

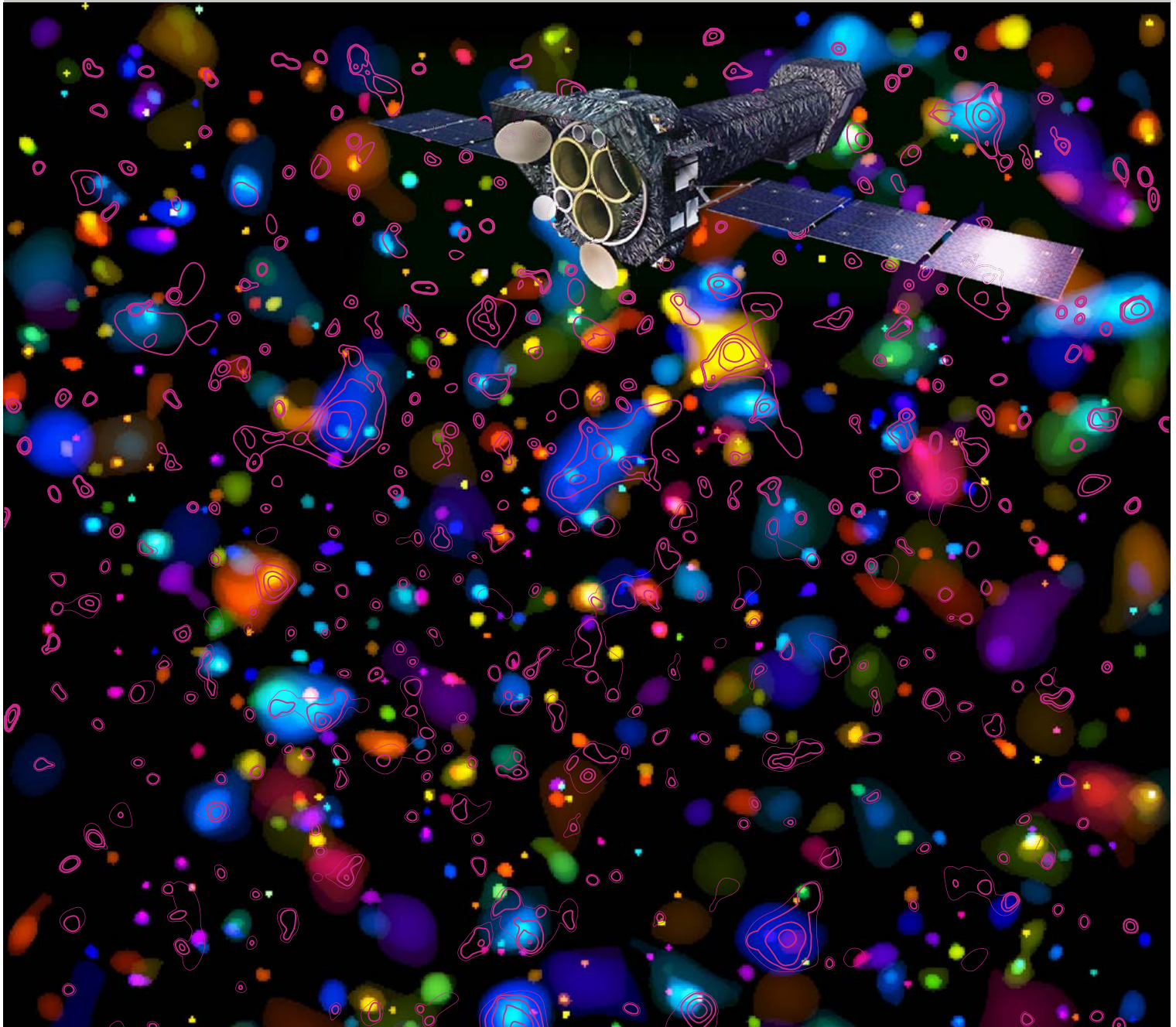


MAX-PLANCK-GESELLSCHAFT

Max-Planck-Institut für
extraterrestrische Physik
Garching



Annual Report 2006



Front Cover:

Colours of the COSMOS: The largest existing sensitive sky survey at many different wavelengths has been performed around legacy programs with the Hubble Space Telescope, with XMM-Newton, Spitzer and Subaru. MPE is leading the X-ray observations in the COSMOS field with XMM-Newton (photomontage). The image displays galaxy concentrations coloured according to their redshift from blue ($z=0.1$) to red ($z=1.2$), overlaid with contours of the extended X-ray emission.



Annual Report 2006

MPE Report 293

Impressum

Responsible for contents: R. Genzel
Editors and Layout: W. Collmar und J. Zanker-Smith
Print: MPE Printshop (R. Hauner)

Text and Figure Contributions: W. Becker, H. Böhringer, U. Briel, M. Brusa, W. Bunk, N. Cappelutti, W. Collmar, R. Davies, R. Diehl, A. Finoguenov, N. Förster Schreiber, R. Genzel, O. Gerhard, J. Greiner, S. Haaland, F. Haberl, G. Hasinger, H. Höfner, A. Ivlev, B. Klecker, C. Knapek, R. Koehler, R. Kompaneets, U. Konopka, D. Lutz, G. Lichti, N. Meidinger, G. Morfill, N. Nowak, G. Paschmann, W. Pietsch, R. Pompl, P. Predehl, C. R ath, R. Saglia, D. Samsonov, L. Str uder, L. Tacconi, K. Tarantik, M. Thiel, M. Thoma, H. Thomas, A. von Kienlin, S. Zhdanov

Further Support: R. Mayr-Ihbe, B. Mory, H. Steinle

1. Edition March 2007

Table of Contents

PREFACE	5
1 RESEARCH AREAS AND INSTITUTE STRUCTURE	9
2 SCIENTIFIC RESULTS	
2.1 Galaxy Evolution, Large-scale Structure and Cosmology	13
2.2 Galaxies, Galactic Nuclei and Massive Black Holes	22
2.3 Stellar Evolution and the Interstellar Medium	32
2.4 Solar System Physics	39
2.5 Complex Plasmas	46
3 EXPERIMENTS AND PROJECTS	
3.1 Space Physics of the Near-Earth Environment	55
3.2 Infrared/Submillimeter Astronomy	57
3.3 High-Energy Astrophysics	
Projects in X-Ray Astronomy	62
Projects in Gamma-Ray Astronomy	66
The MPI Halbleiterlabor – Silicon Detectors for high Speed Imaging	68
3.4 Complex Plasmas	71
3.5 Optical and Interpretative Astronomy	74
3.6 Know-How Transfer	77
4 THE INSTITUTE	
4.1 General Services	83
4.2 Vocational Training and Education	89
4.3 Public Outreach	92
4.4 Social Events	93
5 PUBLICATIONS, TEACHING	97
6 PERSONNEL, COLLABORATIONS	103

PREFACE

This 2006 annual report of the Max-Planck-Institut für extraterrestrische Physik (MPE) provides information about our current science activities, the status and progress of experimental projects, and the development of new hardware. In addition we provide a general overview on the scientific and organisational structure of MPE and its external facilities, introduce our integrated research groups and their ‚daily‘ work environment, and report on our training, educational and social activities.

This report is mainly written for the broader science and astronomy community and for our sponsors, but may also be of interest for the general public and colleagues in industry, education and the media.

The report emphasizes our recent scientific results and the progress of our experiments, projects, and instrumental developments. In the science section we present our main scientific topics by a brief introduction and a summary of our activities, followed by selected highlights. The same structure is used for the experimental and project section.

The past year was again a successful one for our Institute, bringing us exciting new scientific results, as well as key progress and milestones in our projects. Here we mention a few of our scientific highlights, that will be discussed in more detail in the main body of this report, and some milestones achieved in terms of experimental projects:

- discovery of rapidly forming, large, rotating proto-disc galaxies akin to the Milky Way, already three billion years after the Big Bang
 - XMM spots the largest „ball of fire“ in a merging cluster of galaxies
 - ongoing merging activity in the Coma Cluster
 - first direct images of the molecular torus around an Active Galactic Nucleus (AGN)
 - new information on active star formation and evolution in nearby Quasars
 - a major XMM survey of the large ‚COSMOS‘ deep field, with new insights on the evolution of AGN in the universe
 - new evidence on the heating mechanisms of neutron stars surfaces
 - detection of a tumbling, i.e. precessing neutron star
 - the first eclipsing black hole high-mass X-ray binary
 - new insights on the plasma convection in the Earth’s ionosphere
 - clues to the source of energetic solar particles
 - physics of non-newtonian complex plasma fluids and the phase transition of plasma crystals
- „PK-3 Plus“ begins first experiments aboard the International Space Station ISS
 - kick-off of Phase A study of „GRAVITY“, an ambitious near-infrared imaging astrometrical instrument (10 μ arcsec) for the VLT interferometer
 - delivery of the „GLAST Burst-Monitor“ flight model to the GLAST spacecraft
 - completion of the Preliminary Design Review of KMOS, the cooled multi-object, near-infrared spectrograph for the VLT
 - completion of the first MOS (multi object spectroscopy) unit for LUCIFER at the LBT
 - signing of the PanSTARRS contract
 - successful launch of the NASA Mission STEREO
 - first micro-gravity parabola flight campaign for the PK-4 experiment
 - successful completion of the Mission Definition Review for eROSITA
 - start of operation of the PARSEC Laser Guide Star at the VLT
 - installation of two Excellence Clusters (with MPE cooperation) at the Ludwigs-Maximilians University and Technical University of Munich

We thank all colleagues, friends, our industry partners, organisations and sponsors for the excellent cooperation and continuous support.

Professor Reinhard Genzel
Managing Director

1 Research Areas and Institute Structure



1 RESEARCH AREAS AND INSTITUTE STRUCTURE

Our research at the Max-Planck-Institut für extraterrestrische Physik (MPE), located on the University and Research Campus in Garching (Fig. 1), addresses topics of astrophysics and plasma physics. We combine experiments and instrumental development with observations, data analysis and theoretical work. The main themes of our current work are:

- Galaxy evolution, large-scale structure and cosmology
- Galaxies, Galactic nuclei and massive black holes
- Stellar evolution and interstellar medium
- Physics of the Solar system
- Physics of complex plasmas.

On the experimental side, MPE can look proudly back at a forty year record of ambitious and successful projects and experiments in plasma physics and astrophysics. The historically first area concerns particles and electromagnetic fields, in particular their mutual interactions in near-Earth space, that is in the ionosphere, magnetosphere and the solar wind, by means of in-situ measurements. Most of our present experimental work focuses on astronomy with a number of projects, spanning more than twelve decades of the electromagnetic spectrum from millimeter/submillimeter, infrared to optical, X- and Gamma-ray bands. Many of our experiments require telescopes and detectors launched into space by rockets, satellites, and space probes in order to “escape” from the atmospheric absorption which prevents such measurements from the ground. In the infrared and optical bands we also use ground-based or airborne telescopes. Our investigations are complemented by laboratory experiments. Following the discovery of new plasma states (plasma crystals) as a laboratory activity a new research field “Complex Plasmas” has developed, leading to a series of successful experiments aboard the International Space Station. Research groups at MPE also conduct analytical, numerical and observation-related interpretational research and address topics that cover all experimental research areas. The teaming up and strong interaction of theoreticians, observers and experimentalists is a hallmark of our research style.

Our scientific activities are organised into four major research fields, each of which is supervised by one of

the directors: (1) Optical and Interpretative Astronomy, (2) infrared- and submillimeter astronomy, (3) X-ray and gamma-ray astronomy, and (4) theory and complex plasmas. A small group carries out research in space plasma physics. Within these main areas, research is organized in integrated project groups, which include scientists, postdocs, students and technical staff from the Institute’s central division. Currently there are about forty independent project teams. Given our leadership in the development of ambitious space- and ground-based instruments, experiments and telescopes, our technical and engineering branches play a key role, working in



Fig. 1: The research and educational campus in Garching, covering parts of the Technical University of Munich and several research institutes, including MPE. Construction activities for extending the Munich subway to the center of the campus are still ongoing.

close liaison with individual research groups. Over the years, the institute’s emphasis has naturally shifted towards research based on analysis of large amounts of primary data. For coordination of computer hardware and software activities a data-analysis team has been established with representatives from all branches. Other key facilities of the Institute are the X-ray test facility (PANTER) located in Neuried near München (Fig. 2) and a semiconductor laboratory as a collaborative enterprise between MPE and the Max-Planck-Institut für Physik in München on the Siemens campus in München-Neuperlach (Fig. 3). In addition to several technical central groups in mechanical and electronic engineering and their associated workshops mentioned above, our administration and technical services team supports our Institute, as well as the neighbouring Max-Planck-Institut für Astrophysik.



Fig. 2: An aerial photograph of the MPE Panter X-ray test facility in Neuried. The X-ray source and the telescope chamber are separated by a 130m vacuum pipe system.

Know-how transfer from our research into applications is particularly important in two research areas at MPE. The theory division transfers know-how in the area of “analysis of complex systems” into applications in medicine, engineering and pharmacology. The semiconductor laboratory produces X-ray detectors that are applied in other research institutes and in industry.

The implementation of most experimental projects cannot be envisaged without close cooperation with industry, both locally in the Munich area as well as all over Europe and worldwide. Our success record in experimental astrophysics and space research demonstrates the efficiency of such cooperations, primarily with space industry and electronics companies. The challenging technological requirements of our experiments also often lead to technology transfer to industry.

In addition to the institutional support by the Max-Planck-Gesellschaft, that is the most important element of our funding of personnel and projects, our research is also supported by government institutions such as the Federal Ministry for Education and Research

(BMBF) and the German Center for Aeronautics and Space Research (DLR), international organisations such as the European Space Agency (ESA) and European Southern Observatory (ESO) as well as the European Community, with additional financial contributions from the German Science Foundation (DFG), the Humboldt Society and the Dr. Johannes Heidenhain-Foundation.

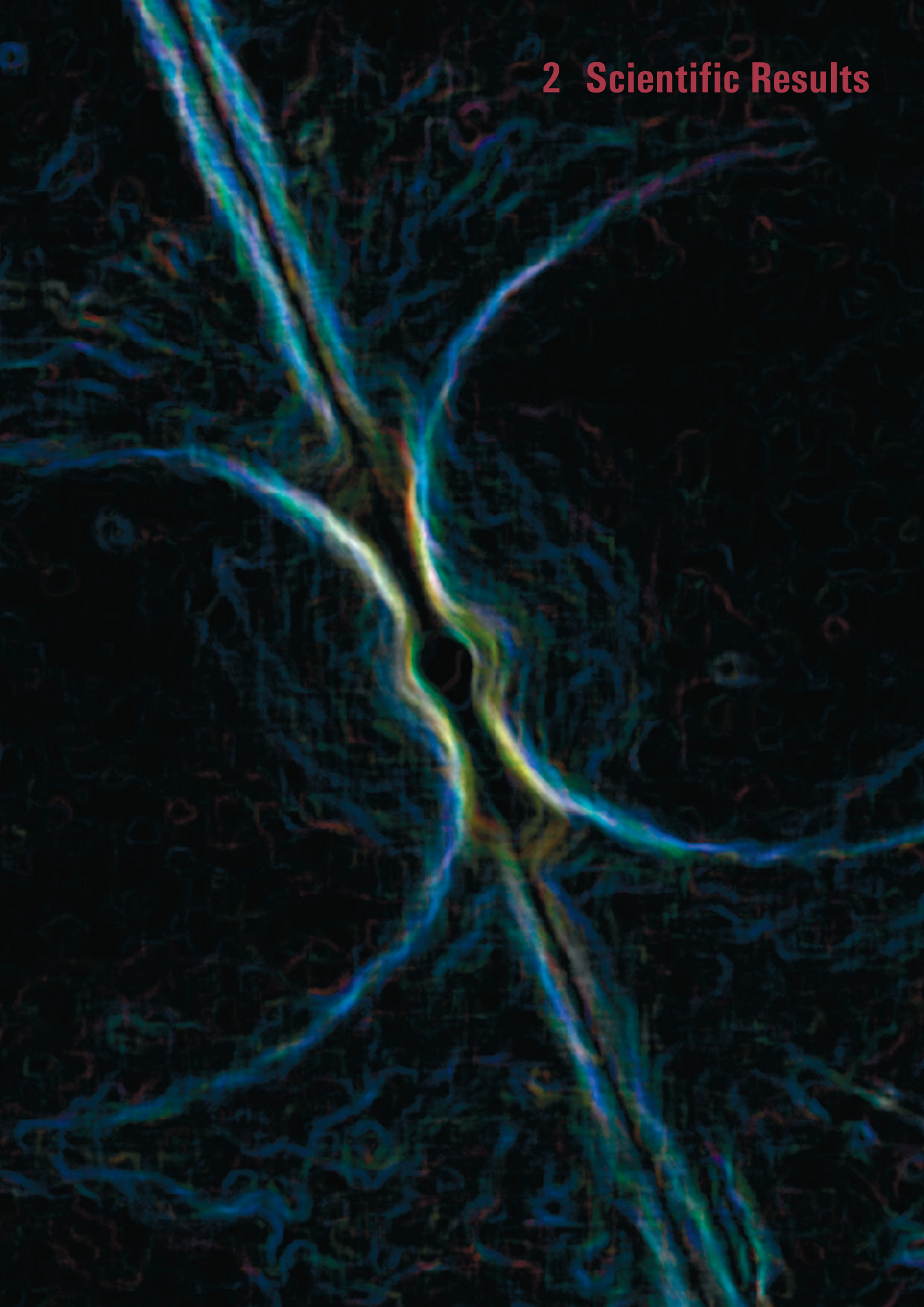
Our institute is strongly engaged in university education: MPE researchers teach at several universities and supervise student research (Diploma, Ph.D.), mainly at both Munich universities, but also in other German universities, and as far

away as the University of California (Berkeley). Seminars, workshops and conferences are held by the Institute in our own and adjacent research fields, often in cooperation with the universities. Our very successful “International Max-Planck Research School on Astrophysics” at the Ludwig-Maximilians-Universität München has resulted in a substantial build up and synergy of the doctoral programs in the Garching/München area.



Fig. 3: The MPI Halbleiterlabor (semiconductor laboratory) on the Siemens campus in München-Neuperlach.

2 Scientific Results



2.1 GALAXY EVOLUTION, LARGE-SCALE STRUCTURE AND COSMOLOGY

Two of the key questions in cosmology are: *How the Universe obtained its structure and appearance that we can observe today and how and when galaxies and larger structures formed?* What can we learn about the global cosmological model describing the evolution of our Universe and about the underlying fundamental physics driving this evolution? These questions are pursued in several wavelength regimes and all groups of the Institute are involved in such investigations.

Deep optical and near infrared photometric surveys provide a census of the galaxy population at various redshifts. The rest frame red and infrared colours provide us with a good measure of the total stellar mass of galaxies and allow us to construct galaxy mass functions for different look-back times. These data combined with stellar population synthesis modelling tell us how the galaxy mass function evolved with time. The surprising result is that the more massive galaxies have essentially been in place at redshifts around one with the same abundance as at present. It is mostly the less luminous galaxies that formed late in the cosmic evolution and consequently still show active star formation activity today.

The star formation rate and the activity of central black holes is probed with the bluer colours of the optical spectrum and, at longer wavelengths, from the properties in the mid-infrared to microwave bands using the Spitzer satellite observatory as well as IRAM mm-observations. The most active objects with the highest star formation rates and most luminous AGN are found at high redshift. The evolution of the star formation rate and the total stellar mass density with time shows approximate consistency in this census.

Very deep infrared observations of distant galaxies can now be conducted from a combination of adaptive optics with integral field spectroscopy with the MPE-built SPIFFI instrument on VLT. These detailed observations provide indications of galaxy internal motion revealing again a surprise: massive spiral galaxies with masses similar to our own galaxy are already found at redshifts of two, indicating the early formation of the more massive objects and posing a challenge to current modelling of hierarchical structure formation. These spectacular results on the kinematics of high redshift galaxies are described in the first article in the present chapter.

The currently most interesting physical processes in galaxy clusters, tied to cosmic evolution, are galaxy cluster mergers – a very dramatic example of these events is illustrated in the second of the following

articles – and the physics of cooling cores, centres of clusters formerly called “cooling flows”. The latter topic was the subject of this years Munich/Garching joint astronomy conference mainly organized by MPE. The increasingly more detailed observations in X-rays and other wavelengths begin to reveal the process with which the massive cooling and condensation of the intracluster medium in cooling core clusters is prevented. Fig. 1 shows as an example such an observational finding in the nearest cooling core region around M87 in the Virgo cluster. The mechanical energy of a jet from the massive black hole in M87 puts out enough energy to heat the surrounding cooling plasma. Detailed XMM spectro-imaging data reveal an excess entropy and therefore heating signatures in exactly the region covered by the radio lobes from the jet.

Galaxy clusters also give rise to gravitational lensing effects, which can be used to reconstruct the mass distribution in clusters. A detailed Hubble Space Telescope image of the cluster Abell 1689 with 107 lensed images of 32 background galaxies provided an absolutely unique study for detailed modelling performed at MPE.

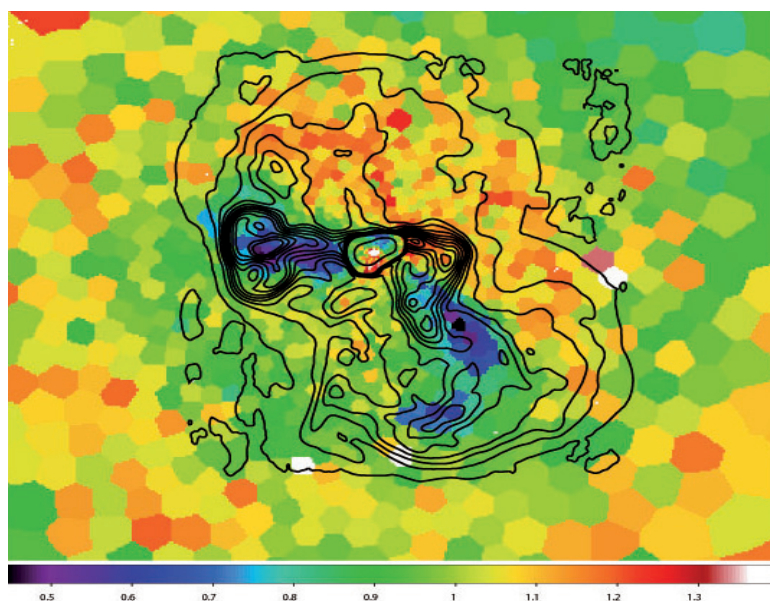


Fig. 1: Entropy-excess map of the X-ray halo M87 with radio map contours overlaid. The red colour in the upper radio halo shows increased entropy, an effect of heating by radio jet interaction.

Several new optical survey projects soon starting, like the ESO KIDS survey, PanSTARRS, and the HETDEX project, have as a main goal the assessment of the large-scale matter distribution of the Universe. These results will be used to test cosmological models with a special emphasis on using particular features (noise peaks) in the large-scale structure statistics called baryonic oscillations. The third article in this chapter discusses this topic.

Far away Galaxy under the Microscope

Observations and theoretical simulations have established a global framework for galaxy formation and evolution in the young Universe. Galaxies formed as baryonic gas cooled at the center of collapsing dark matter haloes, and subsequently grew through mergers and collisions leading to the hierarchical build-up of galaxy mass. It remains unclear, however, over what timescale galaxies were assembled and when and how bulges and disks - the primary components of present-day galaxies - were formed. The „SINS“ survey of distant luminous galaxies now sheds new light on these questions with the discovery of large disk galaxies that must have formed on rapid timescales, only three billion years after the Big Bang. In one of these systems, the combination of adaptive optics techniques with the new SINFONI spectrograph on ESO's Very Large Telescope resulted in a record-breaking resolution of 0.15 arcsecond, giving an unprecedented detailed view of such a distant galaxy.

Our understanding of the formation and evolution of galaxies has improved dramatically over the past decade. This is largely the result of the multitude of surveys carried out at large ground-based telescopes and space-based facilities from the X-ray, ultraviolet, optical, infrared, to radio wavelengths. We now have a robust outline of the global evolution of galaxies since as early as 1 - 2 billion years after the Big Bang. However, we have yet to understand how exactly galaxies assembled their mass and evolved with time. The major limitation is our incomplete knowledge of the relevant mechanisms that control the phase, angular momentum, cooling, and dynamics of the baryonic, or ordinary, matter. The description of galaxy formation in models and simulations remains uncertain because the complex physics of the baryonic processes driving the growth of galaxies lacks observational constraints.

To make further progress, detailed information on the dynamics and physical properties of distant galaxies at early stages of evolution is essential. This is the goal of the „SINS“ (Spectroscopic Imaging Survey in the Near IR with SINFONI) survey, a large and coherent program focussing on the crucial epochs at lookback times of 8 - 12 billion years (cosmological redshifts $z \sim 1 - 4$), when a major fraction of the mass in stars seen in today's galaxies is believed to have

been put in place. SINS takes advantage of the new opportunities afforded by the SINFONI instrument, partly built by the submm/infrared group at MPE and mounted at ESO's Very Large Telescope. SINFONI is a near-infrared imaging spectrometer combined with an adaptive optics system that delivers sharp images simultaneously with high resolution spectral information. Observations at near-infrared wavelengths, between 1 and 2.5 μm , are well-suited to study galaxies at $z \sim 1 - 4$ because many key diagnostic features that are present in the rest-frame optical spectrum of galaxies are redshifted in the near-infrared bands. This includes important emission lines from ionized gas, the spatial distribution and relative motions of which can be fully mapped over the entire galaxies with the unique capabilities of SINFONI.

The most spectacular data set obtained so far as part of the SINS survey is that of the massive star-forming galaxy

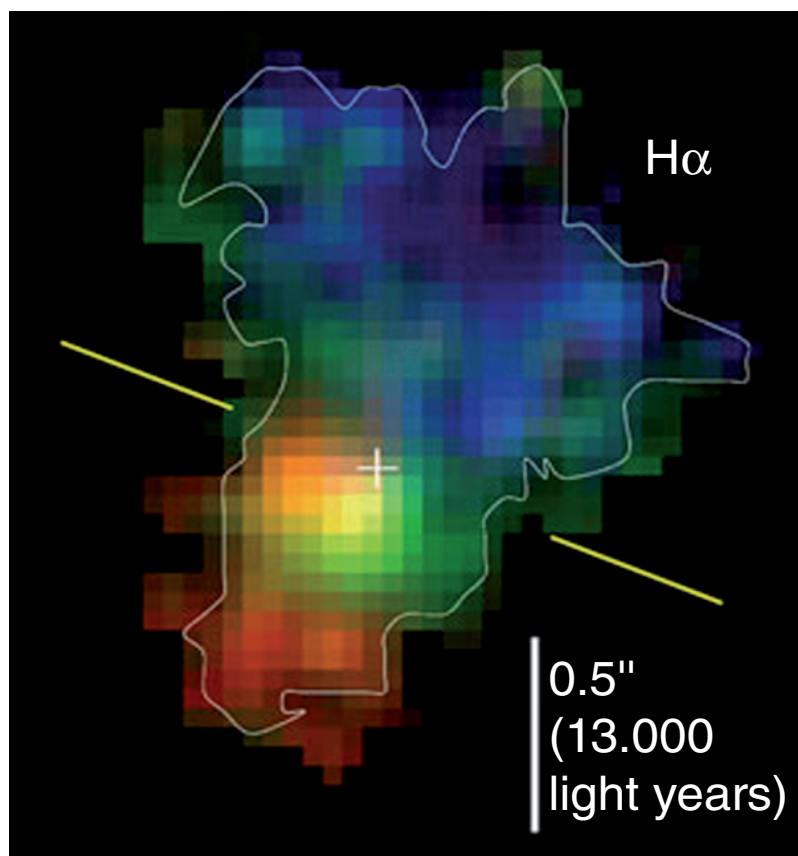


Fig. 1: Hydrogen recombination line emission ($H\alpha$) of the massive star-forming galaxy BzK-15504 about 11 billion light-years away. The colors indicate whether the ionized gas is moving away from us (red), towards us (blue), or is stationary (green), relative to the global motion of the system at its cosmological redshift $z = 2.38$. This galaxy appears to be a disk, akin to the Milky Way, and rotates at a maximum speed of 230 km s^{-1} around an axis (yellow line) passing through the galactic nucleus (white cross).

BzK-15504 at redshift $z = 2.38$, when the Universe was 20% of its current age. The presence of a suitable star for adaptive optics near the source provided the necessary reference light source to correct for the blurring effects of turbulence in Earth's atmosphere (or „seeing“), which otherwise degrade the image sharpness. The angular resolution achieved is about 0.15 arcsecond, or a mere 4000 light-years (1.2 kpc) at the distance of the galaxy. This gives the most detailed view of the ionized gas morphology and kinematics for a galaxy at lookback times around 11 billion years.

The SINFONI observations of BzK-15504 targeted the hydrogen Balmer $H\alpha$ recombination line emission, tracing gas photoionized by the light from hot young stars in star-forming regions. The results reveal a large

fragmentation, and conversion to stars of an initially very gas-rich protodisk, on a timescale of a few hundred million years only. The details of the morphology and kinematics further suggest that this massive ($1.1 \times 10^{11} M_{\odot}$) rotating disk is channelling gas towards a growing central stellar bulge hosting an accreting massive black hole. There are no obvious signs for a major merger, a surprising finding given the high star formation rate and rapid mass assembly. This probably suggests that BzK-15504 assembled its mass via smoother infall, as in the „cold flow“ accretion mechanism proposed as alternative to major mergers, or through a rapid series of minor mergers.

These results confirm the findings for several other of the nearly 30 luminous star-forming galaxies at similar

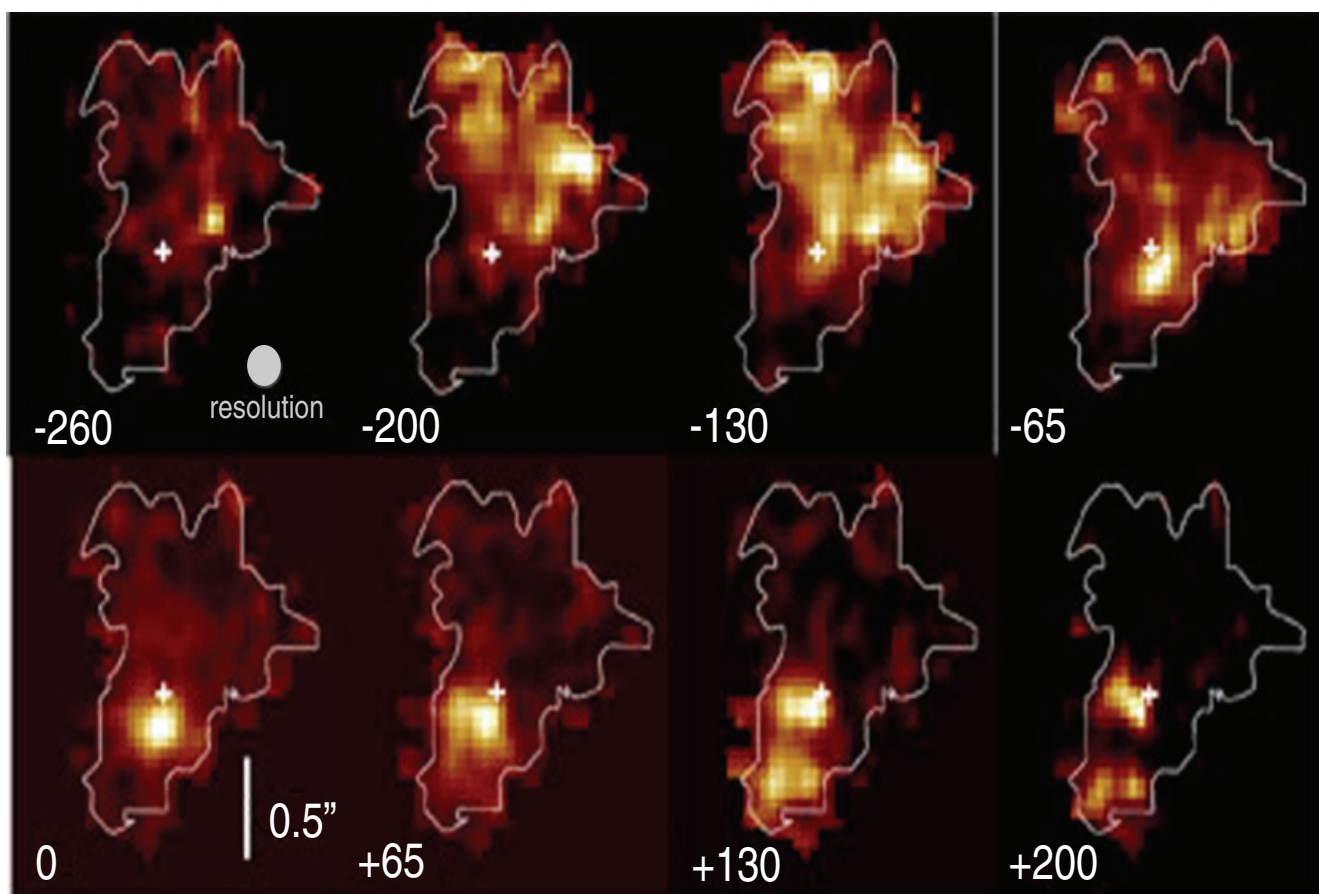


Fig. 2: These high resolution images of BzK-15504 reveal that star formation in this young galaxy is taking place in spectacularly bright and massive complexes, and that gas is flowing rapidly towards the nuclear regions to build up a dense stellar bulge hosting an accreting black hole. This system could later evolve into a massive elliptical galaxy.

galaxy about 53,000 light-years across (16 kpc), with several prominent bright complexes corresponding to the most active sites of star formation (Fig. 2). The relative motions of the gas within the galaxy show that the system is rotating, with a maximum speed of 230 km s^{-1} in the outer parts. The high surface density of gas ($\sim 350 M_{\odot} \text{ pc}^{-2}$), the high rate of star formation ($\sim 150 M_{\odot} \text{ yr}^{-1}$), and the moderately young stellar ages (~ 500 million years) suggest rapid assembly,

redshifts observed to date as part of SINS. Due to the absence of a suitable reference star for adaptive optics near these galaxies, the SINFONI observations were carried out under typical natural seeing conditions, at a resolution of 0.5 - 0.6 arcsecond. For the majority of the larger systems, the ionized gas kinematics exhibit a regular pattern with monotonic variations across the galaxy in spite of an irregular spatial distribution - convincing evidence for orbital motions in a disk configuration. The

case of BzK-15504 offers an unparalleled view into one such system, with three to four times finer detail.

The discovery of so many massive rotating disk galaxies among the SINS sample came as a surprise. In view of the higher rate of major mergers at high redshift, the initial expectation was that most of the larger systems would show more complex gas motions. The properties of these high redshift disks provide new and quantitative constraints for theoretical models. For BzK-15504 and many of the other SINS galaxies at $z \sim 2 - 2.5$, the derived angular momenta of $\sim 1000 \text{ km s}^{-1} \text{ kpc}$ are nearly as large as those of present-day spiral galaxies. Moreover, it appears that the gas in these galaxies could have comparable specific angular momentum as the parent dark matter halos from which they formed, implying little net loss of angular momentum of the baryonic matter upon collapse - an important empirical clue to one of the long-standing questions about galaxy formation. For the best-resolved galaxies, the ratio of the rotation velocity to the random motions velocity can be estimated. The values inferred ($\sim 2 - 4$) are intermediate between those of pressure-supported systems like present-day elliptical galaxies ($\sim 0.1 - 1$) and rotationally-supported disks of spiral galaxies such as the Milky Way ($\sim 10 - 50$). This

implies that their disks are quite turbulent, probably very gas-rich, and likely unstable to global star formation and fragmentation. As some simulations of the evolution of gas-rich galactic disks suggest, the star-forming clumps could later sink towards the gravitational center by dynamical friction against a diffuse underlying gas disk to form a central bulge on a timescale of order of one billion years. This could provide a mechanism whereby some of the young disks uncovered in the SINS survey evolve into elliptical galaxies or disk galaxies with a dominant massive bulge component like those observed in the present-day Universe.

N. Förster Schreiber, R. Genzel



A Puzzling Merger in A3266: the Hydrodynamic Picture from XMM-Newton

XMM-Newton observations have found a comet-like ball of gas, over a billion times the mass of the sun, hurling through the galaxy cluster Abell 3266. This colossal „ball of fire“ is by far the largest object of this kind ever identified. The gas ball is about three million light years across, or about five billion times the size of our solar system. It appears from our perspective as a circular X-ray glow with a comet-like tail nearly half the size of the moon. The event is the consequence of a merging process, the mechanism by which the largest cosmic structures in the universe are thought to form.

Current theories of structure formation are based on hierarchical models whereby small structures form first and, by assembly, build up larger structures. In this picture, mergers play an important role, not only in driving the formation of galaxy clusters, but also in affecting the properties of the intra-cluster medium including their thermodynamic conditions and metal content. A merger event results in dramatic consequences for the systems that take part in it. As a large amount of energy is released in the process, the intracluster medium is strongly stirred up which results in the production of shocks and turbulence. Furthermore, the trans/supersonic infalling subsystem may be stripped off of their gas by ram pressure work. This mechanism may supply the main cluster with low-entropy gas, and perhaps with high metallicity too. In addition, disruption of cool condensations and abundance gradients may result in the cluster center. Until now, however, the evidence for the latter has been only ex post facto in that post-merger systems appear to lack central cool gas reservoirs and central abundance enhancements so that little is known of the intermediate evolutionary stages.

The galaxy cluster Abell 3266 (A3266), located at a redshift of 0.059, is well studied, however not fully understood. A statistical analysis of the kinematic data of the cluster galaxies indicate a merger. They show that the velocity dispersion in the center, ~ 1300 km/s, is higher than the global value of 1000 km/s. This was interpreted as evidence of a relatively localized merger in progress that has increased the internal energy of the cluster primarily in the central region.

XMM-Newton observed A3266 in order to study the properties of its intracluster medium. The high signal-to-noise ratio of the data, together with new reduction techniques, allow to generate statistically accurate maps that describe the thermodynamic state of the intra-cluster medium (ICM) of A3266. While the qualitative picture is confirmed, the new maps provide a much more detailed picture of the merging process. This may serve as a test case for our understanding of the role of gas stripping on cluster scales. In particular, we construct the maps approximating as close as possible the underlying pressure and entropy distribution.

Fig.1 shows maps of pseudo-entropy and pseudo-pressure, as obtained from a wavelet analysis. The pseudo-entropy map reveals the presence of a giant plume of low entropy gas (LEG) extending over $15'$ to the north-east from the cluster center. The distinct value of the entropy of the LEG suggests a common origin for it. The orientation of the LEG is aligned with the projection of the major axis of the merger onto the observer's plane, i.e. the axis of the elongated X-ray morphology. This strongly suggests that the LEG originates with the merger itself. The question is whether the LEG belongs to a cool core in A3266, now undergoing disruption, or is just gas from an infalling subcluster undergoing ram pressure stripping.

The entropy in the LEG has significant structure on small but resolved scales. In particular, local enhancements are clearly visible: these are likely pre-existing as contact discontinuities due to inefficient mixing, but could also have been generated by relatively weak shocks. In fact, all twelve major entropy enhancements (green in Fig. 1) have a corresponding pressure enhancement. Finally, these maps show a great number of the entropy dips that are aligned with galaxies and galaxy subgroups.

The core region exhibits fluctuations on the level of 14% for the entropy and 12% for the pressure, with respect to the typical profiles, as derived for a large sample of clusters. The larger level of fluctuations, 24% for the entropy and 30% for the pressure, seen within a bulk of the cluster, is due to asymmetries in the azimuthal distributions, particularly north-east of the core and are associated with the LEG, which exhibits both $\sim 20\%$ lower entropy and $\sim 30\%$ higher pressure, compared to the expectation. The thermodynamical properties of the A3266 ICM itself are found to be within 10% of the a typical value for clusters of similar temperature. Although the amplitude of the pressure fluctuations is highest in the cluster center, reaching a factor of two, their area filling factor is small, which results in moderate area-weighted values.

In the low entropy regions near the cluster core the total gas mass is $1.3 \times 10^{13} M_{\text{sun}}$. This mass is comparable to the core gas mass of clusters with mass similar to Abell 3266. It is also comparable to the total gas masses of cool, low mass clusters, or to high mass groups. Thus, the extended feature of low entropy gas is either the core of the main cluster or gas stripped off of a secondary merger component with a secondary-to-primary mass ratio of 1:10.

Hydrodynamical simulations show that intracluster gas from a low mass secondary may be stripped as it passes through the high mass, high density core. Nonetheless, it is quite puzzling that the cD (giant elliptical) and other core galaxies sit on the leading edge of the LEG. It is conceivable that we are seeing things in projection so

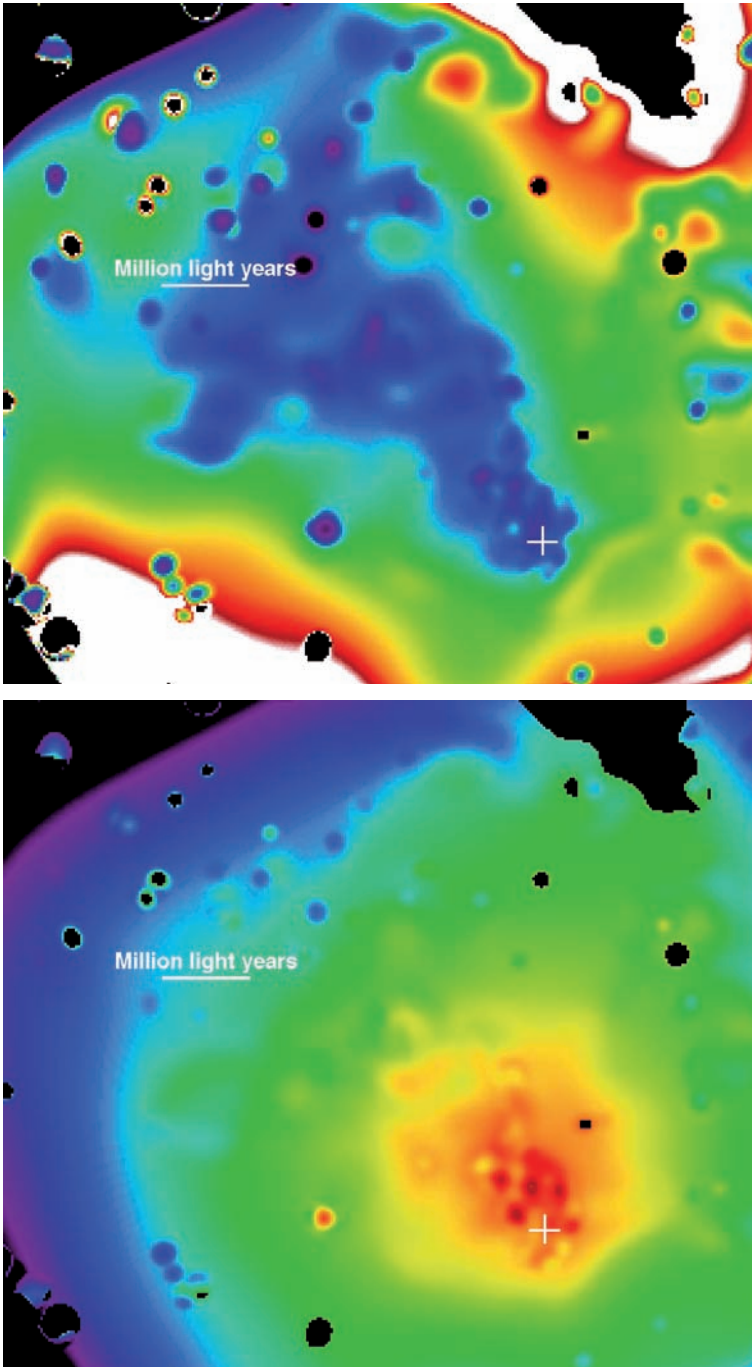


Fig. 1: Top: Wavelet reconstructions of the pseudo-entropy. Point sources are not removed from the maps. Blue, green, yellow, red and white colors correspond to the entropy levels from low to high. Bottom: Wavelet reconstructions of the pseudo-pressure. Blue, green, yellow, red and white colors correspond to the pressure levels from low to high. A size scale and a point of reference (+) were added to compare the images.

measurements of cluster galaxies, can be compared to the gas mass estimate for the LEG. We assume the stripped gas accounts for the bulk of the infalling cluster matter. Based on the average temperature of A3266 of 7.1 keV, the mass-temperature relation, and a gas-mass fraction of 13%, we estimate the total gas mass of the ICM of A3266 to be $1.2 \times 10^{14} M_{\text{sun}}$. The gas mass ratio between LEG and the main cluster is 9, which is within 10% of the dynamical constraint. Both these estimates argue in favor of association of the LEG with the galaxy component infalling from the foreground. The temperature of the infalling cluster is predicted as 2.0 keV and the corresponding initial size of the cluster of 0.59 Mpc. A circle of this radius fits exactly the spatial extent of the tail of the LEG.

Finally we note that Abell 3266 may have a more complex merger history than the single 1:10 mass ratio merger that we propose. On the west side of the cluster, there is an extended collection of entropy debris. Within the debris are several peaks that appear to be associated with galaxies. The masses of the peaks are comparable to group masses. This second region of low entropy gas may indicate an additional episode of merging as A3266 is the most prominent cluster in the southern Horologium cluster concentration.

that the LEG is falling onto the core of A3266 from the foreground, while moving towards the SW in the observer's plane. This scenario may not be so unlikely, as the infalling subclump would aim at the core of the companion cluster (so as to produce a superposition along the line of sight). In addition, such a configuration may explain the increasing apparent velocity dispersion of galaxies towards the center, as being caused by a displacement between the core of the main cluster and the infalling cluster. In order for this to be consistent with the optical data the mass of the subcluster must be in the ratio of no more than 1:10 with respect to the main cluster. This ratio, based on the velocity

A. Finoguenov, H. Böhringer, U. Briel



Baryonic Oscillations

Just like the fluctuations in the Cosmic Microwave Background (CMB), certain length scales are imprinted in the the distribution of mass in the universe. This standard ruler can be found in the phase of the oscillations in the galaxy power spectrum. By comparing the observed phases with the computed length scales using various cosmological models, one is able to constrain cosmological parameters. By using a phenomenological fitting function, to be able to disentangle the amplitude and phase information in the oscillations of the galaxy power spectrum and give constraints on cosmological parameters like the equation of state of dark energy.

According to recent WMAP 3rd year results, the mysterious dark energy constitutes about $\frac{3}{4}$ of the total energy density in the universe today. Although it makes up such a big part of the universe, we know even less about its nature and physics than we know about the equally infamous dark matter, which makes up about 20% of the universe. The 5% of visible baryonic matter we are used to in every day life, can almost be neglected compared to the 95% we are just beginning to understand.

There are a number of particle candidates that could make up dark matter, and particle physicists are exploring various ways to find them.

Constraining the properties of dark energy is even harder. According to elementary particle field theories, there should be about 10^{120} more dark energy than astronomers observe. But this is not the only strange fact concerning dark energy. Contrary to normal energy and matter, it does not slow down the expansion of the universe, but accelerates it. Dark Energy acts as anti-gravity, forcing the universe to expand faster and faster. Some models of dark energy, the so called Phantom Energy, even force the universe to expand so fast that space itself is torn apart in a Big Rip (final Big Bang). Other models, like Quintessence, allow us to solve the question why the dark energy density has exactly the low value that is observed today, which is very improbable. In fact, it is much more probable to win the lotto jackpot 10 times in a row than for dark energy having the density we actually determine. Quintessence circumvents this problem by proposing an energy density that is following

the evolution of the universe and does not have to be fine tuned. Finally, dark energy could be the famous Cosmological Constant, which Einstein added to his field equations to make a stable and infinitely old universe possible. All three models can be characterized by the equation of state ω of dark energy, relating its energy density to its pressure. Normal matter and energy have positive ω values, leading to attractive forces, well known as gravity. Quintessence has a ω value ranging from $-1/3$ to almost -1 , Phantom Energy is called everything with a ω smaller than -1 and the Cosmological Constant's ω is exactly -1 . Of course, theorists also suggest much more elaborate models that allow ω to change with time and even with space. By measuring the effects of dark energy, astronomy provides us with the unique opportunity to learn more about the nature of dark energy. The combination of the most recent measurements yields a ω value of about -1 with an error of 20%, excluding none of the three mentioned possibilities.

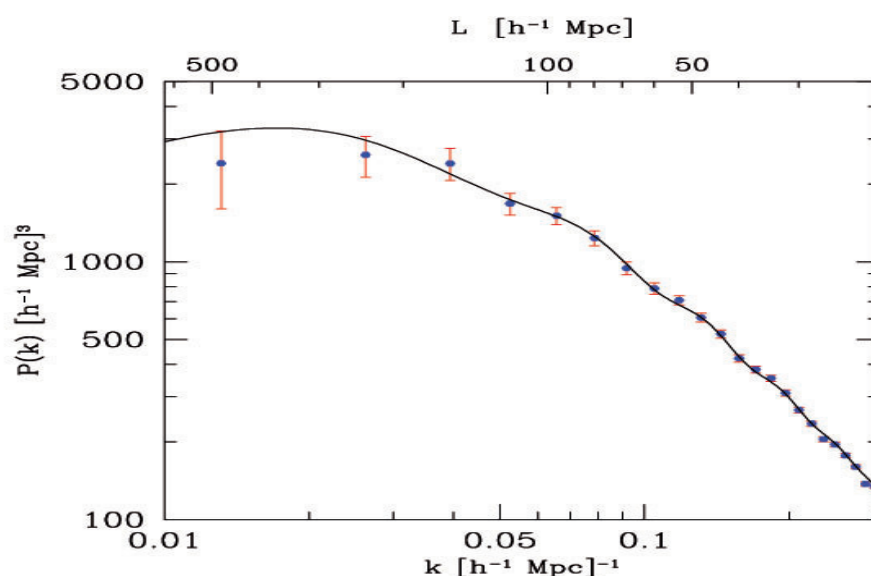


Fig. 1: A matter distribution power spectrum showing the overall clumpiness per inverse distance computed using the Hubble Volume Simulations at redshift $z = 2.3$. It contains the non-oscillatory dark matter part and the Baryonic Acoustic Oscillations on top.

From an astronomical point of view, there are two ways to measure the equation of state of dark energy and thus the ω parameter: The structure growth history of the universe and its geometry. The growth of structures in the universe is mainly dependant on two factors. The actual matter content, and the expansion rate. The more matter there is, the faster it will clump together and form the various large scale structures. A low matter density will lead to less pronounced structures at a later time, while a high matter density enforces pronounced structures early on. Expansion on the other hand works

contrary to this. The faster the expansion is, the less time is available to form structure. The ω parameter is influencing growth by altering the expansion rate. The smaller ω is, the faster the universe is expanding. Thus, the equation of state of dark energy can be constrained by measuring the growth history of structure. The geometry

exact position of galaxies down to a redshift of four. To do this, HETDEX will be able to take about 35,000 spectra per shot utilizing 145 integral field spectroscopy units with 241 optical fibres each. Both ways to measure ω are being used at the moment or will be exploited in the future utilizing various methods. Growth history

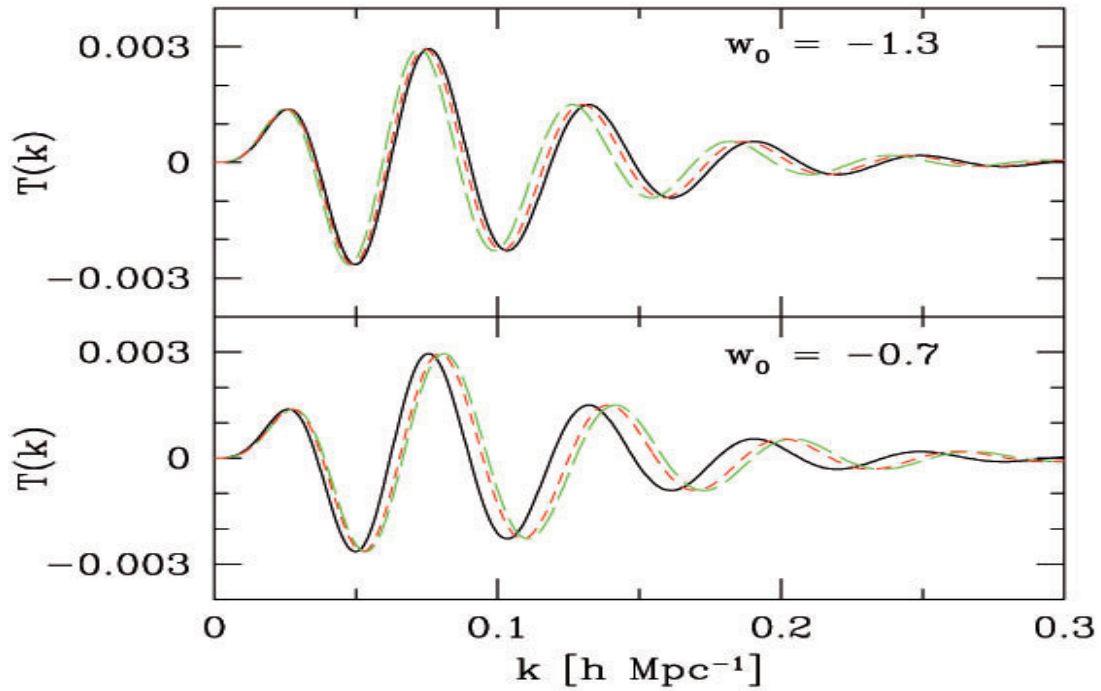


Fig. 2: Behaviour of the extracted Baryonic Acoustic Oscillations using different cosmological models. The wiggles (red, green) get squeezed compared to the reference model (black) when the equation of state of dark energy ω gets smaller, and get stretched when a bigger value of ω is chosen.

of space, on the other hand, is directly influenced by cosmological parameters. The overall energy and matter density of the universe determines its shape in space time. As the ω parameter is influencing this curvature, it can be constrained by measuring the size of different rulers of known size (standard rulers) at different ages of the universe.

The MPE is involved in several large scale surveys that will provide the data for these cosmological tests. In the near future, KIDS, the Kilo Degree Survey, will cover 1500 square degrees with 9 filters to allow for high precision photometric redshifts. PanSTARRS - the Panoramic Survey Telescope & Rapid Response System - is performing an all-sky survey, providing us with photometric redshifts of billions of galaxies. Finally, HETDEX - the **H**obby **E**berly **T**elescope **D**ark **E**nergy **eX**periment - will spectroscopically survey an area of 300 square degrees and more, providing us with the

is probed by counting clusters of galaxies at different redshifts and comparing their distribution. The geometry is determined using Supernovae Ia as standard candles and measuring their relative brightness. Both quantities, geometry and growth history, can be acquired by measuring the distortion of galaxy shapes by weak gravitational lensing, the so called cosmic shear.

A further method are of Baryonic Acoustic Oscillations, which will be used (among others) in KIDS, PanSTARRS and HETDEX. During the better part of its first 300.000 years the universe was filled with a plasma of ionized baryons, electrons and photons. Due to small perturbations, carried over from the inflationary first 10^{-32} seconds of the universe, this plasma was oscillating at various scales. These oscillations can be seen in fluctuations of the Cosmic Microwave Background (CMB) which consists of photons released from the plasma 13.4 billion years ago when the universe became cool

enough to be transparent for the first time. However, not only the photons, but also the baryons carry the imprint of these oscillations, called acoustic, because they were mainly governed by the speed of sound in the plasma. After the release of the photons the baryons moved according to the oscillations, dragging dark matter along via gravitation, and thus ended up being perturbed on various length scales.

By calculating the characteristic length scales and using it as a standard ruler, which can be compared to the measured scales (at various redshifts), we are able to give constraints on cosmological parameters, like the equation of state of dark energy ω . The characteristic length scales can be derived from observations by computing the so called power spectrum out of the matter distribution, which measures the „clumpiness“ of the distribution on various length scales. The fluctuations caused by the Baryon-photon plasma show up as oscillations on top of a smooth dark matter term (Fig.1). However, measuring the oscillations in the power spectrum of the matter distribution cannot be done directly, but indirectly by looking at visible objects. All in all, only about 1% of the matter in the universe is visible. One way to overcome this problem is to measure only the visible part of the matter and assume that the rest is distributed just the same. This introduces a bias, as galaxies tend to form in high density regions like filaments and stay away from low density regions like voids, effectively boosting the clumpiness of the measured distribution. This biasing effect and further complications due to our lack of knowledge about Dark Matter, non-linear effects in structure growth and the fact that we have only less precise redshifts from photometry complicate the determination of the power spectrum.

In our approach at MPE, we cope with these difficulties in the following way: The matter power spectrum consists of two components, the dark matter component, and the baryonic matter component. While the former is monotonically decreasing at the relevant scales, the latter is oscillating on top of it. Thus by fitting a non-oscillating

function to the shape and subtracting it, we are left with the oscillatory part, which we are looking for. The phases of the oscillation are the standard-ruler mentioned above. Effects like biasing, redshift-space, or linear growth only boost the amplitude of these oscillations and thus do not affect phase, as both are orthogonal to each other.

We can now measure the galaxy distribution using, for example, young Lyman Alpha emitting galaxies, at different redshifts and extract the Baryonic Acoustic Oscillations and compare the phase length to cosmological models with different ω values. As ω is affecting the geometry of the universe, the oscillations are either stretched or compressed compared to the theoretical prediction when a wrong ω value is assumed. And this can be done without assuming only very little about Dark Matter and very few sources for systematical errors.

In a further step one can use the amplitude of the oscillations to probe ω using the growth history of the universe. As the amplitude is directly related to the clumpiness of the distribution it can tell us how pronounced structures were at different redshifts. This method is more complicated, because all previously mentioned effects have to be known to good accuracy and to be taken into account. However, after the extraction of the oscillations, the necessary data is available and can be exploited in this way.

The vast amount of data produced by surveys with MPE participation (e.g. KIDS, PanSTARRS and HETDEX) will thus enable us to get further constraints on Dark Matter and Dark Energy, that is one of the biggest mysteries in physics today.

R. Koehler, P. Schuecker



2.2 GALAXIES, GALACTIC NUCLEI, AND MASSIVE BLACK HOLES

Nearby normal, starburst, and active galaxies (AGN) provide the perfect laboratories for detailed investigation of the processes important for galaxy evolution. With the scientific expertise spanning nearly the entire spectrum of wavelengths – from gamma-rays, X-rays, and near-IR through millimetre, at MPE we are in the unique position of being able to study these systems over a wide range of size scales, morphological type, and activity. Much of what we are doing heavily involves instrumentation developed and built in-house, supplemented with data from external facilities, enabling us to undertake unique and pioneering astrophysical research.

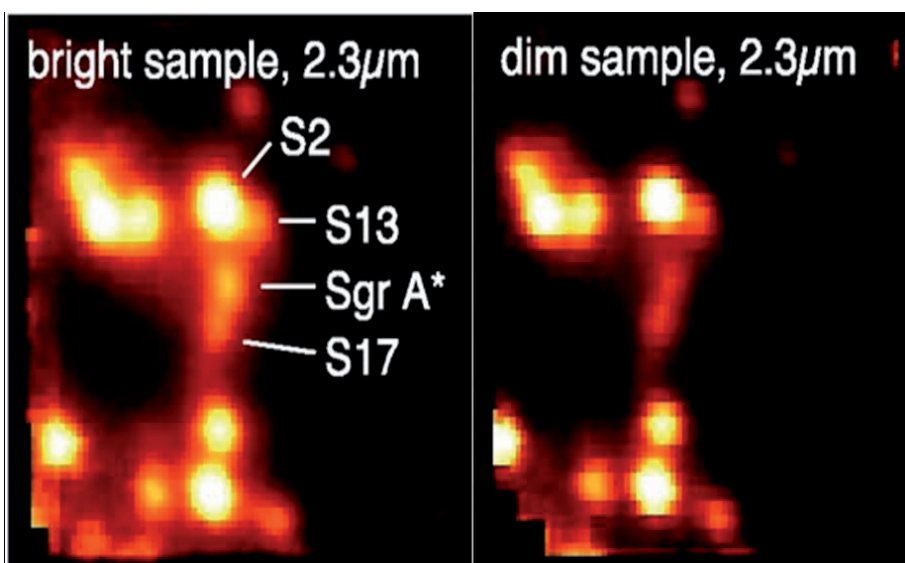


Fig. 1: K-band narrow-band images (centred around 2.3 microns) of a near-infrared flare from Sagittarius A* as seen by SINFONI during bright (left) and dim (right) phases.

Closest to home, the Galactic Centre continues to provide surprises and insights through monitoring campaigns at wavelengths from the near-IR through X-rays as well as detailed high-resolution studies. Using NACO and SINFONI on the VLT, we continue to monitor activity from Sagittarius A* (Fig. 1). For the first time, we have observed spectral variations of a near-infrared flare from Sagittarius A*, as well as a swing of the polarization angle during such a flare.

In local galaxies spectroscopic studies of the central regions at high resolution enable studies of the kinematics and energetics surrounding supermassive black holes at unprecedented resolution. As outlined in the first selected article in this chapter, with SINFONI and adaptive optics techniques we are now measuring black hole masses in nearby nuclei, and are mapping out the distributions of young stars surrounding these black holes on scales of less than 10 pc. With XMM-Newton we are mapping out the hot outflow in local starburst galaxies, such as NGC 253. In that galaxy they find that the energetic O VIII emission line clearly delineates the outflow morphology

out to 750 pc along the minor axis of the galaxy. This is the first time that the hot wind fluid has been detected directly.

In the local Universe and at higher redshifts, we are using observations from Chandra and XMM-Newton to probe the regions immediately surrounding the black holes of active galaxies. With XMM-Newton we have made the first detection of gravitationally redshifted soft X-ray lines in the AGN, Mrk 110. A short exposure surprisingly revealed a broad and redshifted emission line associated with the O VII triplet. The data are in excellent agreement with models, also being worked on at MPE, which predict gravitationally redshifted emission lines from the broad line regions of AGN. Such redshifted lines can be used to estimate black hole masses and spin, as well as constrain parameters of the accretion disk.

On the scales of entire galaxies, at MPE we study the issues of ‘classical’ versus ‘pseudo’ bulges in spiral galaxies, the formation and evolution of bars, and their link to central, supermassive black holes. We want to know whether the black holes in pseudo-bulges follow the same relation as is found for classical bulges. We also analyse the dynamics of early-type galaxies, investigating their dark matter contents and the stellar orbital distributions.

At still larger scales, we are investigating the dynamics of galaxy clusters through observations of intracluster stars, and galaxy evolution through deep-field multi-wavelength imaging and spectroscopy campaigns.

The remainder of this chapter focusses on three selected results from this year’s galaxy and AGN research at MPE. They are: 1) a comprehensive investigation of the kinematics of intracluster evolved stars in the Coma cluster of galaxies to assess the cluster dynamical history; 2) a high resolution study of the nuclei of nearby galaxies and AGN utilizing the unique capabilities of adaptive optics assisted integral field spectroscopy to measure central black hole masses and to investigate star formation in the very centres of these systems; and 3) a major X-ray survey with XMM-Newton as part of the large international Cosmic Evolution Survey (COSMOS) campaign, which covers a contiguous 2 deg² equatorial area of the sky with imaging from radio to X-ray wavelengths, complemented by a multi-wavelength spectroscopic programme.

The Kinematics of Intracluster Stars and the Dynamical History of the Coma Cluster of Galaxies

The Coma cluster is the richest and most compact of the nearby clusters, yet there is growing evidence that its formation is still on-going. A sensitive probe of this evolution is the dynamics of intracluster stars, which are unbound from galaxies while the cluster forms, according to cosmological simulations. With a new multi-slit imaging spectroscopy technique we have measured the line-of-sight velocities of 37 intracluster planetary nebulae associated with the intracluster light in the Coma cluster core, at 100 Mpc distance. These must be the faintest single stars ever detected and the second-most distant after high-redshift supernovae. The measured velocities combined with galaxy redshift and X-ray data argue strongly that the cluster is currently in the midst of a major subcluster merger nearly in the plane of the sky. The two subcluster cores are presently beyond their first and second close passage, during which the elongated distribution of diffuse light has been created.

This diffuse light is believed to originate from stars that were born in galaxies, but were subsequently unbound from them by a variety of dynamical processes, after these galaxies fell into the cluster. In fact, cosmological simulations predict that galaxies should be dramatically modified by interactions during the assembly of galaxy clusters. To test these predictions requires that we measure not only the distribution of the diffuse light stars, as projected onto the sky, but also their motions - the distribution of velocities contains vital information on how and when this component originated.

The only tracers that currently allow us to measure the motions of the diffuse stellar population are Planetary Nebulae (PNe). These dying stars emit $\sim 10\%$ of their luminosity in a single emission line, $[\text{OIII}]\lambda 5007\text{\AA}$, that is redshifted relative to the rest-frame wavelength according to the PN's radial velocity. Unfortunately, the PN phase is brief, and so PNe are rare, about one is seen for every few 100 million stars.

In the Coma cluster at 100 Mpc distance, PNe are also exceedingly faint. The $[\text{OIII}]\lambda 5007\text{\AA}$ line flux from the brightest PNe at this distance is equivalent to ~ 20 photons per minute through the aperture of an 8m telescope, of which ~ 2 will reach the detector for a typical $\sim 10\%$ system efficiency. Such faint sources are no longer detectable with narrow band photometry - their emission disappears in the sky noise. To detect PNe at such distances requires a spectroscopic blind search technique in which only the sky noise within a few \AA dilutes the emission from the PN, and where the positions of these faint PNe do not need to be known beforehand.

In our pilot study, we combined a mask of parallel slits as shown in Fig. 2, with a narrow-

band filter centered on the wavelength of the redshifted $[\text{OIII}]\lambda 5007\text{\AA}$ emission line for the mean recession velocity of the Coma cluster. In this Multi-Slit Imaging Spectroscopy (MSIS) technique, spectra are obtained for all PNe that happen to lie behind the slits. The narrow-band filter limits the length of the spectra on the CCD so that many slits can be simultaneously exposed. For each mask exposure only a fraction of the field is surveyed; to increase the sky coverage the mask is stepped on the sky. The dispersed image resulting from such a mask exposure resembles a brick wall, made up of adjacent 60\AA wide, two-dimensional spectra. Sections of some extracted spectra with a few

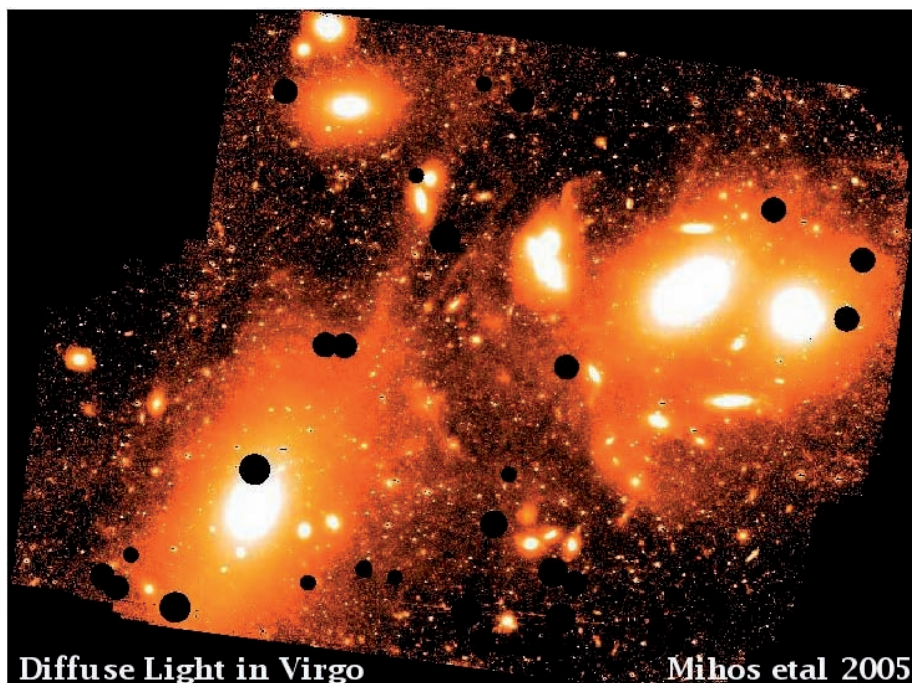


Fig. 1: Deep image of the core of the Virgo cluster, obtained with the Case-Western Schmidt telescope by US colleagues around C. Mihos.

It has become clear in recent years that galaxy clusters contain a diffuse population of stars, spread between the cluster galaxies. About 10% of the stars in typical clusters belong to this diffuse population. A vivid illustration is given by the deep image of the Virgo cluster, obtained by C. Mihos et al. and reproduced in Figure 1. Whereas on typical sky images the large Virgo galaxies like M87 (in the lower left corner of this image), M86 and M84 (both in the upper right) appear well-separated, in this deep image they appear to touch or even overlap. In addition, a multitude of small-scale structures and streamers are visible in this deep image.

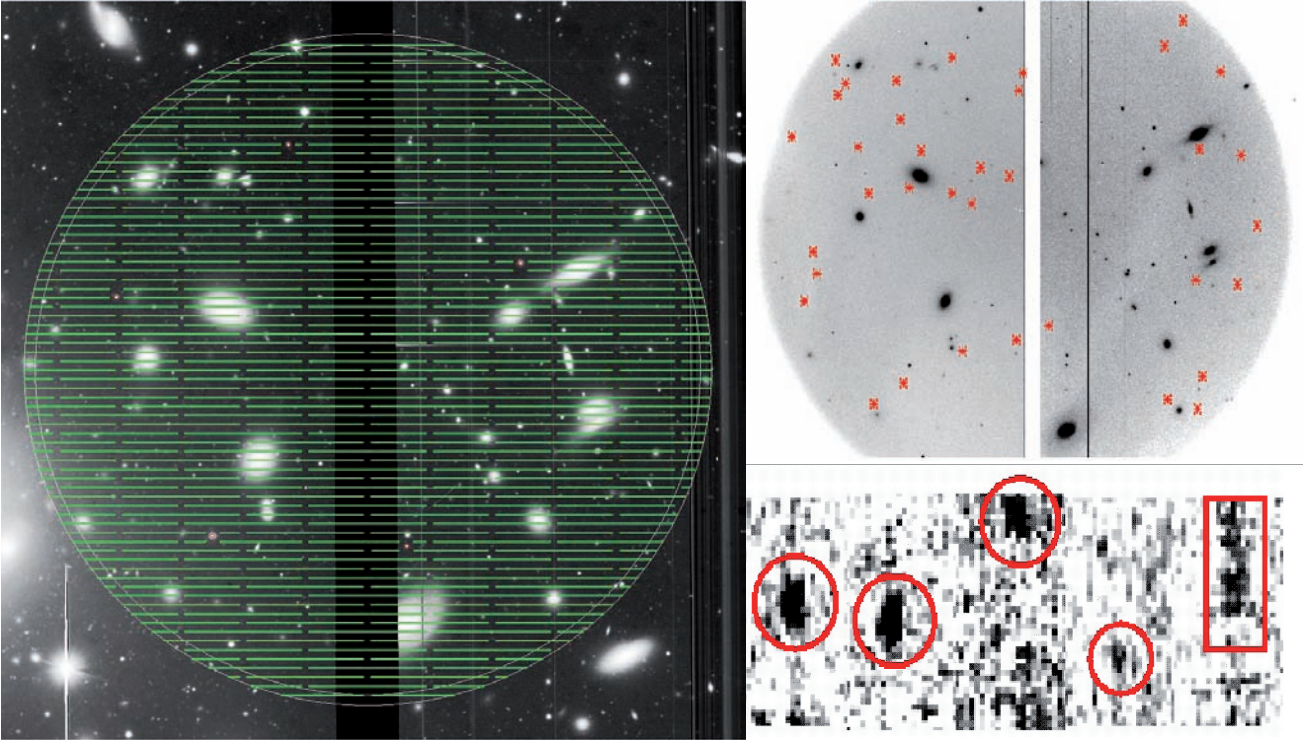


Fig. 2: Left: Multi-slit mask used in the Coma observations, superposed on our field in the core of the cluster. Top right: Distribution of PNe in the observed field. Bottom right: Two-dimensional spectra of some emission sources in the field. The left four sources are monochromatic, point-like sources convolved with the spatial and spectral resolution, and the object on the right is a faint background galaxy. The two objects on the left have the line fluxes of the brightest PNe in the Coma cluster. Object number four is one of the faintest sources with a mere 70 photons in three hours of observation; this is a real source with 95% probability.

PN candidates are shown in the right panel of Fig. 2; in these spectra wavelength is along the vertical axis and the spatial direction is along the horizontal axis. Careful analysis convinced us that the great majority of all PN candidates so detected must indeed be PNe.

The field that we had chosen was known to contain diffuse light. As their distribution in Fig. 2 illustrates, most of the PNe in this field are indeed from the diffuse population; only three out of 40 are close enough both spatially and in velocity to be bound to one of the galaxies in the field.

The distribution of velocities measured from the red-shifted emission lines of these PNe is shown in Fig. 3. It is more or less centered on the systemic velocity of the Coma cluster, but appears to consist of two main components. Of these the bluer (left) peak probably traces diffuse light associated with a group of galaxies which have lower velocities than the cluster mean and currently fall through the cluster from the backside. Such events are quite common in cosmological simulations of galaxy clusters, in which clusters continuously grow by the accretion of smaller substructures.

However, the more surprising result from these observations is that the main peak of the velocity distribution in this field, some 150 kpc south of the giant elliptical galaxy NGC 4874, is 700 km/s off this galaxy's radial velocity and thus cannot be bound to NGC 4874. On the other hand, this peak is very close to the radial velocity of the other giant elliptical, NGC 4889, which is located some 7' east of NGC 4874 (see Fig.3). This kinematic measurement together with the

large elongation of the intracluster light make a strong case that the diffuse stellar population in the core of Coma is in a highly dynamically evolving state.

Previous work on the galaxy velocities, the X-ray emission, and the radio halo in the cluster already suggested that the Coma cluster may currently be in the midst of a merging event. The substructures in the distribution of galaxy velocities together with the velocities of the intracluster stars make it likely that a merger between two major subclusters has occurred nearly in the plane of the sky, where the NGC 4889 subcluster arrived from the ENE direction towards the A2199 cluster (approximately left in Fig. 3) and the NGC 4874 subcluster fell in from the direction of A1367 or A779 in the West (towards the right in Fig. 3). In the Cosmic Web clusters are often connected through filaments along which outlying galaxy groups fall into the dense clusters. The sketched merger scenario seems also consistent with recent X-ray data from colleagues at MPE and in Paris.

In cosmological simulations, subcluster mergers often occur on near-radial orbits. In this case the outer envelopes of both subclusters merge in a slow oscillatory fashion along an essentially unchanging orbital direction. By contrast, the interaction of the subcluster cores is much faster and stronger. If the two central dominant galaxies of the subclusters in Coma, NGC 4874 and NGC 4889, are currently beyond their second close passage on an orbit such as that in Fig. 3, we can naturally explain the elongated distribution of intracluster light and the kinematics of the stars in our MSIS field. These stars, which we now see

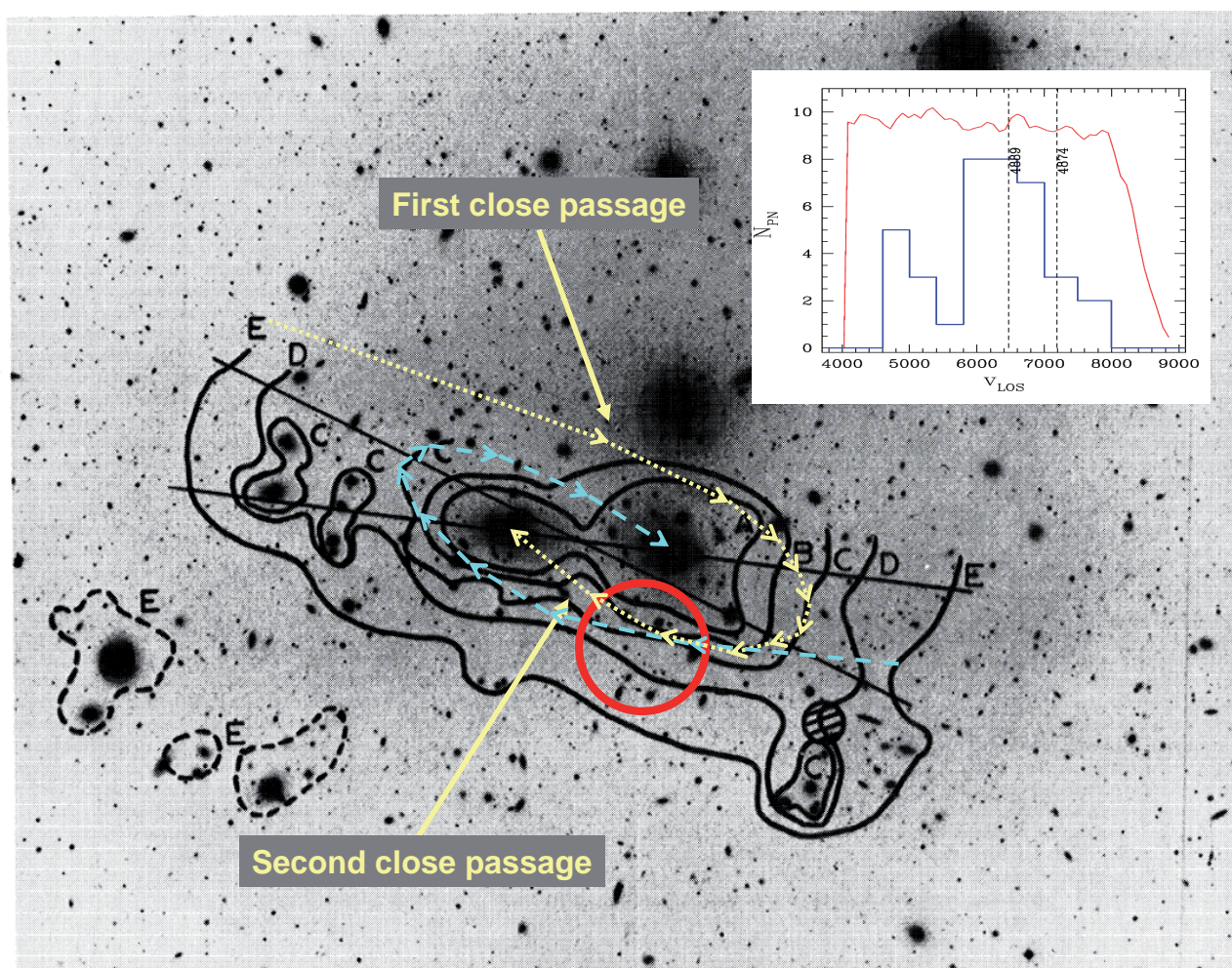


Fig. 3: Image of the core of the Coma cluster, with our MSIS field shown as the red circle, and the isodensity contours of the diffuse light drawn in black. The MSIS field is $5'$ south of NGC 4874; the second giant elliptical galaxy NGC 4889 is $7'$ east (to the left) of NGC 4874. The bright object north of NGC 4874 is a star. Inset: The distribution of measured radial velocities of all intracluster PNe detected in the observed field. The main peak of the distribution is approximately centered on the radial velocity of the more distant NGC 4889, but is ~ 700 km/s offset relative to the velocity of the nearer NGC 4874. These stars are therefore not bound to NGC 4874, but are presumably trailing NGC 4889 after having been tidally dissolved from the halo of this galaxy by the ongoing interaction with NGC 4874. The likely orbits of NGC 4889 and NGC 4874 up to their present positions are sketched by the yellow and magenta lines in the large figure, respectively. The smaller peak in the velocity distribution on the right, blue-shifted relative to the cluster mean velocity, may be related to a group of galaxies infalling into the cluster from behind. The red line shows the wavelength range transmitted by the narrow-band filter.

trailing NGC 4889, were probably unbound from NGC 4889 shortly after the first close passage of both galaxies.

After one or two further orbits, the two giant galaxies and their subcluster cores will have merged. However, with the further arrival of the NGC 4839 subcluster, the Coma cluster may not come to rest for significantly longer. It is not exaggerated to say that this great cluster is still forming now!

As this pilot study showed, we can learn much about the evolutionary history of galaxy clusters from the dynamics of their intracluster stars. Now that we can measure these velocities out to 100 Mpc distance, a representative sample of clusters is within reach.

I would like to thank my collaborators Magda Arnaboldi (ESO), Ken Freeman (Mount Stromlo Observatory, Australia), Nobunari Kasakawa, Sadanori Okamura, and Naoki Yasuda (NOAJ and University of Tokyo, Japan).

O. Gerhard



Zooming in to Active Galactic Nuclei

The unique abilities of our adaptive optics integral field spectrometer SINFONI have been exploited with great success in studying the nuclei of nearby galaxies. Here we describe a few results which include challenging measurements of black hole masses using stellar kinematics, the first direct images of the molecular torus, and new insights on star formation close around active black holes.

Black Hole Masses

It is well established that all galaxies with a massive bulge component harbour central supermassive black holes (SMBHs). The mass of the SMBH correlates both with the mass of the bulge and with the central velocity dispersion. We are investigating whether these relations remain valid, or how they change, for galaxies with very low bulge masses. This is of paramount importance to explain the connection between the growth of seed black holes to the gigantic SMBHs we see in many galaxies, and the formation and evolution of their surrounding bulges. In quiescent galaxies, the evidence of SMBHs comes from gravitational effects on the dynamics of the stars inside the sphere of influence of the black hole. As the angular size of the sphere of influence scales with both distance and black hole mass, only very few SMBHs in low-mass bulges have been measured. In addition,

contains an almost edge-on nuclear disk of stars and dust. A bright star is located ~ 2.5 arcsec from the centre, which makes it one of the rare cases, where natural guide star adaptive optics can be used. We have achieved a spatial resolution of ~ 0.1 arcsec, close to the telescope's diffraction limit under moderate seeing conditions.

We analyzed the motions of the stars in NGC 4486a by measuring the shape of the deep CO absorption bandheads, which are found in the K band at wavelengths $> 2.29 \mu\text{m}$. As illustrated in Fig.1, they confirm the existence of a cold rotating disk (velocity dispersion $\sim 100 - 110$ km/s) inside a dynamically hotter bulge (velocity dispersion $\sim 120 - 130$ km/s). In order to determine the mass of the central SMBH it is not only necessary to know how the stars move, but also the gravitational potential they generate. We have determined this potential by analysing a Hubble Space Telescope (HST) image of NGC 4486a in detail. The mass of the SMBH then was deduced by calculating a large number of model galaxies using the "Schwarzschild method": in the combined potential of stars and a SMBH the orbits of thousands of stars are superposed such that the light distribution of the galaxy is reproduced. We calculated each model galaxy with a different black hole mass and different mass-to-light ratios for disk and bulge. The mass

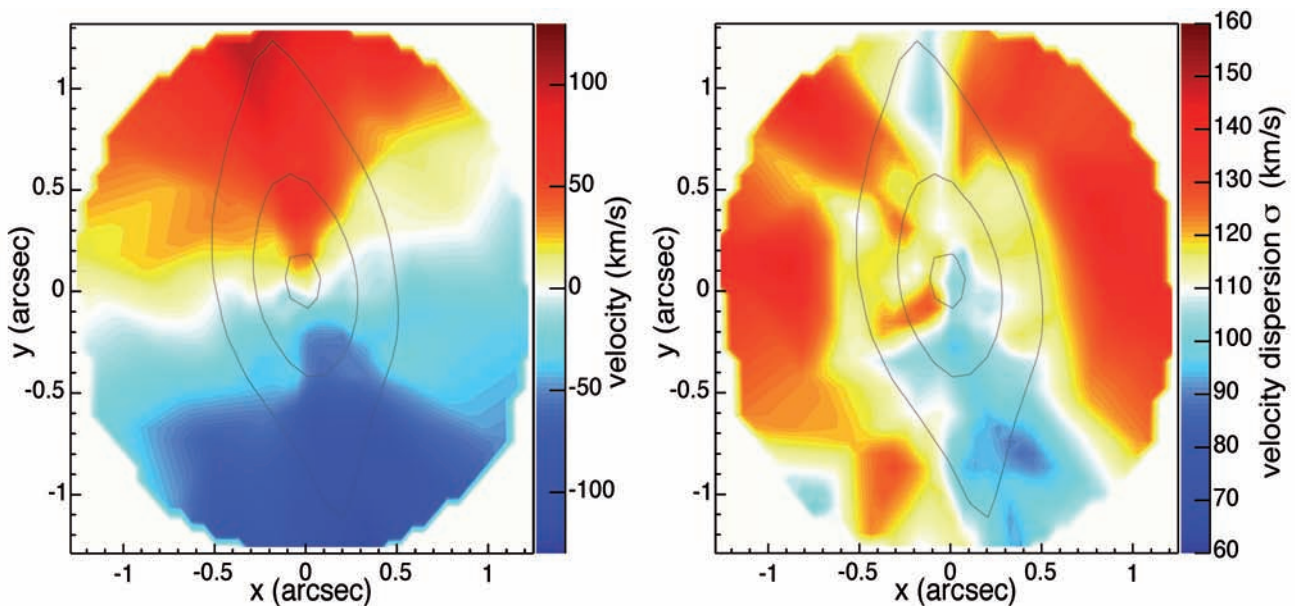


Fig. 1: Two-dimensional map of the stellar velocity (left) and the velocity dispersion (right). The isophotes of the inner part of NGC 4486a are overlaid for comparison.

many of these galaxies have dusty nuclei and can only be studied with near infrared adaptive optics instruments such as SINFONI.

The low-luminosity elliptical galaxy NGC 4486a, located in the Virgo cluster of galaxies at a distance of 16 Mpc,

of the SMBH is then given by the model that produces the best fit to the measured kinematics of the stars. For NGC 4486a a model with a SMBH mass of $1.25 \times 10^7 M_{\text{sun}}$ and mass-to-light ratios of 3.6 and 4.0 for bulge and disk respectively, produces the best reproduction of the

observed kinematics and photometry. Models without a central SMBH are excluded with a probability of 99.999%. This result is in perfect agreement with the predictions of the SMBH mass-velocity dispersion correlation (Fig. 2) and thus strengthens its validity at the low-mass end. The dynamical mass-to-light ratios of disk and bulge agree with old and metal-rich stellar population models.

NGC 4486a is only the first low-mass galaxy in our sample analysed in this way. Recently the Laser Guide Star Facility, necessary to observe faint objects with

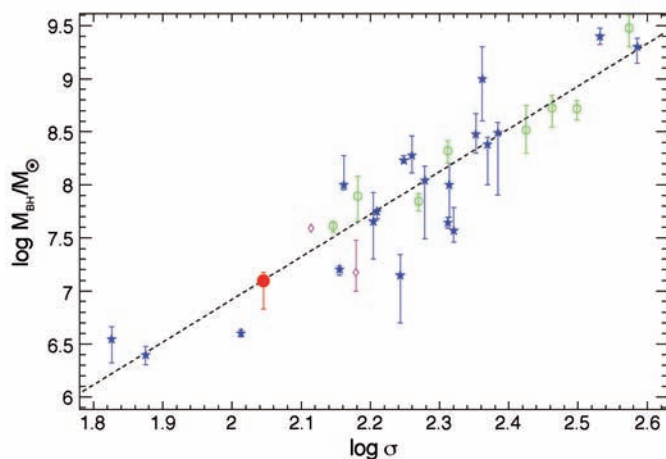


Fig. 2: Correlation between the mass of the supermassive black holes (blue: stellar dynamics, green: gas dynamics, magenta: maser dynamics) and the stellar velocity dispersion σ of the bulge. NGC 4486a is marked in red.

adaptive optics, has been commissioned at the VLT and it will make observation of a large number of galaxies with low-mass bulges possible.

To further explore the interplay between SMBH and a surrounding bulge, it is essential to study SMBHs in their active - material accreting - phase. By measuring black hole masses in AGN dynamically, we are starting to understand black hole growth and how it affects galaxy evolution throughout cosmic history. NGC 3227 is a galaxy, at a distance of 17 Mpc, hosting such an active nucleus. The analysis of SINFONI observations has revealed a black hole mass of $7 - 20 \times 10^6 M_{\text{sun}}$. This mass is lower than indicated by other, less direct, methods, these may overestimate the true mass. It is also a few times less than that implied by the SMBH mass-velocity dispersion relation. There is one other AGN studied with stellar dynamics, where the resulting black hole mass is a few times larger than predicted. This suggests that the scatter in black hole mass estimates for AGN may be significantly larger than those for quiescent galaxies.

Molecular Torus

The cornerstone of the AGN unification scheme is the dense molecular torus that obscures the nuclear region along some lines of sight. Until now, this torus

has never been observed directly. Our SINFONI data of NGC 1068 clearly reveal a compact knot of gas around the central engine (Fig. 3). NGC 1068, the archetypical Seyfert 2, is a nearby galaxy ($1'' = 70$ pc) and it is the object where the torus hypothesis was first exposed to explain measurements of polarised broad emission lines. More than 2 decades later, we now see the gas that is obscuring the unpolarised broad line emission for the first time.

Using our new findings we can start to develop a detailed observational picture of the inner regions of NGC 1068. On scales of <1 pc, radio continuum imaging revealed a thin disk whose rapid rotation is traced by masers. This disk is almost edge-on, and oriented close to east-west, consistent with the direction in which the jet emerges. On scales of a few parsecs, interferometric data were modelled as arising from hot dust within the inner part of the torus. The full extent of the molecular gas in our data now show the torus to be 15 pc across, and having a similar orientation to the inner disk. Remarkably, state-of-the-art clumpy torus models, developed to explain the size of the hot dust emission, predict that the molecular gas should extend over a region similar to the one we have observed. We are now beginning to see an encouraging convergence between models and observations of the elusive molecular obscuring torus.

Star Formation

During recent years, the connection between AGN and star formation in the vicinity of a galaxy's central black hole received attention, since this connection plays a central role in galaxy evolution. Using SINFONI, we mapped the distribution and kinematics of 9 nearby AGN at high spatial resolution. The primary goal was to determine the extent and history of star formation close to the AGN, and to study in detail its relation to the AGN.

Two specific cases provide unambiguous evidence for a nuclear disk hosting a distinct stellar population. At radii of a few arcsec the surface brightness profile is well matched by a single $r^{1/4}$ profile. But when extrapolated inwards, an excess in the central region ($0.5 - 1''$) is found. Similarly, at larger radii, the velocity dispersion is 120 - 150 km/s, decreases at radii approaching the nucleus, reaching 70 - 100 km/s at the centre. Such drops have been interpreted as arising from gas accretion into the central regions followed by star formation. Because the gas is dynamically cool, the newly formed stars will be as well. Thus, in contrast to the spheroidal bulge, their distribution will be rather disk-like. We are able to trace this younger population to radii of ~ 50 pc, and estimate a mass of order $10^8 M_{\text{sun}}$. Under the assumption that the stars are self-gravitating, this implies a vertical scale height of 5 - 10 pc, suggesting that these nuclear disks are in fact relatively thick, and that random motions still provide significant support.

Making careful corrections for contributions from the AGN and its associated phenomena, we constrained the characteristic age of the nuclear star formation to be in the range 10 - 300 Myr, and found the stellar surface brightness to increase at smaller radii. The surface brightness approaches $10^{13} L_{\text{sun}}/\text{kpc}^2$, comparable to that predicted for optically thick star forming disks in ultra-luminous infrared galaxies (ULIRGs). The difference is that in ULIRGs the starburst extends over a size scale

$10^4 M_{\text{sun}}/\text{pc}^2$ in the central regions. The Schmidt law relates this quantity to the star formation rate, stating that as the gas surface density increases, so does the star formation efficiency. A natural consequence, therefore, of the high surface densities we have found is that the star formation rate and efficiency will be high. Based on these observations, a plausible hypothesis for episodic star formation around AGN would be that the high gas density leads to an extremely intense starburst.

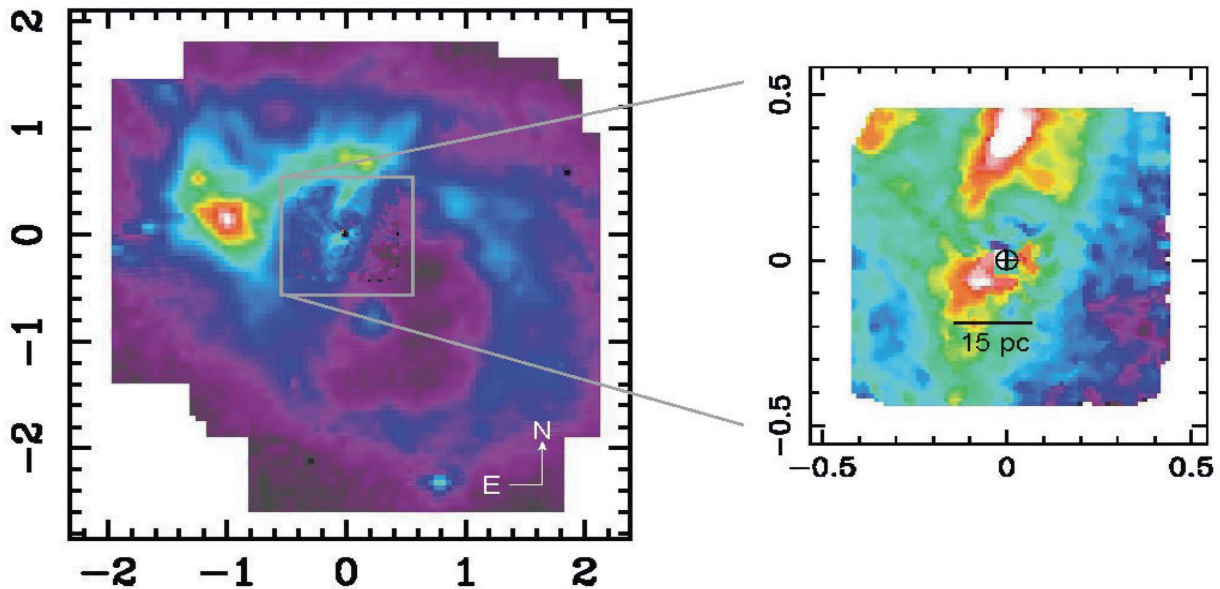


Fig. 3: SINFONI map of molecular hydrogen in NGC 1068, traced via the $2.12 \mu\text{m}$ 1-0S(1) emission line. The scale on the axis is in arcsec. At the distance of NGC 1068, 14 Mpc, 1 arcsec corresponds to 70 pc. The adaptive optics provided an impressive resolution of 0.085 arcsec. The right hand panel shows clear signs of gas around the active black hole (\oplus).

of 1 kpc; in these AGN the most intense starburst is confined to the central few parsec.

ULIRGs are essentially Eddington limited starbursts, because their bolometric luminosity per unit mass is similar to the $500 L_{\text{sun}}/M_{\text{sun}}$ that is sufficient for radiation pressure to halt further accretion. Within the central few tens of parsecs, the AGN we have observed with SINFONI are an order of magnitude below this limit. Intriguingly, the typically low $\text{Br}\gamma$ fluxes imply that although the star formation is recent, it is no longer active. This is important because short-lived starbursts fade very quickly. In the recent past, these nuclear stellar populations could easily have been 10 times more luminous than at present. At that time, they would have been radiating at the Eddington limit for starbursts. To radiate so brightly, the gas must have been converted into stars very quickly. We came to the same conclusion by considering the mass surface densities, which exceed

Because the efficiency is high, the starburst can only be active for a short time before it begins to fade. Inevitably, one then expects the starburst to be dormant until the gas supply is replenished by inflow.

N. Nowak, R. Davies



The XMM-Newton Wide Field Survey in the COSMOS Field (XMM-COSMOS)

We present the first set of XMM-Newton EPIC observations in the 2 square degree COSMOS field. The strength of the COSMOS project is the unprecedented combination of a large solid angle and sensitivity over the whole multiwavelength spectrum. The XMM-Newton observations are very efficient in localizing and identifying AGN (active galactic nuclei) and clusters as well as groups of galaxies. One of the primary goals of the XMM-Newton COSMOS survey is to study the co-evolution of AGN as a function of their environment in the Cosmic web. Here we present scientific results after the first pass of 25 XMM-Newton pointings across the field. In the existing dataset we have detected 1390 new X-ray sources.

Deep X-ray surveys indicate that the cosmic X-ray background (CXB) is largely due to accretion onto supermassive black holes, integrated over cosmic time. In recent years, deep XMM-Newton and Chandra surveys have resolved a large fraction of the CXB, confirming that the main contributors are obscured and unobscured AGN. Now the general interest focuses on understanding the physical nature of these sources, the cosmological evolution of their properties, and their role in galaxy evolution.

The X-ray group at MPE is involved in three of the major on-going X-ray surveys: XMM-COSMOS, the Lockman Hole and the Extended Chandra Deep Field South. In 2006 we focused on the XMM-COSMOS project.

The Cosmic Evolution Survey (COSMOS) is an international project based on a "Treasury project" of the Hubble Space Telescope (HST) that observed a contiguous 2 deg² area at about 10^h in right ascension and about 2° 15^m in declination.

A comprehensive multi-wavelength program is underway to observe the COSMOS field with modern (e.g. VLA,

Spitzer, Subaru, Galex, XMM-Newton and Chandra) and future (e.g. ALMA) observatories from radio to X-rays bands. It is complemented by dedicated optical redshift surveys. The strength of the COSMOS survey is the unprecedented combination of sky area together with a good sensitivity over a broad spectral range. In particular, the high-resolution images will allow measurements of galaxy morphologies, while extensive spectroscopy will allow to relate these studies to the large scale structure, probing the evolution of the galaxies in the universe and the co-evolution with their active nuclei. Once completed, the database of COSMOS will be unique in observational cosmology and will allow to study the evolution of the Universe in the redshift range $z=0.5 - 4$.

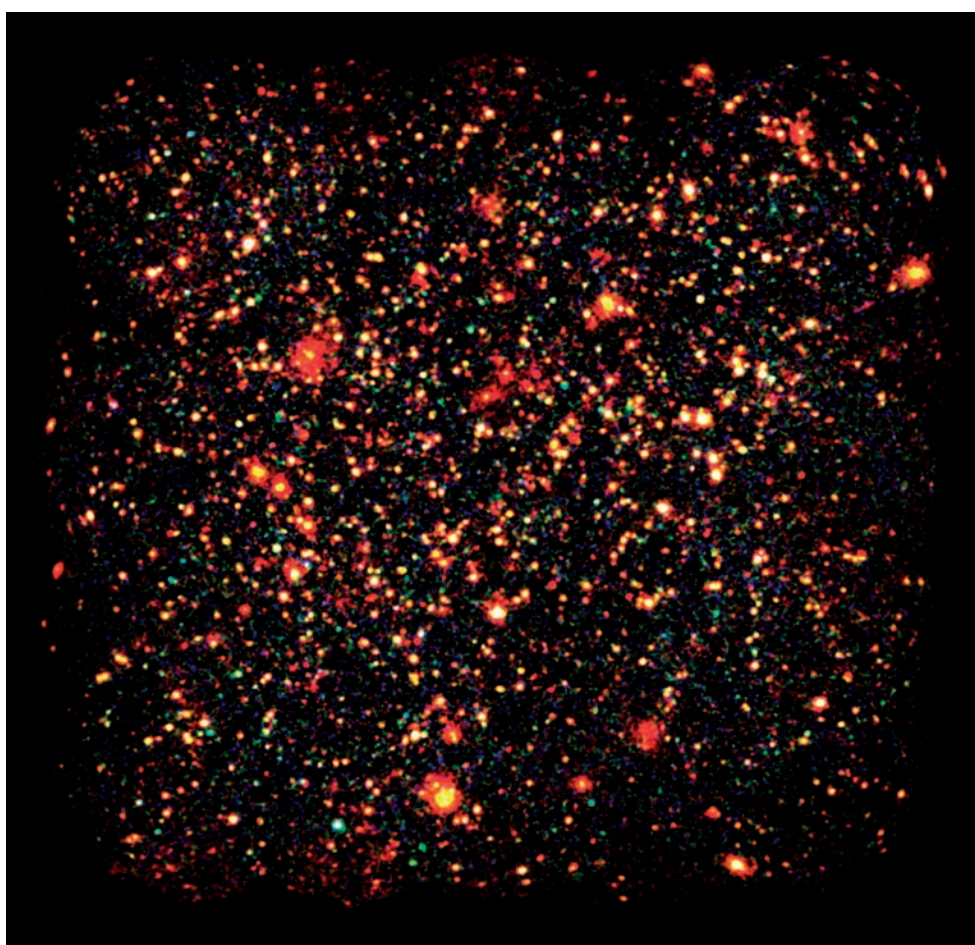


Fig. 1: False color image of the XMM-COSMOS field. The photons were accumulated in three different energy bands: 0.5 - 2 keV (red), 2 - 4.5 keV (green) and 5 - 10 keV (blue). In every energy band images were binned to 4" pixel size, background and exposure corrected, and smoothed with a gaussian kernel with a FWHM of 4". Point sources (mostly AGN) can be readily distinguished from diffuse cluster of galaxies.

The XMM-Newton wide-field survey in the COSMOS field (XMM-COSMOS) provides X-ray coverage from 0.5 - 10 keV (Fig. 1). The very sensitive X-ray observations are a crucial element of the COSMOS surveys, by localizing and identifying AGN and distant clusters of galaxies.

A total of 1.4 Ms of XMM-Newton time has been awarded to this project - the largest project ever approved for XMM-Newton. 53 observations of ~ 30 ks were carried out between November 2003 - June 2006 to build up a mosaic of 25 pointings, repeated twice, with a grid spacing of 15 arcmin. The overlapping pattern of the observations was conceived to optimize the sensitivity as well as the homogeneity of the final mosaic.

The analysis of the entire mosaic of 53 fields is currently ongoing. In 2006 we mainly concentrated on the analysis of the first set of XMM-Newton observations covering 23 fields. The large COSMOS area allows several investigations. We focused on 1) detecting and identifying the X-ray sources in the sky area, 2) perform a detailed spectral study on the brighter sources, and 3) search for peculiar and rare cases.

We searched the 23 fields by a maximum-likelihood source detection algorithm, separately in the soft (0.5 - 2 keV), medium (2 - 4.5 keV), and hard (4.5 - 10 keV) energy bands for X-ray sources. We detected a total of 1390 point-like sources in at least one band. This large number of sources allowed to calculate a sensitive $\log(N>S)$ - $\log(S)$ relation over a wide

Using optical catalogues, we reliably identified $\sim 90\%$ of our detected X-ray sources. The typical location errors of XMM data (a few arcsec in radius) often contain more than one source in deep optical/NIR images. Therefore we applied a likelihood ratio technique to properly identify the counterparts. Only a rather small fraction (10%) of the X-ray sources could not be uniquely identified: either the error circles are empty down to the sensitivity limit of the optical/NIR images (6%), or contain multiple, equally probable counterparts (4%).

About 80% of the counterparts show a very good agreement between the spectroscopic classification, the morphological parameters, and optical to near-infrared colors. The large majority of spectroscopically identified broad-line AGN have a point-like morphology on Hubble Space Telescope images, blue optical colors in color-color diagrams, and an X-ray to optical flux ratio typical for optically selected quasars. Conversely, sources classified as narrow line AGN or normal galaxies are on average associated with extended optical sources, have significantly redder optical to near-infrared colors and span a larger range of X-ray to optical flux ratios. About 20% of the sources show an apparent mismatch

between the morphological and spectroscopic classifications. The most likely explanation is that in these objects the nuclear emission is not dominant with respect to the host galaxy emission in the observed optical band.

We performed detailed spectral analyses on 135 bright and optically identified X-ray sources of the COSMOS field. The majority of the sources are well described by a simple power-law model with no absorption (76%) or a significant amount of intrinsic, absorbing column (20%). The remaining 4% of the sources require a more complex modelling by incorporating additional components to the power-law.

The mean spectral index of the 82 sources in the bright sample is $\langle \Gamma \rangle = 2.06 \pm 0.08$, with an intrinsic dispersion of ~ 0.24 . As expected, the distribution of intrinsic column densities is markedly different between AGN with or

without broad optical emission lines. We found within our sample four so called Type-2 QSOs candidates ($L_x > 10^{44}$ erg/s, $N_H > 10^{22}$ cm $^{-2}$), with a spectral energy distribution well reproduced by a composite Seyfert-2 spectrum. This demonstrates the strength of the wide field XMM-COSMOS survey to detect these rare and

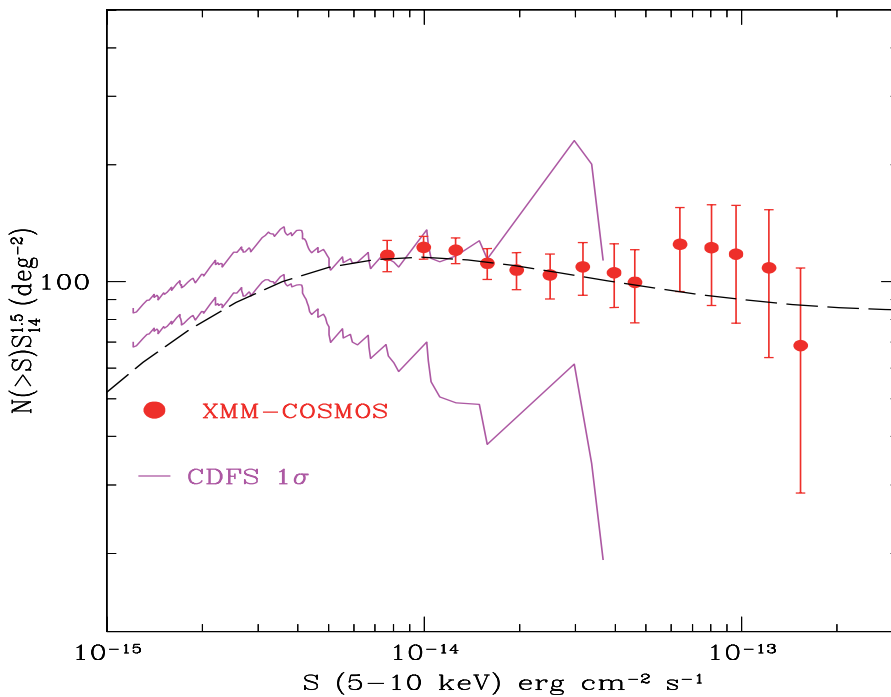


Fig. 2: The $\log(N>S)$ - $\log(S)$ relation (number of source having a flux larger than S) for the X-ray sources (Active Galactic Nuclei) detected in the XMM-Newton COSMOS field. Our results are compared to the results of the Chandra Deep Field South (CDFS) survey, and the most recent model for the cosmic X-ray background (black dashed line).

range of fluxes poorly covered by previous surveys, especially in the 5 - 10 keV band (Fig. 2). A comparison to previous results showed a good agreement in all energy bands in the overlapping flux ranges. Our observed $\log(N>S)$ - $\log(S)$ relations are consistent with the most recent model of the cosmic X-ray background.

under-represented sources. The combination of the optical and X-ray spectral analysis also suggests that the Type2/Type1 source ratio decreases towards high luminosities, in qualitative agreement with the most recent modeling of the X-ray luminosity function evolution.

a redshift of $z=0.125$. The optical diagnostic line ratios put this object among the bulk of the normal Seyfert-2 galaxies and the Balmer decrement indicates a fairly substantial reddening of the emission line region.

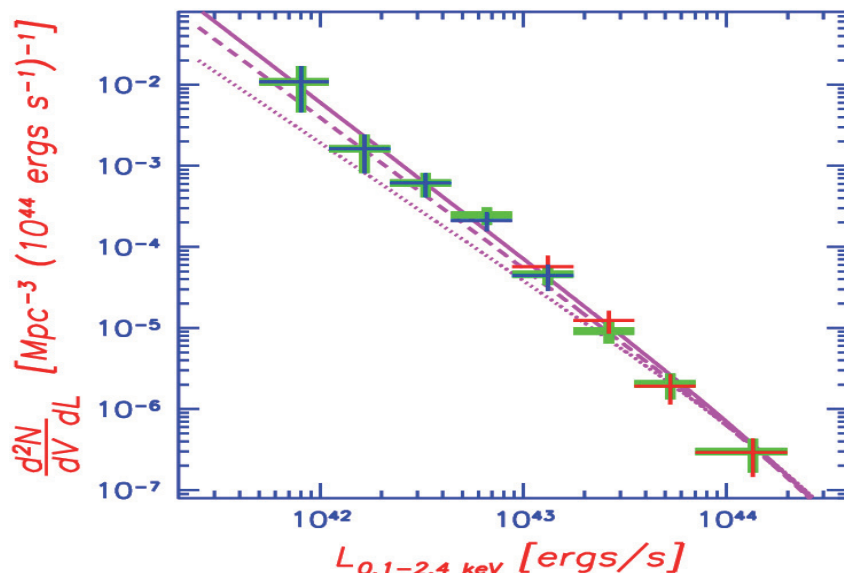


Fig. 3: Luminosity function of clusters in the COSMOS field. Blue crosses indicate the data in the redshift range 0-0.6, green points are the data in the redshift range 0 - 1.3 and red crosses indicate the data in the redshift range 0.6 - 1.3. The dotted line shows the luminosity function of the ROSAT-ESO Flux-limited X-Ray (REFLEX) cluster survey ($0 < z < 0.3$) and the dashed line shows the results of the Bright Cluster Sample (BCS) survey, which illustrates the current uncertainty on the shape of the luminosity function at $z < 0.3$. The solid line shows the best fit to the COSMOS data.

We apply a X-ray color-color analysis by using the three spectral regions. We calculate hardness ratios from different bands, the hard to medium ratio (HR2) and the medium to soft ratio (HR1). In such a color-color analysis, we identify a population of heavily obscured, partially leaky or reflecting absorbers, most of which are likely to be nearby, Compton-thick AGN. An example is the X-ray source with the largest HR2 ratio among those spectroscopically identified. Its location on an X-ray color-color plot can be reproduced with models of heavily absorbed low redshift sources, with some fraction (1-30%) of unabsorbed flux leaking out.

The object is best fitted by a pure Compton-reflection model plus a gaussian line at 6.4 keV rest-frame. The presence of the line is a clear sign that the source is heavily absorbed. An optical spectrum, available from the Sloan Digital Sky Survey (SDSS) archive, indicates

The combination of depth and size of the survey also allows an efficient search for galaxy clusters. Using the first 36 pointings, we reach a depth for a total cluster flux in the 0.5 - 2 keV band of $3 \times 10^{15} \text{ erg cm}^{-2} \text{ s}^{-1}$. Cluster candidates are identified by a wavelet detection of extended X-ray emission. Verification of the cluster candidates is done based on a galaxy concentration analysis in redshift slices of thickness of 0.1 - 0.2 in redshift, using the multi-band photometric catalog of the COSMOS field (see title page). By restricting the search up to redshifts of 1.3 and optical fluxes up to 25 mag, we identified 72 clusters and derived their properties based on the X-ray cluster scaling relations. A statistical description of the survey in terms of the cumulative $\log(N>S)-\log(S)$ distribution compares well with previous results, although yielding a somewhat higher number of clusters at similar fluxes. The X-ray luminosity function of COSMOS clusters matches well the results of

nearby surveys, providing a comparably tight constraint on the faint end slope of $\alpha=1.93 \pm 0.04$ (Fig. 3). For the probed luminosity range of $8 - 200 \times 10^{42} \text{ erg s}^{-1}$, our survey is in agreement with, and adds significantly to the existing data on the cluster luminosity function at high redshifts. It implies that no substantial evolution occurs at these luminosities up to $z=1.3$.

M. Brusa, N. Cappelluti, A. Finoguenov, G. Hasinger



2.3 STELLAR EVOLUTION AND THE INTERSTELLAR MEDIUM

The evolution and fate of stars, individually, as groups, or as entire populations is intimately related to their interactions with the surrounding interstellar medium. We observe stars and such interactions in different evolutionary phases through a variety of astronomical windows of the entire electromagnetic spectrum. Our goal is to complete our picture of the astrophysical processes determining stars from birth to death. At our Institute, we are mainly interested in the extreme phases of stellar evolution, specifically in the conditions of star formation and in the late and remnant phases.

Stars are born through gravitational collapse from dense clumps within interstellar gas clouds. But how exactly such gas clumps lose their turbulent energy to contract and combine to even very massive stars is poorly understood. Infrared and sub-mm studies are capable of probing deep into those star formation environments, revealing protostellar objects and young stars. Our Institute is a key participant in observational programs on 8 - 10 m class telescopes with adaptive-optics technology to search for young stars and planets.

onto the compact star heats up the impact region and its surroundings, and also may lead to acceleration of plasma in jet outflows. In particular the jet formation may occur when stellar-mass black holes are formed, and can be studied in accreting black-hole binaries. One class of gamma-ray bursts may be connected to black-hole formation, and binaries help us to understand physical processes near black hole horizons. Individual and often strongly magnetized rotating neutron stars can be observed also through high-energy emission as pulsars. Such ‘magnetars’ have been recognized recently through giant outbursts of radiation when their magnetosphere releases internal tension.

The interstellar medium plays a key role in the formation of stars, but also for late stellar phases. Still poorly understood are the phase transitions which incorporate the newly-produced elements from stellar explosions into next-generation stars. Towards the end of stellar evolution, ejection of stellar material through winds and supernovae provides turbulent energy for mixing ambient and fresh gas, which is recycled into stars. Radioactive admixtures help to enlighten this recycling of stellar ejecta through decay gamma-rays.

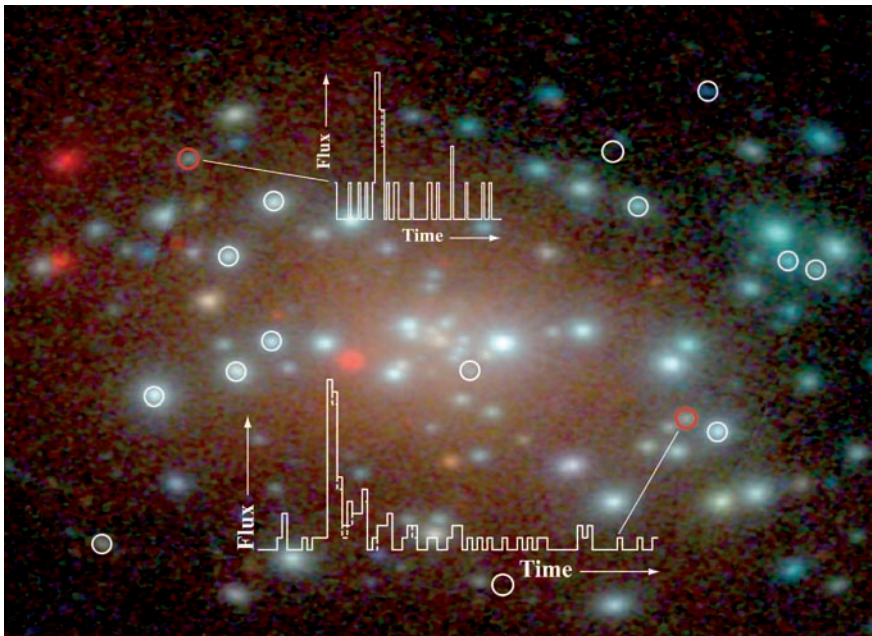


Fig. 1: An X-ray view of accreting-binary sources in the nearby galaxy M31. Flares and outbursts are characteristic for accretion onto compact stars.

Stellar evolution ends in violent events such as novae and supernovae, in particular for the more massive stars, which rapidly consume their nuclear-burning fuel. This evolution finally leads to the creation of compact stars, i.e. white dwarfs, neutron stars, and stellar-mass black holes. New and unusual physical processes become important around such objects. As they accrete mass from a binary companion star, the conversion of gravitational energy into radiation helps us to study these objects, mostly through high-energy emission in X- and γ -rays. The infall

The understanding of this cycle of matter over cosmic time scales requires cross-disciplinary collaborations in astrophysics. Our institute participates in key roles in the XMM-Newton and INTEGRAL projects, where hot plasma, radioactivity, and cosmic ray processes are studied through their specific emission processes. Spatial scales of these research topics extend from the horizons of black holes and the surfaces of neutron stars through the local bubble around the Sun to galaxies as a whole and their cosmic-ray content; even the scale of intergalactic gas is addressed, in the ‘‘cosmology’’ chapter of this report. Star formation is also addressed in the ‘‘Galaxies and AGN’’ chapter, being a key energy source in those objects.

Lessons from specific objects are transferred to populations of sources or entire galaxies, in particular when those objects cannot be resolved. In the 2005 report we highlighted how nearby galaxies can help to illuminate the populations of such sources, and how radioactivities as well as cosmic-ray processes enable inferences on Galactic massive-star populations and their activities. This year, we highlight measurements close to compact stars.

Old Pulsars still have New Tricks to teach us

Pulsars are cosmic beacons which emit their electromagnetic radiation through complex physical processes. The details of these processes are still poorly known, even after 40 years of intense research and observations. Thanks to the unique sensitivity of the European X-ray satellite XMM-Newton an important piece of the puzzle was collected recently. It seems likely that a significant part of the energy, responsible for the million degree hot polar caps observed in middle age neutron stars, is for a large fraction coming from the interior of the star rather than from a bombardment of charged particles on its surface.

The superior sensitivity of ESA's XMM-Newton orbiting X-ray observatory has shown that the prevailing theory of how stellar corpses, known as pulsars, generate their X-rays needs revision. In particular, the energy needed to generate the million degree polar hotspots, seen in cooling neutron stars, may come from the interior of the pulsar, not from the outside.

Cambridge radio astronomers Jocelyn Bell-Burnell and Anthony Hewish discovered pulsars in 1968. Pulsars are the strongly magnetised spinning cores of "dead" stars, each one just 20 kilometres across, yet containing more than 1.5 times the mass of the Sun. Although detected 40 years ago, they even today perplex astronomers across the world.

The theory of how pulsars emit their radiation is still in its infancy. Many models exist but no generally accepted theory. Now, due to recent XMM-Newton observations of several million year old pulsars, a crucial piece of the puzzle probably has been found. It may explain why cooling neutron stars have hotspots at their polar regions.

Neutron stars are formed with temperatures of more than 10^{12} K in the core collapse of massive main sequence stars. Their cooling rate (Fig. 1) strongly depends on the physical properties of the super-dense nuclear matter. Albeit these properties are poorly known, it is agreed that the heat transport in neutron stars is mainly accomplished by electrons. Since electrons are "guided" by magnetic fields, the strong magnetic field of pulsars is expected to significantly influence the neutron star cooling by channeling the heat along the field lines and suppresses the heat flow in a perpendicular direction. Neutron star cooling with a full treatment of the strong magnetic field thus lead to an anisotropic heat flow and subsequently to an anisotropic surface temperature distribution: the polar-cap regions are hotter than the equatorial regions.

Indeed, observations with previous X-ray satellites have shown that the X-rays from several hundred thousand year old cooling neutron stars come from three different regions of the pulsar: The hot surface, the magnetosphere where particles are trapped and moving along the field lines, and hot spots near the magnetic poles.

It is generally believed that these hotspots are heated only by bombardment of magnetospheric particles. These particles are created in the pulsars' magnetosphere and accelerated downwards to collide with the surface at the poles. The recent XMM-Newton observations of million year old pulsars have cast doubt on this view.

While observing a quintet of such pulsars with XMM-Newton, the most sensitive X-ray satellite to date, neither an indication for global surface emission nor for polar hot spot emission was found. The lack of surface emission is no surprise, because since their

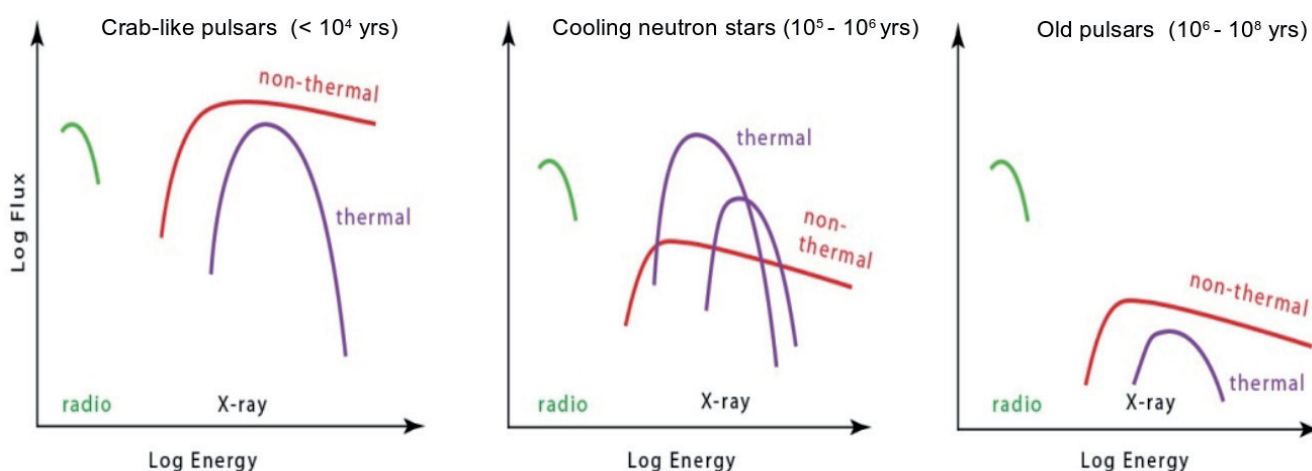


Fig. 1: Emission properties of rotation-powered pulsars are varying with age. Magnetospheric emission dominates in young and old pulsars, thermal emission in middle-aged (so called cooling) neutron stars.

birth, more than some million years ago, their surface has cooled from millions of degrees to less than 500,000 degrees. This temperature made their surface too cool to emit detectable X-rays. However, the lack of the polar hotspots is a big surprise because XMM-Newton detects magnetospheric emission, i.e. the

An alternative view could be, that the heat, trapped in the pulsar since its birth, is guided to the poles by its intense interior magnetic field. This hypothesis suggests that the observed polar spots in young pulsars are generated mainly from a heat flow from the inside of the star rather than by collision of particles from the outside.

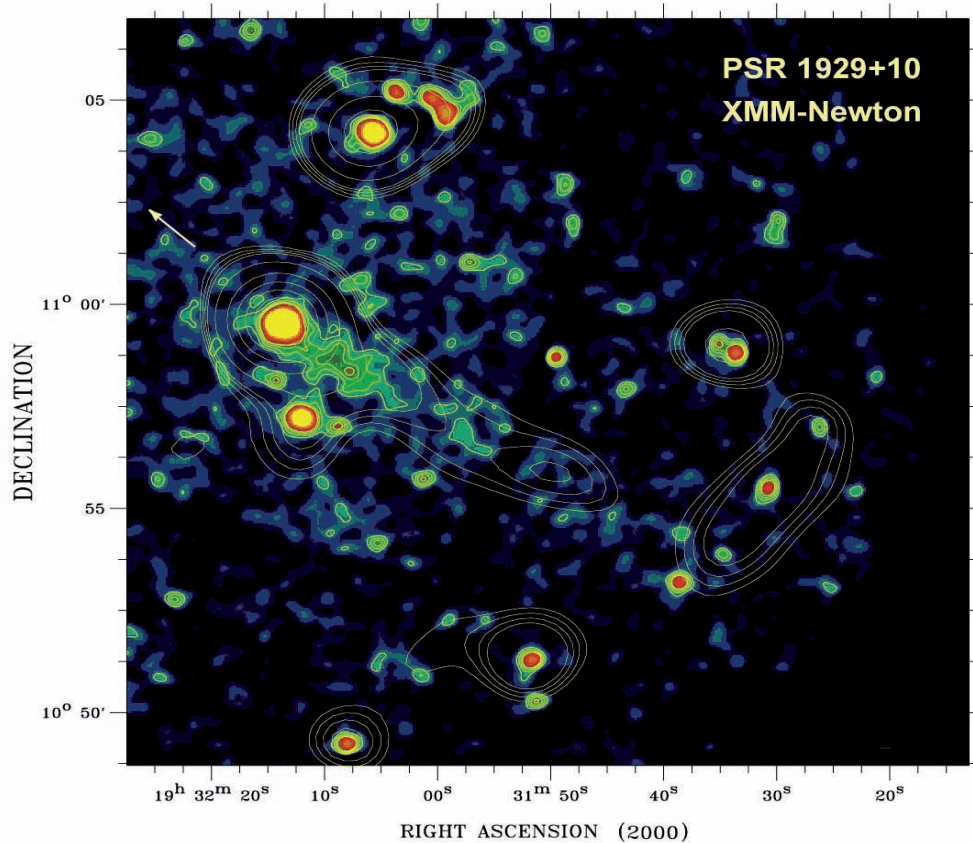


Fig. 2: The faint pulsar PSR B1929+10, captured by XMM-Newton, is moving through space in the direction of the arrow at a speed of 177 kilometres per second. The pulsar leaves a trail of X-ray emitting electron plasma stretching across space.

presence of particles in the magnetosphere. These new observations show, that the particle bombardement from the magnetosphere in old pulsars is not sufficient to heat the polar surface strong enough to emit a significant thermal X-ray component.

A detailed quantitative analysis of the X-ray data of the prototypical old pulsar PSR B1929+10 (Fig. 2) yielded an upper limit of 7% for a contribution of any heated polar region to the total detected X-ray flux. This fact is not in agreement with the conventional theory, that polar spots are created by a bombardement of accelerated magnetospheric particles, and therefore needs to be revised.

Therefore, by a cooling of the neutron stars inside, these X-ray emitting polar spots will fade from view, as the global surface emission does. Although this new theory is still being discussed, it is an interesting alternative to the conventional picture, which the new XMM-Newton findings make quite likely.

W. Becker



Discovery of a Precessing Neutron Star in X-rays

Neutron stars are one of the endpoints in the evolution of massive stars. Observations with the X-ray observatory XMM-Newton led to a surprising discovery: the X-ray spectrum of RX J0720.4-3125 changed on time scales of a few years. These variations are the result of increasing and decreasing temperatures of the neutron star surface. A possible explanation is that the pulsar (RX J0720.4-3125) rotates with a spin period of 8.4 seconds) precesses like a spinning top. Due to this slow tumbling the neutron star exposes different areas of the surface to the observer. RX J0720.4-3125 offers the best opportunity to study precession of a neutron star via its direct and relatively undisturbed X-ray emission from the stellar surface. Precession may allow us to investigate the inner structure of neutron stars and to learn more about the state of the matter in their interior.

Neutron stars as endpoints in the evolution of massive stars are extreme objects in various aspects. They concentrate a mass comparable to that of our Sun in a sphere with a diameter not larger than a medium sized city. Their density with about a billion tonnes per cubic centimeter is even somewhat higher than that of an atomic nucleus. Soon after birth their surface temperature is of the order of one million degrees, their magnetic field is typically several 10^{12} times stronger than that of the Earth, and they rotate with about 100 revolutions per second. The magnetic field only slowly brakes down the rotation. As long as the temperature of an isolated neutron star has not decreased well below a million degrees the bulk of their thermal emission falls into the X-ray band of the electromagnetic spectrum. From theoretical cooling calculations this takes typically a few million years. The magnetic field can be so strong that it influences the heat transport from the stellar interior through the crust leading to hot spots around the magnetic poles on the

star surface. It is the radiation from these hot polar caps which dominates the X-ray spectrum.

From observed supernova explosion rates, the abundance of heavy elements (which are processed in the interior of stars and released in the supernova explosion) in the interstellar medium and from the properties of the radio pulsar population the total number of neutron stars in the Milky Way is estimated to about 100 million up to one billion. However, only very few isolated neutron stars are detectable in the X-ray band. They are expected to show a very "soft" X-ray spectrum, i.e. emit mainly at low X-ray energies and should be extremely faint at optical wavelengths. Despite extensive searches for still unknown objects in the ROSAT data, only seven neutron stars with the expected properties were found. From a comparison of the temperatures inferred from the observed spectra with those obtained from theoretical cooling calculations ages of typically one million years are estimated. The

seven neutron stars (often called "The Magnificent Seven") discovered by ROSAT are particularly interesting because they are among the few which allow us to directly observe the thermal emission from the stellar surface in a relatively undisturbed view.

The Magnificent Seven were investigated with the extremely sensitive instruments on board of the X-ray observatory XMM-Newton (see project part of X-ray astronomy). One of

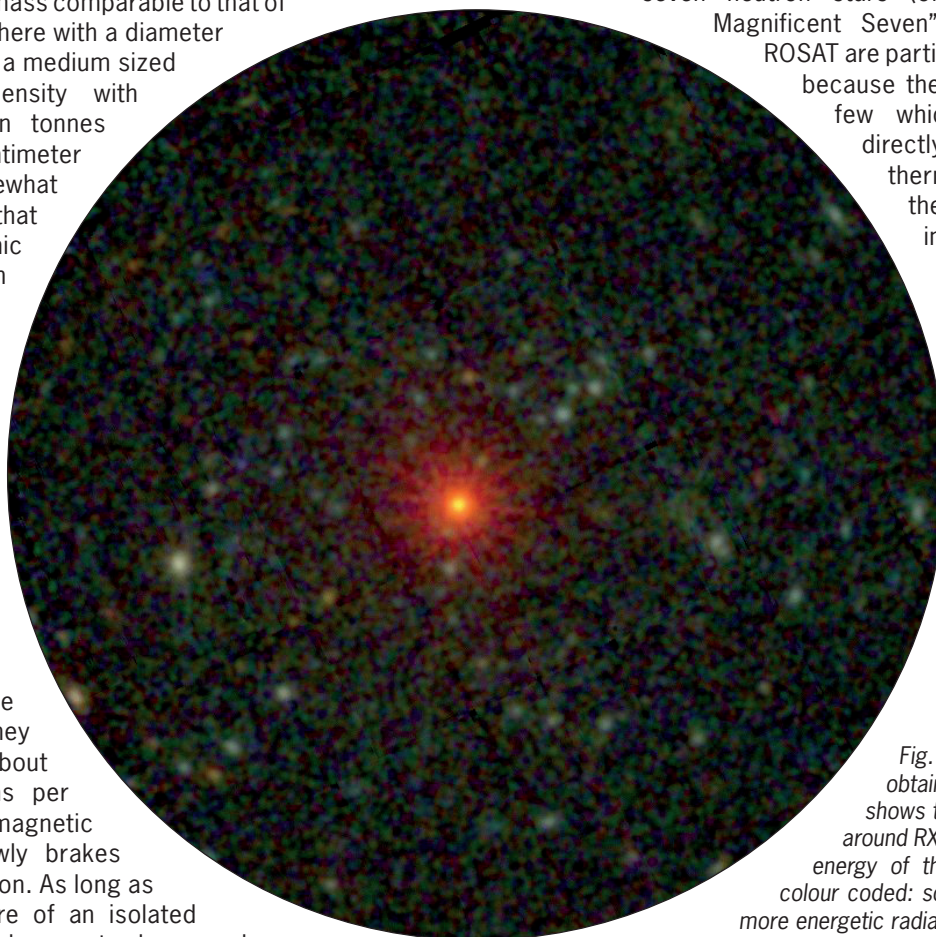


Fig. 1: The X-ray image obtained by XMM-Newton shows the region of the sky around RX J0720.4-3125. The energy of the X-ray photons is colour coded: soft X-rays in red and more energetic radiation in blue. The neutron star appears as bright object in red near the centre of the image.

them is the pulsar RX J0720.4-3125 which rotates with a spin period of 8.4 s at a distance of about 1000 light years. Its optical light is so weak that RX J0720.4-3125 can be observed only with the largest telescopes. However, as X-ray source RX J0720.4-3125 is quite bright

(Fig. 1).

A detailed investigation of the X-ray spectra revealed a surprising discovery: the spectra of the neutron star changed over a few years. Between May 2000 and May 2004 the contribution of hard X-rays in the spectral measurements increased. This means the pulsar emitted X-rays with higher energy on average. Afterwards this contribution decreased again (Fig. 2). This suggests that also the surface temperature of RX J0720.4-3125 varies, in fact, by nearly 100000 degrees. However, it is very unlikely that the global surface temperature of the neutron star changes that quickly in only a few years. The cooling of neutron stars happens over much longer time scales.

The apparent temperature variation is more likely explained by viewing different areas of the stellar surface at different times. If the rotation axis does not rest stable in space but slowly moves around a cone, the viewing geometry changes over years. This precession first moves one magnetic pole and then the other into the field of view of the XMM-Newton instruments. If the polar caps have different temperatures and are of different size they emit unequal shares of hard X-rays. A timing analysis of the X-ray pulses of RX J0720.4-3125 reveals deviations from a gradual braking of the neutron star rotation which is consistent with the precession model. Both analyses indicate cyclic changes with a period of 7 - 8 years, naturally interpreted as the precession period. During the first XMM-Newton observation in May 2000 when the temperature was at a minimum, the cooler and larger spot was mainly visible. Four years later in May 2004 the hotter and smaller spot was better exposed, increasing the measured temperature. The precession model can explain the observed variations in temperature and size of the emitting region as well as their anti-correlation.

The significant temperature difference of the poles can probably be explained by the strong magnetic field of RX J0720.4-3125. The strength of the magnetic field of a pulsar can be estimated from the slow-down rate of the neutron stars' rotation as well as from the energy of absorption lines (if existing) in the X-ray spectrum. If an absorption line can be uniquely identified as a cyclotron resonance line, the most direct determination of the magnetic field strength is possible. RX J0720.4-3125 is one of the few neutron stars where both methods can be applied and consistently indicate a magnetic field strength of a few 10^{13} Gauß. Deviations from a pure, symmetric dipole field, in particular near the surface of the neutron star, then lead to an asymmetric temperature distribution. Different temperatures of the polar regions

were also measured for RBS 1223, one of the other neutron stars from the group of the Magnificent Seven. In this case, like for RX J0720.4-3125, this can be seen from periodic variations in the X-ray spectra in phase with the rotation period. In contrast to RX J0720.4-3125,

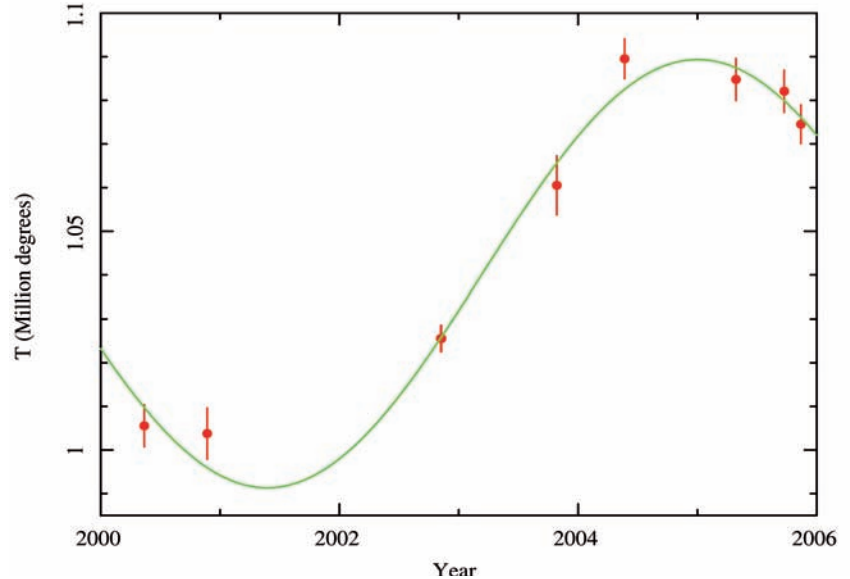


Fig. 2: Temperature variations over a time interval of six years, derived from the X-ray spectra obtained with the EPIC-pn instrument on board of XMM-Newton.

RBS 1223 does not show any sign for precession so far.

How the cosmic top RX J0720.4-3125 started to tumble can only be speculated. From the ratio of the rotation period to the precession period one can estimate the deformation of the neutron star from a perfect sphere. With a value of a few 10^{-8} this converts to a deviation of less than a millimeter for a neutron star radius of 20 km. This unbalanced mass might have been generated in a star quake as it is often observed in young pulsars. However, theoretical investigations suggest that the precession is strongly damped on a time scale of typically 100 precession periods. If that is true the star quake should have happened not much longer than 1000 years ago.

However, all this is strongly dependent on the inner structure of the neutron star, e.g. if it has a superfluid core. Investigating the precession of neutron stars could therefore help to study the inner structure of neutron stars and to learn more about the state of matter in their interior.

F. Haberl



M33 X-7: The First Eclipsing Black Hole X-ray Binary

The Chandra X-ray survey of the local-group galaxy M33 sampled the eclipsing X-ray binary M33 X-7 over a large part of the 3.45 day orbital period and eclipse ingress and egress were resolved for the first time. The occurrence of the X-ray eclipse allows to determine an improved ephemeris of mid-eclipse and binary period, and to constrain the eclipse half-angle. The X-ray spectrum is best described by a disk blackbody spectrum typical for black hole X-ray binaries in the Galaxy. Hubble Space Telescope (HST) images identify the optical counterpart as an O6 III star. Based on the optical light curve, the mass of the compact object in the system most likely exceeds 9 solar masses. The mass, the shape of the X-ray spectrum, and the short-term X-ray time variability identify M33 X-7 as the first eclipsing black hole high-mass X-ray binary.

Messier 33 (M33) is a prominent spiral galaxy of the Local Group, located at a distance of about 2.6 million light years. Observations of the Einstein X-ray satellite about 30 years ago detected and numbered 11 bright X-ray sources in M33.

M33 X-7 (X-7) was already then detected as a variable source. It showed a maximum X-ray luminosity that exceeded 10^{38} erg s^{-1} and stayed active in all subsequent observations. Its variability was explained by an eclipsing X-ray binary (XRB) with an orbital period of 3.45 days, and an eclipse duration of 0.4 days. Evidence for a 0.31 s pulse period was also reported. This, together with the observed luminosity and orbital period, made X-7 very similar to the prominent Small Magellanic Cloud XRB SMC X-1. The position of X-7 correlates with the dense O-B star association HS13 and therefore no individual counterpart could be identified at that time based just on position only.

X-7 was in the field of view during several observations of our XMM-Newton M33 survey from August 2000 to February 2003. These were analysed together with a Chandra observation from the archive. We detected residual emission from X-7 during eclipse, a phenomenon shown by most eclipsing XRBs. The soft X-ray spectrum measured out of eclipse could be best described by bremsstrahlung or disk blackbody models. No regular pulsations of the source were found in the range of

0.25 - 1000 s. In an analysis of optical DIRECT (a project to determine the distances to nearby galaxies, e.g. M33) observations, we identified a B0I to O7I star as optical counterpart. It showed the ellipsoidal heating light curve of a high mass XRB with the X-7 orbital period. The orbital parameters, the optical companion mass, the lack of pulsations and the X-ray spectrum suggested a black hole nature of the compact object in the system. X-7 would be the first detected eclipsing high mass black hole XRB.

In September 2005, an observational program with the Chandra X-ray satellite was started to map M33 in seven deep observations, each 200 ks in length. These observations were carried out over two time periods separated by half a year to catch possible longterm variability of detected X-ray sources. During several of these pointings X-7 was in the Chandra field of view. We analyzed observations of X-7 spread over just two months.

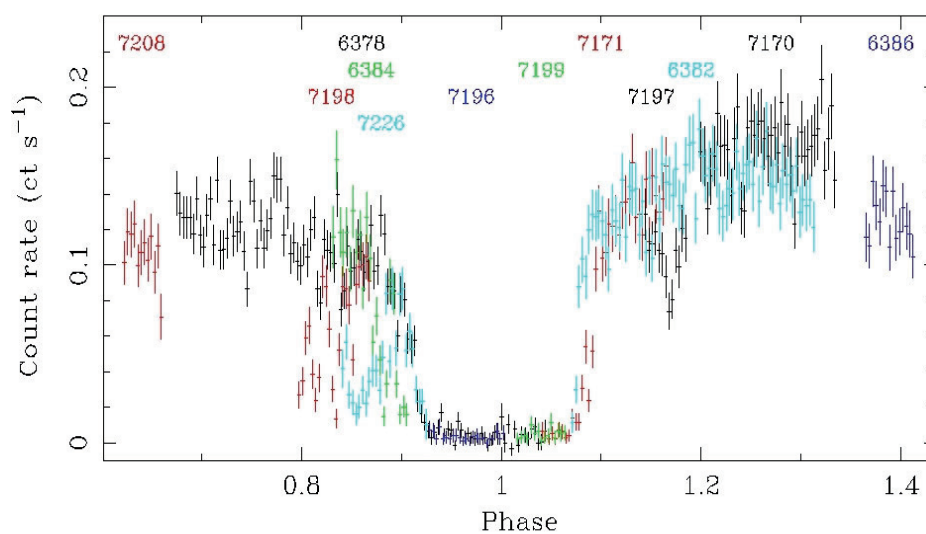


Fig. 1: Chandra light curve of the X-ray binary M33 X-7. Individual observations are color-coded and marked.

In several observations eclipse ingress and egress could be resolved for the first time. While the egress from the eclipse is rather short the ingress takes significantly longer (Fig. 1). As in many other high-mass XRBs, there is stronger variability prior eclipse than thereafter. During this time emission from the compact object is absorbed in the innermost region of the wind from the companion and by dense material following the compact object in its orbit. A search for pulsations with Chandra was unsuccessful, covering the period range 6 - 10000 seconds.

From eclipse ingress- and egress times, separated by two orbital periods, the mid-eclipse ephemeris could be determined to an accuracy of 0.005 days. The eclipse duration is less than 0.147 in phase, corresponding to an eclipse half-angle of 26.5 degrees. We used the better defined eclipse egress times and also re-analysed Einstein and ROSAT data to further improve on the orbital period of the system, and to search for a possible period derivative. Combining all information we derived an orbital decay (period derivative divided by the period) of X-7 of $-4 \times 10^{-6} \text{ yr}^{-1}$, well within the range of values determined for other high mass XRBs such as SMC X-1 for example. Such rapidly decreasing periods in high mass XRBs are most likely caused by tidal interaction between the compact object and its massive companion. As the orbit decays, the Roche lobe, the equipotential surface separating the two stars gravitationally, will descent into the companion's atmosphere, and mass transfer will increase to super-Eddington rates over a relatively short timescale. In the end, the compact object is expected to spiral into the envelope of the companion and in this way terminate the high-mass XRB phase of its evolution.

The energy spectra of the out-of-eclipse observations can be fitted best by a disk blackbody model with an inner disk temperature of $kT \sim 0.99 \text{ keV}$, and an absorbing column which locates X-7 to a position on the near side of M33. The measured fluxes correspond to unabsorbed source luminosities between 5 and $11 \times 10^{37} \text{ ergs s}^{-1}$. From the fitted X-ray absorption, the expected optical extinction and colour corrections can be calculated.

With the unprecedented Chandra point spread function, the position of X-7 could be determined to an accuracy of 0.5". HST images in several filters, taken from the archive, resolve the star association HS13. X-7 is identified with one of a pair of stars with similar luminosities separated by 0.9" (Fig. 2). Its magnitudes, after correction for extinction and colour, point at an O6III star in M33 as companion that should have a temperature of 39,500 K, a radius of $17 R_{\text{sun}}$ and a mass well above $20 M_{\text{sun}}$.

With the improved knowledge on the duration of the X-ray eclipse and the better determined type of the companion star, the mass estimate for the compact object could be improved significantly by modelling the optical light

curve. The inclinations of the orbit can be constrained to be larger than 75° . However, an inclination above 80° is more likely. For such an orbit the mass of the compact object in the system should be larger than 9 solar masses.

The new X-ray data together with the optical analysis clearly determine the black hole nature of the compact

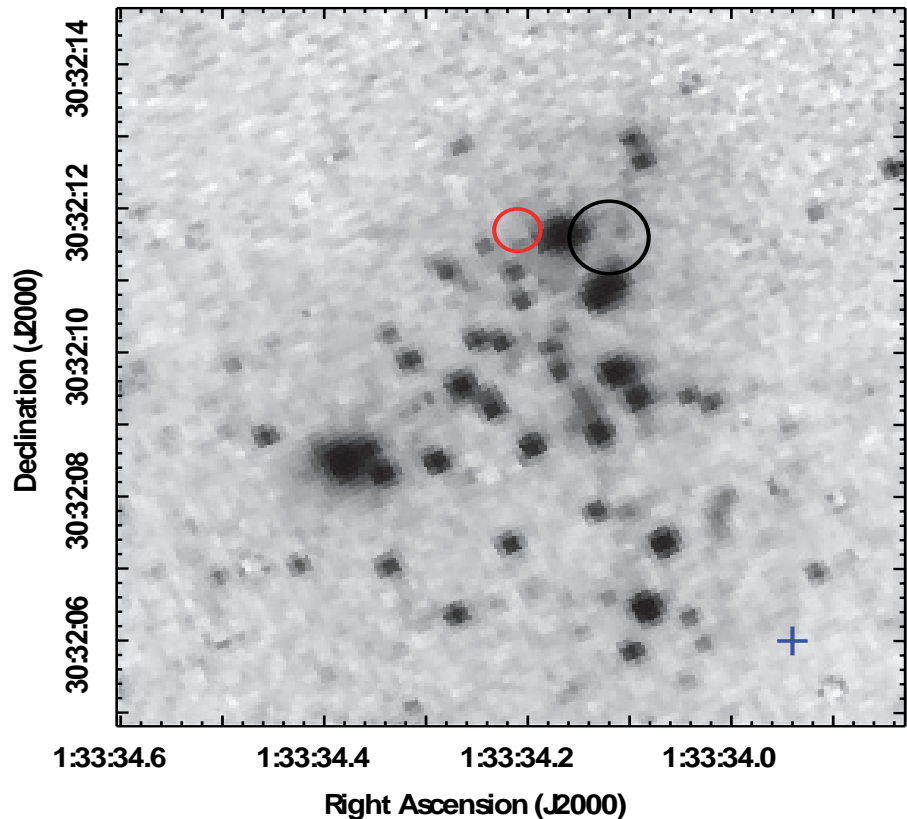


Fig. 2: Hubble Space Telescope (HST) $10'' \times 10''$ image of the OB star association HS13. The Chandra positions (the two circles) are overlaid. The optical counterpart is the source between the circles.

object in X-7. These findings triggered further analyses and observations.

An analysis of optical data, publicly available from the M33 variability survey with the 3.6 m CFHT (Canada-France-Hawaii-Telescope) in 2003 and 2004, confirmed the optical modulation found earlier. Optical spectroscopy of the counterpart of X-7 showed two strong He II absorption lines from the counterpart. A sine fit to their radial velocities revealed a modulation of 109 km s^{-1} and a phase as expected from the X-ray eclipse. The derived optical mass function of 0.46 gives additional support to the black hole identification of the compact object.

W. Pietsch, F. Haberl



2.4 SOLAR SYSTEM PHYSICS

The solar system is comprised of the Sun, the planets, their atmospheres and plasma environs, the small bodies, e.g. comets, down to dust particles, interstellar matter intruding from outside, and the cosmic radiation. At MPE we investigate the plasma physical phenomena in the solar atmosphere, in the Earth's magnetosphere and its boundaries, in interplanetary space and at other planets and comets.

Presently we are involved in several active instruments onboard the Earth orbiting satellites SAMPEX (Solar, Anomalous and Magnetospheric Particle Explorer), FAST (Fast Auroral Snapshot Explorer), Cluster and Double Star, and onboard the interplanetary observatories SOHO (Solar and Heliospheric Observatory), ACE (Advanced Composition Explorer), and STEREO (Solar Terrestrial Relations Observatory).

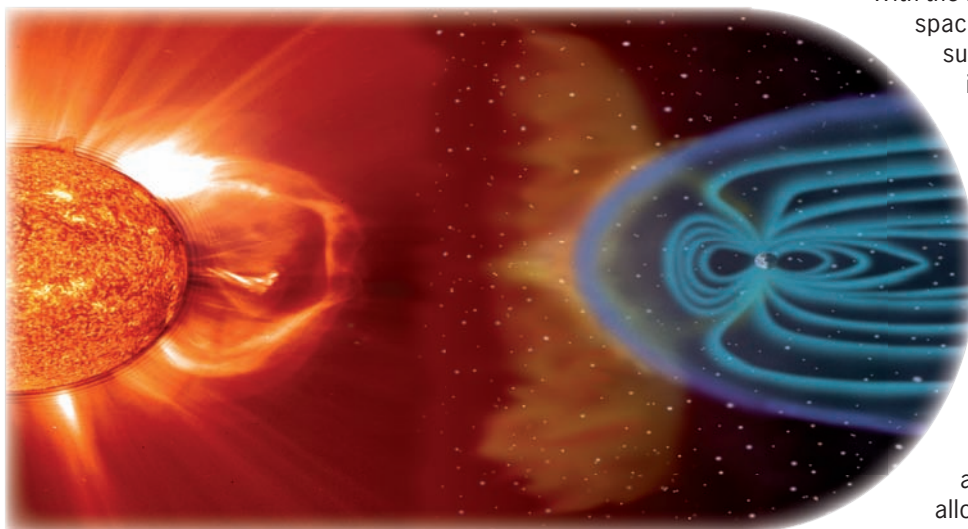


Fig. 1: The release of plasma from the Sun directly affects Earth and the rest of the solar system. This illustration shows a CME directed towards the Earth and its magnetosphere, schematically shown in the right portion of the figure. (Objects and distances are not to scale, illustration courtesy to ESA)

We are, in particular, interested in the interaction of active phenomena of the Sun with the near-Earth environment as illustrated in Fig. 1: The continuous flow of the Solar Wind and its imbedded interplanetary magnetic field shape the Earth's magnetosphere and determine dynamical processes as, for example, reconnection and convection. Furthermore, coronal mass ejections (CMEs) travelling with speeds up to ~ 2500 km/s (the left part of the picture shows an image of a CME taken by SOHO) drive interplanetary shocks that in turn accelerate particles to high energies. A few days later, these CMEs impact on the magnetosphere of the Earth, schematically shown in the right part of Fig. 1, causing magnetic storms, particle acceleration in the magnetosphere, and aurorae.

In order to explore the Earth's magnetosphere, its boundaries and interaction with the solar plasma, and acceleration processes at the Sun, in interplanetary space, and in the magnetosphere of the Earth, over the last decades a number of space-born experiments have been developed at MPE providing plasma and electric field diagnostics, and information on mass, energy, and the ionic charge of the accelerated particle populations.

With the four Cluster and two Double Star spacecraft we are - after 5 years of successful operation of Cluster - in a new age of multi-spacecraft missions in magnetospheric physics. The four Cluster spacecraft with identical instrumentation fly in a tetrahedral formation of variable distance (100 to $>10,000$ km) when crossing regions of interest. These 4-spacecraft measurements allow for the first time to distinguish between spatial and temporal variations and thus allow to investigate the dynamics and structure of boundaries, like Earth's bow shock and magnetopause, in

great detail.

In 2006 we studied, in particular, plasma convection and ion outflow in the polar magnetosphere, structure and motion of the magnetopause, ion beams in the foreshock region of the Earth's bow shock, and solar wind-magnetosphere-ionosphere coupling processes.

Energetic ions of solar origin are measured with our experiments onboard SOHO and ACE. The analysis of ionic charge states provides important information on the particles' sources and the location of the acceleration region at the Sun or in interplanetary space.

Besides the in-situ measurements we obtain results on the interaction of planets or comets with the solar wind from X-ray measurements. These measurements are generally passive. However, the planned collision of the 364 kg copper impactor of NASA's Deep Impact mission with comet 9P/Tempel 1 on 4 July 2006 provided for the first time an 'active' experiment of this kind. The impact with a relative velocity of 10.2 km/s, releasing 10^6 - 10^7 kg of fresh neutral cometary material into the extended atmosphere above the comet, resulted in an enhanced X-ray flux, consistent with the estimates of the additional amount of gas released by the impact.

In the next two articles we report in more detail new results selected from our studies of the magnetosphere of the Earth and of particles accelerated at the Sun and in interplanetary space.

Plasma Convection in Earth's Magnetosphere

We used measurements of the Electron Drift Instrument on board the Cluster spacecraft at large distances within the Earth's magnetosphere have been used to construct detailed maps of the plasma convection in Earth's ionosphere. The derived patterns are exactly what is expected from magnetic reconnection between the interplanetary magnetic field and Earth's magnetic field, with the addition of some feedback from the ionosphere.

The Sun constantly emits a stream of plasma, the solar wind, carrying a magnetic field of variable direction, the interplanetary magnetic field, or IMF for short. When this magnetized plasma encounters the Earth's magnetic field, it is forced to flow around it, leaving behind it a cavity, the magnetosphere, which is separated from the solar wind by a boundary, called the magnetopause. When the IMF has a southerly direction, it can connect with the Earth's northward-directed field at the front of the magnetosphere, via a universal plasma process, referred to as magnetic reconnection. This magnetic connection allows solar wind plasma to enter the magnetosphere. Once connected with the IMF, the terrestrial field lines, and the plasma that sits on them, are carried by the solar wind over the Earth's poles downstream, penetrating deeper and deeper into the Earth's magnetotail, where they eventually reconnect once more to form closed field lines. The field lines are subsequently transported sunward past the Earth, until they again meet the IMF at the magnetopause, allowing the whole process to start all over.

returning at lower latitudes to the dayside via the dawn and dusk flanks.

For northward IMF, the reconnection site moves from the frontside to the region tailward of the cusps, where interplanetary field lines now reconnect with oppositely directed polar cap field lines that were already open. As a result, one expects weak sunward convection over parts of the polar cap.

Statistical maps of the high-latitude plasma convection have been constructed from measurements of the plasma velocity made by the Electron Drift Instrument (EDI) on Cluster between February 2001 and March 2006. EDI is a joint venture with several US groups, under the leadership of MPE. EDI directly measures the two-dimensional drift velocity perpendicular to the magnetic field with unprecedented accuracy. The basis of the electron-drift technique is the injection of two weak beams of 1-keV electrons and their detection after one or more gyrations in the ambient magnetic field. Because of their cycloidal motion, beam electrons can return to the associated detectors only when fired in directions uniquely determined by the magnitude and direction of the plasma drift velocity. Successful operation therefore requires continuous tracking of those directions. The electron beams are amplitude modulated with a pseudo-noise code, to measure the electron times-of-flight. The drift velocity is computed either from the direction of the beams (via triangulation) or from their time-of-flight difference.

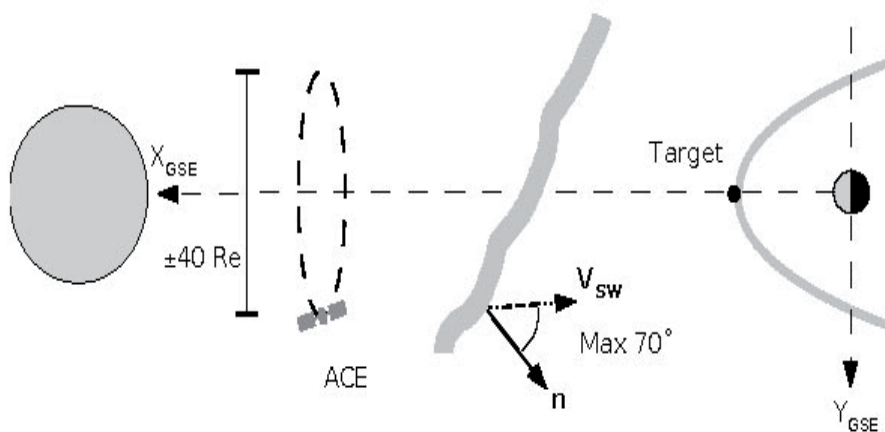


Fig. 1: Determination of the solar wind propagation delay from the ACE spacecraft to Earth's magnetosphere, taking into account the orientation of the 'phase fronts' of the interplanetary magnetic field.

This large-scale plasma and magnetic field circulation extends all the way down to the ionosphere, the ionized portion of Earth's upper atmosphere. The result is a two-cell pattern, with anti-sunward flow over the polar caps,

The Cluster spacecraft, with their 90 degree inclination orbits, completely cover both polar caps twice per year. Cluster measurements are, however, obtained far from the ionosphere at distances between 3 and 19 Earth-radii. Any comparison with ionospheric convection measurements thus requires mapping the EDI measurements to ionospheric altitudes.

To investigate the effect of the orientation of the IMF on the polar cap convection, solar wind plasma and magnetic field data measured by the ACE spacecraft are used. Since ACE is orbiting the L1 libration point at a distance of 1.5 Million km upstream from Earth, its

measurements have to be time-shifted (by typically one hour) to be representative for the conditions at Earth's magnetopause. The standard approach has been to compute this time delay simply as x divided by V_x , where

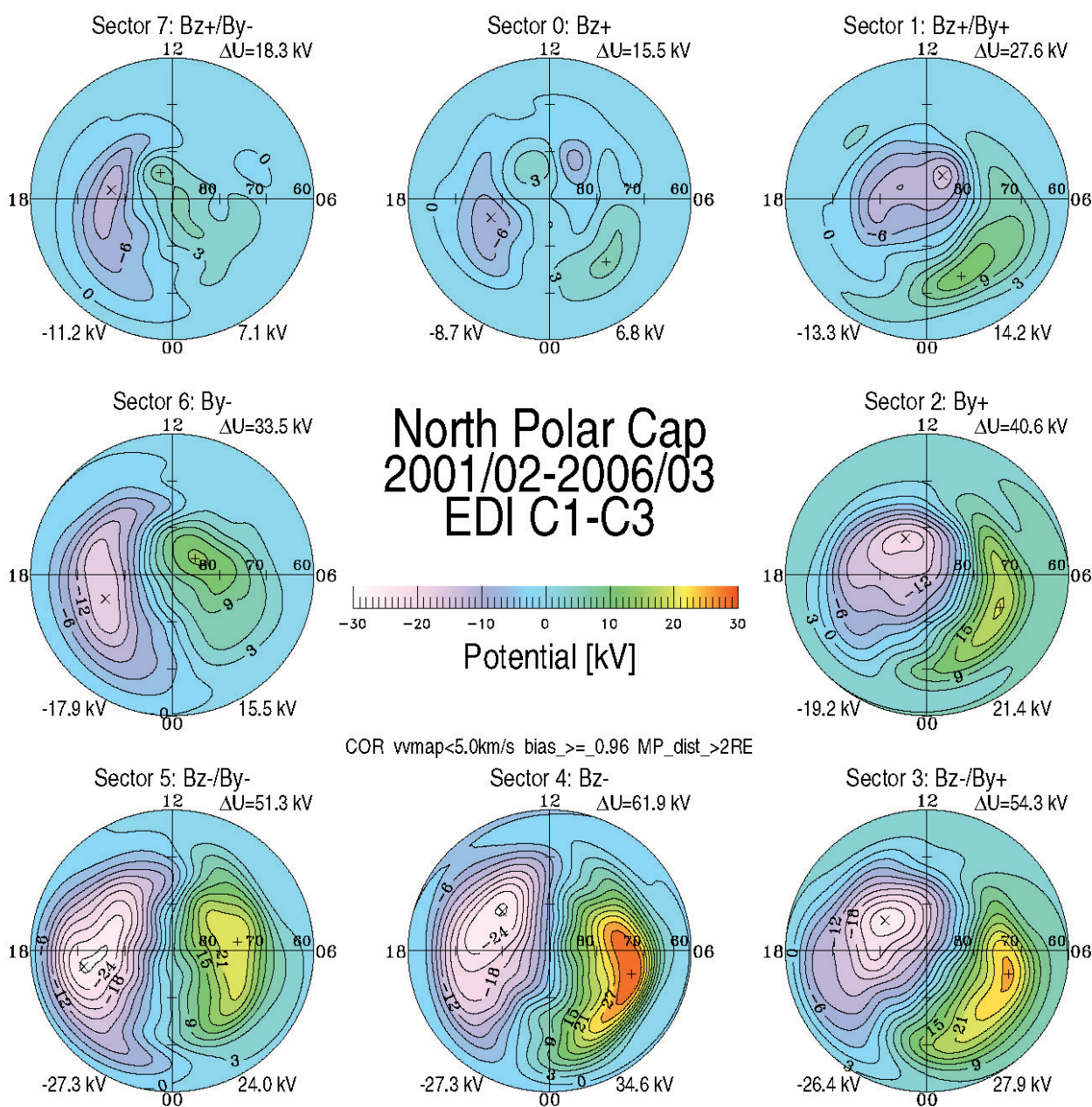


Fig. 2: Electric potential contours in the northern hemisphere, as a function of latitude and magnetic local time, for eight clock-angle orientations of the IMF, obtained by mapping the Cluster EDI velocity measurements into the ionosphere. The background colour shows the value of the potential, according to the colour bar at the center. Lines are drawn at fixed values of the potential, with 3 kV spacing. The minimum and maximum potentials are listed at the bottom, and the total potential drop at the upper right of each map. Because of the equivalence between convection and electric potentials, the contours can also be interpreted as showing the direction of the convective flow.

V_x and x are the solar wind speed and the difference in x-position of the solar wind monitor and the target, respectively. A problem with this method is that the IMF variations appear to occur along surfaces, referred to as 'phase fronts', that can be tilted at arbitrary angles with respect to the solar wind velocity. Figure 1 schematically

illustrates the large effect such a tilt can have on the propagation whenever the ACE spacecraft and the target location are not connected by a solar wind streamline. The orientation of the 'phase fronts' can be obtained by using the property of the magnetic field to show minimum variability in the direction normal to those fronts.

The direction of the IMF is most conveniently characterized in terms of its clock-angle, i.e., the angle between the field, after projection into the plane transverse to the Earth-Sun line, and the northward direction. The clock-angle was computed from 30-minute averages of the measured IMF in terms of its bias-vector, a technique known in meteorology for obtaining average wind directions.

Finally, EDI convection measurements are mapped from the Cluster orbit into the ionosphere, based on an empirical model of the magnetospheric magnetic field. The mapping assumes that the magnetic field lines are frozen into the plasma flow, i.e., the field lines are electric equipotentials.

Since plasma flow in the presence of a magnetic field generates electric fields transverse to the flow, ionospheric plasma convection is equivalent to an electric potential drop across the polar caps. It is thus convenient to turn the global convection results into maps of the electric potential. To obtain absolute values for the potential, a zero-level is defined at the equatorward boundary of the convection zone.

Figure 2 shows the derived potential maps for the northern hemispheres, as a function of the interplanetary magnetic field orientation. For strongly southward IMF (Sector 4), there is the familiar two-cell convection pattern, with strong anti-sunward convection over the poles and return flows at lower latitudes. In the northern hemisphere, the addition of a positive IMF B_y component (Sector 3) skews the convection cells so that a duskward component appears. This is the effect introduced by the asymmetrical addition of open flux to the magnetotail lobes caused by dayside reconnection in the presence

of an IMF B_y . When the IMF is essentially in the positive or negative y -direction (Sectors 2 and 6, respectively), the appearance of one crescent-shaped and one rounded cell is evident. This lack of mirror symmetry in the potential patterns for positive and negative IMF B_y can be understood in terms of the day-night conductivity decrease across the terminator in the E-region ionosphere.

For northward IMF (Sector 0), the large-scale convection is weak, at least on average, as evidenced by the much larger spacing of the contours. On the nightside, anti-sunward convection still prevails. But on the dayside, two more cells appear at high magnetic latitudes (centered at 83 degrees), with sunward flow between them. The creation of two counter-rotating convection cells is expected for reconnection of already open polar cap field lines with a strongly northward IMF, but has never been observed this clearly before.

Except for the extra cells just discussed, much of the features observed in the EDI measurements are clearly evident also in previous statistical studies based on low-altitude satellite and ground-based radar measurements. This good agreement suggests that the magnetic field lines threading the Cluster orbit are equipotentials, at least most of the time.

G. Paschmann and S. Haaland, in close collaboration with M. Förster (now at GFZ Potsdam) and the entire EDI team.



Ionic Charge State Measurements of Solar Energetic Particles: a Clue to the Source

The measurement of the energy dependence of the ionic charge of heavy ions in solar energetic particle events allows inferring the location of the source. In impulsive events, directly related to solar flares, the acceleration is in the low corona, at altitudes <0.3 solar radii (R_s). In gradual events, the particles are accelerated at the coronal and interplanetary shock. High charge states at high energies suggest a contribution of flare particles in the accelerated population that are accelerated near the Sun.

History

The ionic charge of solar energetic particles (SEP) is an important parameter for the diagnostic of the plasma conditions at the source region. Furthermore, the acceleration and transport processes depend significantly on velocity and rigidity, i.e. on the mass and ionic charge of the ions. The variations of elemental and isotopic abundances by several orders of magnitude, and variations in the mean ionic charge at ~ 1 MeV/amu (atomic mass unit) have been used in the last ~ 25 years for dividing SEP events into two classes, *gradual* and *impulsive*, following the classification of flares based on the duration of their soft X-ray emission: (1) *Gradual Events*, showing large inter-planetary ion intensities, small electron to proton ratios, on average elemental abundances similar to coronal abundances, and ionic charge states consistent with source temperatures of $1 - 2 \times 10^6$ K, characteristic for the solar corona and solar wind. These events show long duration soft X-ray emission and are associated with interplanetary shocks, driven by coronal mass ejections (CME). Particles are accelerated at the shock front over a wide range of solar longitudes, propagate along the interplanetary magnetic field, and then reach the orbit of Earth over a wide range of solar longitudes as schematically shown in Fig. 1 (2) *Impulsive Events* show small interplanetary ion intensities, a high electron to proton intensity ratio, enhanced abundances of heavy elements (e.g. by a factor ~ 10 for Fe relative to O), enhancements of ^3He relative to ^4He by up to a factor of 10^4 , and high ionic charge states for Si (14) and Fe (20), which were interpreted as being due to a high temperature of $\sim 10^7$ K in the source region. These events show short duration soft X-ray emission and the acceleration process is thought to be related to the flare. These 'flare particles' (Fig. 1) can reach the spacecraft only from a narrow range of solar longitudes connecting the acceleration site to the spacecraft at 1 AU.

Measurement Techniques

Over the last ~ 30 years, the space plasma group was involved in the development of several methods to determine the ionic charge of energetic ions. At low energies of $\sim 0.01 - 3$ MeV/amu techniques involving electrostatic deflection provided the first direct ionic

charge measurements. At higher energies, the SAMPEX (Solar, Anomalous and Magnetospheric Particle Explorer, launch 1992) instrumentation provided for the first time ionic charge measurements for many elements in the range C to Fe over the extended energy range of 0.3 - 70 MeV/amu, utilizing the Earth's magnetic field as a magnetic spectrometer. Advanced instrumentation with high sensitivity onboard SOHO (Solar and Heliospheric Observatory, launch 1995) and ACE (Advanced Composition Explorer, launch 1997) extended the measurement of ionic charge states during the last ~ 10 years to many SEP events with low interplanetary particle intensity, i.e. in particular to many impulsive events.

New Results in Gradual SEP Events

With SAMPEX, providing for the first time ionic charge measurements in large (gradual) events over an extended energy range, a significant increase of the mean ionic charge (Q) of heavy ions with energy was found in several gradual events, with Q_{Fe} increasing from ~ 10 at 0.3 MeV/amu to $\sim 18 - 20$ at ~ 40 MeV/amu. Recent measurements with SOHO and ACE showed that the mean ionic charge of heavy ions at suprathermal energies (< 200 keV/amu) in these events is usually compatible with solar wind charge states ($Q \sim 10$ for Fe). At somewhat higher energies (0.2 - 0.6 MeV/amu) the mean ionic charge shows a large event-to-event variability. It is either constant or increases moderately with energy, in a few cases by ~ 2 charge units. At energies above ~ 10 MeV/amu, however, the mean ionic charge is often observed to be significantly larger than at low energies, with $Q \sim 20$ for Fe. These results show that our previous interpretation of heavy ion charge states being related to the plasma temperature only was too simplistic.

New Results in Impulsive SEP Events

The new high sensitivity ionic charge measurement with the SEPICA (Solar Energetic Particle Ionic Charge Analyzer) experiment onboard ACE provided ionic charge measurements for a large number of gradual and impulsive SEP events. The distributions of event averages of the mean ionic charge of Fe at 0.18 - 0.25 MeV/amu in ~ 40 gradual events correlated with interplanetary shocks and ~ 40 impulsive events, shows that the distributions of the mean charge of Fe is completely different for the two classes of events: the events correlated with interplanetary shocks show a distribution with a peak around $Q \sim 10$, whereas the corresponding distribution of average charge states in impulsive events is considerably wider and ranges from ~ 14 to 18. Furthermore, all impulsive events, so far without exception, show a strong increase of the average ionic charge of Fe in the narrow energy range of $\sim 0.1 - 0.5$ MeV/amu, with $Q \sim 12-15$ at ~ 0.1 MeV/amu and $Q \sim 18 - 20$ at ~ 0.5 MeV/amu.

The Energy Dependence of the Ionic Charge

A large increase of Q at energies <1.0 MeV/amu, as systematically observed in impulsive events, can only be explained by ionisation in a dense environment. If the particles propagate in a sufficiently dense environment in the lower corona during or after the acceleration, a large increase of the mean ionic charge at energies

$\sim 10^{10} - 10^{11}$ s cm $^{-3}$ and $Q_{eq} \sim 22$ at 1MeV/amu. The new observations also show that the high ionic charge of Fe in impulsive events observed previously at ~ 1 MeV/amu was the high-energy tail of an energy dependent distribution. It is also evident that the new measurements of $Q \sim 12 - 14$ at low energies are not compatible with a high temperature in the source region.

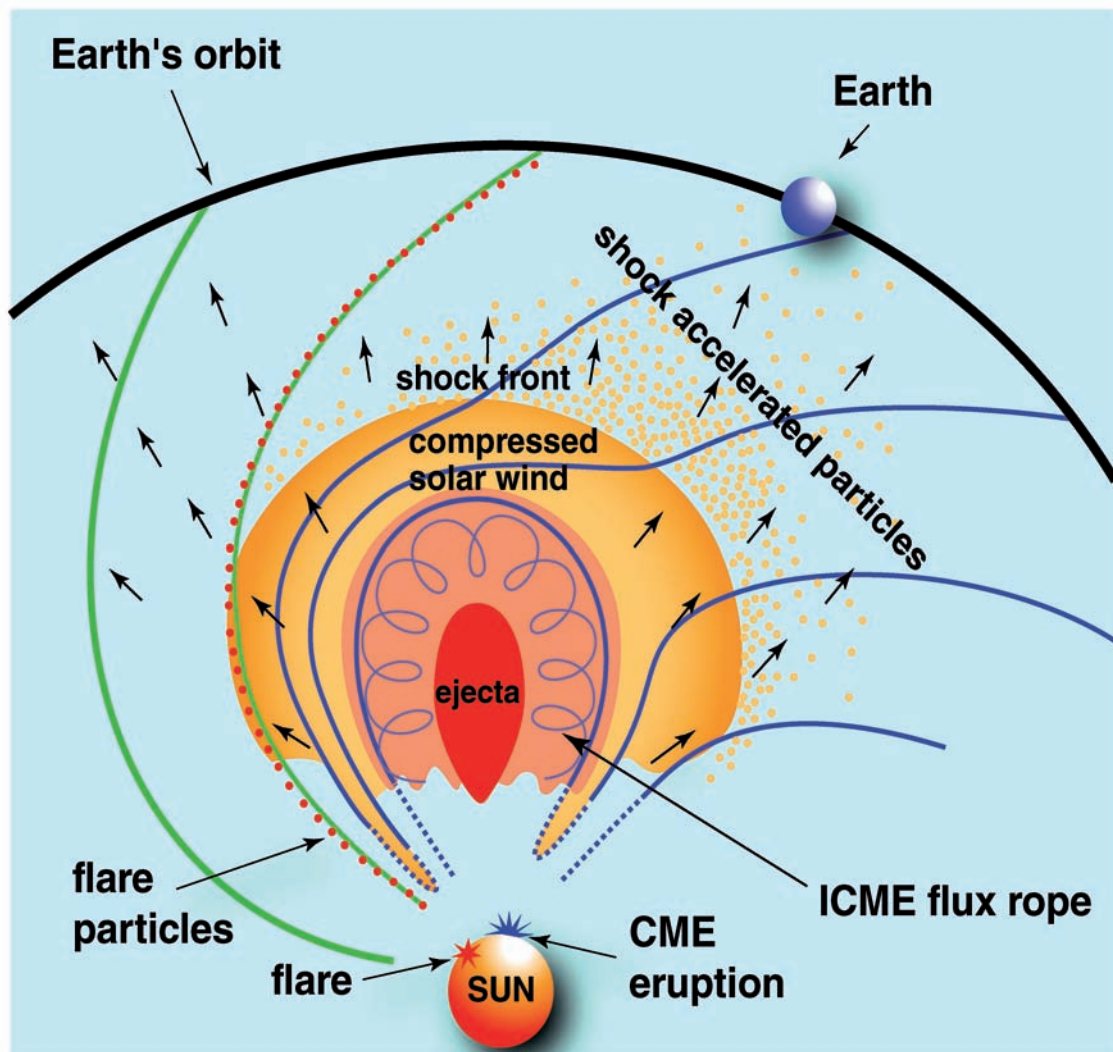


Fig. 1: Schematic view of the acceleration of solar energetic particles by a CME driven interplanetary shock and by a flare at the sun.

of $\sim 0.2 - 1$ MeV/amu is a natural consequence of the cross sections for ionisation by electrons and ions. Calculations of the equilibrium ionic charge of heavy ions as a function of ion speed, including the effects of radiative and dielectronic recombination and ionisation by thermal electrons and ions, show that the mean ionic charge increases monotonically as a function of $N \cdot \tau_A$ where N is the plasma density and τ_A is the acceleration time scale. The ionic charge approaches asymptotically an upper limit (the equilibrium mean charge) Q_{eq} , where $(N \cdot \tau_A)_{eq}$ for $\sim 0.2 - 1.0$ MeV/amu Fe ions is

A Model for Acceleration and Propagation

The increase of Q with energy is typically observed at somewhat lower energies than predicted by the equilibrium model. It has been demonstrated recently that this difference between the observed and predicted energy dependence of Q can be explained by propagation effects: on their way from the acceleration site at the Sun to 1 AU low energy particles can lose a significant fraction (\sim factor of two) of their energy. This results, for an average ionic charge $Q(E)$ at the Sun, in a lower

energy E' at 1 AU. For a quantitative comparison of the observations with model calculations, more realistic models are needed, including the effects of acceleration, ionization, and propagation at the Sun, and propagation in interplanetary space. In these models, the intensity-time profiles and anisotropies of particles with different mass per charge ratio (e.g. H^+ , He^{2+} , electrons) are used to infer the injection profile at the Sun and the propagation characteristics in interplanetary space. Then, the observed energy spectra and charge spectra of heavy ions are used to infer the model parameters for the acceleration and the plasma parameters of the acceleration environment. The model parameters are $N \cdot \tau_A$, τ_A/τ_D , and T_e , where N and T_e are plasma density and temperature, and τ_A and τ_D are the time scales for acceleration and diffusion in the source region at the Sun. The model calculations show that a steep increase of the ionic charge with energy by 4 - 6 charge units can only be explained with contributions from two regions with different temperature. These 2 regions could, for example, be two loops with different plasma parameters as schematically shown in Figure 2.

For a solar energetic particle (SEP) event on September 9, 1998, for example, the initial spectra of particles injected close to the Sun were obtained for the acceleration parameters $\tau_A/\tau_D = 0.1$, $T_e = 1.58 \times 10^7 K$, and $N \cdot \tau_A = 5 \times 10^{11} s cm^{-3}$ for region 1 and $T_e = 10^6 K$, $N \cdot \tau_A = 10^{11} s cm^{-3}$ for region 2. With these parameters, both the energy spectra and the observed energy dependence of the ionic charge could be reproduced satisfactorily.

Consequences for the Source Location

The model calculations show that the steep increase of the ionic charge of Fe ions in the energy range < 1 MeV/amu as observed in impulsive SEP events requires values of the parameter $N \cdot \tau_A \sim 10^{11} s cm^{-3}$. If we assume acceleration time scales in the range of ~ 10 to 100 s, compatible with X-ray and electron measurements in these events, this corresponds to densities of $\sim 10^9 - 10^{10} cm^{-3}$, i.e. the ionization, and probably also the acceleration, of the particles is very low in the corona, at altitudes $< 0.3 R_s$ above

the photosphere. The large variability of $Q(E)$ can be understood in terms of different acceleration rates and non-equilibrium conditions for charge stripping.

The ionic charge of heavy ions in gradual events, in particular the ion population observed near the interplanetary shock at < 0.3 MeV/amu, is compatible with the ionic charge of the solar wind and suprathermal particles, suggesting local acceleration. The increase of

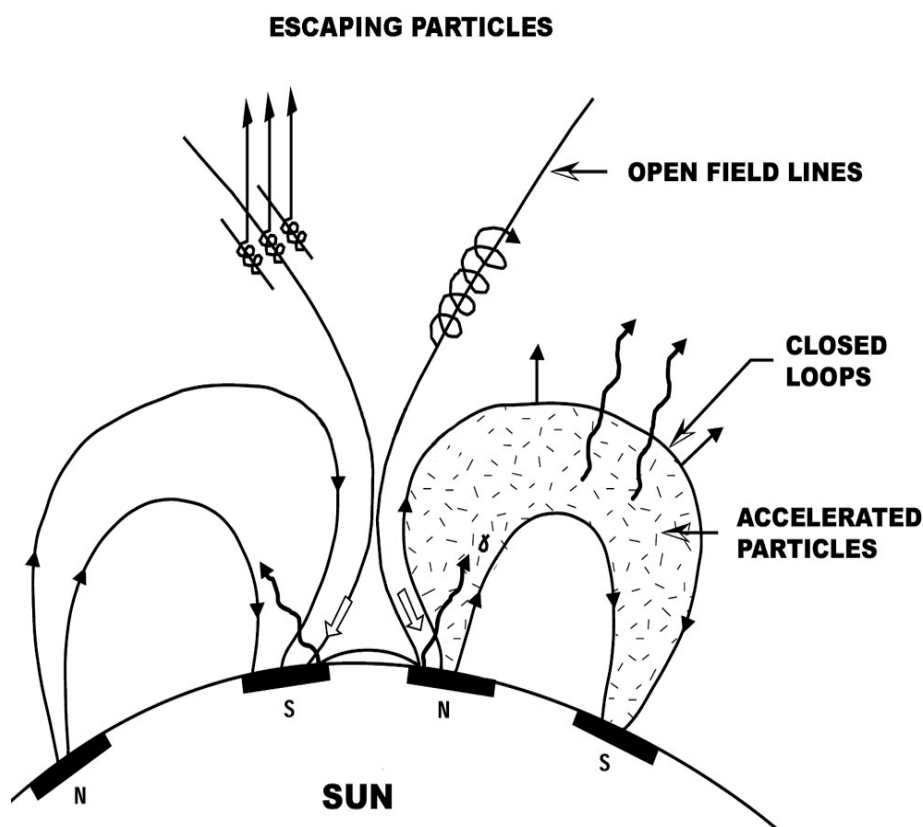


Fig. 2: Simplified description of an acceleration region, consisting of two magnetic loops with different plasma parameters.

Q at high energies as often observed can be explained by injection of flare particles (with high charge states) into the shock acceleration process near the Sun.

B. Klecker, in close cooperation with E. Möbius, M.A. Popecki, UNH.



2.5 COMPLEX PLASMAS

Complex or dusty plasmas are plasmas, i.e. ionized gases, containing microparticles, e.g. dust grains. In low-temperature discharge plasmas these microparticles collect mainly electrons on their surface. The charge of the microparticles is typically between 1000 and 100.000 elementary charges. The typical interparticle distance is of the order 100 μm . The microparticles build a strongly-coupled system, i.e., their interaction energy is larger than their thermal energy. Due to screening of the particle charge within the plasma the interaction potential is of the Yukawa type (screened Coulomb potential).

In 1986 it was predicted that the microparticles in a complex plasma can due to their strong interaction arrange themselves in regular structures, the so called plasma crystal. In 1994 such a plasma crystal was generated and observed for the first time within a collaboration between the MPE and the German Space Agency DLR. For this purpose a radio-frequency discharge in a small plasma chamber is used to produce the background plasma in a noble gas (e.g. Argon) at pressures of the order of 0.1

microscopic and kinetic level. Also the liquid phase is of great interest, in which for example shear flow and turbulence can be studied. Therefore complex plasmas are ideal models for understanding crystallization and other dynamical processes (phase transitions, instabilities, dispersion relations, etc.) on the microscopic level in solid state, fluid, and plasma physics.

Other applications of complex plasmas can be found in astrophysics and plasma technology. There are many situations in space where dusty plasmas occur. Among them are comets, planetary rings, accretion disks, interstellar clouds and others. Plasma etching and coating, on the other hand, is a widely used technology, e.g. for producing microchips. In these plasma reactors dust arises and grows, leading to possible contamination problems. Therefore a detailed understanding of the origin and growth of dust and its interaction with the plasma is desirable. Furthermore dust plays a role in fusion reactors. Due to this variety of applications, complex plasma physics is a rapidly growing field.

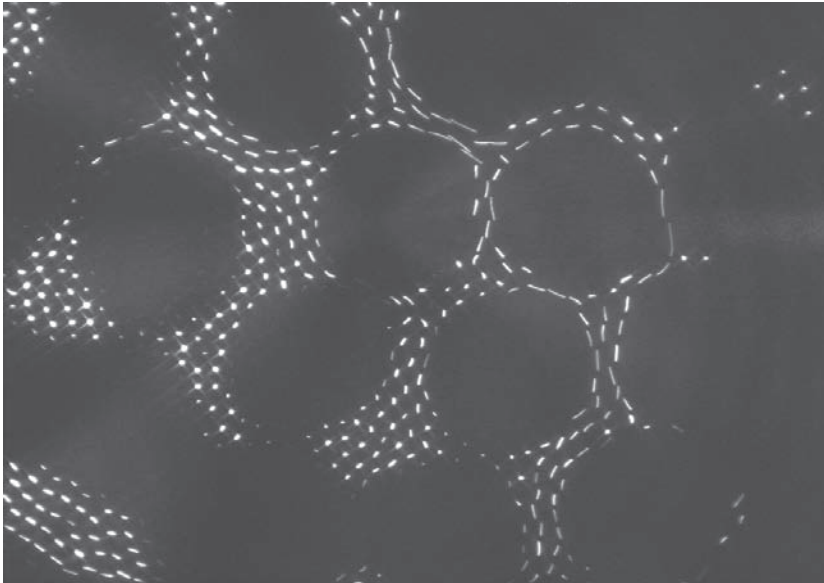


Fig. 1: Microparticles (white dots) illuminated by a laser forming a crystal (top view) within a complex plasma.

to 1.0 mbar. Afterwards monodisperse plastic spheres with diameters of the order 1 to 10 μm are injected. The charged microparticles are then levitated and confined by the electric field surrounding the plasma in the plasma sheath above the lower electrode. The microparticles, illuminated by a laser sheet, are observed by a camera. In this way, complex plasmas, e.g. in the crystalline phase (Fig. 1), can be investigated directly.

The formation and melting of plasma crystals, their structure, phonon spectra etc. can be observed on the

In the laboratory on earth many experiments are hampered by gravity effects, restricting the system to the plasma sheath. Hence often only small, quasi two-dimensional systems can be produced and gravity influences the structure and dynamics of the microparticle system. Furthermore, the background plasma in the plasma sheath is rather complicated (non-neutral and anisotropic) which renders the interpretation of the experiments difficult. Therefore we perform microgravity experiments with complex plasmas since 1996 in sounding rockets and parabolic flights. Since 2001 (see section 3.4.) complex plasmas are also investigated on board of the International Space Station ISS in cooperation between MPE and the Institute for High Energy Densities in Moscow.

At MPE complex plasmas are investigated experimentally and theoretically. Laboratory experiments, e.g. the properties and behaviour of complex plasmas in strong magnetic fields (Fig. 1) or in a dc discharge, as well as microgravity (parabolic flight campaigns, ISS) experiments are constructed and performed. Analytic models and numerical simulations are developed for an understanding of the physical processes.

In the following we report on two recent results of our investigations of complex plasmas, namely the non-Newtonian behaviour of complex plasma fluids and the recrystallization of a two-dimensional plasma crystal.

Non-Newtonian Complex Plasma Fluids

Rheological and structural properties of complex plasma fluids were studied. First, the shear viscosity was measured using the PK-4 setup. The shear flow was induced either by an inhomogeneous gas flow or with laser radiation. Complex plasmas exhibited substantial shear-thinning and shear-thickening in a broad range of shear rates. Second, the formation of a string fluid phase in electrorheological complex plasmas was investigated, by applying an external AC electric field and measuring the induced structural anisotropy. The observed isotropic-to-string phase transition is believed to be of second order, and thus is a good candidate to study kinetics of critical phenomena.

One of the remarkable features of complex plasmas is that although they are intrinsically multiphase systems, the rate of momentum exchange through collisions between the charged microparticles can significantly exceed the coupling to the background neutral gas. Therefore fluid complex plasmas can act as an essentially single-fluid system. This opens up a unique opportunity to investigate generic phenomena occurring in strongly coupled media at the kinetic level, and to get insights into microscopic properties of hydrodynamics as well as thermodynamics of fluids, which is considered as one of the outstanding problems in fundamental physics.

Fluids exhibit a rich variety of rheological properties. Along with conventional Newtonian fluids (e.g., air, water, gasoline) that have constant viscosity, there exists a broad class of non-Newtonian fluids with their rheology strongly depending on the flow conditions (e.g., fluids with shear-thinning and shear-thickening effects, viscoelastic fluids). Classic examples encountered in everyday life include paint, ketchup, gelatine, etc. Other fluids such as molten polymers and slurries are of considerable technological importance.

Another remarkable class of non-Newtonian fluids are the so-called electro- or magnetorheological (ER/MR) fluids. The interparticle interaction in such fluids and, hence, their rheology is determined by external electromagnetic fields: At low fields they may be “normal” fluids, but above a critical field, at low shear stresses ER/MR fluids behave like solids, and at stresses, greater than a “yield stress” they flow with enhanced viscosity. ER/MR fluids have potential use in industrial applications as, e.g., hydraulic valves, clutches, brakes. Moreover, for colloidal ER/MR fluids, the possibility to tune the crystal structure of these suspensions by an external field makes them appealing for display production and photonic applications.

Our recent experiments demonstrated that complex plasmas are very well suited to study the kinetics of “microscopic” processes that govern the non-Newtonian behavior. We investigated shear flows in complex plasma fluids (by applying stresses of different magnitudes and measuring the dependence of the viscosity on the local shear rate), and studied the formation of a string fluid phase in ER complex plasmas (by applying an external ac electric field and measuring the induced structural anisotropy).

We developed a theoretical model of the non-Newtonian viscosity of complex plasmas. The model is based on the assumption of local balance between viscous heat deposition and neutral friction sink, which yields a

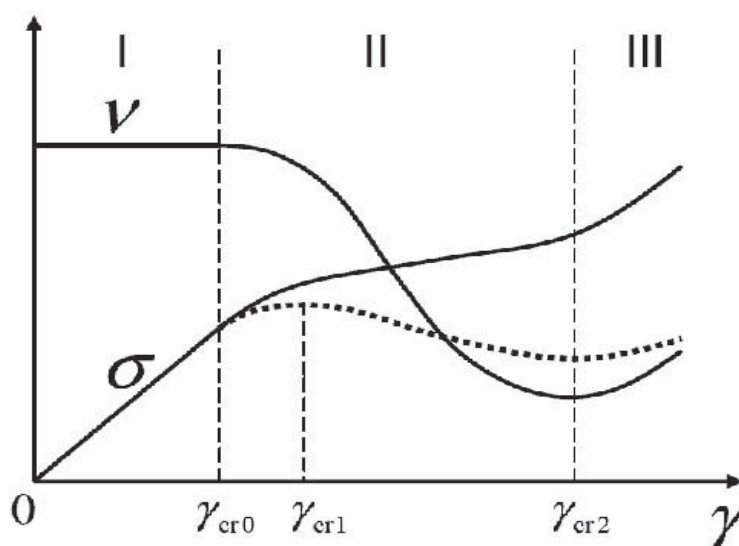


Fig. 1: Qualitative dependence of the viscosity ν and the shear stress $\sigma = \nu\gamma$ on the velocity shear rate γ . Three ranges of γ are indicated, corresponding to the Newtonian (constant-viscosity, I), shear-thinning (II), and shear-thickening (III) regimes. The $\nu(\gamma)$ dependence may have an anomalous N-shaped profile (dashed line).

local relation between the shear rate γ and the kinetic temperature T of the microparticles. Along with the known dependence of the kinematic viscosity ν on T , this gives a parametric dependence for $\nu(\gamma)$. According to the model, there are three distinct regimes shown schematically in Fig. 1: If γ is small enough, the temperature remains constant and the viscosity does not depend on γ , the shear stress $\sigma = \nu\gamma$ has a linear scaling (regime I). At larger γ , the temperature starts increasing and the behavior becomes non-Newtonian: $\nu(\gamma)$ falls off showing shear-thinning (regime II). Note that in some cases the behavior can become anomalous, $d\sigma/d\gamma < 0$ (dashed line). As γ grows further, $\nu(\gamma)$ and hence $\sigma(\gamma)$ increase again (shear-thickening, regime III). The transition from regime II to III is due to the interplay between the so-called “potential” and “kinetic” parts in

the $\nu(T)$ dependence, determining the viscosity at low and high temperatures, respectively.

We performed a series of shear flow experiments using the PK-4 prototype setup (Fig. 2). The particles formed a very elongated 3D cloud (of length 3 - 10 cm and diameter of 4 - 6 mm) that was oriented along the axis of the discharge tube. The shear flow (along the axis) was induced by two different methods: (i) we used the gas flow in the tube (the velocity of the gas has a parabolic profile and hence exerts shear stresses due to coupling to microparticles), or (ii) applied laser radiation (along the tube axis). The gas-induced flow turned out to have an one-dimensional plane topology with zero net flux (resembling the Couette flow between parallel plates), the laser-induced flow, on the other hand, had cylindrical symmetry (similar to the Poiseuille flow in a tube).

We performed a two-parametric fit of the measured velocity profile with solutions of the Navier-Stokes equation for (i) our non-Newtonian viscosity model and (ii) the conventional constant-

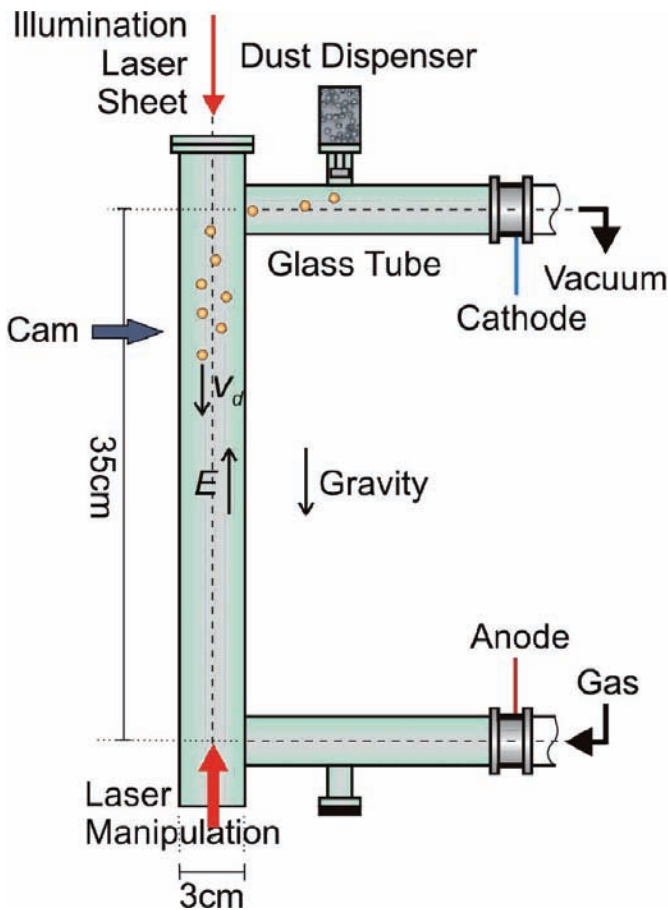


Fig. 2: The PK-4 prototype setup. A camera (left) is recording the plasma kinetics.

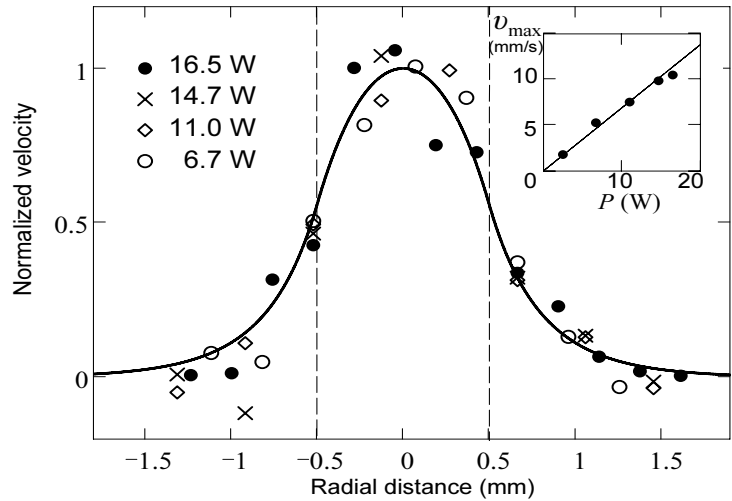


Fig. 3: Experimental velocity profiles (symbols) of the laser-induced shear flow measured for different laser power P . The profiles are normalized by the maximum velocity at the center of the beam v_{\max} . The beam boundaries are indicated by the vertical dashed lines. The solid line represents the theoretical fit (for $P = 16.5$ W) with constant viscosity. The inset shows the dependence of v_{\max} on P .

viscosity case. The non-Newtonian viscosity yields an extended region of quasi-linear profile and thus provides good agreement. In contrast, for the constant-viscosity model the curve is of fairly different shape, which allows a qualitative distinction from the non-Newtonian case. Quantitatively, the distinction becomes evident by chi square-fitting. The theoretical fit allows us to retrieve an explicit dependence of the viscosity on γ with well-pronounced shear-thinning and -thickening.

For the laser-induced flows, the cylindrically symmetric velocity profiles were measured for different values of the laser power P and normalized to the maximum velocity at the center v_{\max} , as shown in Fig. 3. Qualitatively one can see that the normalized profiles seem to be similar for different P , and v_{\max} grows linearly with P . This, along with the assumption that the laser force on a particle is proportional to P , suggests that - if hydrodynamics still works - the effective viscosity should be constant. Such a hypothesis is well confirmed by the corresponding fit shown in Fig. 3.

The range of shear rates achieved in our experiments with the gas-induced flow was sufficiently broad to reveal a non-Newtonian behavior of 3D complex plasmas, accompanied by substantial shear-thinning and shear-thickening effects. At the same time, the shear was small enough to expect hydrodynamics to be applicable. In contrast, the inhomogeneity of the flow induced by the laser was very high - the velocity changed significantly at the scale of the interparticle distance. Thus, a combination of both methods of the flow generation made it possible to cover the entire range of γ up to the edge where complex plasmas cannot be considered as a continuous medium. Nevertheless, the formal hydrodynamic description of "extreme" laser-induced shear flows gives reasonable results. Apparently, the

transport properties in this case are no longer local and in equilibrium, and further investigations of the mechanisms governing the momentum exchange in such flows would be highly desirable.

The derived magnitude of the kinematic viscosity in the Newtonian regime is $\sim 100 \text{ mm}^2/\text{s}$, which is about the viscosity of, e.g., glycerin. The observed shear-thinning, however, diminishes the viscosity by factor of 10, making it close to the viscosity of air at atmospheric pressure. Hence, in terms of viscosity the fluid complex plasmas are very similar to ordinary classic fluids.

Electrorheological complex plasmas were investigated with the plasma crystal experiment PK-3 Plus under microgravity conditions on board the ISS. We employed a modulation with an external electric field at 100 Hz (well above the eigenfrequency of the microparticles) that caused a periodic polarization of the plasma cloud around each microparticle, so that the resulting interaction between the particles was identical to that in conventional dipolar (Stockmayer) fluids. Such electrorheological fluids are famous because of their exceptionally diversified phase diagram that includes a number of second-order structural phase transitions. Thus, electrorheological complex plasmas may allow us to investigate at the kinetic level critical phenomena accompanying such transitions.

The “string” formation in gaseous ER complex plasmas is one of the candidates for the second-order phase transition: Theory predicts that for a given thermodynamic state there exists a critical amplitude of the electric field above which the isotropic gaseous phase loses the thermodynamic stability and particles form lines oriented along the field. Experiments seem to confirm the theory: At low fields the microparticles form an isotropic gaseous-like phase shown in Fig. 4a, whereas above a certain threshold an ordering of the particles along the field emerges. At sufficiently large fields the string fluid can be observed by naked eye - vertically, particles form clear strings (see Fig. 4b), but horizontally there is no apparent order. The magnitude of the critical field for the transition is in good agreement with the theoretical prediction.

Further kinetic investigations of 3D fluid complex plasmas will require the development of a convenient technique for

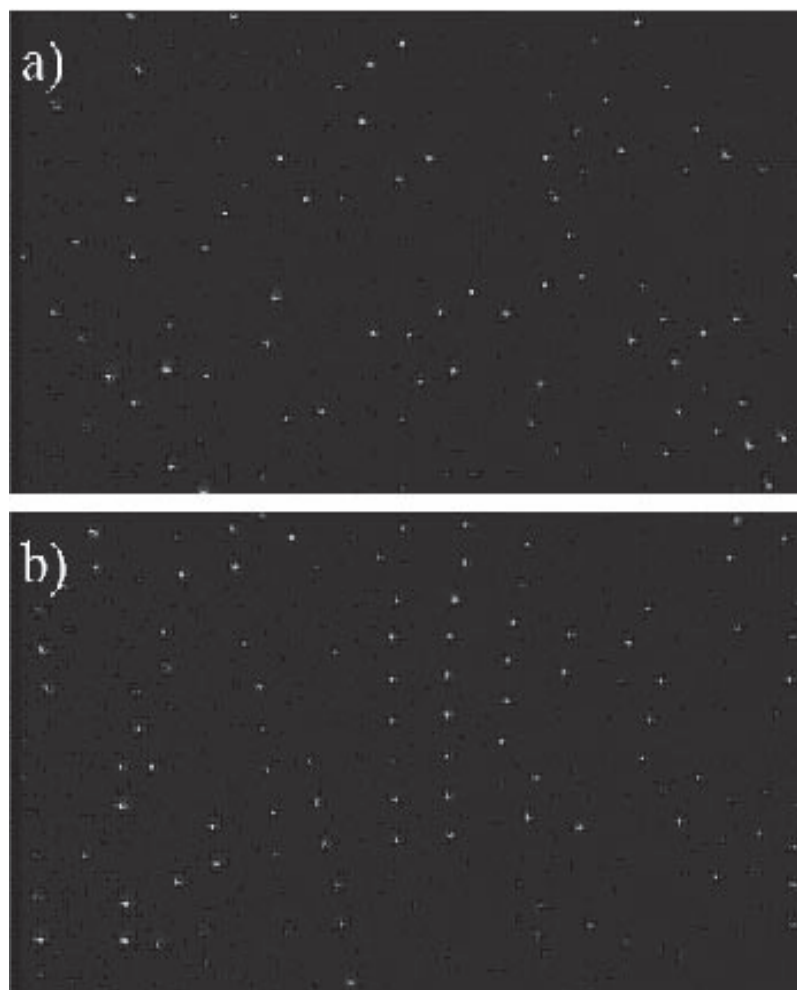
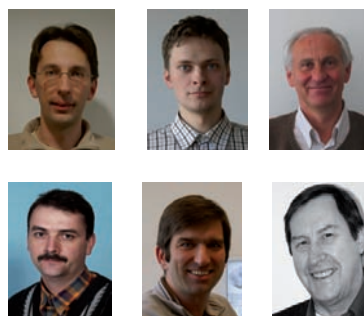


Fig. 4: Isotropic-to-string phase transition observed in experiments with electrorheological complex plasmas. The dipolar interaction between microparticles is induced by an external vertical AC electric field with a tunable amplitude at 100 Hz. Particles are visualized by a vertical laser sheet of about $200 \mu\text{m}$ thickness. At small fields the particles form an isotropic gas-like phase (a), at larger fields the “string fluid” phase with vertical order emerges (b).

individual particle tracking. In particular, such technique is essential for reliable temperature measurements in the fluid phase, and its development will be one of the main challenges for our future work.

A. Ivlev, R. Kompaneets, H. Höfner, H. Thomas, C. R ath, G. Morfill



Recrystallization of a 2D Plasma Crystal

A monolayer plasma crystal consisting of micron-sized particles, levitated in the sheath of a radio frequency discharge, was melted by applying a short electric pulse to two parallel wires located at the height of the particles. Structural properties and the particle temperature were examined during the stage of recrystallization. A liquid-like phase was followed by a transient state characterized by energy release and the partial restoring of long range order. Numerical simulations revealed the same regimes of recrystallization as those observed in the experiment.

Phase transitions, solid to liquid and back, of 2-dimensional systems are a subject of great interest. Theory describes a continuous melting transition with the appearance of a so called "hexatic" phase, which is characterized by long range orientational order, but no long range positional order, between the solid and liquid state. Plasma crystals provide an ideal opportunity to observe phase transitions of 2D

The crystal can be melted into a gaseous state by application of a strong negative electric pulse. The observation of the following transition from the molten unordered state back to an ordered crystal gives information on the processes happening on the level of the particle motion itself.

An Argon plasma has been ignited in a vacuum chamber by applying a radio frequency power between a horizontal electrode and the grounded chamber walls, and dust particles (melamine-formaldehyde spheres with a diameter of $9.19\ \mu\text{m}$) have been injected. The particles levitate in a plane above the lower horizontal electrode at the height where downward gravitational and upward electric forces are in balance. They arrange in a 2D hexagonal crystal due to their mutual interactions and the radial confining forces given by the shape of the lower electrode. Two parallel wires were mounted horizontally at both sides of the crystal, approximately at the height of the particles. To these, an electric pulse of $-253\ \text{V}$ lasting for $0.2\ \text{s}$ was

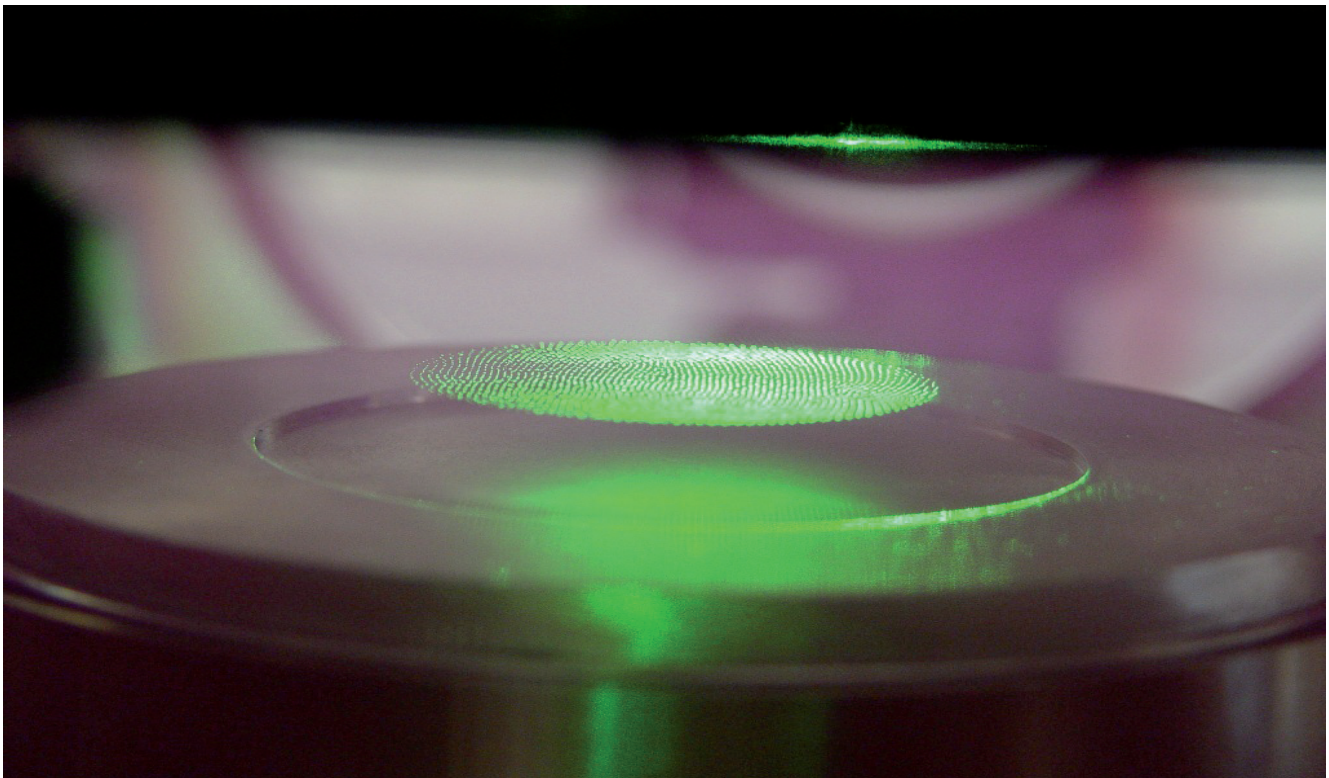


Fig. 1: A two-dimensional plasma crystal of charged microparticles illuminated by a green laser and levitated above the circular electrode by an electric field.

systems at the kinetic level due to the direct visualization of the individual particles and the short restoring time they need to reach equilibrium after a perturbation. A single layer of micron-sized spherical particles arranged in a hexagonal crystalline structure can easily be generated in the sheath of a plasma. An example for such a crystal is shown in Fig. 1.

applied, which pushed the particles from both wires to the center of the chamber and melted the crystal. The particles were illuminated by a horizontally spread laser sheet from the side. A digital high speed camera recorded the whole process of melting and recrystallization from the top view with a frame rate of 500 frames per second (fps).

From the images, we extracted particle coordinates by searching for contiguous regions of a few pixels with brightness values above a given threshold, and identified those as particles. These particles were then traced from frame to frame to obtain velocities. For our analyses we used 2300 such particles, located in a chosen region of the field of view.

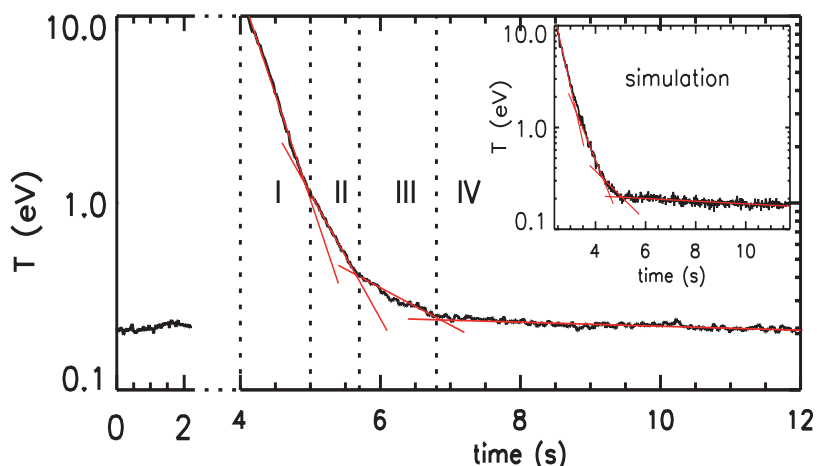


Fig. 2: Particle temperature versus time during the recrystallization. The vertical dashed lines mark the regimes I - IV of different temperature decay. The inset shows the temperature decay found in computer simulations. The red solid lines represent exponential fits.

The mean particle temperature T was derived for each time step from the velocity distributions. The temperature T is highest for the melted state (Fig. 2). Then follows a regime (I) where the dust particles are slowed down mainly by the collision with neutral gas atoms in the plasma. This process, called Epstein damping, implies an exponential decay of T with time, whose slope is given by the plasma conditions. After 1 second of this state, the decrease of T slows down but is still exponential. We found two consecutive regimes (II, III), where some release of energy seems to heat the particles and weakens the effective cooling rate. The temperature reaches its initial value (before melting) after about 4.5 seconds in regime IV. A simulation of a particle system, having the same conditions as in our experiment, yielded the same behaviour (inset in Fig. 2).

Our aim then was to connect the kinetic behaviour of the system to structural properties, being a measure for the order, i.e. the state (e.g. crystalline or fluid) of the system at each time step. The degree of order depends on the positions of particles relative to each other. Here we distinguish between the local structure in the nearest vicinity of a particle, and the global appearance - the continuity of this structure over larger distances. In a liquid for example, particles are distributed randomly over the system on global scales. However on a local scale, they are subject to their mutual interactions, implying a certain interparticle distance. In an ideal 2D plasma, crystal particles are arranged in a continuous hexagonal lattice with a constant interparticle distance and 60° angles between the nearest neighbour bonds.

The range of order is described by means of the pair- and bond correlation functions. The pair correlation function gives the probability to find a particle at a distance r to another particle. By a fitting process, we obtained the translational correlation length for each image. The larger its value is, the larger is the distance scale on which the system is highly ordered. Similarly, the bond correlation function is a measure

for the long range orientational order. It measures the average orientation of nearest neighbour bonds, separated by a distance r in the crystal. The bond correlation function decayed by a power law in the initial state, and exponentially elsewhere. The latter defines an orientational correlation length, comparable to the translational correlation length.

Locally, order can be destroyed by defects. Particles with a number of nearest neighbours differing from the canonical value of six in case of a hexagonal lattice, we call defects. Most common are defects with five or seven neighbours. They often appear in pairs. We calculated their fraction in each frame.

We found that both, defects fraction and correlation lengths, evolve according to power laws proportional $(T - T_c)^\alpha$, where T_c is a critical temperature. We found similar absolute values for the exponent α , ranging

from 0.25 - 0.35. This behaviour holds for all regimes of the temperature decay.

While the defect fractions and the translational correlation length return to their initial values, the orientational order shows a different behaviour after melting. The bond correlation function decays exponentially with increasing correlation length, in contrast to the initial power law decay. According to theory, this behaviour would indicate a liquid state. This however, is in conflict with the general appearance of the system, being highly ordered also on larger scales (Fig. 3).

The orientational order is investigated closer by means of the local bond order parameter. It is calculated from the angles between the bonds from one center particle to all its nearest neighbours, which define the unit cell around this particle. The parameter provides information on the closeness of the unit cell to an ideal hexagon, and on the orientation of the cell with respect to an arbitrary chosen fixed axis. Fig. 3 shows colour-coded maps of selected frames. The brighter the colors the closer the cells are to ideal hexagons. The arrows indicate the orientation of the unit cells. Further, defect locations are marked by red (5 neighbours) and blue (7 neighbours) dots. After an unordered state (Fig. 3b), crystallization proceeds first to a system of small ordered 'crystallites' with arbitrary orientations separated by strings of defects. As the system cools down, these crystallites grow and merge with neighbouring regions (Fig. 3 c-d). A metastable state is reached which is characterized by highly ordered adjoined crystalline domains (Fig. 3e). Since the orientation of unit cells changes abruptly across the

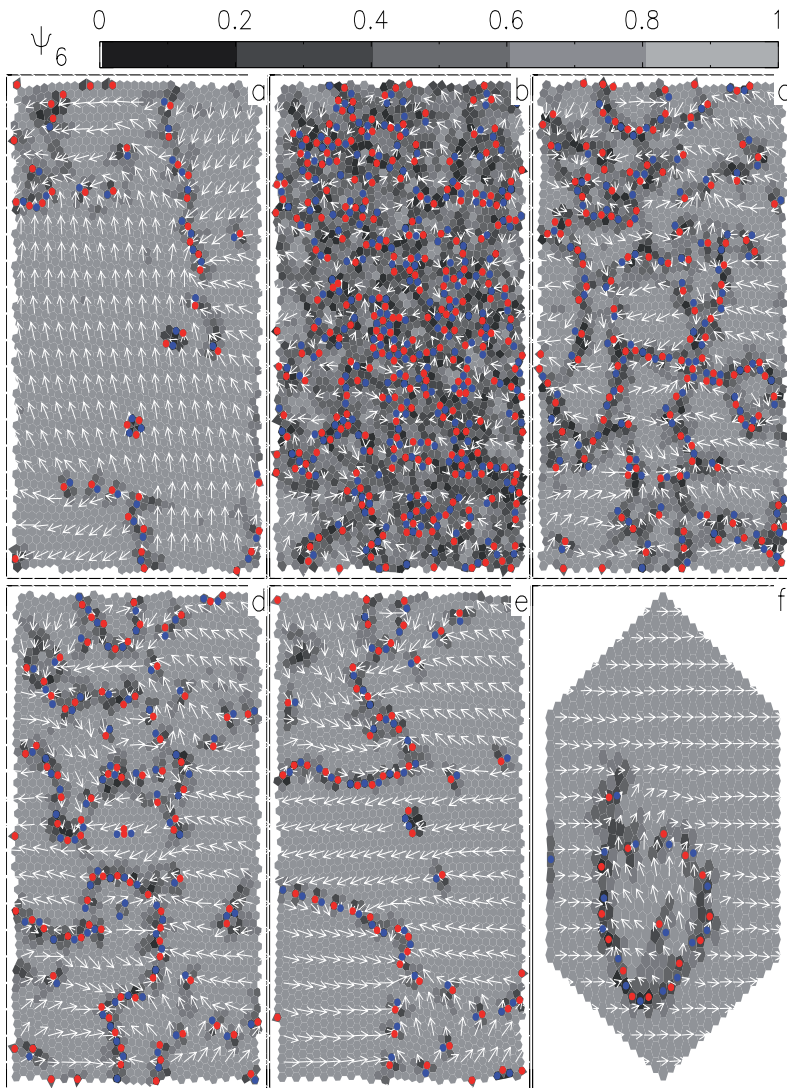


Fig. 3: Color-coded maps of the crystal for different regimes of recrystallization. The background color corresponds to the value of the modulus of Ψ (see colorbar at the top). The arrows represent the vector field of $\arg(\Psi)$. Defects are marked by red (5-folds) and blue (7-folds) dots. a) Crystal structure before melting; b) liquid-like state immediately after melting (regime I); c),d) consecutive regimes II,III of crystallization; e) metastable regime IV; f) crystallite structure observed in simulations.

domain boundaries - even to directions with opposite signs for adjoining domains - long range orientational order cannot be found in the final state of the system, in contrast to the initial state (Fig. 3a). The formation of a crystallite was also observed during the cooling regime in the simulation data (Fig. 3f).

In conclusion, the transition of a liquid-like state of a monolayer of particles to a state of high translational order and low defect fraction was investigated. The exponential temperature decay changes from pure Epstein damping to a slower decay rate until the temperature of the initial state is reached. Defect fraction and translational order are also restored to their initial values. Long range orientational order is not present due to the non-uniform orientation of domains across the crystal. It was found that the crystal slowly returns to a more uniform state after a sufficiently long time (approximately 30 minutes). The regime of slow temperature decay (II and III in Fig. 2 and 3) deserves special attention. The occurring “heating”, i.e. the slower temperature decay, could have two origins: Either, latent heat released by the dissolution of lattice defects and the tilting of nearest neighbour bonds into the (hexagonal) ground state, or the strong coupling between the particles, which would simulate successively larger (more massive) “unit cells” or “effective” particles. Finally, a unique classification of the found regimes with respect to the existing theory – especially regarding the hexatic phase – can not be carried out, since not all of the quantities which describe the structural properties exhibit the predicted behaviour.

C.A. Knapek, D. Samsonov, S. Zhdanov, U. Konopka, G.E. Morfill



3 Experiments and Projects



3.1 SPACE PHYSICS OF THE NEAR-EARTH ENVIRONMENT

In this branch of the institute we are investigating plasma physical processes inside the solar system. For these studies, we develop scientific instruments for the in-situ investigation of these processes, for example in the magnetosphere of the Earth and in interplanetary space.

Presently we are involved in several active instruments for the determination of plasma parameters in the near-Earth environment and for the measurement of energy-, mass-, and ionic charge distributions of solar wind, suprathermal, and energetic ions in interplanetary space. These instruments are onboard the Earth orbiting satellites SAMPEX, FAST, Cluster, and Double Star, and onboard the interplanetary observatories SOHO, ACE, and STEREO. The Cluster mission, together with SOHO, is the first “cornerstone” of ESA’s scientific program “Horizon 2000”.

Cluster Mission: The prime purpose of Cluster is the identification and detailed study of the processes at plasma boundaries of the Earth’s magnetosphere. The four Cluster spacecraft with identical instrumentation fly in a tetrahedral formation when crossing regions of interest. This enables us for the first time to study the dynamics of boundaries, like the Earth’s bow shock and magnetopause, because the 4-spacecraft measurements make it possible to distinguish between spatial and temporal variations. The distance of the 4 Cluster spacecraft is being varied during the mission to investigate space plasma phenomena on different length scales in different regions of the magnetosphere. In 2006 a new configuration with a ~10.000 km tetrahedron was used for both the cusp and central tail crossings. In 2005 the Cluster mission was extended by four years to 2009. This extension will (1) provide more measurements at so far not sufficiently covered large distances of ~10.000 km and more, and (2) provide access to new regions in Earth’s magnetosphere in 2008 and 2009, e.g. to the sub-solar magnetopause and to the auroral acceleration region. The final decision for the full extension will depend on the results of a mid-term review in 2007.

Double Star: Based on an agreement between ESA and the Chinese National Space Administration (CNSA), the Cluster fleet has been complemented by two spacecraft of the Double Star mission (TC-1, TC-2) in 2003 and 2004. With Cluster and Double Star coordinated measurements

with up to 6 spacecraft in the same region of the magnetosphere are now becoming possible for the first time. The operation of the two Double Star spacecraft has been extended this year to 30 September 2007, i.e. Double Star will be supported until the predicted re-entry date of TC-1 on 10 October 2007. MPE has been heavily involved in two instruments of the Cluster science payload: the Electron-Drift Instrument, EDI, and the Cluster Ion Spectrometer, CIS. One of the two CIS sensors (HIA) is also implemented onboard the equatorial Double Star spacecraft TC-1 (s. a. Annual Report 2004).

Cluster Active Archive (CAA): The long-term CAA is supported by ESA in the framework of the International Living with a Star (ILWS) program. The purpose of the CAA is, to make all relevant Cluster data available for a large international scientific community, in particular data relevant for the study of sun-Earth connections. This year archiving of EDI data was continuing and data sets for the years 2001 to 2004 have been processed and submitted to the CAA.

German Cluster Data Center (GCDC): The GCDC located at MPE is one of the 8 National Data Centres building the Cluster Science Data System (CSDS). The GCDC is responsible for processing the scientific data for the German instruments, RAPID (Research with Adaptive Particle Imaging Detectors) from the MPS and EDI from our institute. The resulting datasets are distributed among the various data centres such that each centre is in the possession of the data from all Cluster instruments. These data, presently ~ 60 Gbyte, can then be retrieved from any scientist in Germany participating in the Cluster data analysis via a web-based interface. Currently, there are on average ~1200 requests to the GCDC per month with a total data transfer of ~1 GByte. The GCDC is also responsible for the production of survey plots of all Cluster instruments that are distributed to the other data centres.

SOHO: The Solar and Heliospheric Observatory (SOHO) is now in the 11th year of successful operation and is presently approved to continue at least to 2007. MPE is involved in the Charge, Element, and Isotope Analysis System (CELIAS) that provides near real-time solar wind parameters, solar wind isotopic composition, and the elemental and ionic charge composition of suprathermal particles accelerated in solar flares and by interplanetary shocks.

The PLASTIC Instrument onboard STEREO

The twin spacecraft of the Solar Terrestrial Relations Observatory (STEREO) provide for the first time a 3-D stereoscopic view of the Sun and of coronal mass ejections (CMEs). MPE is involved in the Plasma and Suprathermal Ion Composition (PLASTIC) experiment. PLASTIC provides the key parameters of the solar wind and supplies diagnostic measurements of the mass and ionic charge state composition of heavy ions to characterize CMEs and ambient coronal plasma.

STEREO: The primary objective of the **Solar TERrestrial Relations Observatory (STEREO)** mission of NASA is to understand the origin and consequences of coronal mass ejections (CMEs), the most energetic solar eruptions. CMEs, responsible for the largest solar energetic particle events, are the primary cause of major geomagnetic storms, and may play an important role in the solar cycle via the removal of magnetic flux generated by the solar dynamo.

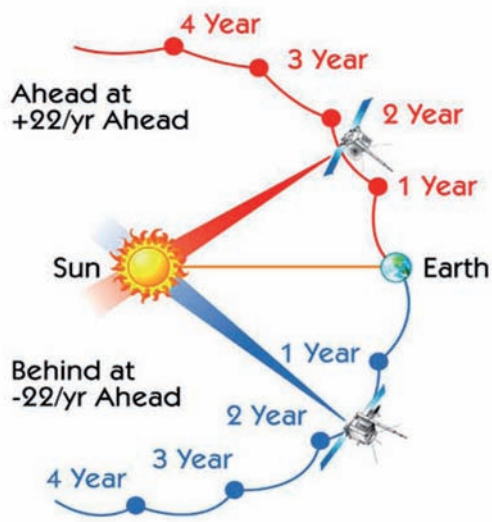


Fig. 1: The orbit of the two STEREO spacecraft, projected onto the ecliptic plane, with fixed Earth-Sun line. The distance in solar longitude between the 2 spacecraft will increase by 45° per year, providing a 3-D stereoscopic view of the Sun and of CMEs.

STEREO Orbit: STEREO with its two identical spacecraft will enable us to study the sun, the solar wind and solar energetic particles from two vantage points, separated in solar longitude. The distance in longitude between the twin spacecraft will increase by 45° per year, providing for the first time 3-D stereoscopic images of the sun and of CMEs. STEREO was successfully launched on October 26, 2006 with a Delta II rocket from Cape Canaveral. The commissioning phase is expected to be completed at the end of January 2007. Nominal mission duration is two years, with a possible extension thereafter.

STEREO Instruments: The two STEREO observatories carry identical payloads with a total of 13 instruments on each spacecraft. The instruments include EUV imagers, White-Light Coronagraphs, an Heliospheric Imager, radio wave trackers, and two packages for the in-situ measurement of the interplanetary magnetic field, of thermal and suprathermal solar wind ions and electrons, and of energetic ions and electrons up to energies of ~ 40 MeV/nuc.

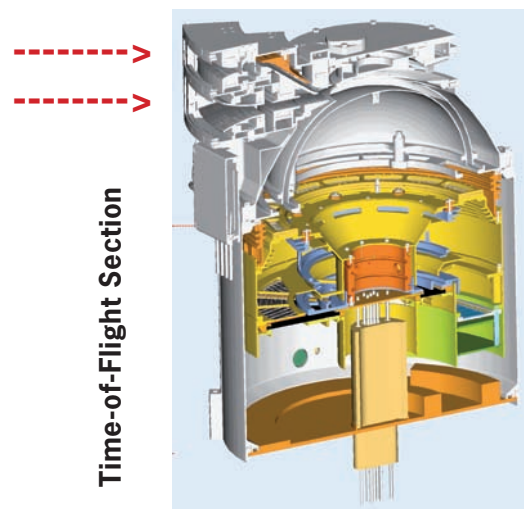


Fig. 2: Cross-sectional view of the time-of-flight section (bottom) and entrance aperture (top section) of the PLASTIC sensor onboard STEREO. The two arrows indicate the entrance aperture for solar wind protons and alpha particles (top) and heavy ions (bottom), respectively.

PLASTIC: The Plasma and Supra-Thermal Ion Composition (PLASTIC) experiment is the primary sensor onboard STEREO for studying the Solar Wind and suprathermal ions. The PLASTIC instrument provides solar wind density, velocity, and temperature, and supplies key diagnostic measurements of the mass and charge state composition of heavy ions to characterize CMEs and ambient coronal plasma. PLASTIC is based on the design of the CIS-CODIF sensor onboard Cluster, with significant improvements to provide mass, ionic charge, and energy of solar wind ions and of suprathermal particles in the energy range 0.2 to 100 keV/e. A cut through the PLASTIC sensor is shown in Fig. 2. The sensor combines energy/charge determination with a quadrispherical electrostatic analyzer with separate apertures for solar wind protons and alpha particles (top arrow) and heavy ions in the mass range C - Fe (bottom arrow) with a time-of-flight and energy measurement (lower section of Fig. 2).

3.2 INFRARED/SUBMILLIMETER ASTRONOMY

Our group is pursuing development programs for high resolution near-infrared instrumentation for 8m class telescopes as well as space-based and airborne far-infrared instrumentation. Our intention is to tackle a few key scientific questions, simultaneously using a wide range of observing wavelengths and methods.

The commissioning in 2006 of the Very Large Telescope (VLT) Laser Guide Star Facility including our PARSEC-Laser (see selected article) is enabling further our previous developments for VLT instruments using adaptive optics, namely the NACO near-infrared camera and spectrometer (commissioned 2002) and the SINFONI near-infrared integral field spectrograph (commissioned 2004).

MPE and other German institutes hold a 25% share in the Large Binocular Telescope (LBT) on Mount Graham, Arizona, two 8m telescopes on a common mount and separated by 16m. Our first major instrument contribution to this project is the cryogenic multi-object spectroscopy unit that is part of the near-infrared imager/spectrograph LUCIFER being built by a German consortium. For the two 'eyes' of the LBT, two complete LUCIFER instruments are being built. The first multi-object spectrograph unit including cryogenic mask and cabinet exchange mechanisms has been completed in 2006 and is being tested in the laboratory. The LBT itself has undergone extensive testing and commissioning activities in 2006. Science Demonstration with the optical prime focus camera will start in January 2007. We are comparing options to further extend the scientific potential of the LBT by adding a Laser Guide Star system. In particular, the powerful multi-object spectroscopy capability of LUCIFER could benefit from sharpening the point spread function by means of a ground layer adaptive optics system. In the same context, we are exploring advanced phase shifting laser guide star concepts in a prototype experiment. The study of an integral field spectroscopy unit for the interferometric combined focus of the LBT (SERPIL/LIINUS), in collaboration with Cologne university, has continued with emphasis on theoretical investigation of lenslet/fiber concepts for dual beams.

The Phase A study has started in 2006 for GRAVITY, a 2nd generation instrument for the VLT Interferometer optimized for highest precision (10 μ arcsec) astrometry in the near-infrared K-band. Probing the physics and strong gravity next to the Galactic center black hole is one of the key goals of this instrument developed in collaboration with Paris Observatory, MPIA, and Cologne University.

In collaboration with ESO, we set up at MPE a laboratory experiment to integrate and test the PRIMA astrometric facility for the VLT interferometer.

We are developing the analysis software for the near-infrared multi-integral field unit spectrograph KMOS being built for the VLT by an international consortium including MPE. The final design review is scheduled for mid 2007.

A success story has been completed with the end of the active archive phase of the Infrared Space Observatory (ISO) and the closure of our ISO Spectrometer Data Centre at the end of 2006. The last activities were devoted to preparing the final archive of the data obtained during ISO's 1995-1998 mission, which has produced a wealth of exciting results for our group as well as the general community.

Testing of the flight model of the far-infrared camera/spectrometer PACS for ESA's Herschel Space Observatory, currently our biggest instrumentation project and due for launch in 2008, has begun in fall 2006 (see selected article).

Development of GaAs far-infrared photoconductors, in collaboration with University of California Berkeley, Lawrence Berkeley National Laboratory and Naval Post-graduate School in Monterey came to an intermediate point of completion. The requested purity of the material could be achieved with the liquid phase epitaxy centrifuge system, but recent technology progress with chemical vapour deposition suggests replacement by this technology enabling the growth of larger wafers and aiming for the required low concentration of minority carriers.

The far-infrared integral field spectrometer FIFI-LS for the US/German airborne observatory SOFIA has seen first light in the laboratory for its long wavelength channel. Tests suggest sensitivity consistent with the expectations. After a period of intense budget discussions on the US side, the SOFIA project is entering its test phase with scientific operations expected for 2009.

We are studying spectrometer concepts, cryo-mechanisms, detectors, and science case for a next generation far-infrared imager and spectrometer. This 'European Science Instrument' ESI may be contributed by a European consortium to the fully cryogenic infrared space observatory SPICA, with 3m mirror diameter, that is under study by the Japanese Space Agency.

A New Star Shines over the VLT

In 2006, we have commissioned our PARSEC laser guide star at ESO's Very Large Telescope. Using the laser guide star and adaptive optics, high spatial resolution observations in the near infrared will for the first time be possible for many important celestial objects.

Adaptive optics (AO) is a powerful technique that corrects blurring due to atmospheric turbulence, thereby providing extremely high spatial resolution. This uses the full potential of modern large telescopes. AO already makes a significant impact in many areas of infrared astronomy: from the Galactic Center, to nearby active galactic nuclei, and even high-redshift galaxies. But its greatest limitation is the need for a bright star near the science target, which is a rare occurrence. The Laser Guide Star Facility for the 8-m Yepun telescope at the

layer of sodium atoms fluoresce at a height of 90 km in the atmosphere. The whole system has to be very stable, running for a whole night with little adjustment. And a considerable degree of remote control and automation has to be incorporated so that it can be operated from the Control Room of the VLT by staff with no expert knowledge of lasers.

We started the project in the autumn of 2000, and 18 months later the design concept was approved in a laser selection test of the prototype. Then in March 2004, PARSEC was granted Preliminary Acceptance in Europe by ESO. Once testing of the complete LGSF was concluded, the entire system was shipped to Paranal Observatory in Chile, where it was installed. The system was commissioned during 2006, and service mode operation for guest observers will begin early in 2007.

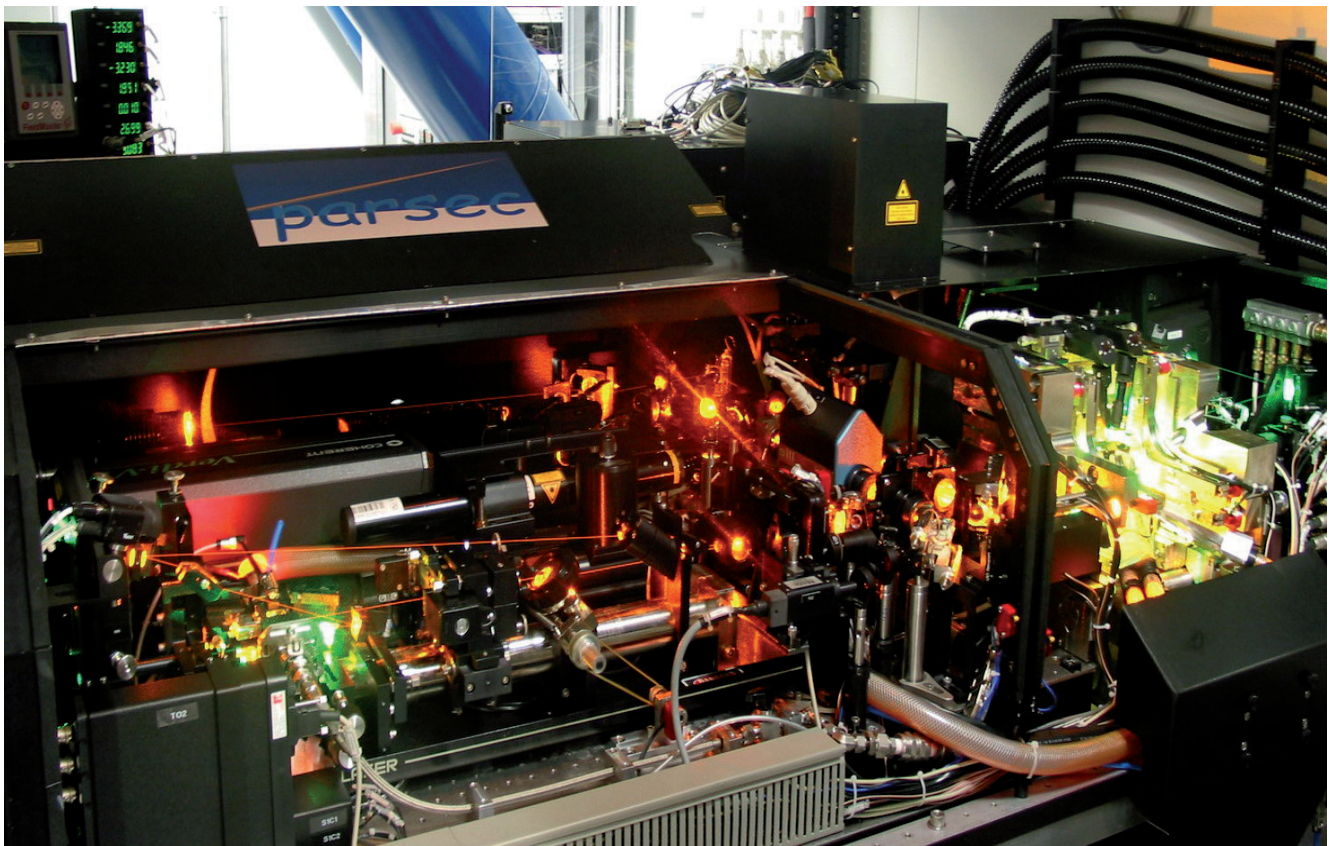


Fig. 1: The PARSEC laser installed in the Laser Clean Room under the Nasmyth platform of UT4 at the VLT.

ESO's Very Large Telescope (VLT) is designed to address exactly this issue by creating an artificial star anywhere in the sky where needed. The PARSEC laser - designed and built at our institute - forms the heart of this system which is currently operational at Paranal Observatory.

From its outset the PARSEC project posed substantial challenges. The laser has to produce a high quality laser beam with a power of at least 10 W and the wavelength of the emitted light has to be exactly right to make the

To minimize the development risk, we based the design on an innovative use of well known dye laser technology. A commercial ring laser acts as a master laser, producing a low power 2 W single frequency and single mode beam. The gain medium for the laser is a liquid dye solution, which is pumped through a 200 μm thick channel in a sapphire nozzle at a pressure of 27 bar. The dye molecules in the resulting jet are excited by a 10 W solid state green laser. The wavelength of the emitted radiation can be tuned by adjusting the length

of the resonant cavity. This wavelength is locked to a sodium cell. Detection of a fluorescence signal from the cell guarantees that the atmospheric sodium will also fluoresce, hence creating the laser guide star.

The beam from the master laser is used to seed the power amplifier. The amplifier has a novel symmetric 3-dimensional design with 2 dye jets. In contrast to standard planar lasers which need corrective optics to compensate astigmatism, the amplifier cancels astigmatism by design. In addition, no frequency selective optics are needed, therefore the cavity is extremely efficient. The highest output power measured is 24 W and its length is maintained to an accuracy better than 1 nm.

The position of the laser beam is stabilised to within a few microns using active steering mirrors. Additional control loops maintain the alignment of both the master laser and amplifier. And numerous diagnostics are able to monitor the power, quality, and polarisation of the beam.

Another novel aspect of the laser is its LIDAR mode which provides the ability to measure the height and density profile of the sodium layer. Variations in this layer, where the laser guide star is created, have a crucial impact on the focus of the wavefront sensor, and how efficiently it must be controlled. In addition, it may affect the size of the laser spot - with a narrower layer being associated with a smaller spot size. This in turn impacts the quality of the adaptive optics correction.

PARSEC is now operating at Paranal Observatory, where it is installed in a dedicated Laser Clean Room. The generated beam is fed into a single mode photonic crystal fibre, which takes it to the 50-cm launch telescope mounted behind the secondary mirror of the 8-m telescope. From there it can be projected anywhere in the sky, creating a bright artificial star which is used by AO systems of NACO and SINFONI.

The possibilities offered by the Laser Guide Star Facility have generated a great deal of excitement within the community, and the response to the first calls for proposals was overwhelming. The hope is that near infrared astronomy is poised on the brink of a revolution.

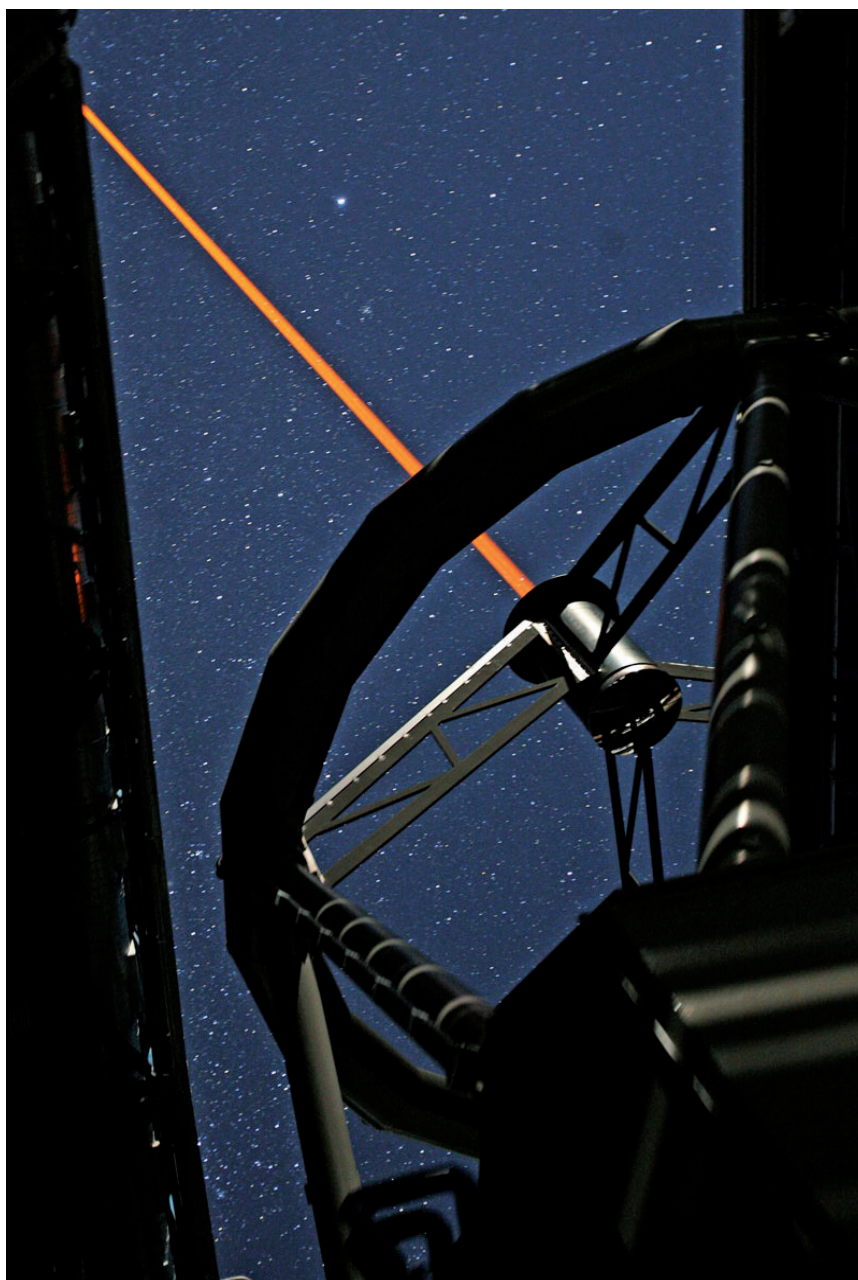


Fig. 2: The laser beam produced by PARSEC, projected from the Launch Telescope mounted behind the secondary mirror of the 8-m telescope Yepun.

The future is bright. The future is orange.

Key players in the PARSEC project currently at MPE: R. Davies (project manager), S. Rabien (laser physics), T. Ott (software), S. Kellner (electronics), S. Huber (mechanics).

Getting Ready for L2 – Final Integration and Tests of Herschel-PACS

Final laboratory tests are well advanced for our PACS instrument, to be launched with ESA's Herschel Space Observatory in 2008 and sent to the Sun-Earth Lagrange point 2 (L2). PACS will offer unprecedented capabilities for imaging and spectroscopy at far-infrared wavelengths, with a wide range of applications from searches for forming stars to resolving the cosmic infrared background.

The Photodetector Array Camera & Spectrometer (PACS) for ESA's Cornerstone Mission "Herschel" is the largest project that we at MPE presently are pursuing. The reason for investing a good fraction of our institute resources in such an endeavour is easily seen from a brief look at the spectrum of the Cosmic Background (Fig. 1). In the far infrared the Cosmic Background has a peak around 150 μm . Here as much energy is reaching us than in the sum of the UV, optical, and near IR, i.e. many cosmic sources contribute to this emission. One of the central

cooled 3.5m telescope and the large format detector arrays in our instrument, will - for the first time - provide the mapping sensitivity and angular resolution to achieve this goal. We expect much improved insights in the history of star formation and galaxy evolution from *photometric surveys* at these wavelengths and from *complementary spectroscopic investigations*. The far-infrared hosts a good set of highly diagnostic lines, which are accessible with no or little extinction from interstellar dust.

With this strong scientific motivation in mind, MPE took on the leadership in a large European consortium of 15 partner institutes and their industrial contractors to build and operate PACS, one of three focal plane instruments aboard Herschel. The instrument covers two slightly offset fields of view in the telescope focal plane; a larger one for imaging photometry in 3 bands around 70 μm , 110 μm , and 170 μm , and a smaller one for imaging spectroscopy between 57 μm and 210 μm .

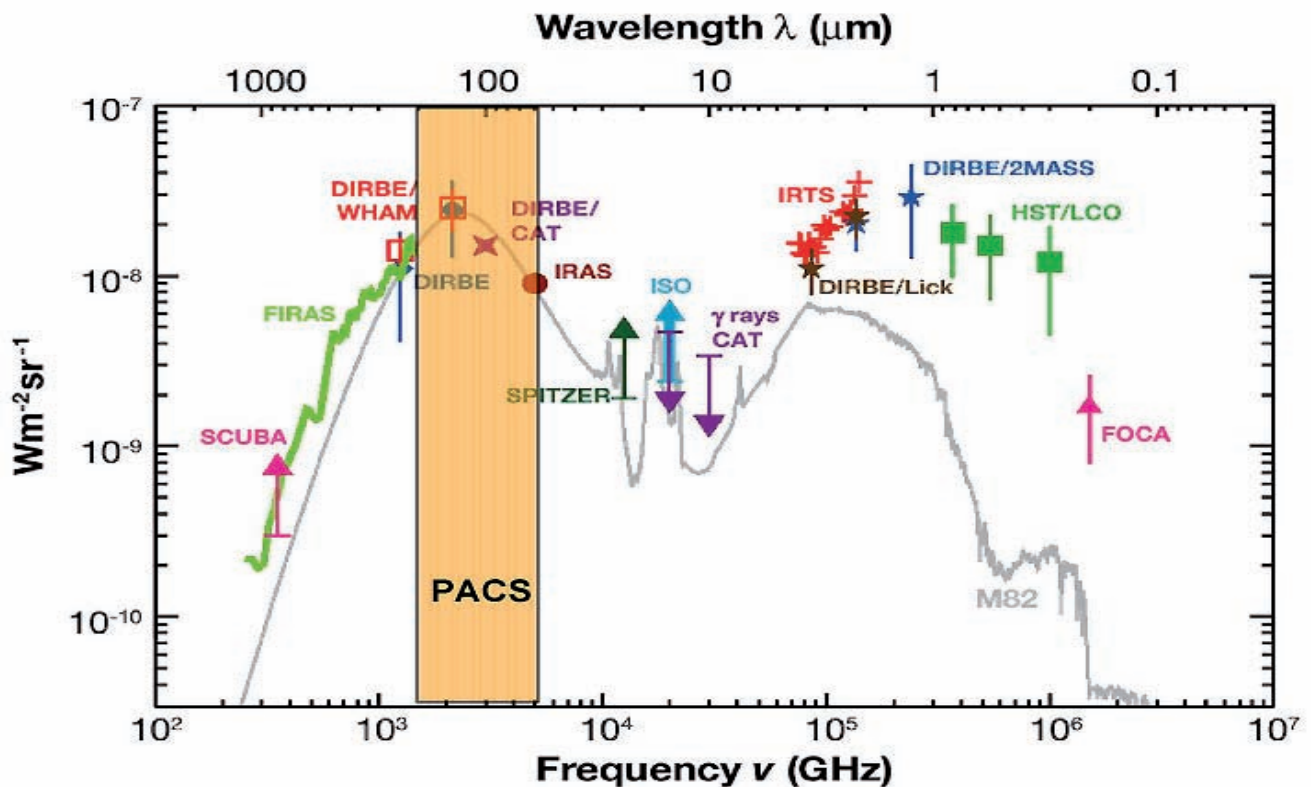


Fig. 1: Spectrum of the Cosmic Background from the mm- to the UV-band. The wavelength range observable with PACS is indicated.

tasks for PACS on HERSCHEL will be to estimate the contributions of different source types to this emission. Probably it consists mostly of re-processed light from stars and/or nuclear activity in galaxies that are heavily obscured by dust. Herschel (Fig. 2), with its passively

The spectrometer field of view is fed into an integral field unit, which re-arranges the field into a long slit at the entrance to a grating spectrometer. The resulting spectra are sorted by grating order and detected with two 25x16 pixel germanium photoconductor arrays.

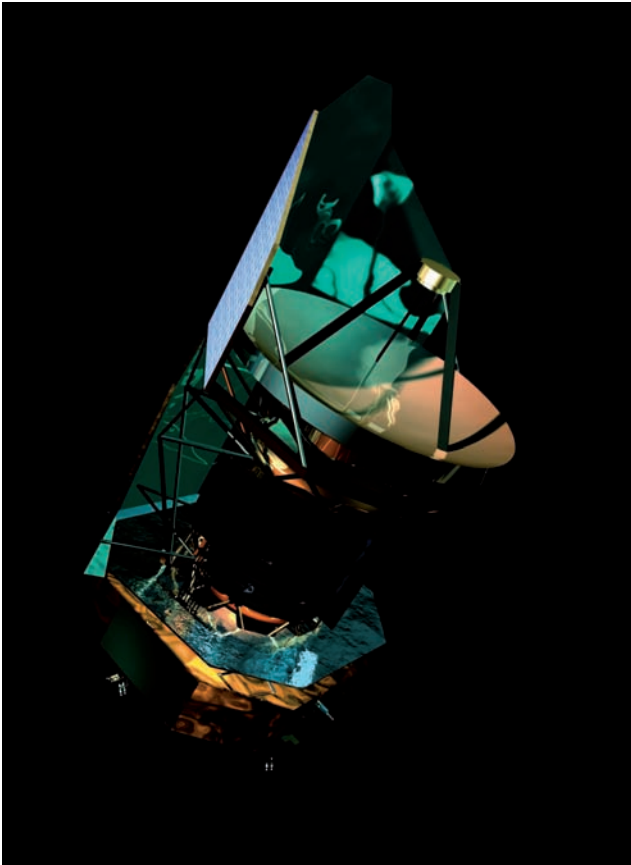


Fig. 2: An artist's view of the Herschel Space Observatory.

The photometric field of view is re-imaged onto two filled bolometer arrays, one for the $170\ \mu\text{m}$ band, with 32×16 pixels, and one for the $70\ \mu\text{m}$ and $110\ \mu\text{m}$ bands, with 64×32 pixels - small compared to any current optical/near-infrared detector, but the largest array ever built for the far-infrared, and sufficient to provide adequate beam sampling over the PACS field of view.

Detectors and the complex optics of this combined photometer/spectrometer instrument are part of the Focal Plane Unit, which also contains calibration sources, filter changers, the grating with its drive mechanism, and a chopper mirror.

After eight years of instrument development, the PACS team at MPE entered into the final phase of the Flight Model assembly, integration and testing. What started out as

a carefully orchestrated effort between all partners required a lot of on-the-spot modifications of the original planning in order to cope with delays and difficulties encountered in many places (as one should expect for a system with the complexity of PACS). One major milestone was the cryovibration test in July/August. After a close inspection upon return to MPE and a last-minute filter exchange we were glad to finally close the lid on the Focal Plane Unit on August 29, 2006. After the integration of the Focal Plane Unit with the test optics in the test cryostat and the connection to the warm electronics units - partly supplied by our collaborators - we started our instrument level test, which will continue until the delivery of PACS to ESA in early 2007.

The test laboratory at MPE with its big test cryostat (Fig. 3) allows us to verify the operation of the instrument in a satellite-representative environment and to measure all relevant performance parameters, like image quality, spectral resolution, and system noise. The campaign to date has demonstrated that PACS can operate and perform as designed and predicted; the beam shapes of our diffraction-limited optics are as calculated, the spectral resolution measured at several wavelengths with the help of a far-infrared laser is nominal, and the detector noise in the system is as measured at subsystem level. However, some problems in the on-board software and with the hardware remain to be fixed before PACS can travel aboard Herschel to its final destination, the Sun-Earth Lagrange point 2 (L2) at a distance of about 1.5 million kilometres from Earth.

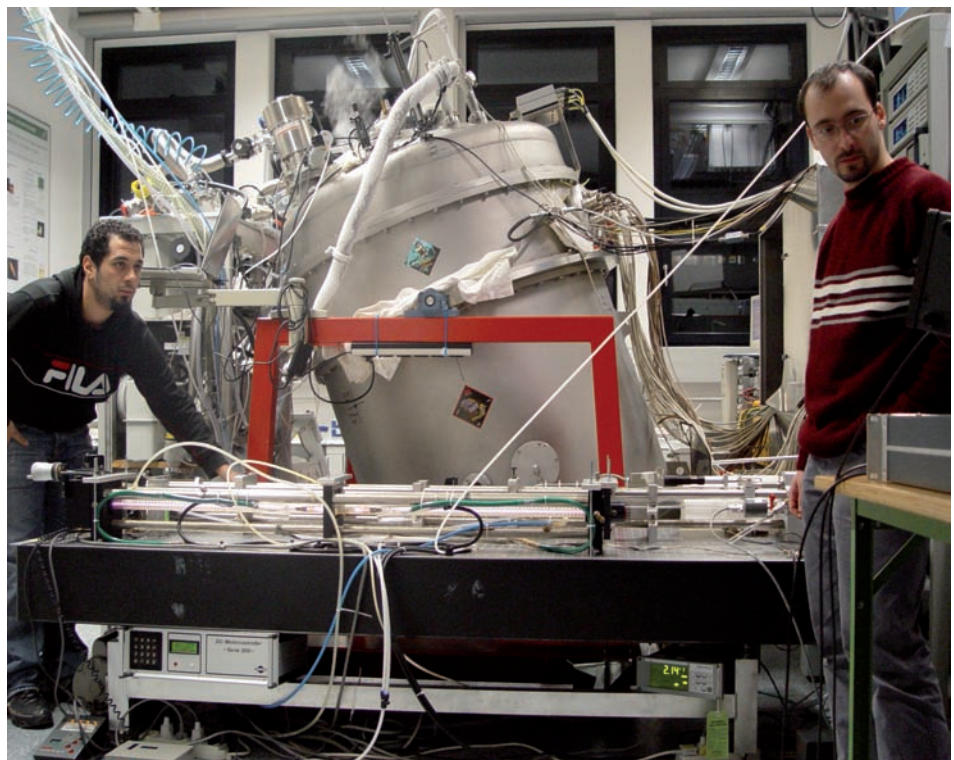


Fig. 3: For laboratory testing, PACS is mounted together with calibration units in the big cylindrical cryostat in the center. Additional calibration signals, here far-infrared laser emission, can be injected from outside the cryostat.

3.3 HIGH-ENERGY ASTROPHYSICS

Projects in X-Ray Astronomy

The X-ray group at MPE is on the one hand dealing with the development of X-ray instruments for future astronomy projects, and on the other hand with the scientific analysis of X-ray data. This year we undertook major steps in the design of new telescopes and the development of CCDs for eROSITA (see selected article). Studies for Simbol-X and the ESA mission XEUS (see below) continue. Currently the scientific data is largely collected by the two main X-ray observatories in orbit: XMM-Newton and Chandra. We were strongly involved in the development, testing and calibration of instrumentation for both missions and are still performing the in-orbit calibration of the EPIC-pn camera onboard of XMM-Newton.

Our archive of Chandra low-energy transmission grating spectrograph (LETGS) data was reprocessed and extended with better quick-view images for all publicly available data sets. Ongoing calibration of the low-energy end of the LETGS yielded an improved effective area for the instrument.

To develop astronomical data bases and their access in a more general way we are involved in the GAVO (German Astrophysical Observatory) and AstroGrid projects. We worked on the implementation of data access protocols for datasets at MPE, in particular a spectral access protocol for optical follow-up spectra of X-ray sources and an image access protocol for the ROSAT pointed observations and all-sky survey fields. The contributions to the AstroGrid-D project were concentrated on Clusterfinder, an algorithm which combines information from optical and ROSAT surveys to identify clusters of galaxies.

The X-ray group operates the X-ray test facilities PUMA and PANTER which are used to measure new detectors for X-ray astronomical applications, and also to characterize new X-ray optics. In the past year there have been several highlights concerning the calibration of X-ray mirrors. For the first time tandems of pore optics were measured, which could be used e.g. for the XEUS mission. These are built up of silicon plates (as used in semiconductor applications) and excel in a low mass to area ratio. Moreover, first samples of glass pore optics were characterized at the PANTER test facility, which are even lighter and could be applicable for BepiColombo, a possible ESA mission to Mercury. Finally, multilayer mirror shells were calibrated, which show high reflectivities in the hard X-ray band and are thus relevant for the Simbol-X mission.

In the context of future lightweight segmented mirror systems for large X-ray telescopes we extended our studies of the glass slumping technique by own experimental work. In a special furnace built up for this purpose we

manufactured thin-walled Wolter-I mirror segments from glass and, for the first time, documented the temporal progress of the slumping process by imaging. The goal is to find a connection between the process parameters and the imaging quality of the manufactured mirrors thus being able to optimize the slumping procedure.

The high energy X-Ray satellite Simbol-X, a European collaboration (France/Italy/Germany), is currently in a Phase A study. The project aims at two goals: the verification of the formation flight of two satellites and to observe celestial targets up to an energy of about 100 keV at an unprecedented sensitivity. The plan is to build two satellites: a mirror satellite with a Wolter-type telescope of 100 nested mirror shells, and a detector satellite with a sandwich-detector for the energy band from 0.5 to 100 keV. Our contribution is twofold: the test and calibration of the mirror module, and the development, test and calibration of the low-energy pixel detector.

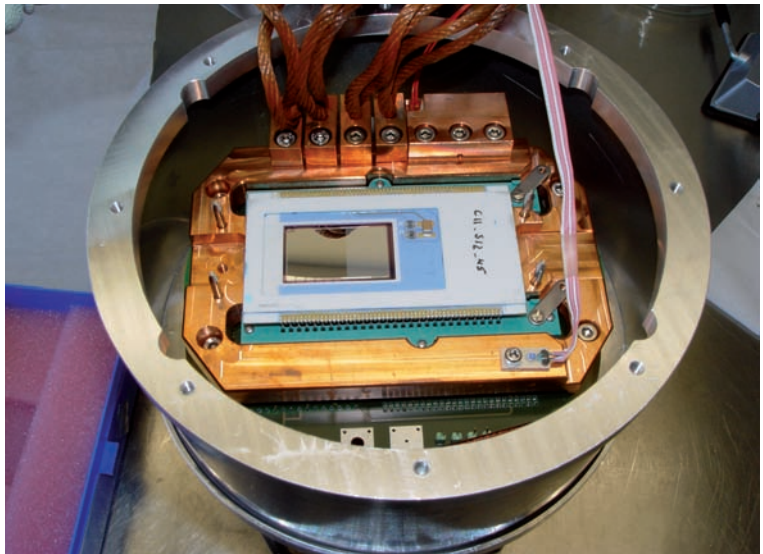


Fig. 1: The PANTER test facility was equipped with a new imaging detector, a 2cm x 2cm framestore pnCCD camera with 75 μm pixel size. The view into the camera housing shows the CCD mounted on a ceramic board.

At CERN the Axion-Helioscope CAST (CERN Axion Solar Telescope) is still in operation. It tries to detect so-called solar axions which might be produced in the core of the Sun. During the first period finished in 2004, the CAST experiment was sensitive to axions with a mass of $m_a < 0.02$ eV. During 2006 we reconstructed the experiment to a new setup which allows to extend the sensitivity range up to an axion mass $m_a < 0.3$ eV. In 2007 CAST will be transferred to a new configuration allowing to be operated with ^3He . This will further extend the sensitive mass-range to $m_a < 1.1$ eV. A significant signature of an axion signal could not yet be detected.

The X-ray Observatory XMM-Newton

Seven years after launch XMM-Newton continues to provide a wealth of scientific data. The X-ray group is strongly involved in the in-orbit calibration of the EPIC-pn camera and developed methods to improve the data quality.

XMM-Newton, the European X-Ray satellite, is now in orbit for more than seven years. XMM-Newton is a cornerstone project in the ESA Horizon 2000 programme and is the biggest science satellite ever built in Europe. Imaging cameras (EPIC) together with high resolution spectrographs behind three X-ray telescopes observe the X-ray sky simultaneously. Its mirror system was designed for a large collecting area in order to address many cosmic mysteries of the violent Universe. The

of the three XMM-EPIC CCD chips (the pn-CCD). Since the launch of XMM-Newton in December 1999, we are responsible for the maintenance and in-orbit calibration of the pn-camera and for several tasks within the XMM-Newton Survey Science Center.

As an example of our work on the performance of the pn-CCD, we show in Fig. 1 the results of a method we have developed for improving the data quality. This method restores the spectral information in specific pixels which were disturbed by the passage of energetic particles, and suppresses potential noise events on a statistical basis, utilizing an empirical model of the spatial and spectral properties of the noise. In the example shown in Fig.1, two thirds of the original events at

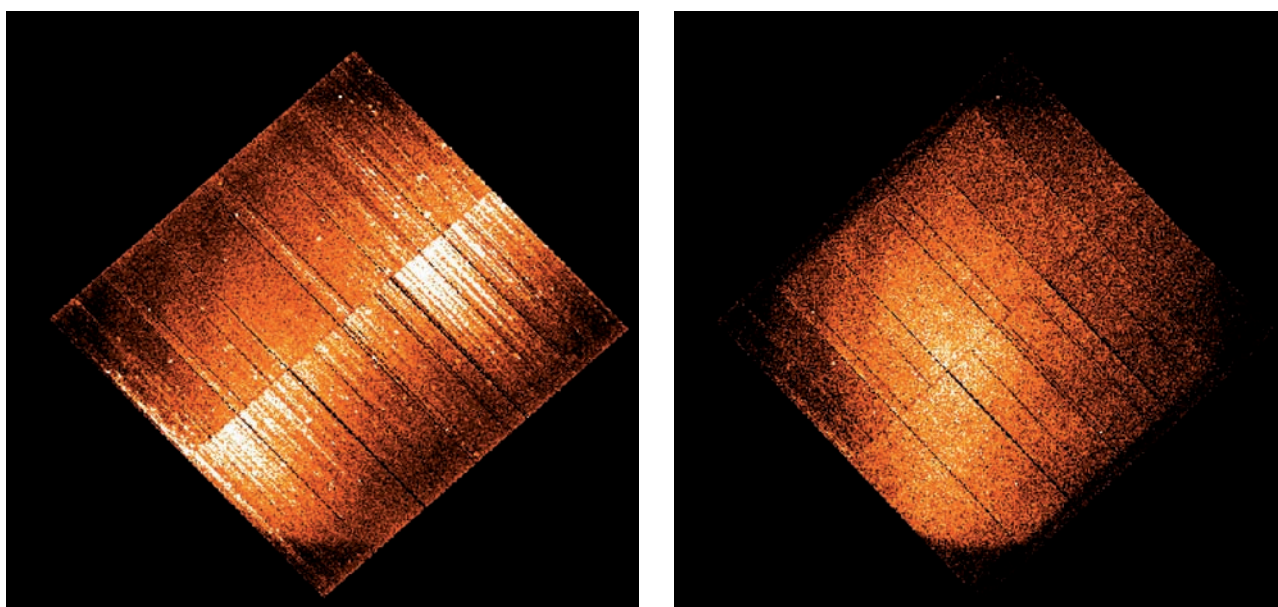


Fig. 1: XMM EPIC-pn images of part of the Vela Supernova Remnant, before (left) and after (right) applying the corrections. For these images, only the lowermost energy channels were selected, covering the instrumental energy range 120 - 200 eV. The correction reveals the presence of diffuse soft X-ray emission which was previously hidden in the detector noise.

high sensitivity allows us to investigate the early history of the universe, the formation of galaxies and active galactic nuclei which are powered by super-massive black holes. With XMM-Newton we can probe the extreme environments of black holes and neutron stars, the endpoints of stellar evolution. XMM-Newton is one of the most successful scientific satellite missions. By now, more than 1300 refereed scientific papers have been published. Our institute was involved in about 25% of them.

We at MPE were and still are significantly involved in this project, in the development, test and calibration of the three X-Ray mirror modules and, on the detector side, our Semi-Conductor-Laboratory developed one

120 - 200 eV were suppressed due to detector noise. While these corrections are most evident in images accumulated at low energies, the spectral quality is improved throughout the full spectral range.

After seven years of smooth operation of the EPIC-pn camera the in-orbit calibration of the spectral detector response reached a high level of accuracy. The main emphasis in the calibration concentrates now on the cross-calibration of the various instruments on board of XMM-Newton which simultaneously observe the same area of the sky. This cross-calibration work of high-energy instruments will be extended to other high-energy satellite missions, like INTEGRAL.

The future X-Ray Telescope „eROSITA“

Over the last year eROSITA passed a number of major milestones in the definition and funding of the instruments. The launch on the Russian satellite mission Spectrum-Röntgen-Gamma is planned for 2011. During four years of all-sky survey, eROSITA will detect about 100.000 clusters of galaxies. From the study of their large-scale distribution we will learn more about the origin, geometry and dynamical evolution of our Universe.

A medium size Russian satellite called „Spectrum-Röntgen-Gamma“ (Spectrum-RG or SRG) is planned for launch in 2011 (Fig. 1). A Soyuz-2 rocket will carry the satellite from Baikonur/Kazakhstan into a 600 km orbit with 30° inclination. Besides eROSITA („extended ROentgen Survey with an Imaging Telescope Array“), the payload includes the wide field X-ray monitor LOBSTER (Leicester

eROSITA will test cosmological models to assess the origin, geometry, dynamics, and the growth with time of our Universe via the study of the large-scale structure in the matter distribution. Galaxy clusters are ideal tracers of the large-scale structure. The amplitude and shape of the cluster power density spectrum, and its growth with time, depend sensitively on Dark Matter and Dark Energy. During the four years lasting all-sky survey, eROSITA will detect about 100 thousand clusters of galaxies. This sample size is necessary for example to precisely characterize the cluster mass function and power spectrum in at least ten redshift bins, to follow the growth of structure with time. Baryonic wiggles due to the acoustic oscillations at the time of recombination are still imprinted on the large scale distribution of clusters and thus can give tight constraints on the curvature of

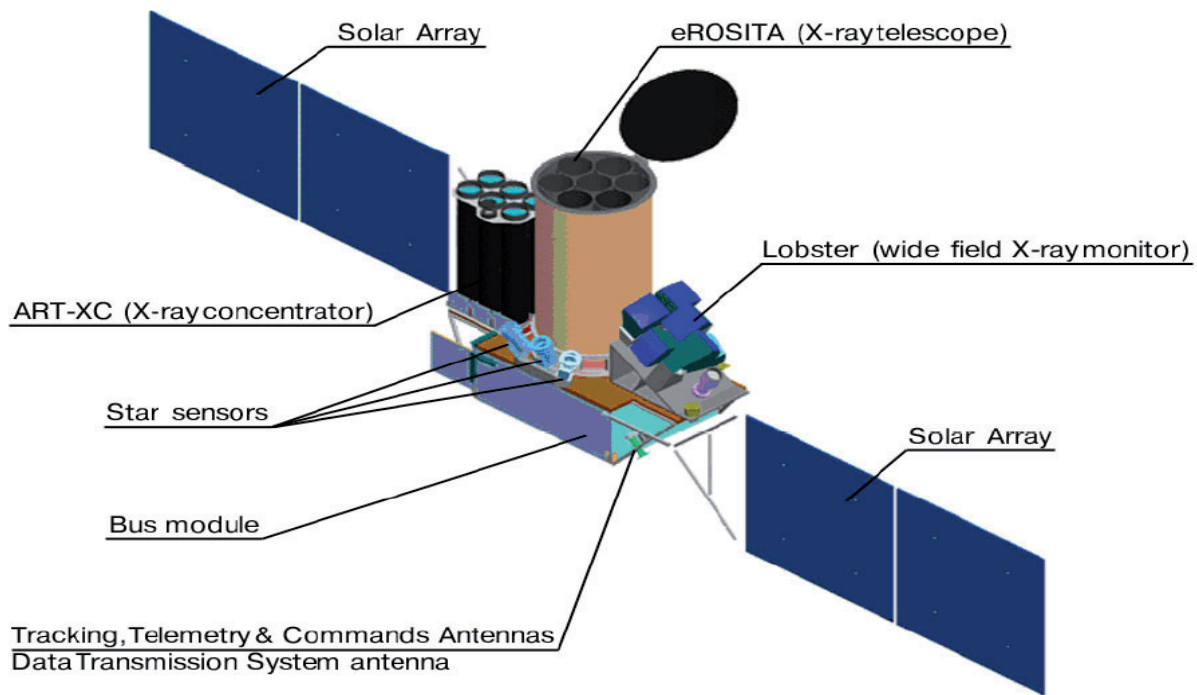


Fig. 1: Preliminary design of the Spectrum-Röntgen-Gamma mission. The different instruments, including eROSITA, are shown.

University), the X-ray concentrator ART („Astronomical Roentgen Telescope“, IKI, Moscow) and a gamma ray burst detector built by a Russian consortium.

On its way of getting approved and funded by the German Space Agency (DLR), eROSITA has passed a series of milestones, making a funding and realisation of the mission very likely. In 2006 we concentrated on designing a concept for the telescope structure which is able to fulfil the requirements regarding stiffness, stability and weight. Furthermore, the cooling of the CCDs down to - 80°C turns out to be a challenging task in a low-earth orbit when using passive means only.

space at different epochs. A statistics of at least 50,000 to 100,000 clusters is necessary to reveal the baryonic oscillations in the cluster distribution power spectrum.

The eROSITA flux limit of the survey in the 0.5 to 2 keV band will be $\sim 4 \times 10^{-14}$ erg s⁻¹ cm⁻² (an order of magnitude deeper than the ROSAT Survey) over most of the sky and about ten times deeper in the poles of the survey scan pattern. At this flux the X-ray sky is dominated by clusters and AGN, which can be separated with an angular resolution of 25 arcsec.

The detection of all (including obscured) AGN in the local Universe is one of the main goals of the new eROSITA

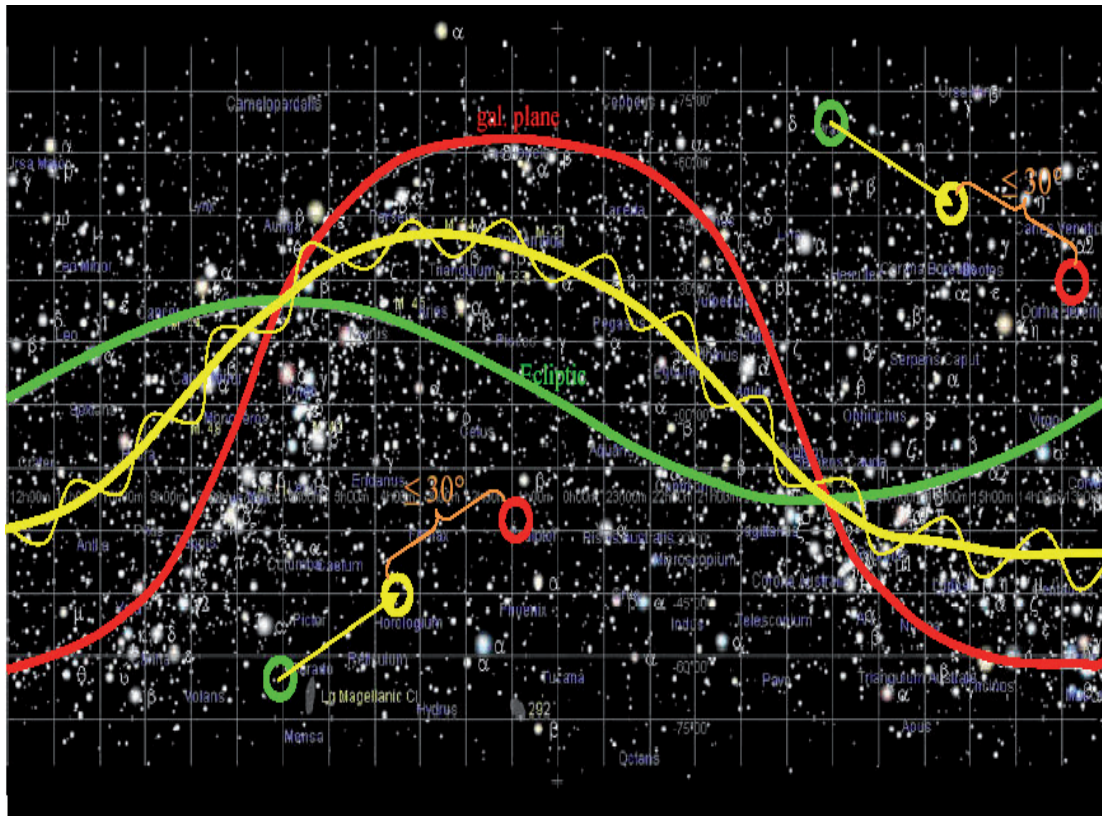


Fig. 2: Galactic equator and poles (red line and circles, respectively) and ecliptic equator and poles (green), and the scan geometry (yellow).

instrument. Many hidden, but still very active black holes should be lurking in rather nearby galaxies, waiting to be detected by a hard X-ray survey. We expect to detect more than three million AGN with eROSITA.

In addition there are other science goals which can be studied with eROSITA like gamma-ray burst afterglows. They will be observable for two days after the burst. We expect to detect 600 afterglows during the four years of the all-sky survey.

The scientific goals require a variety of mission phases and observing modes, respectively: (1) an all-sky survey, i.e. a continuous scan with one revolution per orbit, (2) an extragalactic survey (20,000 square degrees outside the Milky Way), (3) a deep Survey close to the galactic poles, where the Milky Way is most transparent and (4) pointed observations on selected individual objects. In order to keep the spacecraft operations as simple as possible, we will combine the three surveys into a single one.

The rotation axis directed towards the Sun would lead to an overlap of all great circles at the ecliptic poles. Tilting the rotation axis towards the galactic plane would automatically give the extragalactic sky a higher exposure, in particular near the galactic poles. A tilt of

$<30^\circ$ away from the Sun seems to be compatible with other constraints, e.g. the minimum Sun angle (Fig. 2).

The mirror system consists of 7 mirror modules with 54 mirror shells each with a diameter of the outermost shell of 360 mm. The inner 27 mirror shells are replicated from refurbished ABRIXAS mandrels, and therefore the focal length (1,600 mm) are kept the same. Unlike on ABRIXAS, the seven optical axes are co-aligned. Since the entire field of view (FoV, $\sim 1^\circ$ diameter) is used for the surveys, the measure for sensitivity is the product of the FoV-averaged effective area and the solid angle of the FoV.

Each of the seven mirror modules has its own CCD camera in the focus. These CCDs are advanced versions of the pn-CCD camera onboard of XMM-Newton: the pixel size is reduced to $75 \mu\text{m}$ square, corresponding to ~ 10 arcsec. The sensitive area is $\sim 3 \text{ cm}^2$ (or 384×384 pixels). A frame-store area is added to the sensitive area which allows the fast shift from the image area in order to reduce so called out-of-time events, photons which are recorded during charge-transfer. The use of 6 inch silicon wafers with $450 \mu\text{m}$ thickness gives higher quantum efficiency at higher energies. We could also improve the low energy response and the energy resolution by modifying the fabrication process.

Projects in Gamma-Ray Astronomy

The gamma-ray group at MPE has been working primarily with data from the ESA-mission INTEGRAL. Our prime scientific interests are in the analysis of nuclear lines (Al, Ti), the global diffuse gamma-ray emission in our Galaxy, the emission from active galactic nuclei and gamma-ray bursts. The two main INTEGRAL instruments IBIS and SPI are providing very significant results, among them the discovery of the galactic Doppler profile in the Al emission (see selected project report).

MPE, in collaboration with the companies Jena-Optronik GmbH (Jena) and Astrium (Immenstaad), has delivered the 14 flight detectors, 12 NaI and two BGO detectors, and the complete electric power supply of the GLAST Burst Monitor (GBM). During the last year the flight hardware was subjected to comprehensive system tests (thermal-vacuum and electromagnetic-compatibility tests) which was led by our GBM-partners at MSFC (NASA) and the University of Alabama (USA). In August 2006, GBM was delivered to Spectrum Astro Space Systems in Phoenix/Arizona, where the integration of the GBM detectors to the GLAST satellite started. In autumn 2006 a BGO detector was calibrated at high gamma-ray energies using a Van-de-Graaf accelerator in Stanford/California, extending the previous calibration (15 keV - 6 MeV). The GBM, together with the Large-Area Telescope (LAT), will measure the spectra of gamma-ray bursts (GRBs) over more than six energy decades. From these measured spectra we expect new insights into the complex emission process of the gamma rays, especially about the high-energy emission above 100 MeV which is not yet understood.

Swift, launched in November 2004 and successfully operating since then, has measured more than 200 gamma-ray bursts. MPE participated in the project with the calibration of the X-ray telescope at the PANTER facility. In addition, we supported the mission operations by participating in the so-called Burst Advocate scheme (with the group at Leicester/UK). Our prime science interest is in the follow-up observation of Swift-detected GRBs, and the all-sky survey of the Burst Alert Telescope in the 14 - 170 keV band.

GROND (Gamma-Ray Burst Optical and Near-Infrared Detector) is a 7-channel imager for follow-up observations of gamma-ray bursts, and is nearing its completion in the lab at MPE. We performed a variety of system tests and aligned all optical components and 7 detectors. Also, substantial preparatory work was carried out on the MPI 2.2m telescope at ESO La Silla (Chile) where GROND will be commissioned in 2007. The prime scientific objective is to rapidly measure the redshift of GRB afterglows to allow dedicated follow-up spectroscopy with the VLT

within the same night.

OPTIMA is a high-time resolution photo-polarimeter, which is able to determine instantaneously the state of linear polarization of highly time variable optical sources. The primary goal for this instrument is to observe linear polarization in the early optical afterglow of gamma-ray bursts. High-energy objects like cataclysmic variables, BL Lac AGN and optical pulsars are also of interest. We have used the new integrated system of detector and telescope control, called 'OPTIMA-Burst', during a long campaign at the Skinakas Observatory (SKO), Crete, Greece from June 25 to September 28, 2006. Although we did not receive a suitable GRB trigger from Swift (2 - 3 were expected), extensive photo- and polarimetric observations of CVs and coordinated measurements of optical and TeV emissions (with HESS and MAGIC) of BL Lacs were performed.

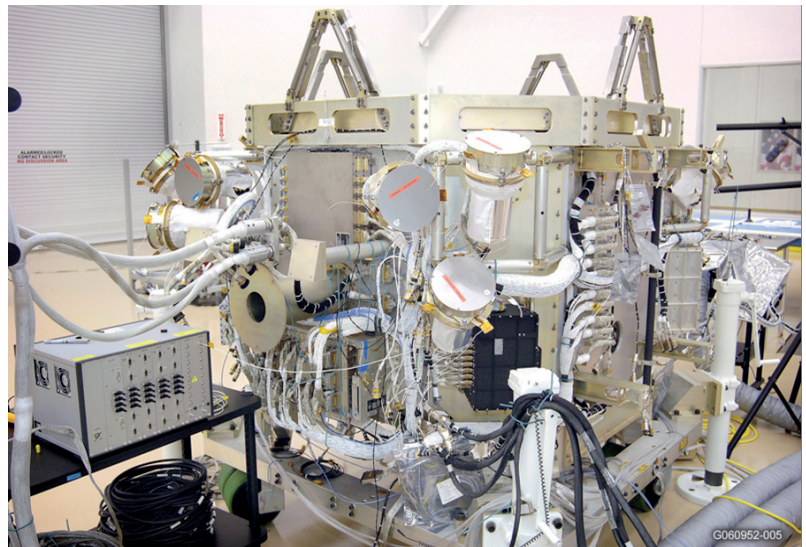


Fig. 1: The GLAST Burst Monitor is integrated on the GLAST spacecraft. Six cylindrical sodium iodide detectors (red labels on the detector cover) and the power box (black box) are visible on the image.

In 2005 we started to develop very efficient pnCCDs for fast imaging of single photons in the visible/near-IR range (350 - 1100 nm). This project is part of the EU funded consortium OPTICON and aims to develop new technologies for high-time resolution astronomy. The essential modifications of the 'classical X-ray' back-illuminated pnCCDs with column parallel readout are the application of a wide band optical anti-reflective coating on the entrance window and the on-chip implementation of avalanche amplifiers operated in the linear regime with amplifications up to a few thousand. The frame rate should be as high as 1.000 frames a second. The first fabrication tests of the avalanche structures are finished and show the expected good results with respect to leakage current, onset and stability of the avalanche process, and in the response to injected photons.

The INTEGRAL Observatory Mission

INTEGRAL is a medium-sized space mission of ESA for high-energy astrophysical observations in the supra-thermal energy range (15 - 8000 keV). It was launched in October 2002 for a nominal mission duration of 3 years. With excellent performance of all components and its scientific success, ESA decided quickly to extend operations of this mission. At present, the mission is funded till end of 2010.

INTEGRAL features two main telescopes, an imager with unprecedented imaging resolution (arcmin) in this energy domain, and a spectrometer with unprecedented spectral resolution adequate for nuclear-line spectroscopy. Monitoring instruments for X-rays, the optical sky, and background radiation complement these main instruments. INTEGRAL's high-excentricity 3-day orbit reaches out to 150000 km, chosen to minimize instrumental background from cosmic-ray activation during radiation belt passages. Belt passages at perigee,

~100°C for several days. This annealing procedure has now been applied eight times, with great success. The spectral resolution of the SPI spectrometer instrument is maintained at the level required for this unique fine spectroscopy of nuclear lines.

In its first mission years, INTEGRAL revealed new aspects of the Galaxy and its sources: The penetrating power of gamma-rays showed that accreting binaries are embedded inside dense interstellar clouds, young pulsars with high magnetic fields found to have tails of substantial high-energy emission.

The Galactic ridge seems to contain a yet-unidentified source population with rather high-energy dominated spectra. The emission from annihilation of positrons was seen by the spectrometer as surprisingly concentrated in a bright bulge. The imaging properties of the spectrometer allowed to see the signature of Galactic rotation in Doppler shifts of ^{26}Al line (Fig. 1), the ^{60}Fe

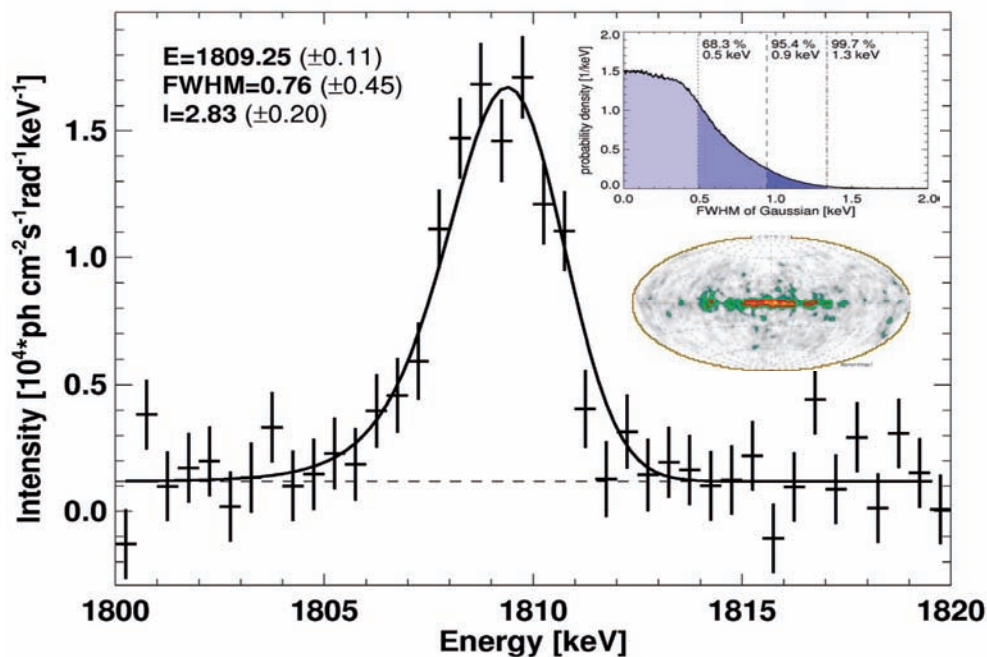


Fig. 1: SPI measurement of the ^{26}Al line profile. Doppler broadening from interstellar gas motions is constrained to below ~1 keV or 130 km s^{-1} (see insert).

but more so the solar and Galactic high-energy particles, are responsible for the still high instrumental background level typically constraining γ -ray instruments. Cosmic ray bombardment degrades the charge collection properties of the Ge semiconductor elements which are the core of the spectrometer. For the first time in space, therefore, an annealing procedure had been devised to cure these defects in the crystal lattice by heating detectors from their cryogenic operating temperatures to

from massive stars, and also from ^{44}Ti in the Cas A supernova remnant, have been seen, and are puzzling in view of conventional theories of massive-star structure and core-collapse supernovae, respectively. INTEGRAL's measurements of hard-X/soft γ -ray emission from AGN also helps to understand these sources and their contributions to the diffuse hard X-ray background. MPE is Co-I institute of the spectrometer SPI.

The MPI Halbleiterlabor – Silicon Detectors for High Speed Imaging

The MPI Halbleiterlabor (MPI-HLL) was founded in 1992 in a joint effort of the MPE and the Max-Planck-Institut für Physik. It is the aim of the MPI-HLL to develop innovative semiconductor detectors, commercially non-available, for the experiments of the institutes.

For the MPE astrophysics mission eROSITA our activities focused on the design, fabrication and testing of the pnCCD camera. The work is well under way and in agreement with the project schedule. The second priority is development of the macropixel monolithic active pixel sensors (APS) based on DEPFETs (Depleted P-channel Field-Effect Transistor) for the X-ray spectrometer on ESA's BepiColombo mission and the low energy detector (0.5 keV to 20 keV) on the French-Italian SIMBOL-X mission. Both telescopes rely on the XEUS detector technology and represent a helpful intermediate step towards the anticipated ESA mission XEUS. A new fabrication of DEPFET arrays, 16 times larger than the previous detectors will help us to continuously approach the final XEUS flight type devices with more than 10^6 pixels.

As the optical properties of the pnCCDs are outstanding (high quantum efficiency from 300 nm to 1150 nm, no fringing, high speed, low noise etc.) they are now being tested as wave front sensors for adaptive optics systems in cooperation with ESO. For high time resolution astrophysics experiments we currently develop an avalanche amplifier, on-chip coupled to a MOSFET (Metal Oxide Semiconductor Field-Effect Transistor). Operated in a linear mode, this concept enables us to achieve single photon counting capabilities in the optical. All columns of the pnCCD are terminated by one avalanche amplifier, allowing us to keep the readout speed high. Another technique to operate at very low noise is the repetitive readout of the same signal charge. At temperatures around -40°C the best measured noise is already below 0.2 electrons (rms) – the world record in low

noise performance in linear amplifier systems.

After the tremendous success of the Mars rovers Spirit and Opportunity (NASA), equipped with Silicon Drift Detectors (SDDs) from the MPI-HLL, the follow-on mission EXOMars (ESA) also intends to equip a Mössbauer spectrometer with SDDs. The MPI für Chemie and the Universität Mainz are the main partners. The SDDs are increasingly popular for all kind of spectroscopic applications - scientific and industrial.

The pnCCD test system has equally proven in 2006 its popularity in the scientific community: as a 2D-spectroscopic imager at the BESSY synchrotron and at HASYLAB, as an low energy X-ray imager at the MPI for Quantum Optics, as an electron imager in transmission electron microscopy at the MPI für Biochemie in Martinsried and as an electron detector in channeling radiation experiments at the University in Göttingen.

In 2006 the shape of the new MPG initiative Center for Free Electron Laser studies (CFEL) became more visible. Inside CFEL the MPI-HLL will have its role in developing new instruments for the 2-dimensional intensity measurements of the scattered monochromatic X-rays from 0.3 keV up to 25 keV.



Fig. 1: Mounting and bonding of devices in the semiconductor laboratory.

pnCCD Detector Development for eROSITA

In 2006 the MPI Halbleiterlabor (MPI-HLL) carried out extensive tests with the present pnCCDs, the prototype detectors of the eROSITA mission, before the production of the flight pnCCDs was started. The pnCCD and its analog signal processor CAMEX are based on the concept of the very successful XMM-Newton pnCCD detector, which performs X-ray spectroscopy and imaging since 2000. The eROSITA instrument will be finally equipped with seven identical and independent pnCCD cameras.

The state-of-the-art pnCCD is a 3-phase, back-illuminated charge coupled device with fully depleted chip thickness of 450 μm . The transfer registers and the photon entrance window are realized by boron implantations in ultra-pure n-type silicon. They have to be accomplished ultra-shallow in case of the radiation entrance window

source of the transistor to the input of an analog signal processor channel of the CAMEX ASIC (Application Specific Integrated Circuit). The programmable CAMEX (CMOS Amplifier and MultiPlEXer) allows amplification and shaping of signals in 128 channels in parallel.

The prototype pnCCDs were produced on double-sided polished wafers with 150 mm diameter and $\langle 100 \rangle$ lattice orientation. They have a 2 cm x 2 cm large image area composed of 256 x 256 pixels. For the eROSITA flight pnCCD a larger image area of 3 cm x 3 cm is requested to increase the grasp of the instrument. The new image area, enlarged to 384 x 384 pixels, allows for a field of view of 1° diameter. Since essentially the number of pixels is changed but not the pixel size of 75 μm x 75 μm , its structure or the photon entrance window, the results measured with the prototype pnCCDs

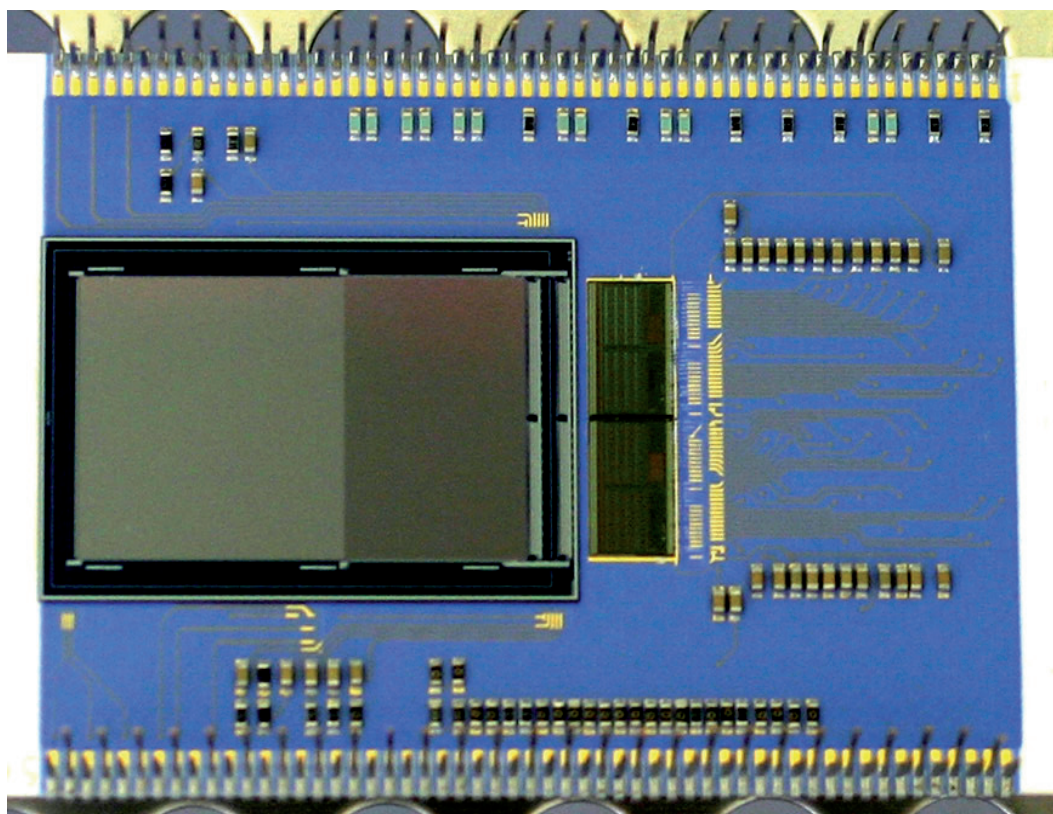


Fig. 1: The figure shows a pnCCD detector used for the measurements in the laboratory to qualify the pnCCDs and the total detector. You see the front side of the large pnCCD chip on the left side and the two adjacent CAMEX ASICs to the right. X-ray photons enter the back-illuminated detector from the opposite side.

(back side) and homogeneous over the entire image area. The quantum efficiency is thus above 90% from 0.3 keV to 11 keV. The charge is transferred in a depth of about 7 μm below the front side. All CCD transfer channels are equipped with an anode and a JFET (Junction Field-Effect Transistor) for on-chip amplification and fast parallel readout of the X-ray signals. A bond wire connects the

should be basically the same as later on for the flight devices.

Layout, production and tests of the devices are carried out in our semiconductor laboratory (MPI-HLL). The aim of the prototype pnCCD tests was to obtain sufficient information about detector performance

with the objective to accomplish a redesign of the eROSITA flight pnCCDs and to start the flight pnCCD production in 2006.

The eROSITA prototype CAMEX was tested at first on wafer level, then as part of the pnCCD detector system. The results were of course again important for the design of flight type ASICs, in particular for the purpose of operation and performance optimizations.

The detector assembly consists mainly of a multi-layer printed circuit board (PCB), two CAMEX chips (and three CAMEX chips finally for the larger eROSITA CCDs respectively) and the pnCCD (Fig. 1).

A data acquisition system (DAQ) as well as analysis software was developed for the experimental test of the CCD detector with CAMEX analog signal processor. The whole setup was appropriate for the laboratory tests, i.e. of course not flight or space qualified but offering the flexibility which is necessary during the development.

The average readout noise of the pnCCD, measured under eROSITA relevant operating conditions regarding temperature (-80°C) and frame rate (20 images/s), amounts to 2.2 electrons rms. This is a decrease of noise by even more than a factor of two compared with the XMM-Newton type pnCCD detector. The number of pixel defects could be further minimized; several pnCCDs showed even no pixel defect at all. The measurements revealed a small non-linearity in energy of the CAMEX amplifier which will be corrected in the redesign of the ASIC. The pixel is by a factor of four smaller compared with the XMM-Newton pnCCD. As a result we obtain mainly split events, which means that the signal electrons generated by an X-ray photon are distributed over up to four pixels. Proper rejoining of the split events is thus necessary for the analysis of energy resolution.

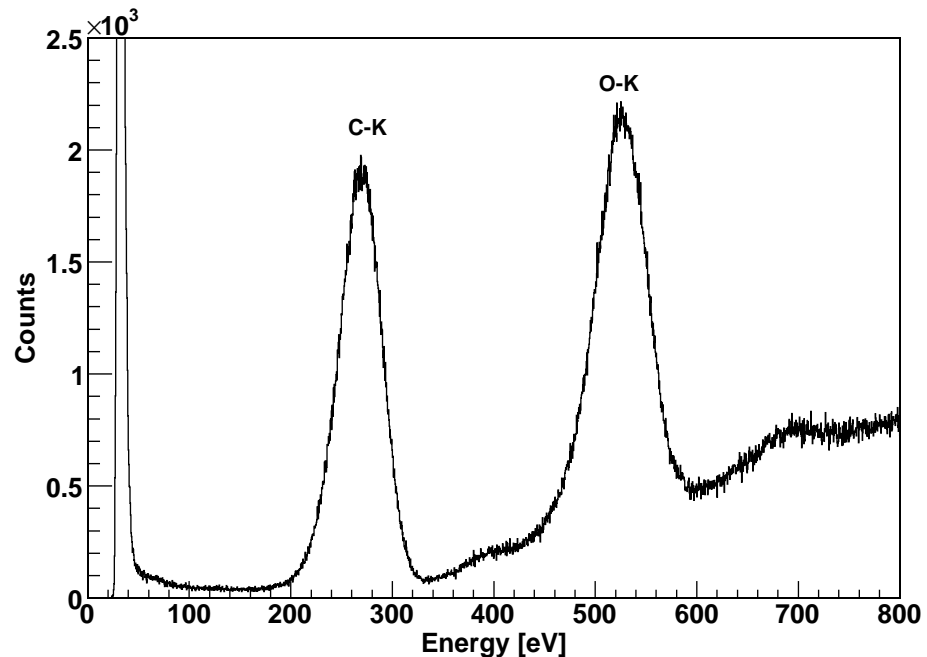


Fig. 2: C-K (277 eV) and O-K (525 eV) spectrum measured with an eROSITA prototype pnCCD in standard frame store mode. The photon entrance window is equipped with the optical and UV light filter, as requested for the operation in space. As operating temperature, we used -60°C (even 20°C higher than planned for eROSITA); the cycle time was set to 50 ms. The spectral lines were generated by an X-ray tube, which causes additionally a bremsstrahlung continuum, in particular at higher energies.

At very low X-ray energies (< 0.5 keV), we measured in contrast to the XMM-Newton pnCCDs an excellent energy resolution, e.g. for the C-K line at 277 eV a FWHM of 50 eV (Fig. 2).

The new pnCCDs allow in contrast to the XMM-Newton type pnCCDs an operation in frame transfer or frame store mode, i.e. to store the previous image during readout in a frame store area on the device. By this operation mode, a smearing of the image in transfer direction is suppressed.

The pnCCD and its analog signal processor CAMEX showed excellent performance in the tests; even better compared to the previous pnCCD detectors including the XMM-Newton pnCCD. Nevertheless, we identified small drawbacks which were addressed in the redesign of both devices. The eROSITA flight pnCCDs and CAMEX ASICs are presently produced.

One of the already tested pnCCD detectors will be applied at the PANTER test facility for calibration of various X-ray telescopes.

3.4 COMPLEX PLASMAS

Complex plasma research is a fast growing field covering fundamental physics with applications in many other fields, e.g. solid state physics or fluid physics. The reason for the latter is that in complex plasmas phenomena like melting can be investigated on the most fundamental, i.e. the kinetic level. This is due to the fact that the crystal or fluid is formed by particles of micrometer size in distances of millimeters in a classical manner by electrostatic interaction. The so-called microparticles can be illuminated by a laser beam and the scattering can be easily observed with CCD cameras allowing us to follow the particles over long time in high precision. This allows us to use the complex plasma as a model system for crystals and fluids. Beside this, the microparticles' charge fluctuations and cannibalism, so-called Non-Hamiltonian effects, add new physics which makes complex plasmas interesting to investigate on their own.

The coverage of a broad phase space of complex plasmas makes it necessary to investigate in different setups, each with different and special features. Therefore we installed many laboratories over the last 9 years, since the experimental group has been established at MPE. Especially during the 5 years of our cooperation with the MPI for Plasma Physics (IPP) within CIPS (Centre for Interdisciplinary Plasma Science), specially funded by the Max Planck Society, new labs could be founded, like the Strong Magnet Lab, a 4 Tesla setup allowing for the first time to investigate the complex plasma in a strongly coupled strongly magnetised regime, or the PAGE lab, a Particle Growth Experiment with the intention to grow diamond particles of very high quality (this is a cooperation with IPP). CIPS could be continued on a smaller scale by the research group "Experimental Complex Plasmas". Other labs were partly funded by DLR, like the Adaptive Electrode and the Cryo lab, and of course, the science labs for the microgravity experiments PK-3 Plus and PK-4.

Microgravity research is a mandatory part of the research of complex plasmas. Microparticles are about 10^9 times heavier than atoms with sizes like dust particles and gravity plays an important role leading to stress and inhomogeneity of the system. Therefore we started the investigation of complex plasmas under

microgravity conditions already quite early in the history of this new research, strictly speaking the idea of the crystallisation of complex plasmas without gravity was the starting point at the Institute. In 1996 the era of research under microgravity started with parabolic flights, followed by two sounding rocket experiments. Since 2001 our Institute has a permanent laboratory on the International Space Station ISS. The latter is a cooperation with the Russian Academy Institute for High Energy Densities in Moscow. PKE-Nefedov was the first long term experiment on complex plasmas on the ISS operational over more than 4½ years. Since January 2006 the follow-up laboratory PK-3 Plus is operational (see selected article).

Even the future laboratory PK-4 is in the pipeline; a Phase A/B study financed by ESA started in the beginning of the year. PK-4, compared to its precursors, will be a fully new developed apparatus. Its main goal is the investigation of the fluid behaviour of complex plasmas,



Fig. 1: PK-4 parabolic flight measurements in Bordeaux during a period of micro-gravity.

like the transition from laminar to turbulent flow or the supercritical fluid and the critical point. The project is based on laboratory developments since 2002 and parabolic flights. The breadboard assembly was flown on parabolic flights in October in Bordeaux. The main goal of this short time microgravity experiments (each of the 93 parabolas provides about 20 sec low-g) was to test technical achievements on its microgravity relevance. Beside the pure technical reason some interesting scientific results could be obtained.

PK-3 Plus – Complex Plasma on the ISS

The operational phase of our Plasma Crystal Laboratory PK-3 Plus on the International Space Station ISS started in 2006 successfully. PK-3 Plus was mainly built at MPE with assistance from the German Space industry Kayser-Threde and financed by German Space Agency (DLR). The PK-programme is a joint cooperation between our Institute and the Russian Academy Institute for High Energy Densities in Moscow. This partnership provides the free access of accommodation and resources on the ISS.

The International Space Station ISS is a perfect platform for research under microgravity conditions. MPE together with its Russian partner Institute IHED makes use of this special opportunity since right from the beginning of the colonisation of our outpost in Space in 2001. PKE-Nefedov, the first long-term natural science laboratory on the ISS was operational over more than 4 years with a scientific yield of more than 30 refereed publications. While performing experiments and gaining more and more know-how we designed and fabricated an advanced follow-up laboratory. This so-called PK-3 Plus laboratory was launched in December 2005 by a Progress rocket from Baikonur. Since January 2006 it is operational and has been used four times for experiments during the reporting period.

PK-3 Plus' special features allow the detailed investigation of complex plasmas under microgravity conditions. Compared to the precursor experiment PKE-Nefedov the system provides a much better homogeneity and symmetry of the complex plasma and highly advanced diagnostics. This is mandatory for many detailed experiments, like the formation and investigation of plasma crystals.

The first experimental mission has been performed by cosmonaut Valery Tokarev from 10th to 16th January. After



Fig. 1: Scientists follow the first experiment on the ISS performed by cosmonaut Valerie Tokarev in January 2006 from the control centre in Korolov (see also insert).

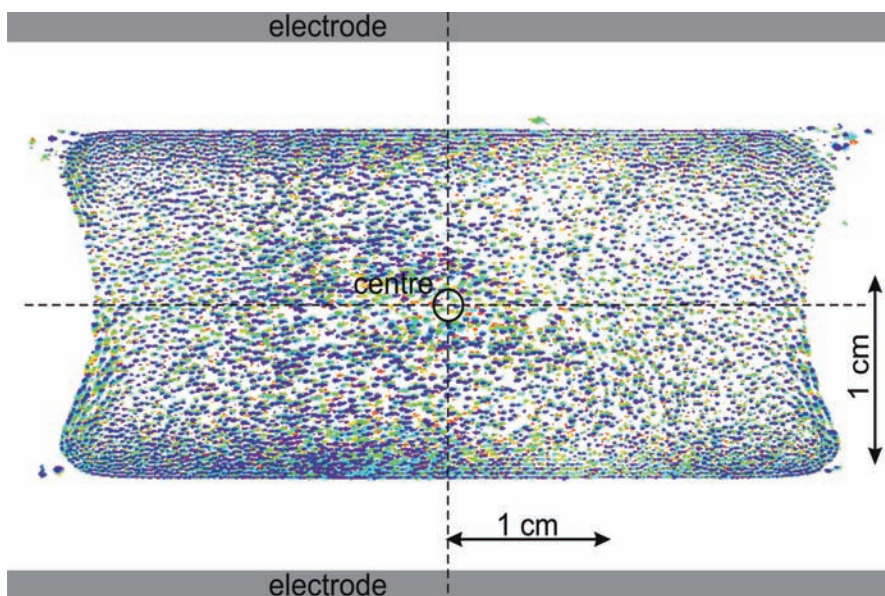


Fig. 2: Homogeneous distribution of a complex plasma under microgravity conditions, one of the main achievements of PK-3 Plus. This allows many interesting investigations in the crystalline and fluid phase.

the assembly, which has to be done before every experimental mission since the accommodation place is always temporarily, the three experiments have been conducted on the 12th, 13th and 16th. Already the first live video that was transferred to ground during the experiments showed the advanced features, mentioned above, of PK-3 Plus, especially concerning homogeneity and iso-tropy of the complex plasma. Fig. 2 shows this from a dynamic point of view. The group of scientists, engineers and officials from Russian and German side followed these experiments keenly and enthusiastically in the control centre in Korolov near Moscow (Fig. 1). The scientists received the experimental data after their transport with Sojus



Fig. 3: German ESA Astronaut Thomas Reiter on board of the ISS with the PK-3 Plus laboratory. The Experiment Container is mounted in the Service Module. (Courtesy of NASA)

back to Earth in the cosmonauts hand luggage in April, right in time for the planning of the next set of experiments in August.

In August we performed a double mission with a total of six experiments on consecutive days. The crew time was split between cosmonaut Pavel Vinogradov and the German ESA astronaut Thomas Reiter. For Thomas Reiters' Astrolab Mission we opened the project for ESA scientists on a cooperation basis. This, in principle, pure Russian-German laboratory gained from this commitment, since new topics for the research of complex plasmas could be defined and additional experiments could be performed. Especially the research or search for the critical point in the gas-liquid phase transition of complex plasmas is one of the hot topics here. Vinogradov and Reiter performed, beside practically automatic running experiments, each one manual experiment, where the astronaut/cosmonaut had to control the apparatus as a real experimenter. This requested special training of the astronaut. The scientists on ground in the control centre were following these experiments and were permanently informed by the cosmonaut/astronaut via an audio connection to the ISS.

Thomas Reiter also performed a second series of experiments in October. These were again ESA funded experiments. Additionally, Thomas Reiter gave a lecture from the ISS about the PK-3 Plus lab and science in front of a group of students taking part in the EuMAS Masters

Programme in Aeronautics and Space technology. The students from the Technical University in Munich were listening in the Columbus Control Centre in Oberpfaffenhofen near Munich, others from the partnering Universities via the internet. Prof. G. Morfill was the second lecturer on ground.

Russian cosmonauts and heroes Yuri Baturin, Yuri Gidzenko, Sergey Krikalev and Valerie Tokarev joined the first scientific PK-3 Plus symposium held at the MPE in the beginning of October. Additionally, we invited a large delegation from our Russian partners, including scientist, engineers from RKK-Energia and officials from the Cosmonaut training centre. As a start of the symposium the delegation was taken to the Oktoberfest, to teach them old Bavarian tradition. After the



Fig. 4: Cosmonaut, Russian hero and world record holder of stay in orbit Sergey Krikalev during his first attempt to open a beer barrel (insert) and with the scientific leader of the PK-3 Plus experiment, Gregor Morfill, during a celebration at the Institute.

celebration, the full delegation met on a Symposium on two consecutive days at our Institute for the discussion of the past, present and future of our research on the ISS. Beside the most recent scientific results from the mission in August, detailed information on implementation of the experiments and background about the hard- and software of the apparatus used on the ISS were given by the attending cosmonauts.

In total, the first year of operation of the PK-3 Plus laboratory on the International Space Station was a great success.

3.5 OPTICAL AND INTERPRETATIVE ASTRONOMY (OPINAS)

During the past year the MPE OPINAS group was involved in a number of hardware projects and related software and science case developments. They include the KMOS near-infrared spectrograph for the VLT, the upgrading of the Wendelstein observatory, the HETDEX project for the HET telescope, the KIDS and VIKING ESO public survey programs with the VST and VISTA telescopes, the AstroWise software package for the reduction of the wide-field imager surveys, and PanSTARRS.

The participation in the construction of KMOS (K-band multi-object spectrograph) continued successfully as planned. KMOS is one of the second generation instruments for the VLT. It is a near infrared spectrograph with 24 deployable integral field units, each able to deliver 196 spectra of a 2.8"x2.8" area sampled by 0.2"x0.2" pixels. The wavelength range goes from the I to the K band at R~4000 resolution. The consortium building KMOS is composed of the UK Astronomy Technology Center, Durham and Oxford Universities, the MPE and the Universitätssternwarte der Ludwig-Maximilians-Universität (LMU) in partnership with ESO. In 2006 the project reached a significant milestone, passing the Preliminary Design Review in June-September 2006, by presenting a prototype of the 24 arms able to match the required performances in cryogenic conditions. The Final Design Review is expected during 2007, after which the actual construction of the instrument will start. The project is on schedule to bring KMOS at the telescope by 2010.

The LMU-part of the OPINAS group runs the Wendelstein Observatory of the LMU, 60 kilometers south of Munich, where an 80cm telescope is available. Three major developments happened during 2006. First, the construction of a two-channel camera is almost completed. This allows the simultaneous observations in the B, V and R, I bands, delivering 12"x12" images with 0.35" pixel scale. The camera will replace the 10 years older MONICA camera and will be able to operate on the new 2m telescope. The second development concerns the replacement of the 80cm telescope with a 2m robotic telescope. The funding for the project is secured and the official authorisation for the beginning of the works was released in December 2006. A call for tenders will be prepared soon, with the goal of starting constructions in 2008 and see first light in 2010. Finally, the OPINAS group participates in the "Cluster of Excellence for Fundamental Physics" of the LMU together with the Max Planck Gesellschaft, the Technische Universität München and ESO. There, 1.7 Million Euros are foreseen to build a new optical/near infrared camera for the new 2m Wendelstein telescope. The design and construction will be performed in collaboration with the MPE X-ray group.

We participate in the Hobby-Eberly Telescope (HET) with a 7% share of the observing time. HET is the fixed-elevation 10m telescope of the McDonald Observatory in Texas. Together with astronomers of the Texas University

in Austin, we started a study to define the second-generation instrument for HET, the Visible IFU Replicable Ultracheap Spectrograph (VIRUS) for the HET Dark Energy eXperiment (HETDEX). VIRUS will consist of 145 copies of a unit spectrograph fed by 247 fibers, arranged in rectangular blocks and each with a diameter of 1 arcsec. It will be able to deliver spectra of ~7.8 arcmin² of the sky simultaneously, covering the wavelength range 3300-5700 Å. The main scientific driver for the project is the study of the equation of state of Dark Energy at redshift 1.8 to 3.7. To reach this goal, the power-spectrum of millions of Ly- α emitters will be measured over a region of 500 deg². The funding for the construction of HETDEX is secured to ~50%, with further promising grant applications running to cover the remaining half. VIRUS-P, a prototype of the spectrograph unit, has been completed and tested on the 2.7 m McDonald Telescope. Due to the different scale, the fiber bundle covers ~0.86 arcmin² of sky and is only 4.5 m long (for comparison, the HETDEX fibers will be 11 m long). The OPINAS group contributed to the prototype by purchasing the optics and writing software for the data acquisition and reduction. In the next six months the instrument will be tested to verify that the sensitivities aimed for HETDEX can be indeed achieved, and that the surface densities of Ly- α emitters match the expectations.

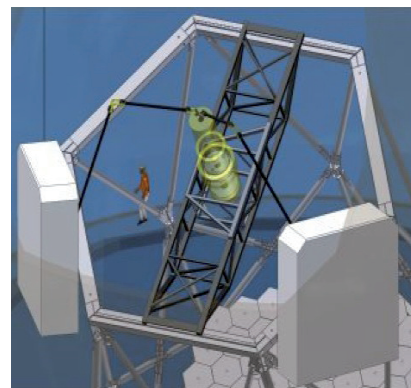


Fig. 1: An artist's view of the VIRUS spectrograph at the Hobby-Eberly Telescope (HET).

Finally, the projects KIDS (Kilo Degree Survey) and VIKING (VISTA Kilo-degree INfrared Galaxy survey), with the OmegaCam instrument on the VST (VLT Survey Telescope) and VISTA (Visible & Infrared Survey Telescope for Astronomy), and the 3 π survey with the PanSTARRS1 telescope were defined, to cover large areas of the sky with multi-band optical and near-infrared photometry. These will allow the determination of photometric redshifts for millions of galaxies and the investigation of the equation of state of dark energy, the mysterious component making 70% of the energy density of the Universe. The next two contributions describe the projects in detail, discussing also the software foreseen to handle the expected conspicuous dataflow.

OmegaCam and the KIDS and VIKING Surveys

In the next 4 years the KIDS and VIKING ESO public surveys will cover ~ 1500 deg² of sky with multi-band optical and near-infrared photometry, using the OmegaCam camera at the VST and the VISTA telescope, reaching magnitudes limits 2 mag deeper than the SLOAN project. The software package AstroWise has been developed to cope with the expected large dataflow.

The 1 deg² camera OmegaCam for the VST telescope at ESO-Paranal, built by the OPINAS group and a Dutch-Italian consortium (see Annual Report 2004), is still waiting to be delivered to the mountain due to continuing delays in telescope construction (Fig. 1 shows the dome on Paranal). In the mean time the OPINAS group finalized the definition of two ESO Public Surveys that will make use of a large fraction of the observing time at the VST and the VISTA telescope, the Near Infrared counterpart of the VST. The KIDS project is a German-Dutch-French-Italian-British collaboration to map 1500 deg² of sky in optical bands to approximately two magnitudes deeper than SLOAN with much better seeing (in particular 0.7" FWHM in the optical r band). The science drivers are: (1) to constrain the equation of state of Dark Energy using the Baryonic Acoustic Oscillations as a standard ruler at a mean redshift ~ 1 , by using photometric redshifts of ~ 50 millions of galaxies, (2) to measure the cosmological weak lensing shear and the statistical properties of galaxy dark matter halos from galaxy-galaxy lensing, (3) to discover rare luminous, high-redshift quasars and galaxies, and (4) to provide a census of an unprecedented number of massive, high redshift clusters of galaxies. The Near Infrared counterpart of KIDS is the VISTA Kilo-degree INfrared Galaxy survey (VIKING). The survey will cover the same area as KIDS in infrared bands, 1.5 magnitudes deeper than the ongoing UKIRT Infrared Deep Sky Survey (UKIDSS).

Combined with the KIDS photometry, the VIKING survey will allow the determination of photometric redshifts accurate to 2% for galaxies brighter than $r=23.5$, providing an optimal dataset to perform the BAO experiment discussed above. Moreover, it will allow the discovery of ultra-cool white dwarfs and brown dwarfs. KIDS and VISTA have been approved by the ESO Observing Programs Committee, and should hopefully start operations in the second half of 2007. Survey completion is expected on a 3 - 4 year time scale.

The AstroWise package is the software backbone of the projects. Their expected dataflow is considerable and can be managed only with the help of the software AstroWise which was developed by an European-funded

collaboration involving the OPINAS group, Groningen and Leiden Universities in Holland, Paris in France and the Neapolitan Capodimonte Observatory in Italy. The project ended in November 2006 with the delivery of the code and relative documentation. The package implements an innovative approach to astronomical data reduction, allowing the user to "pull" the data through the pipeline (for example, by searching the data available at a given position on the sky) in contrast to the classical approach of "pushing" the raw data through the pipeline to obtain reduced data releases at fixed dates. The key feature of the system, that will allow us to manage the KIDS and VISTA projects on a distributed set of nodes, is the possibility to federate a database with remote databases across the world. This opens the possibility to share calibration files, control software versions and achieve homogenous quality standards.



Fig. 1: The dome of the ESO VLT Survey Telescope (VST) on the mountain Cerro Paranal in Chile.

The PanSTARRS1 Project

In the next 4 years the PanSTARRS1 project will image $\frac{3}{4}$ of the sky in the grizy - optical to near-infrared - bands at least one mag deeper than SLOAN, with two major variability studies.

The OPINAS group, together with the Max-Planck Institute for Astronomy (MPIA) in Heidelberg, universities in the USA (Harvard, John-Hopkins) and the UK (Durham, Edinburgh, Belfast) joined the PanSTARRS1 (PS1) project of the University of Hawaii in September 2006.

PanSTARRS stands for Panoramic Survey Telescope & Rapid Response System. PS1 consists of a 1.8m telescope with a CCD camera of the unprecedented size of 1.4 Gigapixel which will image 7 sq.deg. of the sky with 0.3" resolution in one exposure. PS1 is the pilot project for PanSTARRS4 which will comprise four telescopes and cameras of the size and type of PS1. The PS1 telescope has been installed on Haleakala, Maui, and had first light in June 2006 (Fig. 1). The construction of the different parts of the system (Dome, Telescope, Camera, Filters, Dewar, Hardware and Software for front-line data taking and reduction) is proceeding according to plans and should allow the start of regular operations in fall 2007. The 64x64 red-sensitive CCDs (each with 600x600 pixels) of the camera are the most innovative parts of the system, allowing for orthogonal charge transfer and therefore "on-chip" tip-tilt correction with drastic improvement of the image quality. The filters span the green to near-infrared wavelength range, including g, r, i, z and y („grizy“) bands.

The main scientific project of PS1 is the 3π survey. The aim is to cover the sky observable from Hawaii in the grizy bands 14 times during the 3.5 years project duration, reaching limiting magnitudes in the final summed images ~ 1.5 mag deeper than the SLOAN survey. The 14 pointings will allow to investigate variability and test the algorithms searching for asteroids. Here, our main interest stems from the possibility to derive for a large number of galaxies (the so-called Red Bright Galaxies) over a huge area of the sky accurate photometric redshifts to constrain the power spectrum and therefore the equation of state of Dark Energy, similar to what is described above. Further 82 sq.deg. will be observed at much deeper limits (~ 26 mag). Here interesting aspects of galaxy evolution (luminosity functions, star formation rate densities, etc) can be investigated thanks to the faint limits reached. Finally, the OPINAS group, together with the MPIA, triggered two further variability projects. The first, PAndromeda, will monitor M31 to search for massive compact halo objects (so-called MACHOS) through the pixel-lensing effect and quantify the baryonic fraction of the dark halo of M31. When a MACHO passes through the line of sight

of a star (in M31), its gravitational attraction focuses the light emitted by the star causing a brightening of the corresponding pixel with a well defined temporal behaviour. A detailed analysis of the relative light curves allows the statistical determination of the MACHO properties, such as mass spectrum and spatial distribution. The second, PanPlanets, will search for extrasolar planets with the transit method, measuring the light curves of millions of stars in dense galactic stellar fields and looking for the signature of an orbiting Jupiter-like giant planet, the 1 - 2% dimming during the 2 - 3 hours eclipse.



Fig. 1: The PanSTARR1 telescope on the summit of Haleakala, Maui (Hawaii).

Beyond supporting operations, the Max Planck Society also assigned funds to provide adequate computing power for the analyses of the expected huge dataflow (12 TBytes per month).

3.6 KNOW-HOW TRANSFER

The working group „complex systems“ is part of the theory department of the MPE and is very much concerned with the development and the application of advanced scientific data analysis methods. The various techniques are in particular derived from concepts of nonlinear data analysis, from ideas of graph theory and from principles of information theory.

Based on these concepts we deal with the appropriate embedding of the data in multidimensional state spaces and with the quantitative description of the resulting point distribution by means of their scaling behaviour or attractor properties. We study in particular similarities and synchronization phenomena between data sets using measures from information theory that are sensitive to linear and nonlinear correlations, as well. Relations between objects are investigated with the help of distance

Data analysis problems are considered from a theoretical and generic point of view e.g. by studying (nonlinear) model systems such as the Rössler or Lorenz system. The techniques developed for the various model systems are afterwards applied to natural systems. The applications associated with a variety of interdisciplinary projects range from studying synchronization of brain activity, voice recognition, to text mining problems in extended unstructured text data bases. A few topics will be summarized briefly and presented in the selected articles.

In cooperation with the Klinikum Rechts der Isar (Technical University Munich) parameters for the risk assessment of osteoporosis from non-invasive obtained medical images are investigated. The access to high resolution μ -ct images (Fig. 1) allows a further improvement of

our methodological approach, which uses a realization for computing the pointwise dimension in state spaces, the scaling index method. Hereby, the quantitative characterization of the bone structure by means of the scaling indices yields a measure for the mechanical strength of the bone and helps to identify patients with high fracture risk.

In a series of experiments, together with LMU Munich, we studied the atomic force microscope (AFM) which can be viewed as an impact oscillator. These systems are a special class of continuous

time dynamical systems which undergo intermittent impact collisions and have dynamical trajectories in state space which are piecewise continuous, however, with discontinuities in the velocities resulting from the collisions of the tip with the surface. Even if the system is linear in the absence of impacts, such as a freely oscillating AFM cantilever, the overall dynamics of the AFM exhibits a rich variety of behavior because of the non-linearity introduced by the impacts of the tip. A new chaotic mode of the AFM has been found that has not been observed so far. Understanding the dynamics of the system could help to improve the overall system performance and its imaging quality.

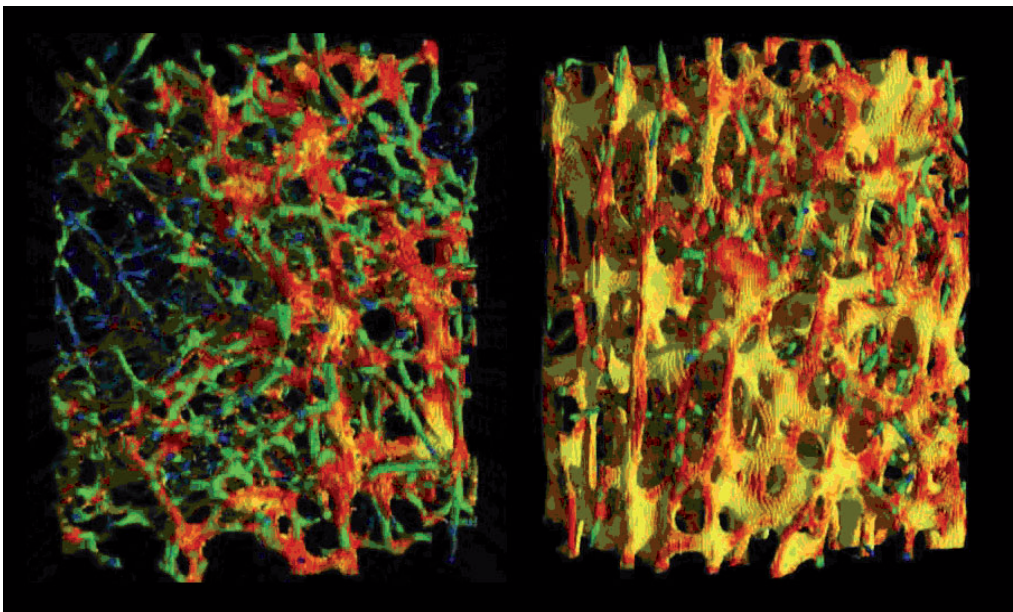


Fig. 1: Visualization of an osteoporotic (a) and a healthy (b) bone structure by means of the scaling index method. Both samples of μ -ct images have a diameter of ~ 6 mm. The calculated scaling indices of each voxel allow for a differentiation between point-like structures (blue), rod-like structures (green) and sheet-like structures (red and yellow) and help to identify patients with high fracture risk.

measures derived from several information measures (as for example the mutual information or the Kullback-Leibler distance) and represented with hierarchical trees. Hereby, the data sets under study are of very different modality, comprising time series, images or maps, and spectra in different wavelengths.

For a quantitative description of complex systems the use of statistical methods and newly developed surrogate data techniques is essential. Therefore, a lot of attention is concentrated in the development and study of techniques for generating such surrogate data sets that preserve selected properties of the data and can be used for an appropriate test statistics.

Test for non-Gaussianities in CMB using a new Surrogate Technique

A new technique for generating surrogate data, which explicitly controls the randomization of the Fourier phases has been developed. It is applied to simulated Cosmic Microwave Background (CMB) maps for investigating future model-independent tests of non-Gaussianities in the cosmic microwave background.

In cosmology, one of the fundamental questions is whether the observed fluctuations were Gaussian, because this gives important information about the nature of fluctuations and how they were generated. Thus, one ultimately obtains deeper insight in the physical processes governing the very early universe. To test for non-Gaussianities, one usually compares observations with simulations based on a best fit power spectrum and randomized Fourier phases. For these tests a detailed cosmological model is a necessary prerequisite.

the same power spectrum, while wiping out all higher order spatial correlations. The widely used iterated amplitude adjusted Fourier transform (IAAFT) algorithm puts emphasis on reproducing the power spectrum and implicitly assumes that the randomized phases remain uncorrelated. We performed a detailed analysis of the Fourier phases of the surrogates with the help of phase mapping techniques and could demonstrate that in many IAAFT-surrogate realisations phase correlations, thus higher order correlations, are induced (Fig. 1). Hence, the suitability of this algorithm is highly questionable. To improve upon the quality of the surrogates, we modified the scheme in such a way that the randomness of the phases is explicitly controlled (iterated phase adjusted Fourier transform = IPAFT- algorithm). Although the power spectrum is no longer exactly preserved, it can still be reproduced sufficiently well (Fig. 1, lower left panel). With these IPAFT-surrogates reliable, model-independent tests

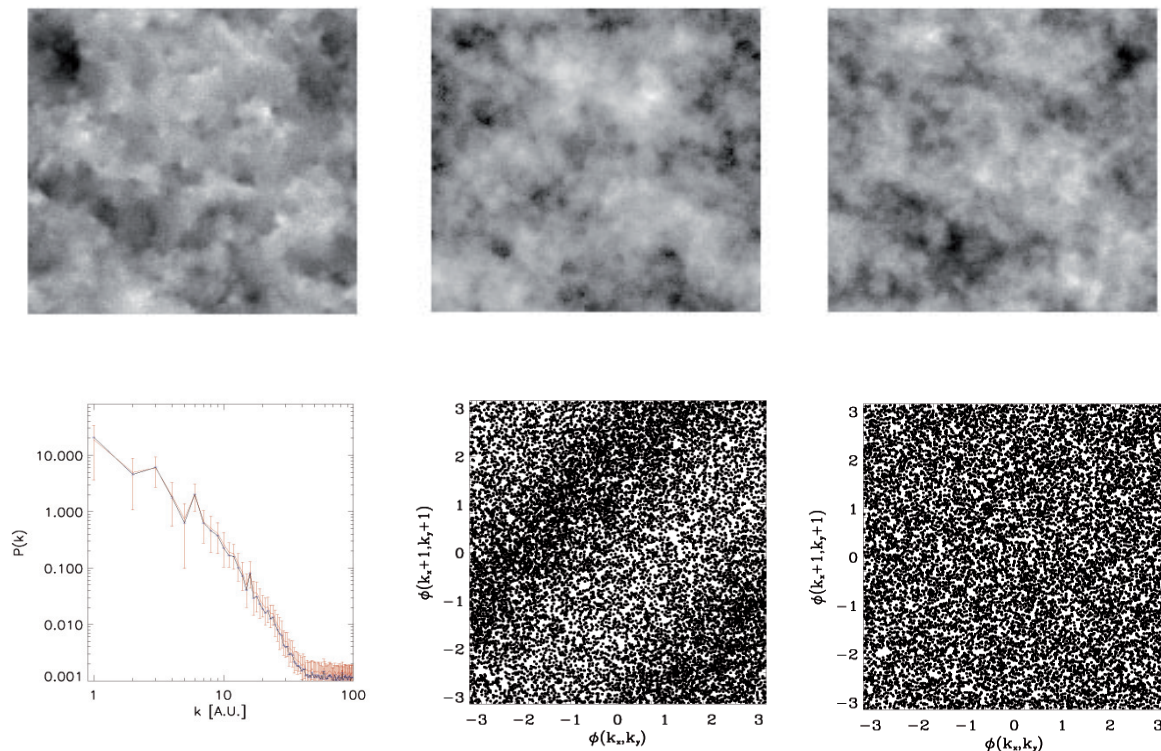


Fig. 1: Upper panels from left to right: Simulated CMB map with superimposed noise containing non-Gaussian signatures coming from topological defects (Butterfly-patterns), IAAFT-surrogates and IPAFT-surrogates. Lower panel: Corresponding power spectra for the original data (black), IAAFT (blue) and IPAFT-surrogates (left). The phase correlations in IAAFT-surrogates are obvious (example of phase map, lower middle panel), while the newly developed PAFT-algorithm ensures now correlation-free phases (lower right).

Alternative approaches, which were originally developed in the field of non-linear data analysis, offer the possibility to perform model-independent tests for non-Gaussianities. These tests involve so-called surrogate data sets, which retain some predefined properties with the original data, while all other features are randomized. In our case, we want the surrogates to have

for non-Gaussianity of the CMB using e.g. projections of patches of the WMAP-data are applicable. In general, it turns out that for using surrogates it is crucial to test their quality, not only with respect to the reproduction of the linear properties but particularly to the absence of any higher order correlations.

Plasma Medicine

In the project “plasma medicine” the suitability of atmospheric low-temperature plasma in the treatment of chronic wounds is investigated in a cooperation with the LMU Munich/Hospital München Schwabing and ADTEC Plasma Technology Co., Ltd. (Japan). New developments and tests with respect to its medical compatibility allow for the first clinical study of „plasma“ wound healing worldwide.

The bactericidal effect of plasmas is well known and utilized for the sterilization of surfaces e.g. of medical instruments. Their properties, like contact-free treatment and penetration into small cavities, makes this technique highly attractive for medical in-vivo applications, e.g. for the treatment of leg and foot ulcer.

It is generally accepted that bacterial colonization of the wounds prolongates or even inhibits the healing process, which is further complicated by germs that are resistant to many antibiotics. A significant reduction of the bacteria load by the plasma treatment should lead to a better healing process. Another benefit from this application is expected from the avoidance of unwanted side-effects of established methods: Since the sterilization mechanism is different from antibiotics, bacteria cannot acquire resistances. Furthermore our own ex-vivo studies proved that even multi-resistant bacteria types can be treated successfully with this technique.

To this clinical purpose a new plasma device (a microwave plasma torch, working at atmospheric pressure) has been developed by our group and tested with respect to medical compatibility. In particular, the temperature of the plasma at it's operating range is of about 37°C, low enough for 'in vivo' applications. The results of comprehensive preclinical ex-vivo tests of human blood, skin and cell samples did not reveal any medical incompatibilities. Meanwhile we are conducting the worldwide first clinical study of wound healing with the help of atmospheric plasmas. The available study results confirm a reduction of the bacteria load on the wounds. Also, no unwanted side-effects have been observed and the patients did not report any painful sensations during or after the treatment.

The objective of our investigation however is not only to proof the efficiency of the treatment but also to understand the underlying biophysical mechanisms. The sterilizing effect of plasma treatment can be attributed to several (possibly superimposed) mechanisms, including e.g. the UV radiation, charged particles and generated radicals. Beside physical diagnostics we use different microscopic imaging techniques such as optical, fluorescent, Raman- and atomic force (AF) microscopy for answering this

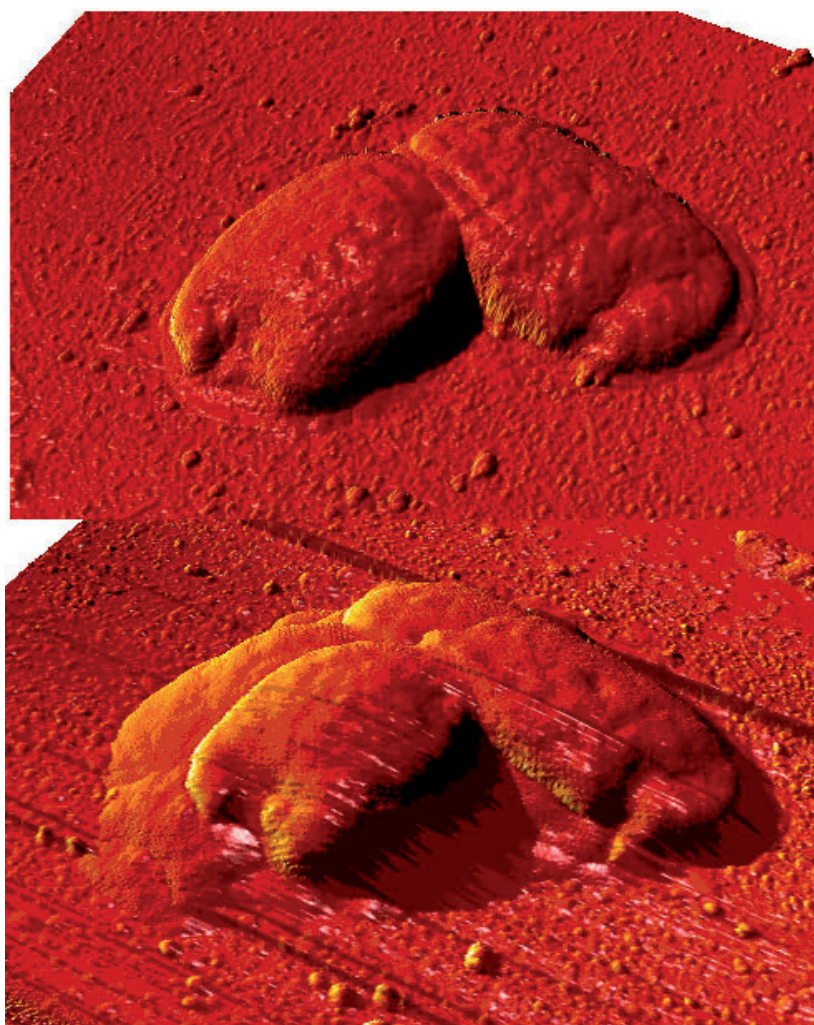


Fig. 1: AFM-images of *E.coli* bacteria (field of view: $\sim 5 \mu\text{m}$). The image shows two bacteria before treatment (upper panel) and the same bacteria after three minutes of plasma-treatment (lower panel).

question. Figure 1 shows high resolution AFM-images of two *E.coli* bacteria, before and after a three minute plasma treatment. The bacteria are highly damaged after the treatment (disruption of their cell walls).

4 The Institute



4.1 GENERAL SERVICES

Electrical Engineering

The department of electrical engineering, together with the departments of mechanical engineering, the mechanical workshop and the data processing group, is part of the central technical services at the MPE. 27 staff members (at the MPE in Garching and the Semiconductor Laboratory in Neuperlach) altogether, are working in the areas of electronic development and the electronic workshop. The assignment of the electrical engineering division is versatile, from the planning

future space projects. Along the development of CCDs and their read-out ASICs (Application Specific Integrated Circuit), test facilities and data acquisition systems are designed and manufactured there. In 2006, for example, they developed a data acquisition system for the 64x64 pixel DEPFETs (Depleted P-channel Field Effect Transistor) detector and a read-out ASIC in 0.35 μm AMS (Austria Microsystems) technology for DEPFETs.

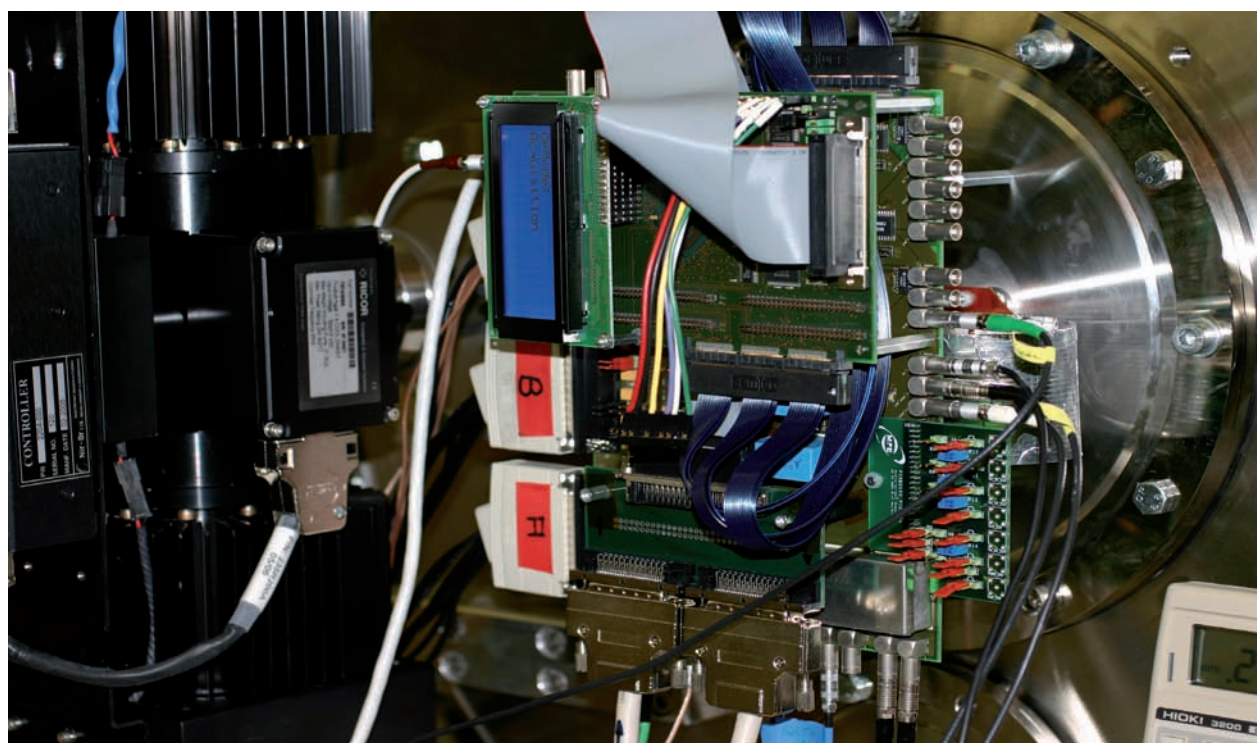


Fig. 1: A complete DEPFET (Depleted P-channel Field Effect Transistor) data acquisition system set up in our laboratory.

phase (drafting concepts), designing and manufacturing to commissioning of instrumentation for terrestrial and extraterrestrial observations and scientific experiment design for the International Space Station. Our group technically supports ongoing missions and observations. The staff is expected to demonstrate substantial knowledge of electrical engineering, confident handling of modern design and simulation tools and also to be well informed about electronic components. Experience in the areas of vacuum-, cryo-, laser technique as well as other areas is required to transform scientific visions efficiently into real projects. The electronic workshop is occupied with tasks like simple cable assembly, assembly of complex printed circuit boards, but also with wiring of experiments suitable for space missions.

The Semiconductor Laboratory in Neuperlach is mainly occupied with the development of new detectors for

In 2006 our group supported, among others, the following scientific projects:

At the PUMA test facility in Garching and the PANTER test facility in Neuried we performed a series of studies and tests for the development of the future cameras for the new project eROSITA (see 3.3). For the control of the cameras the essential electronics was developed and assembled. A prototype of the eRosita camera with a 256x256 CCD chip and two CAMEX (CMOS amplifier and multiplexer) components was developed, manufactured and tested by members of the electronic group in close collaboration with colleagues from the semiconductor laboratory. Along the extensive development, we drew up concepts, provided documentation and carried out thermal studies for application of the cameras on the satellite. Members of the electronic group were also involved in discussions with national and international

companies and institutions about the eROSITA satellite platform, the mirror and orbit as well as the mission of the future satellite.

For the instrument HERSCHEL-PACS (see 3.2), being in the completion phase, we carried out a variety of optical adjustments, calibrations and tests. The work had to be planned and prepared thoroughly because opening up the instrument is very time intensive and can only be executed under clean-room conditions. Conducting necessary vibration tests on the instrument at extreme low temperatures was another important task. The characterisation and calibration of the flight model detectors could only be done at temperatures near absolute zero, at 2 degree Kelvin (-271°C). Most of the tests and calibrations were accomplished at test facilities in Belgium.

In 2006 the Plasma-Crystal experiment PK-4 was in the phase of “conceptual design”. Together with scientists we determined all relevant physical parameters and the general framework. Therefore extensive investigations and experiments in the laboratory and on parabolic flights (tests at zero gravity) were necessary. Members of our group developed various laboratory layouts and modified the experiment layout for parabolic flights and, participated in the conduction of the experiments. After completion of the investigations, we started to develop a concept for the controlling hard- and software. Simultaneously, we developed, built and tested various electronic and mechanical components, for example a particle dispenser and high voltage- and RF-generator control units.

In the area of plasma medicine, we installed the low-energy plasma source (6 electrodes) at the hospital München-Schwabing for a clinical study to test its in-vivo application on patients. We also examined possibilities to improve the efficiency and practice-orientated handling in the laboratory. Therefore we tested new types and materials of electrodes, examined new ways for reducing line loss and phase alignment, tested a gas-mix-procedure and enabled the integration of a safety guard for patient security. Parallel to this we identified toxic substances that appear in atmospheric plasmas with mass-spectroscopy and electro-chemical measurements and applied optical spectroscopy to determine the plasma emission.

An additional activity was the concept development and assembly of a “laser scattering experiment” to determine the reflection behaviour of doped varnished

surfaces. Therefore we measured angular dependences at different laser wavelengths.

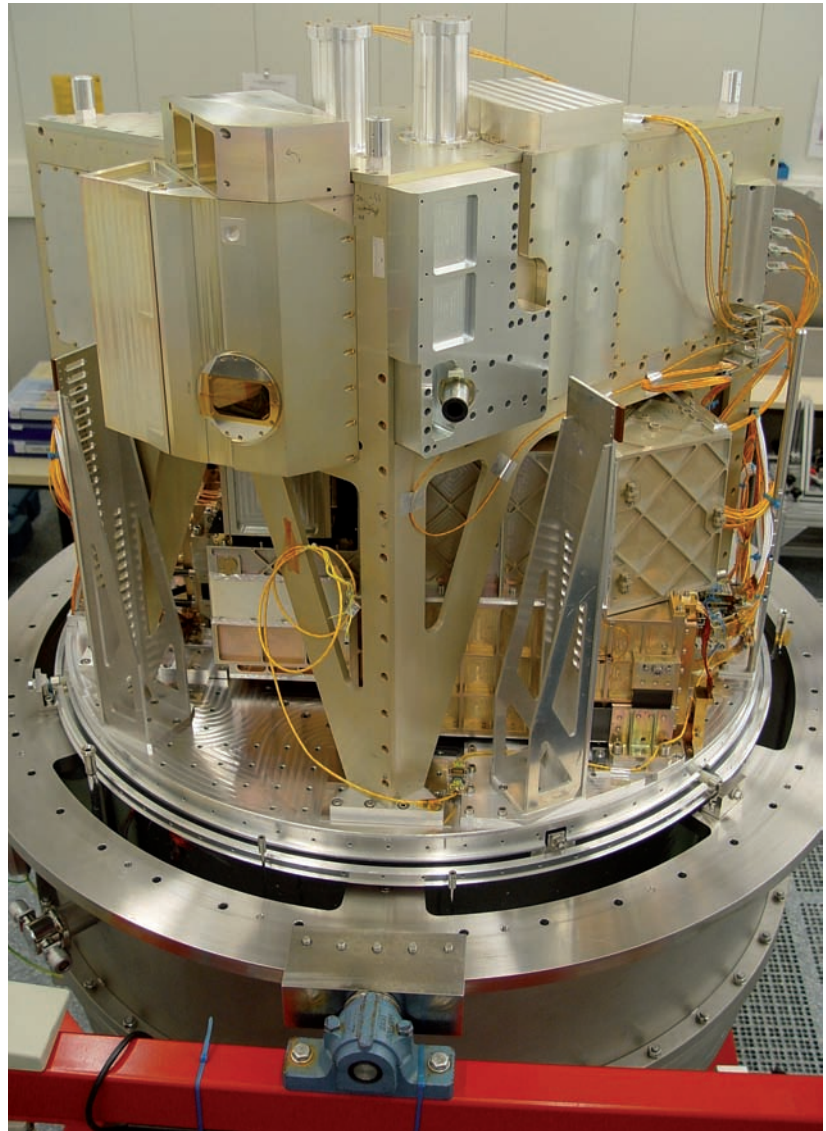


Fig. 2: The PACS Flight Model and Herschel telescope simulator optics, integrated with cryostat for Instrument Level Test at MPE.

Beside the described key projects, members of the electronic group also supported the following projects:

- GROND (Gamma-Ray Burst Optical and Near-infrared Detector)
- XEUS Optik (X-ray Evolving-Universe Spectroscopy Mission)
- OPTIMA (Optical Pulsar TIMing Analyzer)
- FIFI-LS (Field-Imaging Far-Infrared Line Spectrometer)
- PK-3 Plus (see 3.4)

Mechanical Engineering

The Mechanics department includes

- the mechanical engineering and design group,
- the test laboratory for environmental testing,
- the mechanical workshop with plastic and adhesives laboratory, locksmith's shop, joiner's workshop and
- the training workshop.

In close cooperation with the scientific groups, MPE's electronics engineers and with external colleagues from industry or partner institutes, the Mechanics department plays an important role in the development and manufacture of instruments for experimental astrophysics. To support a variety of scientific projects, a wide range of disciplines has to be covered, reaching from high-precision instrument engineering via special-purpose machines to extreme lightweight design. Typical examples are infrared and X-ray detectors or cameras, spectrometers, entire instruments for ground telescopes, scientific payloads for ballistic rockets or satellites and laboratory experiments. In many cases, the engineering work is governed by extraordinary requirements such as cleanliness, extreme stress due to vibration loads during rocket launch or the operation of instruments in vacuum at cryogenic temperatures down to absolute zero.

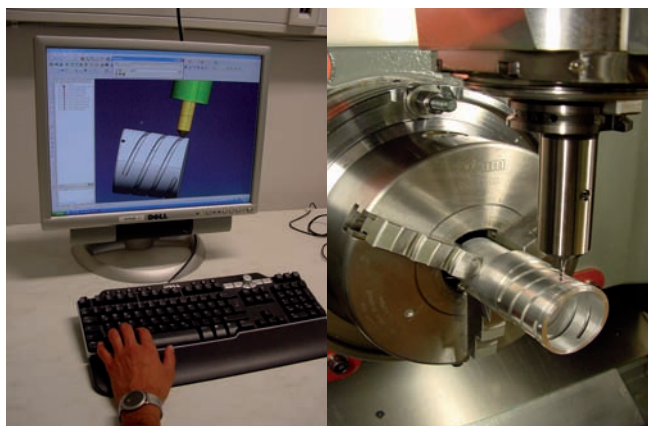


Fig. 1: CNC manufacture with the five-axis machining centre: Sequence programming at the CAM workstation and machining of a part for the focus mechanism of a slit spectrograph.

The mechanical engineering and design office (9 people) is in charge of the mechanical development process, from conceptual design to manufacturing drawings and control, using state-of-the-art 2D/3D-CAD tools. Furthermore, the engineers conduct modal, strength and thermal analyses with finite element (FE) software. Other important tasks are product assurance during assembly, integration and verification by test. For that purpose, an environmental test laboratory with two employees,

equipped with a shaker system, two thermal-vacuum chambers and a climatic chamber cooperates closely with the mechanical engineering group.

The mechanical workshop currently employs 12 mechanics

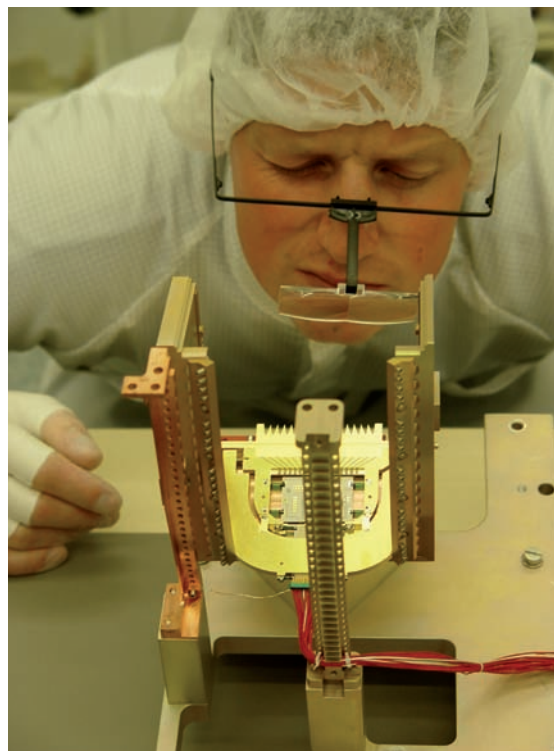


Fig. 2: Integration of the PACS Ge:Ga detector modules in the MPE cleanroom.

and technicians, another 6 people work in the plastic laboratory, locksmith's and joiner's workshops. We are equipped with a total number of nine milling machines, mostly numerically controlled, and six turning lathes. 2D/3D-CAD data can be directly exchanged between the design office and the workshop's CAM-workstations, a modern machining centre allows simultaneous five-axis milling of complex parts. Another important job for us and plastic laboratory is the assembly and integration of scientific instruments at the institute and at our partner's premises.

In 2006, high emphasis was given to the projects HERSCHEL-PACS and GROND. By end of the year, we almost completed the assembly of both instruments and started final system-level tests.

For integration and testing of the far-infrared instrument PACS (see 3.2) we designed and manufactured several testing devices and assembly tools like e.g. external calibration sources for the test cryostat and several cryogenic test rigs. Furthermore, the Ge:Ga detectors of the flight model were integrated and, in cooperation with the contractor Kayser-Threde, the entire instrument was finally assembled. In order to support the 1,5 Kelvin

cooling links of the PACS instrument, our group designed, manufactured and assembled a set of support structures. Finally, the engineering group and the workshops played a decisive role during preparation and conduction of the acceptance test programme with the PACS flight model (thermal vacuum and cryogenic vibration test campaign).

The mechanical engineering group participated on system-level in a phase-A study for the 2nd generation interferometry instrument GRAVITY, an instrument for the ESO VLT. Here we developed a laboratory test setup of the metrology and a cryogenic test rig for the characterization of mono-mode fibre waveguides. Another test bench was built up in cooperation with ESO for the PRIMA (PRISma Mass Analyzer) instrument.

In order to reduce the weight of the telescope GROND our group designed a lightweight titanium housing, and conducted an finite element analysis to study thermally-induced deformation

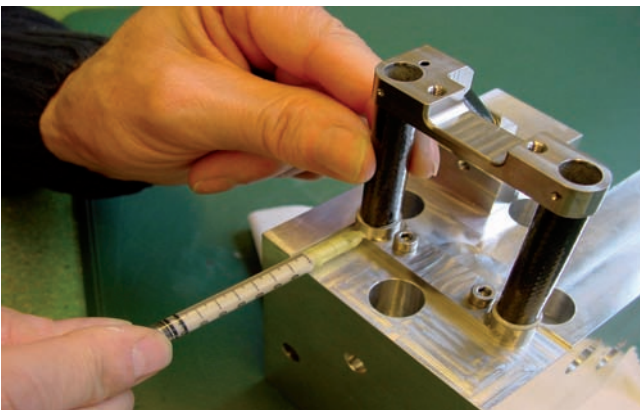


Fig. 3: Adhesive bonding of a support structure for 1,5-Kelvin cooling links in the plastic and adhesives lab.

of the instrument's optical structure, a measurement and adjustment device for the optical alignment was designed and installed. The integration of the optical components and detectors was close to being completed by the end of the year and an interface structure to the 2.2 m Telescope in La Silla was developed and manufactured.

Furthermore our group was involved in baseline design and development of future X-Ray projects, like design studies for the low-energy detector unit of SIMBOL-X (a new-technology hard X-ray telescope), and thermal optimisation of the X-ray camera for eROSITA (see 3.3). In addition first design concepts for the telescope structure have been established and studied. The design office and workshops continuously supported the X-Ray test facilities and the MPE semiconductor laboratory.

In the field of Complex Plasmas the Mechanics department participated in the projects PK-4 (design of a laboratory test setup and the parabolic flight unit, participation in

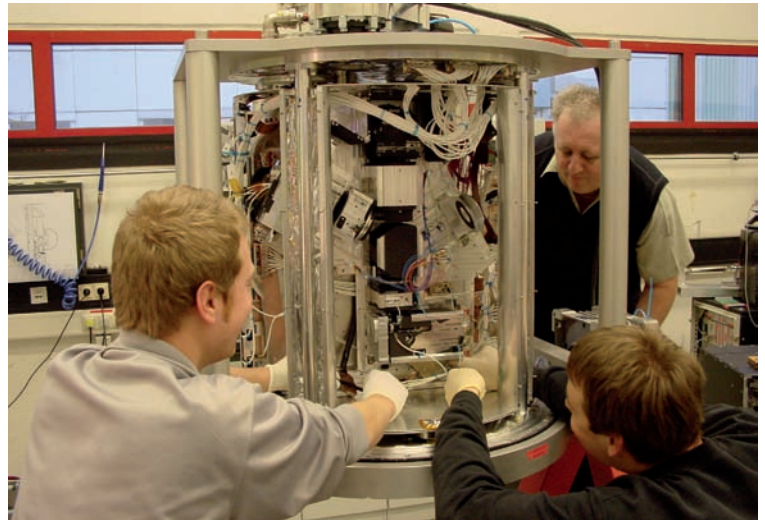


Fig. 4: Assembly of the telescope instrument GROND at the MPE integration facility.

a parabolic flight campaign) and PK-4-ISS (conceptual design of the lab test setup and the instrument to be operated on the International Space Station). Moreover we designed and manufactured a test model of a miniature plasma-medical treatment device.

Both the mechanical engineering group and workshop are continuously supported by external design offices and workshops, in most cases the external contractors are directly supervised by MPE engineers.

The training workshop is closely tied to the main workshop and offers eight training posts for young industry mechanics. In many cases, the trainees were directly involved in the scientific projects.

In 2006, the test laboratory conducted numerous environmental tests, both for MPE projects and for external partners. In total, twelve vibration campaigns, partly very extensive, and 22 thermal vacuum tests were carried out.

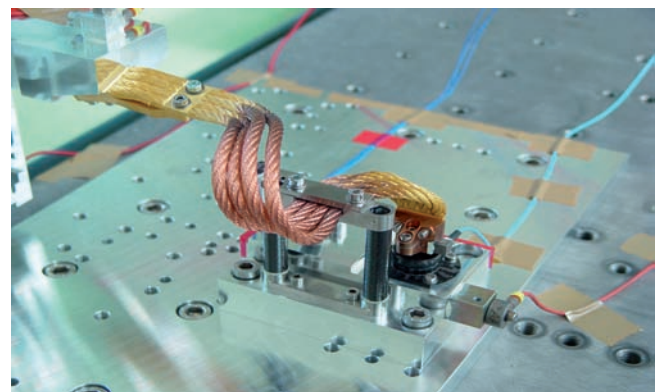


Fig. 5: Vibration test with a 1,5-Kelvin cooling link and a CFRP / titanium support structure.

Administration

The Max Planck Institute for Extraterrestrial Physics (MPE) and the Max Planck Institute for Astrophysics (MPA) share one Administration whose executive support extends also to the two branches of the MPE - the PANTER Test Facility and the Semiconductor Laboratory in Munich-Neuperlach, which is run together with the Max Planck Institute for Physics. The management of a guest house in Berkeley, California, is also taken care of by the Administration.

The Administration's structure is classic, comprising the departments of finances, personnel, purchasing, and other services. Its main areas of work involve the handling of personnel matters relating to its own staff as well as to junior researchers and visiting scientists from abroad, the procurement of scientific and other equipment, and the organization and maintenance of the Institute's infrastructure. Additional tasks include the planning and administration of institutional and third-party funds, along with the appropriate processing of receipts

and disbursements, supplying proof of the correct usage of appropriated funds. In performing these functions, the Administration is required to comply with the laws, legal provisions, and guidelines applicable to the Max Planck Society and its institutes. The Administration advises the directors on the implementation of these rules and guidelines.

The increase in international projects and collaborations, as well as the general internationalization of science and the worldwide mobility of scientists, PhD students and fellows have led to a change of the Administration's tasks. Providing advice as well as practical assistance to this group of persons (housing, handling of paperwork with the authorities, health insurance, language courses, etc.) are new tasks. Of particular importance in this context is the International Max-Planck Research School, which is attended almost exclusively by talented young undergraduate students from abroad.

Publication Services and Print Shop

The Institut's copyshop produces reports, brochures, as well as business products such as forms, note papers and envelopes for the MPE and, to limited extend, other Max-Planck-Institutes in the northern part of Munich and

the central administration. It owns exclusively digital print machines (b/w and colour). Our graphics group is able to prepare all kinds of graphics and images for publications, brochures, posters and websites.

Library

The "Astrobibliothek" is a facility jointly run by the MPI for Astrophysics (MPA) and the MPE. The fact that this library has to serve the needs of two institutes with differing research emphases - predominantly theoretical astrophysics at the MPA and observational/instrumental astrophysics at the MPE - explains its size. The library currently (2006) holds about 22,000 books and conference proceedings, 22,000 periodicals, as well as ca. 6,500 reports and observatory publications. It holds print subscriptions for about 240 periodicals and it manages online subscriptions for about 400 periodicals. It keeps copies of the Palomar Observatory Sky Survey (on photographic prints) and of the ESO/SERC Sky Survey (on film).

The MPA/MPE library catalogue includes monographs, text books, conference proceedings, periodicals, doctoral dissertations, habilitation theses, reports, observatory publications, bibliographical metadata, and links to online publications.

To serve the users' and librarians' needs, the library provides access to several photocopiers, and is equipped with a microfiche reader/printer, a book scanner, several PCs and terminals, two laser printers, and a fax machine.

In addition, the library maintains a closed archive of MPA and MPE publications. Starting with the launch of the "Edoc" systems by the Max Planck Society in 2003, all institute publications (MPA and MPE) are archived electronically. The library staff administrates and maintains the "Edoc" systems which currently (2006) comprises about 900 publications. The library also participates in the "VLIB" (Virtual Library) project which is the portal of the Max Planck Society. It provides a common interface that makes various scientific information resources available.

Datamanagement

The data handling - mangament and processing - at MPE is generally done in a collaborative effort between the MPE computing support group and the individual science groups. The computing support group covers the central tasks and, in addition, supports the science groups in their specific work by IT-knowledge and man power.

Due to requirements of the many experiments developed and carried out at MPE as well as by national and international collaborations, the demands for the MPE computing group are numerous and complex. Therefore software development tasks and preparation of experimental data are carried out within the scientific groups.

Coordination of computing and data processing activities is handled by a data-analysis committee with representatives from all areas of the Institute. It is supported by a central group for system support and programming. The main tasks of the working group are the coordination and evaluation of new hardware and software procurement, the conception and control of central installations such as the local-area network and its security, the access to external networks and the public printers. In addition, this working group coordinates

the collaboration with the Garching Computer Centre (RZG) and takes care of the IT-related training of MPE members.

The members of the central computing support group are responsible for the acquisition and operations of the central MPE IT-structure (network, printer, servers) and for the maintenance of the central IT-services (www, ftp, mail, etc). In addition, the group maintains - in collaboration with the scientific groups - the contents of the MPE web pages. Additional task are the acquisition and distribution of software and associated licenses, the configuration of servers, workstations and laptops. New MPE members - employees, guests - are adviced and supported with respect to software installation and programming tasks.

About half of the group members spend the majority of their working time as software consultants and developers within the scientic groups to support our main science projects like XMM-Newton, INTEGRAL, Cluster, Herschel, PanSTARRS, and complex plasmas. This guarantees a significant synergy between computing support group and the different science groups.

4.2 VOCATIONAL TRAINING AND EDUCATION

The International Max-Planck Research School (IMPRS) on Astrophysics

The Max Planck Society for the Advancement of Science has realized the importance of educating and training junior scientists for the future of science and research. Subsequently they, together with the Association of Universities, established a program called the International Max Planck Research Schools in the year 2000. These schools offer especially gifted students from Germany and abroad the excellent opportunity of studying at the highest possible level of science. In the framework of this program, the Max-Planck-Institute for Extraterrestrial Physics and the Max-Planck-Institute

Planck Society the common foundation of the education is of central importance. It is the cornerstone for future cooperation without national boundaries. Graduates that received a doctorate through the IMPRS on Astrophysics in Garching, have the best chances for an international scientific career. Renowned Professors, private lectures and scientists lecture at the participating institutes and the students learn about the most recent results from new observations and experiments. This is the best foundation for the educational development of the scientists of tomorrow.

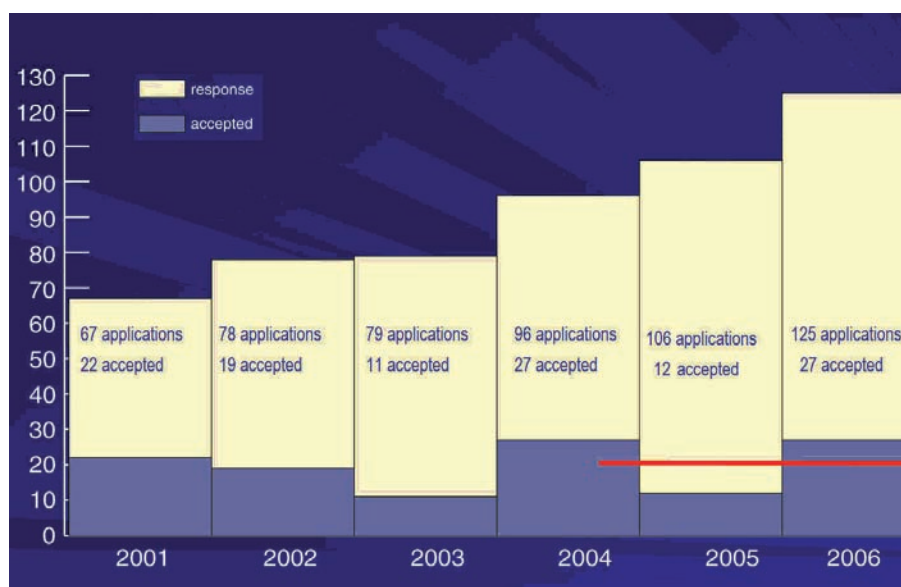


Fig. 1: Summary of annual applications for the participation in the IMPRS program in Garching. Since its start in 2001 a total of 648 students applied for participation in the program.

At the IMPRS for Astrophysics, 20 - 25 students on average are selected per year, out of more than 130 applications. The increasing number of applications reflects the high international interest as well as the success of the program. The number of applications has increased every year since the start of the school in 2001. 65 students participated in the program in the academic year 2006, and a total of 684 students from Germany and abroad have applied for it since its start. Of the accepted students about 20% are from Germany and ~50% are from European and associated countries. 40% of all PhD students are females. To accommodate the wide international interest in the program, the IMPRS in Garching received additional funding from the European Commission. Since June 2004

for Astrophysics launched the school in a joint venture supported by the Observatory of the Ludwig-Maximilians University and the European Southern Observatory. Therefore the IMPRS in Garching is a unique system worldwide where the cooperation of four leading scientific institutes enables rich educational opportunities for the next generation.

The IMPRS on Astrophysics tries to optimize the academic development of their graduate students by providing the possibility to prepare their dissertation in one of the leading centres of Astrophysics. The close teamwork between students and scientists, encouraged by the IMPRS, promotes continuing collaborations among them. Studying together in Garching will enhance the probability to collaborate also in the future. For the Max

the IMPRS on Astrophysics at the Ludwig-Maximilians University of Munich is a Marie-Curie early stage training site of the European Commission for PhD students of Astrophysics.

So far, about 40 students have successfully defended their PhD at one of the two Universities located in Munich. About 85% of the PhD thesis were submitted to the Ludwig-Maximilians University of Munich and 15% to the Technical University in Munich. The affiliation of the supervisors determines the university.

Initially approved for a period of six years, the funding for the IMPRS on Astrophysics was extended by the president of the Max Planck Society for six more years until the year 2013.



Fig. 2: The IMPRS students, who started their PhD for Astrophysics in Garching in September 2006.

Student Experiment “Plasma Crystal“

Since 2003 we offer a student experiment, called “plasma crystal”, as part of the physics education (“Fortgeschrittenen Praktikum”) at the Technical University Munich and the University Ulm. The aim of this experiment is the creation and investigation of a plasma crystal (structure, dynamics, correlations) in an rf discharge plasma by the students. For this purpose a complete set-up on the basis of the PKE-Nefedov chamber (see section 3.4) is provided at our institute. About 15 groups consisting of 2 - 3 students from the Technical University perform this experiment every semester. In addition, a practical course for students from the University Ulm takes place once a year for one week.



Fig. 1: The student experiment “Plasma Crystal“.

Vocational Training

Education is a socio-political responsibility to which the MPE, as a publicly funded research institute, feels committed. In addition to the scientific “offspring”, the vocational training of young people is also supported at our Institute.

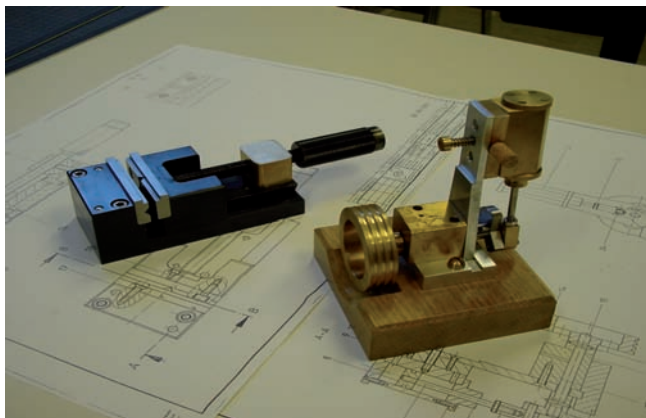


Fig. 1: Drillscrewblock and standing steam-engine - Projects for the 1st and 2nd year of training.

Last year eight apprentices, two per year of training, were instructed as industrial mechanics with the emphasis on mechanics at the educational workshop of the Institute. Furthermore 12 pupils completed a week-long orientation placement, and four student apprentices a six week manufacturing placement. Two of our apprentices completed their vocational training very successful in February 2006, and subsequently joined the mechanical workshop team.



Fig. 2: Mounting an optical experimental-setup to test the PRIMA instrument by 3rd year apprentices.

In the first two years of the apprenticeship, the emphasis is on a broad, occupational orientated basic training, with the main goal being familiar with the basic skills of the profession. Working independently and team-orientated is promoted as well as learning security regulations. Around half way through the second year of training, apprentices support the mechanical workshop with simple turn-, milling- and assembly jobs. In the third year of training they are assigned for three months to the mechanical workshop, where they gain further expert experience. Then they already accomplish essential contributions for the Institute.

In 2006 the MPE apprentices attended various work specific training courses in the areas of pneumatics and E-pneumatics at the Munich public services department and completed seminars at Siemens-Education, preparing them for their exams.

Visiting informational events like the international exhibition for production engineering and automation, METAV, is also part of their training. A notable highlight was the participation at the special exhibition “Talents 2006” at the international trade fair in Munich where we showed a split-spectrograph, built in our educational workshop.



Fig. 3: Various development phases of the split-spectrograph.

The open day with the children’s program was another highlight where all the young people from the workshop participated with great enthusiasm.

The MPE also trains people in the profession of office administrator. In this officially recognised job (that requires training) young people are trained in the areas of personnel administration, salary handling, accountancy and cost calculation as well as application- and invoice processing. Through work placements we also offer the opportunity to young people to gain an insight into the tasks and general schedule of an apprenticeship.

4.3 PUBLIC OUTREACH



Fig. 1: How to assemble a rocket ?

Astrophysical topics are subjects of increasing interest to the public and the media. As a publicly financed institution MPE feels a special obligation to reach out to the community, offering guided tours through the institute, hands-on courses for pupils, and public lectures by institute members on various technical levels. In addition the projects and scientific publications of all groups are found on the MPE web site <http://www.mpe.mpg.de>.

In 2006 a total of 23 guided tours were organized, each consisting of a group of up to 30 people. Most participants were pupils and teachers of science oriented schools, but tours were also organized for clubs and various occupational groups. We offer review talks from the different scientific teams, laboratory visits and hardware exhibits from the different projects.

A highlight of these activities was the “Open Day” on Sunday, October 15, which was organized campus-wide by all institutes to celebrate the opening of the subway station in the centre of the campus.

The whole range of our research activities was presented to the visitors in an approachable way. At hourly intervals public talks were presented which enjoyed great popularity. In total, more than 1500 visitors demonstrated the enormous interest of the public in modern astrophysical research.



Fig. 3: The main entrance on Open Day.



Fig. 2: Intergalactic ice cream factory.

A very special attraction of our institute turned out to be the children’s program, which caused amongst even the youngest excitement for extraterrestrial research. The program covered a wide range: from astronomically motivated handicraft and experiments for the youngest, mass launches of self-built rockets, up to an “institute rally” for the older kids who could thus improve their astronomical knowledge. More than 400 enthusiastic children flooded the institute, presenting an impressive sign of gratitude for the many volunteers who helped to run this event.

4.4 SOCIAL EVENTS



Fig. 1: A group of MPE-skiers in the Tirolean mountains.

An important aspect of a „living“ institute is certainly common social activities, supporting the daily life at the institute, in particular the personal communication within the institute groups and among members of different groups, as well as the integration of new institute members. These social activities at MPE range from group-internal celebrations of particular events (e.g. successful completion of a larger project or a PhD, special birthdays) via MPE-wide celebrations, like the annual Christmas party, to the three well-established annual trips.

In February a group of mixed nationalities and skiing skills went on a skiing trip to Ellmau in Tirol, Austria. Although the snow conditions were good some participants did not take the „skiing trip“ to literally and went sledding and hiking. The skiers enjoyed the day in different groups according to their skills. Fortunately without any severe injuries, all gathered in the evening again for a common dinner and could fulfill their duties at MPE the next day.



Fig. 3: Oktoberfest

For our annual works outing in summer we visited the baroque city of Eichstätt, located in the lovely valley of the river Altmühl. After a guided tour through the baroque city centre and inside the Eichstätt cathedral during the morning hours, the afternoon was free for self-chosen leisure activities, of which canoeing on the river Altmühl seemed to be most attractive. However, this generally quiet and cozy floating was not that peaceful for all crews. Some canoe „battles“ ended in an overturn, cooling off the high spirits of some crews. The calories lost during the sporty afternoon activities could be replenished in a solid meal of medieval style at the castle of Eichstätt in the evening.



Fig. 2:

Left: One of the many baroque squares in Eichstätt.

Below: Canoeing on the river Altmühl.



The fall highlight was, certainly, the annual visit to the Munich Oktoberfest. Last but not least the offer of a reduced board price convinced many of our locals, foreign staff and guests to join the event. With the spirits continuously rising during the afternoon and early evening, the „end of work“ was shifted to the late night by most of the colleagues.

5 Publications, Teaching



5 PUBLICATIONS, TEACHING

Here we present a tabular and graphical summary of our publication activities in 2006. The publications are counted by science group and publication type. The complete lists of the individual references for the different

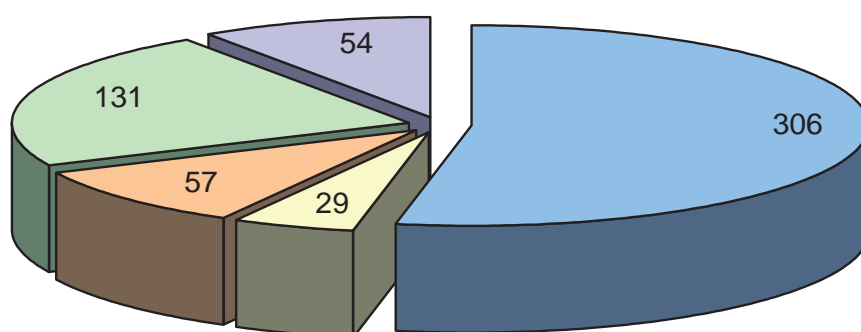
categories are given on the enclosed CD. They can also be viewed on or downloaded from our MPE web pages (<http://www.mpe.mpg.de/popus.html>).

Summary of MPE Publications in 2006

Science Groups	refereed Publications	refereed Proceedings	instrumental Publications	non-refereed Publications	Telegrams/Circulars	Talks	Poster
Plasma	39 (12)	10 (5)	0	21 (7)	0	26 (10)	7
IR	43 (12)	3 (0)	14 (7)	21 (12)	0	67 (48)	7
X-Ray	110 (44)	6 (2)	39 (11)	46 (26)	11 (6)	159 (101)	7
Gamma	31 (11)	5 (3)	0	11 (6)	32 (14)	26 (17)	10
Theory	52 (31)	4 (3)	1 (1)	17 (11)	0	74 (32)	18
Opinas	31 (6)	1 (0)	3 (1)	15 (6)	12 (0)	19 (16)	3
Total	306 (127)	29 (13)	57 (20)	131 (68)	54 (20)	371 (225)	52

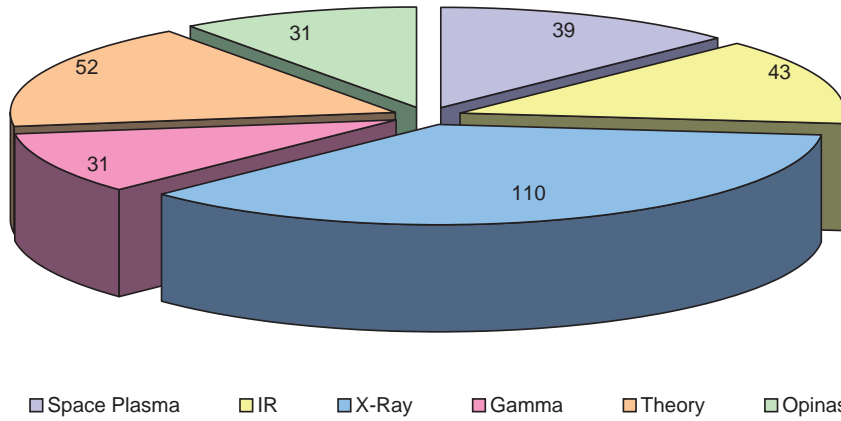
The red numbers in brackets give the number of publications with a first author from MPE or invited talks, respectively. Publications with contributions from more than one research group are counted for the group of the leading author. Posters are counted if the first author is a MPE member.

Total Publications 2006 (by Type)



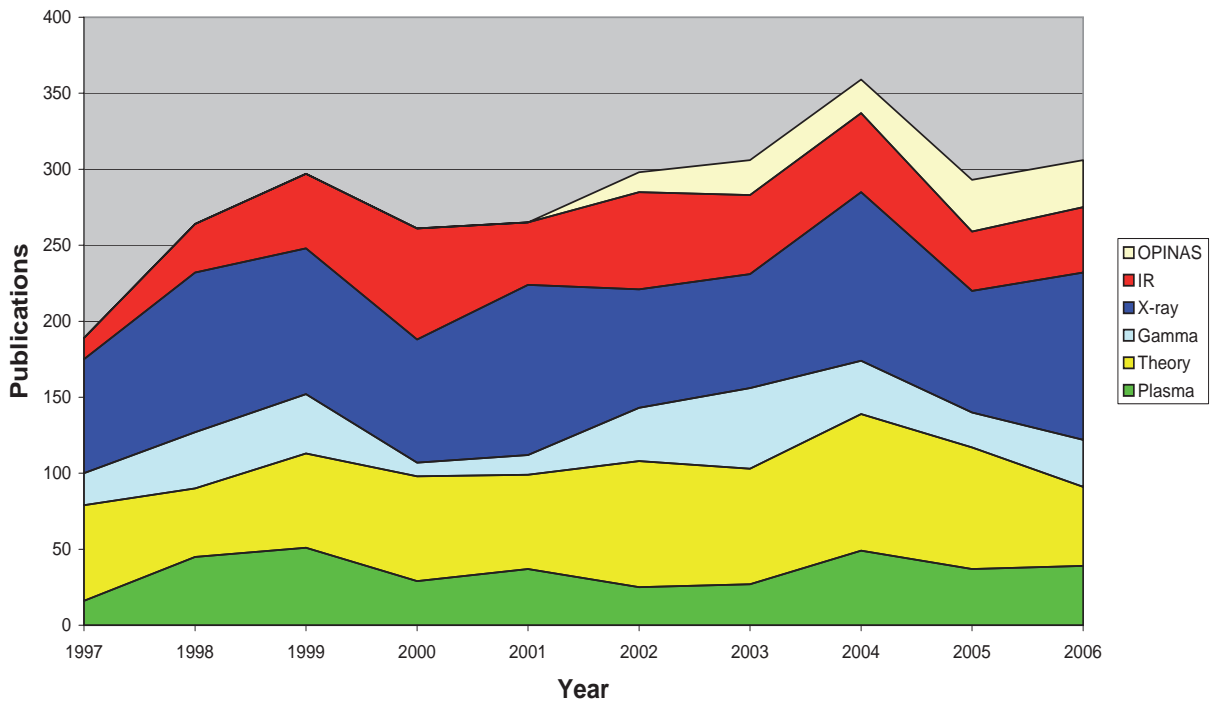
■ refereed Publications
 ■ refereed Proceedings
 ■ instrumental Publications
 ■ non-refereed Publications
 ■ Telegrams/Circulars

Refereed Publications 2006 (by Science Group)



Space Plasma IR X-Ray Gamma Theory Opinas

History of MPE Refereed Publications (by Science Group)



OPINAS
IR
X-ray
Gamma
Theory
Plasma

Teaching

IMPRS Garching

Bender

Introductory Course Astrophysics (WS 06/07)

Gerhard

IMPRS Advanced Course II: Stellar dynamics, galaxy structure, simulation of galaxies and the intergalactic medium. Part 2 on Structure of the Milky Way (WS 06/07)

Schuecker

Cosmology, Large-Scale Structure, and Stellar Structure (SS 06)

Cosmology, Large-Scale Structure, and Stellar Structure (SS 06)

International University Bremen

Haerendel

Dynamo Theory, in High Energy Astrophysics (Astrophysics III) (April 06)

Discontinuities and Shocks, in Space Physics II: Space Plasma Physics (April 06)

Johann Wolfgang Goethe-Universität Frankfurt am Main

Boller

Einführung in die Astronomie II (SS 06)

Astrophysikalisches Praktikum (SS 06)

Einführung in die Astronomie I (WS 06)

Astrophysik III (WS 06)

Ludwig-Maximilians Universität München

Annaratone

Introduction to Complex Plasma (WS 06/07)

Low Temperature Plasma Physics (SS 06)

Becker

Weißer Zwerge, Neutronensterne und Schwarze Löcher (WS 06/07)

Doktorandenseminar über Aktuelle Themen aus der Astrophysik (WS 06/07)

Gravitationswellen und ihr Nachweis (SS 06)

Doktorandenseminar über aktuelle Themen aus der Astrophysik (SS 06)

Bender

Astronomisches Hauptseminar zur Astrophysik: Schwarze Löcher in Theorie und Praxis, Teil 2 (SS 06)

Astrophysikalisches Praktikum „B“ und Übungen (SS 06)

Astronomisches Kolloquium (SS 06)

Extragalactic Journal Club (E) (SS 06)

Extragalactic Group Seminar (E) (SS 06)

Gravitational Lensing (E) (WS 06/07)

Astronomisches Hauptseminar zur Astrophysik: „Tools in Modern Astrophysics“ (WS 06/07)

Astrophysikalisches Praktikum „A“ und Übungen (WS 06/07)

Astrophysikalisches Praktikum „B“ und Übungen (WS 06/07)

Astronomisches Kolloquium (WS 06/07)

Extragalactic Journal Club (E) (WS 06/07)

Extragalactic Group Seminar (E) (WS 06/07)

Böhringer

Inflation und dunkle Energie in der Kosmologie (WS 06/07)

Jamitzky

Java Programmierkurs (WS 06/07)

Java Programmierkurs (SS 06)

Grenzflächen und weiche Materie (SS 06)

Grenzflächen und weiche Materie (WS 06/07)

Schuecker

Beobachtende Kosmologie (SS 06), mit Böhringer

Kosmologie der Inflation und Dunklen Energie (WS 06/07)

Trippe

Seminar „Schwarze Löcher“ (SS 06), mit Gillessen

Seminar „Tools in modern astrophysics“ (WS 06/07), mit Gillessen

Technische Universität München

Diehl

Advanced Astrophysics Seminar: „The Dark Universe“ (WS 05/06), mit Hasinger, Hillebrandt, Müller

Advanced Astrophysics Seminar: „Astrophysical and Astronomical Measurements: Exploiting Observations“ (WS 05/06)

Advanced Astrophysics Seminar: „The Dark Universe“ (SS 06), mit Hasinger, Hillebrandt, Müller

Advanced Astrophysics Seminar: „Spectroscopy of Cosmic Light: Elements throughout the Universe“ (WS 06/07), mit Hasinger, Hillebrandt, Müller

Cosmic Nuclear Reactions: Nucleosynthesis (WS 05/06)

Hasinger

Einführung in die Astrophysik (SS 06)

Einführung in die Astrophysik (WS 06)

Thoma

Betreuung Fortgeschrittenen Praktikum „Plasmakristall“ (SS 06), mit Kretschmer

Betreuung Fortgeschrittenen Praktikum „Plasmakristall“ (WS 06/07), mit M. Kretschmer

Universität Gießen

Thoma

Quantenfeldtheorie (SS 06)

Theoretische Kernphysik II: Kernreaktionen (WS 05/06)

Hadronen, Quarks und Symmetrien (WS 06/07)

Universidad Nacional de La Plata (Argentina)

Monetti

Aplicaciones de la Teoría de Caos en Medicina (April 06)

University of Padova

Boller

High Energy Astrophysics (SS 06)

6 Personnel, Collaborations



6 PERSONNEL, COLLABORATIONS

Directors

Prof. Dr. R. Bender, Optical und Interpretative Astronomy, also Professorship for Astronomy/Astrophysics at the Ludwig-Maximilians-University Munich

Prof. Dr. R. Genzel, Infrared und Submillimeter-Astronomy, also Prof. of Physics, University of California, Berkeley, USA (Managing Director)

Prof. Dr. G. Hasinger, X-Ray- and Gamma-Ray Astronomy

Prof. Dr. G. Morfill, Theory, Non-linear Dynamics, Complex Plasmas

Prof. Dr. G. Haerendel (emeritus)

Prof. Dr. R. Lüst (emeritus)

Prof. Dr. J. Trümper (emeritus)

Manager's Assistant

Dr. H. Scheingraber

Scientific Secretary

Dr. W. Brinkmann (until 31.10.2006)

Dr. W. Collmar (since 1.11.2006)

External Scientific Members

Prof. Dr. V. Fortov, IHED, Moscow (Russia)

Prof. Dr. R. Z. Sagdeev, University of Maryland (USA)

Prof. Dr. M. Schmidt, CALTECH, Pasadena (USA)

Prof. Dr. Y. Tanaka, JSPS, Bonn; MPE (Germany)

Prof. Dr. C.H. Townes, University of California, Berkeley (USA)

Curators (together with the MPI for Astrophysics)

Dr. L. Baumgarten, Vorstandsmitglied DLR

Prof. Dr. A. Bode, TU München

W.-M. Catenhusen, Staatssekretät im BMBF, Berlin

H.-J. Dürrmeier, Süddeutscher Verlag, München

Prof. Dr. W. Glatthaar, DG Bank (Chair of the Curatorium), Frankfurt

Dr. G. Gruppe, Bayerisches Staatsministerium für Wirtschaft, Verkehr und Technologie, München

Prof. Dr. B. Huber, Rektor der LMU München

Dipl.-Ing. R. Klett, Kayser-Threde GmbH, München

Dr. M. Mayer, Mitglied des Bundestages, Höhenkirchen

Prof. Dr. E. Rohkamm, Thyssen Krupp AG, Düsseldorf

Scientific Advisory Board

Prof. Dr. R. Davies, Oxford University (UK)

Prof. Dr. R. Ellis, CALTECH (USA)

Prof. Dr. N. Gehrels, NASA/GSC (USA)

Prof. Dr. F. Harrison, CALTECH (USA)

Prof. Dr. O. Havnes, University of Trømsø (Norway)

Prof. Dr. P. Léna, Université Paris VII (France)

Prof. Dr. R. McCray, University of Colorado (USA)

Prof. Dr. M. Salvati, Osservatorio Astrofisico di Arcetri (Italy)

External / Interdisciplinary Scientific Advisors

Prof. Dr. H. Gleiter, Forschungszentrum Karlsruhe

Prof. Dr. R. Sauerbrey, Forschungszentrum Rossendorf, Dresden

Humboldt Awardee

Prof. Dr. P. Henry, University of Hawaii (USA)

Prof. Dr. B. Sonnerup, Dartmouth College (USA)

Prof. Dr. V. Tsytovich, Russian Academy of Sciences, Moscow (Russia)

Prof. Dr. H. Netzer, Tel Aviv University (Israel)

Friedrich Wilhelm Bessel - Research Award of the A. von Humboldt Stiftung

Dr. A. Cimatti, Istituto Nazionale de Astrifisica (INAF), Arcetri (Italy)

A. v. Humboldt Fellows

Prof. Dr. D. Jaffe, University of Texas (USA)

Dr. F. Martins, Observatoire Midi-Pyrénées (France)/ Geneva Observatory (Switzerland)

Dr. V. Yaroschenko, Universiteit Gent (Belgium)

MPE Senior Research Fellow

Dr. D. Porquet (until 30.9.2006)

Dr. K. Iwasawa (since 1.10.2006)

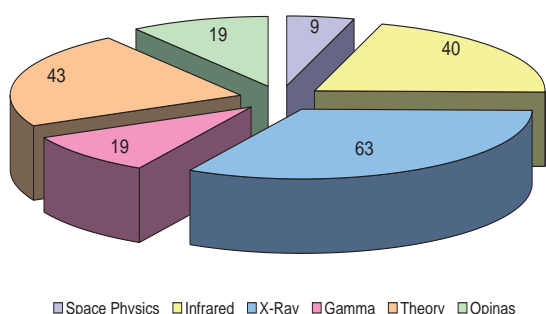
Scientific Honours, Appointments

Genzel, R.: Celsius Lecture, Uppsala University, Schweden, February 2006.

Trümper, J.: Marcel Grossmann Award, July 2006.

Science Groups

Staff Members by Science Groups



Space Physics of Near-Earth Environment

Team Assistant: Zanker-Smith, J.

Georgescu, Dipl.-Phys. E.; Haaland, Dr. S.; Kis, Dr. A. (until 30.6.); Klecker, Dr. B.; Leistner, Dipl.-Phys. G.; Marghitu, Dr. O. (until 30.4., 12.-19.6., since 1.11.); Pitout, Dr. F.; Volwerk, Dr. M.

Guests

Bunescu, Dr. C. (1.11.-31.12); Comisel, Dr. H. (2.6.-31.7., 1.10.-31.12); Dröge, Dr. W. (7.2.-6.3.); Kartavykh, Dr. J. (6.2.-5.3.)

PhD / Diploma

Blagau, A. (Klecker); Ilie, D. (until 30.4.);

Infrared/Submillimeter Astronomy

Secretary: Harai-Stroebl, S.

Abuter, Dr. R. (until 15.1.); Agudo Berbel, A. (since 23.10.); Bauer, Dipl.-Phys. O.; Bouche, Dr. N.; Contursi, Dr. A.; Cresci, Dipl.-Phys. G. (since 1.9.); Davies, Dr. R.; Eisenhauer, Dr. F.; Feuchtgruber, Dipl.-Phys. H.; Fridjof, A. (1.2.-31.7.); Friedl, A.; Geis, Dr. N.; Gemperlein, H.; Gillissen, Dr. S.; Gräter, A. (since 1.8.); Hamaus, N. (28.6.-30.9.); Hartinger, Dr. C.; Hicks, Dr. E. (since 1./9.10.); Hofmann, Dr. R.; Katterloher, Dr. R.; Kleiser, A.; Kornberg, Dr. M.; Krombach, H.; Lehnert, Dr. M. (until 15.11.); Lutz, Dr. D.; Müller, Dr. T.; Osterhage, S.; Paumard, Dr. T. (until 30.9.); Poglitsch, Dr. A.; Raab, Dr. W.; Rabien, Dr. S.; Schmid, Dr. W.; Schreiber, Dr. N.; Seidenschwang, K. (until 30.4.); Sturm, Dr. E.; Tacconi, Dr. L.; Verma, Dr. A. (until 31.8.); Wetzstein, Dr. M.; Wildgruber, G.

Guests

Jaffe, Prof.. D. (1.-30.6.); Cimatti, Dr. A. (3.4.-20.7.); Netzer, Prof. H. (until 31.1.)

PhD / Diploma

Buschkamp, P. (Hofmann); Dasyra, Dipl.-Phys. K. (until 20.8., Tacconi); Genel, S. (since 1.9., Genzel); Gobat, R. (until 31.3., Lehnert); Harayama, Dipl.-Phys. Y. (until 31.1., since 1.8., Eisenhauer); Hönle, Dipl.-Phys. R. (until 31.7., Poglitsch); Ihle, S. (until 31.10., Eisenhauer); Müller-Sanchez, F. (Davies); Nesvadba, Dipl.-Phys. N.

(until 30.9., Lehnert); Schropp, M. (since 9.10., Rabien); Schweitzer, Dipl.-Phys. M. (Poglitsch/Sturm); Trippe, Dipl.-Phys. S. (Genzel); Valiante, Dipl.-Phys. E. (Lutz/Sturm); Viehhauser, Dipl.-Phys. W. (until 30.8., Poglitsch)

X-Ray Astronomy

Secretary: Boller, B. / Jakobs, I. (until 31.1.)

Andritschke, Dipl.-Phys. R.; Aschenbach, Dr. B.; Becker, Prof. Dr. W.; Boller, Prof. Dr. T.; Böse, Dr. G. (until 30.9.); Braig, Dipl.-Phys. C. (until 30.4.); Bräuninger, Dr. H.; Briel, Dr. U.; Brunner, Dr. H.; Brusa, Dr. M.; Burkert, Dr. W.; Burwitz, Dr. V.; Carlson, Dr. A. (since 9.1.); Dennerl, Dr. K.; Donnert, J. (6.6.-31.7.); Finoguenov, Dr. A.; Frankenhuizen, W.; Freyberg, Dr. M.; Friedrich, Dr. P.; Fürmetz, M. (6.3.-31.7.); Gallo, Dr. L. (until 30.11.); Geppert, Dr. U. (until 31.3.); Gruber, Dr. R. (until 30.4.); Haberl, Dr. F.; Hambaryan, V. (1.3.-31.8.); Hartner, Dipl.-Math. G.; Hirschinger, M.; Iwasawa, Dr. K.; Kahabka, Dr. P.; Kim, Dr. J.W. (until 31.1.); Kimmel, Dipl.-Phys. N. (until 15.9.); Komossa, Dr. S.; Lange, R. (until 31.10.); Lemson, Dr. G.; Mainieri, Dr. V. (until 31.7.); Meidinger, Dr. N.; Mießner, D.; Misaki, K.; Misanovic, Z. (until 31.1.); Müller, Dr. A.; Naumann, A. (15.2.-15.3.); Nosenko, V. (since 4.9.); Pfeiffermann, Dipl.-Phys. E.; Pietsch, Dr. W.; Porquet, Dr. D. (until 31.10.); Porro, Dr. M.; Predehl, Dr. P.; Ramirez, J.M.; Schaller, G.; Schopper, Dr. F.; Shen, Dr. S.; Silverman, Dr. J.; Stojetz, W. (4.9.-6.10.); Strateva, Dr. I. (since 1.3.); Strüder, Prof. Dr. L.; Szokoly, Dr. G.P.; Treis, Dr. J.; Trill, M. (3.-17.8.); Voges, Dr. W.; Vongehr, M.; Wöhrl, S. (6.-16.6., 31.7.-25.8.)

Guests

Carrera, J. (26.9.-19.11.); Filipovic, M. (8.9.-4.10.); Giodini, S. (1.10.-30.11.); Griffiths, R. (11.7.-15.8.); Henry, Prof. Dr. P. (15.6.-14.8.); Miyaji, T. (27.8.-1.10.); Schmidt, M. (26.10.-15.11.); Tanaka, Prof. Dr. J.P., Trichieri, Dr. G.; Xu, Dr. D. (8.8.-22.9.)

PhD / Diploma

Balestra, Dipl.-Phys. I. (Boller); Bauer, Dipl.-Phys. M. (Pietsch); Cappelluti, Dipl.-Phys. N. (Hasinger); Deresch, A., (until 31.5., Pfeiffermann/Predehl); Fan, Dipl.-Phys. Y. (until 31.8., Komossa); Huang, Dipl.-Phys. H.-H. (Becker); Hui, D. (Becker); Hyde, E. (Meidinger); Mühlegger, Dipl.-Phys. M. (since 1.9., Hasinger); Posselt, Dipl.-Phys. B. (Haberl/Voges); Stiele, H. (since 1.5.), Pietsch/Hasinger); Trepl, L. (since 1.4., Becker); Trill, M. (until 18.5., Burwitz); Wölfel, Dipl.-Phys. S. (Strüder); Zhang, C. (until 31.10., Strüder);

Gamma-Ray Astronomy

Team Assistant: Frankenhuizen, W.

Brunschweiler, J. (20.2.-15.7.); Diehl, Dr. R.; Falke, L. (until 31.1.); Greiner, Dr. J.; Halloin, H. (until 30.8.); Kanbach, Dr. G.; Kienlin von, Dr. A.; Lichti, Dr. G.; McBreen, Dr. S. (since 1.4.); Mühlegger, Dipl.-Phys. M. (1.5.-16.6.); Petry, Dr. D. (since 1.9.); Rehm, D.; Sala, Dr. G. (since 1.5.); Savaglio, Dr. S. (since 1.3.); Strong,

Dr. A.; Willis, Dr. D. (until 31.8.); Yoldas, A.; Zhang, Dr. X.-L. (since 15.9.)

Guests

Dogiel, Prof. V. (1.-31.8.); Harris, Dr. M. (1.10.-31.12.); Hartmann, Prof. D. (3.-28.7.); Iyudin, Dr. A., Longo, F. (1.-28.2.); Slowikowska, A. (until 1.9.); Zeh, A. (1.6.-31.8.)

PhD / Diploma

Ajello, Dipl.Phys. M. (until 30.9., Kanbach); Andritschke, Dipl.Phys. R. (until 5.12.); Brunschweiger, J. (since 13.11., Greiner); Bissaldi, E. (since 1.9., Lichti); Bottacini, E. (Collmar); Clemens, C. (Greiner); Duscha, S. (Kanbach); Huber, B. (since 1.4., Kanbach); Kretschmer, Dipl.Phys. K. (until 31.8., Diehl); Krühler, T. (since 1.11., Greiner); Küpcü Yoldas, Dipl.Phys. A. (until 31.7.); Lang, M. (since 17.7., Diehl); Mühlegger, M. (until 31.3., Kanbach); Orlando, E. (Strong); Prymak, N. (Greiner); Schächner, G. (Kanbach); Stefanescu, Dipl.Phys. A. (Kanbach); Wang, W. (Diehl)

Theory & Complex Plasmas

Secretary: Langer, A. / Collmar, E.
 Andreani, P. (until 31.5.); Annaratone, Dr. B.M. (until 31.12.); Aschenbrenner, Dr. T.; Böhringer, Dr. H.; Brinkmann, Dr. W. (until 30.11.); Broeg, C. (since 1.8.); Bunk, Dr. W.; Fell, J. (since 18.9.); Höfner, Dipl.Phys. H.; Ivlev, Dr. A.; Jamitzky, Dr. F.; Kluge, M. (27.3.-13.4., 27.6.-31.8.); Klumov, Dr. B.; Konopka, Dr. U.; Khrapak, Dr. S.; Kretschmer, Dr. M.; Li, Dr. Y. (since 1.11.); Martin, Dr. J. (until 31.10); Monetti, Dr. R.; Nosenko, Dr. V. (since 4.9.); Pierini, Dr. D.; Pompl, Dr. R.; Pratt, Dr. G.; Pustynnik, M. (since 9.10.); Râth, Dr. C.; Ratynskaia, Dr. S. (until 30.9.); Rohr, S. (13.2.-3.3.); Rubin-Zuzic, Dr. M.; Samsonov, Dr. D. (until 15.3.); Sato, T. (until 31.1.); Schachenmayer, J. (13.3.-21.4.); Scheingraber, Dr. H.; Schwabe, M. (1.6.-10.7.); Shimizu, Dr. T.; Shimizu, Dr. S.; Shukla, N. (1.9.-31.10.); Sidorenko, Dr. I.; Thoma, Dr. M.; Thomas, Dr. H.; Yaroshenko, Dr. V.; Zhdanov, Dr. S.

Guests

De Angelis, Prof. U.; Fortov, Prof. V.; Horanyi, Prof. M. (1.9.-31.10.); Khrapak, Prof. A.; Martin, Dr. J. (until

31.10.); Steinberg, Prof. V. (until 30.4.); Takahashi, Dr. K. (until 31.3.); Tsytovitch, Prof. V. (until 30.4., 3.-29.7.); Vladimirov, Prof. S. (1.-31.5.)

PhD / Diploma

Antonova, Dipl.-Phys. T. (Annaratone); Braglia, F. (Böhringer); Chaudhuri, M. (Morfill); Elsaßer, A. (until 31.10.); Faßbender, Dipl.-Phys. R. (Böhringer); Fink, Dipl.-Phys. M. (Morfill); Gonzalez Tapia, Dipl.-Phys. E. (until 27.11., Morfill); Heidemann, R. (since 1.7., Thomas); Huber, Dipl.-Phys. P. (Morfill); Knapek, Dipl.-Phys. C. (Morfill); Kompaneets, Dipl.-Phys. R. (Morfill); Mitic, S. (since 1.11., Morfill); Mokler, Dipl.-Phys. F. (until 31.10., Morfill); Santos, J. (Böhringer); Schwabe, M. (since 1.8., Konopka); Simionescu, A. (Böhringer); Sütterlin, Dipl.-Phys. R. (Morfill); Zhang, Y.-Y. (Böhringer)

Optical and Interpretative Astronomy

Secretary: Rieperding, M.
 Burkert, Prof. Dr. A. (since 1.10, MPE Fellow); Drory, Dr. N. (since 1.9.); Feulner, G. (until 30.4.); Gabasch, Dr. A.; Gebhardt, Dr. K.-H. (until 31.7.); Gerhard, Prof. Dr. O.; Hopp, Dr. U.; Milvang-Jensen, Dr. B. (until 31.3.); Muschiello, Dr. B.; Noyola y Loya, Dr. E. (since 1.9.); Phleps, Dr. S.; Riffeser, Dr. A. (until 28.2.); Saglia, Dr. R.; Schücker, Dr. P. (until 30.11.); Snigula, Dr. J.; Wilman, Dr. D.; Zibetti, Dr. S.

Guests

Bauer, A. (1.9.-15.12.); Coccato, L. (9.11.-10.12.); Kormendy, Dr. J. (24.5.-27.12.)

PhD / Diploma

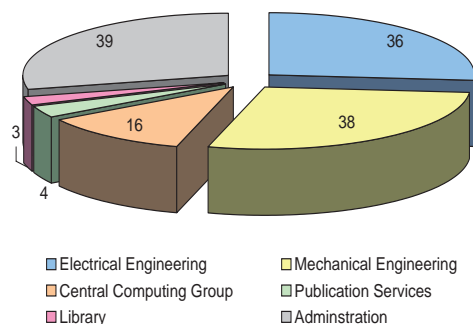
Balaguera Antolinez, A. (since 28.8., Schücker/Bender); Das, P. (since 15.9., Gerhard); De Lorenzi, Dipl.-Phys. F. (Gerhard); Hirschmann, M. (since 15.10.); Köhler, R. (Bender); Köppenhöfer, Dipl.-Phys. J. (until 31.1., Saglia); Nieves, Dipl.-Phys. L.A. (Bender); Nowak, Dipl.-Phys. N. (Saglia); Pannella, Dipl.-Phys. M. (since 1.2., Bender); Riffeser, Dipl.-Phys. A. (until 28.2., Bender); Ulubay Siddiki, Dipl.-Phys. A. (Gerhard); Ventimiglia, G. (since 1.9., Gerhard); Walch, Dipl.-Phys. S. (Burkert)

Engineering and Workshops

Electronic Engineering

Hippmann, Dipl.-Ing. H. (until 31.8 Head of Electronics)
 Tarantik, Dipl.-Ing. K. (since 1.9. Head of Electronics)
 Albrecht, Dipl.-Ing. S. (since 1.6.); Albrecht, F. (since 1.12.); Barl, Dipl.-Ing (FH) L.; Bornemann, Dipl.-Ing (FH) W.; Burghardt, Dipl.-Ing (FH) T.; Cibooglu, H.; Deuter, M.; Emslander, A.; Fumi, Dr. F.; Gressmann, R.; Hagl, Dipl.-Ing (FH) T.; Hälker, Dipl.-Ing (FH) O.; Hans, O., Hengmith, M.; Herrmann, Dipl.-Ing (FH) S.-C.; Jakob, Dipl.-Ing (FH) G.; Karing, W. (until 30.6.); Kellner, Dipl.-Ing (FH) S.; Kink, Dipl.-Ing (FH) W.; Lange, R. (until 31.10.); Langer, P.; Lederer, R.; Lieb, W.; Müller, Dipl.-Ing (FH) S.; Oberauer, F.; Rau, Dipl.-Ing (FH) C. (since 1.2.); Reiss, P.; Rothermel, Dr. H.; Rupprecht, T.; Schneider, M.; Schrey, F., Steffes, B.; Tarantik, Dipl.-Ing. K. (until 31.8); Yaroshenko, V.; Zanker-Smith, J. (since 1.9.)

Engineering, Workshop and Central Services Staff



Diploma

Ziegleder, J. (since 1.9.)

Mechanical Engineering

Thiel, Dipl.-Ing. M. (Head of Mechanics)
 Bayer, R.; Blasi, T. (since 1.3.); Brandstetter, J., Brara, A.; Budau, B.; Czempiel, S.; Deuschle, G. (until 31.10.); Deysenroth, C.; Deysenroth, M. (since 1.10.); Dietrich, G.; Dittrich, Dipl.-Ing (FH); K.; Eibl, J.; Feldmeier, P.; Gahl, J.; Goldbrunner, A.; Haug, Dipl.-Ing. (FH) M.; Heidelberg, T. (until 28.2.); Honsberg, M.; Huber, N.; Huber, S.; Huber, F.-X.; Huber, Dipl.-Ing (FH) H.; Kestler, H.-J.; Kettenring, Dipl.-Ing. G. (until 30.6.); Liebhardt, J. (since 1.3.); Mayr, R.; Mayr-Ihbe, R.; Mican, Dipl.-Ing. B.; Plangger, M.; Rohe, C.; Sandmair, R.; Schnell, P.; Schunn, W.; Soller, F.; Straube, P.; Wildmoser, T. (30.10.-8.12.); Zaglauer, Dipl.-Ing. (FH) W. (until 24.5.)

Apprentices

Arzt, S.; Bibracher, M.; Blasi, T. (until 28.2.); El-Masry, J.; Hartwig, J.; Liebhardt, J. (until 28.2.); Niemetz, E. (since 1.9.); Schindlmeier, M.; Schneider, A.; Urban, T. (since 1.9.)

Work Experience (Schools)

Anzer, G. (29.5.-2.6.); Bieringer, M. (20.-24.2.); Cavdar, C. (8.-12.5.); Cziasto, D. (15.-19.5.); Maßmann, F. (3.-7.4.); May, J. (17.-21.7.); Ostwald, R. (26.-30.6.); Paulini, R. (10.-14.7.); Plattner, M. (30.10.-3.11.); Preisler, C. (10.-13.4.); Sigl-Beck, C. (18.-21.4.)

Work Experience (University)

Hüsson, P. (19.6.-28.7.); Prunkl, E. (6.-31.3.); Stäbler, D. (28.2.-3.3.); Steinberger, B. (28.8.-13.10.)

Central Services

Computing

Central Computing Committee

Bauer, Dipl.-Phys. O.H. (Head)
 Bohnet, Dipl.-Phys. A.; Brinkmann, Dr. W. (until 30.11.); Burwitz, Dr. V.; Collmar, Dr. W. (until 31.10.); Haberl, Dr. F. (deputy); Jamitzky, Dr. F.; Leistner, G.; Lutz, Dr. D.; Müller, Dipl.-Ing. (FH) S.; Ott, Dr. T.; Petry, Dr. D. (since 1.11.); Rubin-Zuzic, Dr. M. (since 1.12.)

Central Computing Support Group

Bauer, Dipl.-Phys. O.H. (Head)
 Baumgartner, H. (network, system support); Bohnet, Dipl.-Phys. A. (system support Optical and Interpretative Astronomy); Collmar, Dr. W. (GRO, INTEGRAL, IMPF); Kleiser, A. (Printer support); Klose, L. (network, System support); Oberauer, A. (Software, PC support); Ott, Dr. T. (system support Infrared); Paul, J. (X-ray, data security); Post, C. (network, system support PC and Linux); Sigl, Dipl.-Ing. (FH) R. (network management); Steinle, Dr. H. (data archives, archive systems, WWW); Vaith, Dipl.-Phys. H. (since 1.7., system support Optical and Interpretative Astronomy); Voges, M. (programming); Wieprecht, Dipl.-Ing. E. (Herschel-PACS); Wiezorrek, Dipl.-Ing. (FH) E. (Herschel-PACS)

Publication Services and Copy Shop

Hauner, R.; Karing, W.; Mayr-Ihbe, R.; Mory, B.

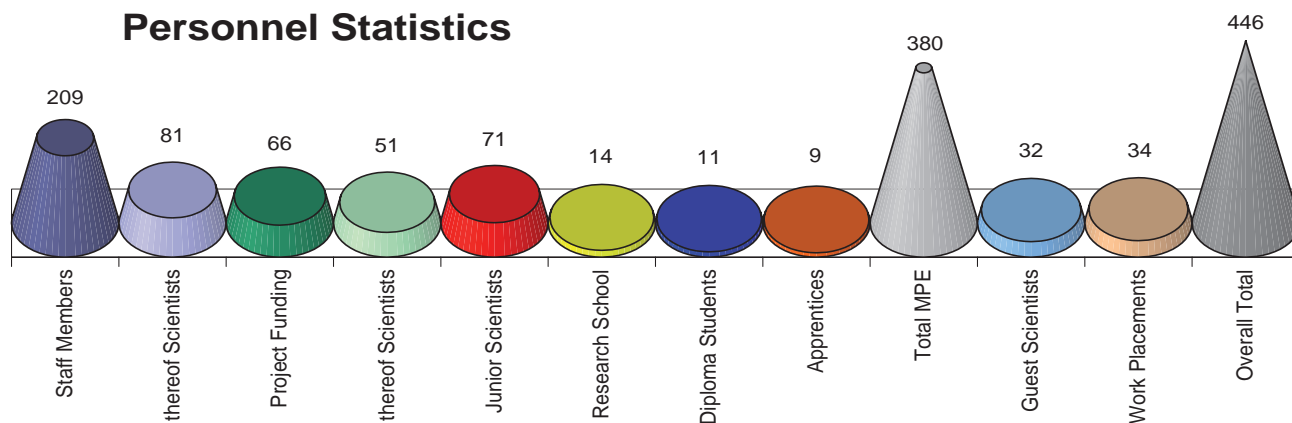
Library

Chmielewski, E. (Head)
 Hardt, C., Schurkus, R.

Administration

Ihle, M. (Head)
 Secretary: Kliem, V.
 Apold, G.; Arturo, A.; Bauernfeind, M.; Bidell, M.; Bitzer, U.; Blaschek, M.; Cziasto, U.; Cziasto, S. (17.5.-31.7.); Doll, E.; Ertl, M.; Gleixner, W. (until 31.7.); Goldbrunner, S.; Grasmann, M.; Gschnell, H.-P.; Hübner, R. (3.-5.1., 2.-23.6., 3.8.-8.9.); Inhofer, I.; Jäkel, T.; Karing, W. (since 1.7.); Keil, M.; Kestler, L.; Kürzinger, T.; Kus, H. (until 5.9.); Lochner, C.; Mazur, A. (since 2.10.); Nagy, A.; Neun, A.; Peischl, M.; Preisler, C.; Reither, A.; Rochner, R.; Rossa, E.; Sandtner, P.; Scheiner, B.; Schneider, D.; Sedlmeir, G. (1.-30.6., 31.7.-15.9.); Seeger, Dipl.-Ökonom G., Steinle, R.; Strecker, R. (6.-23.6., 7.8.-1.9.); Strecker, R.; Thiess, L.; Troll, P.

Personnel Statistics



Science Project Teams

(Project managers underlined)

Space Physics of Near-Earth Environment

ACE / SEPICA

Klecker, Zanker-Smith

CLUSTER / CIS

Klecker, Marghitu, Paschmann, Pitout, Scholer.

CLUSTER / Data Center

Georgescu, Klecker, Leistner, Volwerk.

CLUSTER / EDI

Georgescu, Haaland, Paschmann, Treumann, Vaith.

Double Star

Georgescu, Haaland, Klecker, Paschmann, Pitout.

ROSETTA-Lander

Haerendel (IUB), Thiel.

SAMPEX / HILT

Klecker, Scholer.

SOHO / CELIAS

Klecker, Scholer, Zanker-Smith.

STEREO / PLASTIC

Klecker, Zanker-Smith.

Infrared/Submillimeter Astronomy

Deputies to the Director of the Group

Lutz, Tacconi.

GRAVITY

Abuter, Eisenhauer, Gillessen, Gräter, Haug, Hofmann, Ihle S., Kellner, Paumard, Rabien, Thiel, Ziegleder.

Herschel-PACS

Barl, Bauer, Berg v., Bickert Cesarsky, Contursi, Eibl, Feuchtgruber, Friedl, Geis, Hartinger, Igl, Jakob, Katterloher, Kleiser, Kornberg, Krombach, Lutz, Müller T., Osterhage, Poglitsch, Schmid, Schubert, Seidenschwang, Sturm, Thiel, Wetzstein, Wieprecht, Wiezorrek, Wildgruber, Yaroshenko.

ISO Spectrometre

Bauer, Feuchtgruber, Lutz, Müller T., Sturm, Verma, Wieprecht.

KMOS

Agudo Berbel, Davies, Förster-Schreiber, Hofmann, Lehnert.

LBT, Lucifer

Buschkamp, Eisenhauer, Gemperlein, Gillessen, Gräter, Hofmann, Lederer, Lehnert, Straube.

LBT IFU

Eisenhauer, Haug, Müller-Sanchez.

PARSEC

Davies, Huber S, Kellner, Ott, Rabien, Schropp, Ziegleder.

PRIMA testbed

Abuter, Eisenhauer, Gräter, Haug, Kellner, Rabien, Thiel.

Sofia-FIFI-LS

Fumi, Geis, Hönle, Klein, Oberauer, Poglitsch, Raab, Schweitzer, Viehhauser.

GaAs-Detektoren

Jakob, Katterloher.

Galactic Centre

Abuter, Eisenhauer, Genzel, Gillessen, Maness, Martins, Ott, Paumard, Trippe.

Galactic Nuclei

Contursi, Dasyra, Davies, Friedrich S., Genzel, Gilbert, Hicks, Hamaus, Lutz, Müller-Sanchez, Netzer, Schweitzer, Sturm, Tacconi, Verma.

Galaxies at large redshifts

Abuter, Bouché, Buschkamp, Cresci, Eisenhauer, Förster-Schreiber, Genel, Genzel, Gobat, Lehnert, Lutz, Nesvadba, Sturm, Tacconi, Valiante, Verma, Viehhauser.

X-Ray Astronomy

Astrogrid-D

Carlson, Voges.

CAST

Bräuninger, Strüder.

Chandra

Burwitz, Predehl.

Euro-VO_DCA

Lemson, Voges.

GAVO

Kim, Lemson, Voges.

ROSAT

Boese, Gruber, Haberl, Voges.

eROSITA

Andritschke, Aschenbach, Bornemann, Bräuninger, Briel, Brunner, Burkert, Eder, Freyberg, Friedrich, Hälker, Hartmann, Hartner, Hasinger, Hengmith, Hermann, Hippmann, Hirschinger, F. Huber, H. Huber, Kettenring, Kink, Meidinger, Müller, Pfeiffermann, Predehl, Rohe, Strüder, Vongehr.

SDSS

Böhringer, Boller, Gallo, Hasinger, Huber M., König, Voges.

SIMBOL-X

Briel, Hälker, Hasinger, Herrmann, Hippmann, Huber, Lechner, Pietsch, Strüder, Treis.

Skinakas Observatory

Bauer, Hasinger, Lieb.

SWIFT

Ajello, Brunschweiler, Greiner, Hartner, Hasinger, Strong, Voges.

XEUS

Aschenbach, Boller, Bräuninger, Braig, Burkert, Friedrich, Hasinger, Meidinger, Schaller, Strüder, Trümper, Vongehr.

XEUS-WFI

Andritschke, Hälker, Herrmann, Meidinger, Mießner, Schopper, Strüder, Treis.

XMM-Newton

Aschenbach, Bohnet, Boller, Bornemann, Briel, Brunner, Burkert, Dennerl, Freyberg, Gallo, Gruber, Haberl, Hartner, Hengmith, Hippmann, Hirschinger, Huber, Kettenring, Kink, Lange, Meidinger, Müller, Pfeffermann, Pietsch, Predehl, Strüder, Trümper.

Gamma-Ray Astronomy

COMPTEL

Collmar, Diehl, Strong.

EGRET

Kanbach.

GLAST

Collmar, Diehl, Greiner, Kanbach, Kienlin v., Lichti, Steinle, Strong.

GROND

Bornemann, Clemens, Fueger, Greiner, Hasinger, Huber H., Schrey, Szokoly, Thoene, Wölfl, Yoldas, Zaglauer.

INTEGRAL

Diehl, Kienlin v., Kretschmar, Kretschmer, Lerusse, Lichti, Pottschmidt, Strong.

MEGA

Andritschke, Kanbach, Schönfelder, Schrey, Zoglauer.

OPTIMA

Kanbach, Schrey, Steinle H., Stefanescu.

Jet-Sources

Ajello, Bottacini, Collmar, Greiner, Kanbach, Pottschmidt, Sala, Willis, Zhang.

Nuclear Astrophysics

Cierniak, Diehl, Kienlin, Kretschmar, Kretschmer, Lang, Lichti, Strong.

Relativistic Particle Accelerators

Ajello, Collmar, Diehl, Duscha, Kanbach, Mühlegger, Orlando, Slowikowska, Stefanescu, Strong.

Gamma-Ray Bursts

Clemens, Greiner, Huber B., Kanbach, Krauss, Krühler, Küpcü-Yoldas, Primak, Stein, Steiner, Thöne, Willis, Yoldas.

Theory and Complex Plasmas

IMPF

Annaratone, Hagl, Höfner, Huber, Ivlev, Konopka, Morfill, Rothermel, Sütterlin, Tarantik, Thoma, Thomas, Rubin-Zuzic.

PK-3 Plus

Annaratone, Bigelmayr, Hagl, Huber, Ivlev, Konopka, Morfill, Rothermel, Stöcker, Sütterlin, Tarantik, Thomas, Rubin-Zuzic.

PK-4

Deysenroth, Fink, Höfner, Kretschmer, Morfill, Ratynskaia, Tarantik, Thoma.

PKE-Nefedov

Annaratone, Hagl, Huber, Ivlev, Khrapak, Klumov, Konopka, Kretschmer, Mokler, Morfill, Rothermel, Rubin-Zuzic, Samsonov, Sütterlin, Thomas, Zhdanov.

Student Experiment "Plasma Crystal"

Kretschmer, Morfill, Rothermel, Thoma.

Strip-Electrode

Annaratone, Deysenroth, Höfner, Konopka, Morfill, Steffes.

Adaptive Electrode

Annaratone, Chauduri, Huber, Morfill, Steffes, Thomas.

Diamant-Laboratory

Dose, Jakob, Morfill, Rothermel, Shimizu, Thomas.

3-D-Diagnostics

Antonova, Chauduri.

High-Energy Astrophysics

Arevalo, Braglia, Böhringer, Brinkmann, Faßbender, Pierini, Pratt, Santos, Simionescu, Zhang, Zimer.

GEC-Laboratory

Knappek, Konopka, Morfill, Samsonov, Sütterlin, Thomas, Rubin-Zuzic.

High-Field Laboratory

Deysenroth, Konopka, Kretschmer, Morfill, Schwabe, Steffes, Tarantik, Tichmann.

Nonlinear Dynamics, Complex Systems
Aschenbrenner, Böhm, Bunk, Jamitzky, Monetti, Müller,
Pompl, R  th, Scheingraber.

Paramagnetic-Laboratory
Huber, Knappek, Morfill, Samsonov, Steffes, Zhdanov.

Plasmaphysics
Scholer, Sidorenko, Treumann.

Plasma Torch
Bunk, Morfill, Sato, Shimizu, Steffes.

Optical and Interpretative Astronomy

ASTRO-WISE
Bender, Saglia, Wilman.

Galaxy Dynamics

Bender, Gerhard, Saglia, Thomas.
KMOS
Bender, Saglia.

Large Scale Structure
Bender, Phleps, Sch  cker, Saglia, Wilman.

MUNICS
Bender, Hopp, Drory

OmegaCAM
Bender, Hopp.

PanSTARRS
Bender, Hopp, Phleps, Saglia, Wilman.

Stellar Populations and Galaxy Evolution
Bender, Hopp, Pierini.

Scientific Collaborations in Projects

Argentina

Observatorio Astronomico Felix Aguilar (OFA), Universit  t San Juan, and Instituto de Astronomia y Fisica del Espacio (IAFE), CONICET, Buenos Aires: H-alpha Solar Telescope for Argentina (HASTA).

Australia

Australian National University: Galaxy formation.
Melbourne University: Astro-Plasma Physics.
Swinburne University of Technology, Victoria: Millisecond Pulsars.

Austria

Institut f  r Weltraumforschung der   sterreichischen Akademie der Wissenschaften, Graz: CIS; EDI on CLUSTER; Geomagnetical tail.
Universit  t und TU Wien: Herschel-PACS.

Belgium

CSL Li  ge, Katholieke Universiteit Leuven: Herschel-PACS, INTEGRAL-Spectrometer SPI,
European Commission, Joint Research Centre (JRC-IRMM), Geel: Development of large-area X-ray filters for eROSITA.

Brasil

Universidade de Sao Paulo: Galaxy formation.

Chile

Universidad de Concepcion: X-Ray Binaries.
Universidad Catolica Santiago: X-Ray Binaries.

China

Institute for High-Energy Physics (IHEP), Peking: AGN and unidentified Gamma sources of COMPTEL and INTEGRAL.
University of Hongkong: Radiation mechanisms of pulsars from X-rays to Gamma-rays.

France

CEA, Saclay: INTEGRAL-Spectrometer SPI; Herschel-PACS; CAST; SIMBOL-X.
Centre d'Etude Spatiale des Rayonnements (UPS), Toulouse: INTEGRAL-Spectrometer SPI; CIS/Cluster; Double Star.
Centre d'Etudes des Environnements Terrestres et Plan  taires (CNRS), St Maur des Foss  s: FAST – auroral physics; IMPF.
GREMI-Lab, Orleans: Complex Plasmas; Plasma-crystal experiment on ISS.
IGRP Marseille: Herschel-PACS.
Observatoire de Meudon: ASTRO-WISE.
Observatoire de Paris / LESIA: GRAVITY
Universit   d'Orl  ans CNRS: PKE-Nefedov.

Germany

Astrophysikalisches Institut Potsdam: eROSITA; XMM-Newton; GAVO; OPTIMA, GROND.
Christian-Albrechts-Universit  t, Kiel: IMPF; Complex Plasmas; STEREO.
DLR Berlin: SOFIA.
DLR-K  ln Porz: Plasma-Crystal Experiment; Rosetta Lander (ROLAND); PKE-Nefedov.
European Southern Observatory (ESO), Garching: KMOS Multiobject spectrograph for VLT; GRAVITY; PARSEC for the VLT Laser Guide Star Facility; ISO (extragalactic program); ROSAT (MIDAS); Galaxy formation; ASTRO-WISE; OmegaCAM, PRIMA testbed.
Fraunhofer Institut f  r Festk  rper-Technologie, M  nchen: XEUS; eROSITA.
Fraunhofer Institut f  r Mikroelektronische Schaltungen und Systeme, Duisburg: Development of micro electronics; CAMEX 64B; JFET-CMOS Prozessor; XEUS; eROSITA.
International University Bremen: Astro-Plasma Physics, CLUSTER

Institut für Festkörperphysik und Werkstoff-Forschung, Dresden: Development of magnetically soft materials.

Institut für Astronomie und Astrophysik Tübingen (IAAT): XMM-Newton; eROSITA.

Klinik für Dermatologie, Allergologie und Umweltmedizin, Krankenhaus München Schwabing: Plasma medicine.

Landessternwarte Heidelberg-Königstuhl: Near-Infrared Spectrograph LUCIFER für LBT; Galaxy formation.

Ludwig-Maximilians-Universität, München: OmegaCAM; ASTRO-WISE; KMOS.

Max-Planck-Institut für Sonnensystemforschung, Katlenburg-Lindau: Experiment CELIAS on SOHO; Experiment CIS on CLUSTER; Rosetta Lander (ROLAND); Theory on multi-ion plasmas.

Max-Planck-Institut für Astronomie, Heidelberg: GRAVITY; PARSEC; Herschel-PACS; PanSTARRS, SDSS.

Max-Planck-Institut für Astrophysik, Garching: GAVO; SDSS; OPTIMA.

Max-Planck-Institut für Physik, Werner Heisenberg Institut, München: Development of CCDs; Active pixel detectors (APS); JFET-Electronics and drift detectors for X-rays; CAST.

Thüringer Landessternwarte Tautenberg: GROND; Gamma-Ray Bursts.

Technische Universität Braunschweig, Institut für Geophysik und Meteorologie: Hybridcode-Simulations; Mirror-Modes.

Technische Universität Darmstadt: CAST.

Universität Bochum: Complex Plasmas.

Universität Bonn: Test of pixel detectors for XEUS; OmegaCAM; ASTRO-WISE.

Universität der Bundeswehr München: Venus Express.

Universität Greifswald: Complex Plasmas.

Universität Köln: Galactic Centre; GRAVITY.

Universitätssternwarte Göttingen: OmegaCAM.

Universität Siegen; Compton Camera

Greece

University of Crete and Foundation for Research and Technology Hellas (FORTH), Heraklion: Development and operation of the Skinakas Observatory; Studies of wind-accreting X-ray binaries; Development and application of the OPTIMA photometers; Optical identifications and monitoring of X-ray selected.

Israel

Ber Sheva University: Astro-Plasma Physics.

School of Physics and Astronomy, Wise Observatory, Tel Aviv: Active Galaxies; Interstellar medium; ISO extragalactic program.

Weizmann Institut, Rehovot: Complex Plasmas; Galactic Centre.

Italy

Brera Astronomical Observatory: Jet-X; Sky survey for clusters of galaxies; XEUS.

IFCAI-CNR Palermo: XMM-Newton observations of neutron stars and pulsars.

INAF Trieste: Gamma-Ray Bursts.

INFR Frascati: SIDDHARTA

Istituto di Fisica Cosmica e Tecnologia, Mailand: INTEGRAL-Spectrometer SPI.

Istituto di Fisica dello Spazio Interplanetario (CNR), Frascati: ESIC; Herschel-PACS; CLUSTER/CIS; Double Star.

OAA/LENS Firenze: Herschel-PACS.

OAP Padua: Herschel-PACS; OmegaCAM.

Osservatorio Astrofisico di Arcetri, Florenz: Hardpoints for primary mirror of LBT.

Osservatorio di Capodimonte, Napoli: OmegaCAM; ASTRO-WISE.

Osservatorio di Padova: OmegaCAM.

Politecnico di Milano: low-noise electronics; detector development for X-rays.

Universität Neapel: Complex Plasmas.

Japan

Tokio Institute of Technology (TITECH), Ookayama: ASCA/XMM-Newton observations of AGN.

Institute of Space and Astronautical Science, Yoshinodai: Suzaku; Astro-F Solar System Observations; Astro-Plasma Physics.

Kyushu University: IMPF.

Tohoku University: Complex Plasmas; IMPF.

University of Tokyo: Astro-F Solar System Observations; Astro-Plasma Physics.

Kroatia

Ministry of Science and Technology, Zagreb: CAST.

The Netherlands

ESTEC, Noordwijk: XMM-Newton-TS mirror calibration; CCD development; Radiation Performance Instrument; INTEGRAL.

SRON, Utrecht: COMPTEL; Chandra-LETG.

Sterrewacht Leiden: SPIFFI/SINFONI; ASTRO-WISE; OmegaCAM.

TU Delft: Reflexion measurements on black colours.

University Eindhoven: Complex Plasmas; IMPF.

University of Groningen, Kapteyn Institute: Reconstruction of the density distribution of the universe; OmegaCAM; ASTRO-WISE.

Norway

Universität Trømsø: Complex Plasmas; IMPF.

Portugal

Universität Lissabon: Complex Plasmas.

Rumania

Institute for Space Sciences, Bucarest: Plasma physics; FAST; CLUSTER.

Russia

Institute for High Energy Densities of the Russian Academy of Science, Moscow: Plasma-crystal experiment (PKE); IMPF.

Institute Physics of Earth, Moscow: Plasma physics; Astro-Plasma Physics.

Space Research Institute (IKI) of the Russian Academy of Science, Moscow: Calibration of JET-X, eROSITA.

IHED Moscow: PKE-Nefedov; PK-3 Plus; PK-4.

Skobeltsyn Institute of Nuclear Physics, Moscow: Nuclear astrophysics and Gamma-Ray Bursts.

Switzerland

CERN, Geneva: CAST.

International Space Science Institute, Bern: Plasma physics; Astro-Plasma Physics.

Observatoire de Genève Sauverny, Geneva: ISDC.

Universität Bern: SOHO/CELIAS; STEREO/PLASTIC.

Spain

Instituto de Astrofísica de Canarias (IAC), Laguna: Herschel-PACS.

Universidad Valencia, Department de Astronomia, Valencia: INTEGRAL-Spectrometer SPI.

Universidad de Zaragoza: CAST.

Taiwan

National Central University, Chungli: IMPF.

Turkey

Bogazici University, Istanbul: IMPF; CAST.

UK

BRUNEL University: XEUS.

John Moores University, Liverpool: Sky survey of clusters of galaxies.

Rutherford Appleton Laboratory, Council for the Central Laboratory of the Research Councils: SIS-Junctions; Complex Plasmas; Rosetta Lander (ROLAND); JSOC for CLUSTER.

University of Birmingham: INTEGRAL-Spectrometer SPI; XMM-Newton.

University of Bristol: KMOS.

University of Durham: KMOS, PanSTARRS.

University of Edinburgh: KMOS, PanSTARRS.

University of Leicester: XMM-Newton data analysis; XEUS; Swift.

University of Liverpool: Complex Plasmas.

University of Wales, Cardiff: Filter for Herschel-PACS and SOFIA.

University Oxford: Complex Plasmas; IMPF, KMOS.

University of Sheffield: Astro-Plasma Physics.

USA

Brookhaven National Laboratory: radiation hard JFET-electronics; radiation-hard detectors.

California Inst. of Technology, Pasadena: SAMPEX; ACE; X-ray survey, STEREO.

Clemson University: Gamma-Ray Bursts; Nuclear astrophysics.

Dartmouth College, Hanover, NH: Space-Plasmaphysics, CLUSTER.

Harvard University: PanSTARRS.

Institute for Astronomy, Hawaii, Honolulu: Galaxy formation, PanSTARRS.

Johns Hopkins University: PanSTARRS

Lawrence Berkeley National Laboratory, Berkeley: Manufacturing of Ge:Ga detector elements for Herschel-PACS and SOFIA; Charakterisation of GaAs detector material.

Marshall Space Flight Center, Huntsville: GLAST Gamma-Ray Burst Monitor; XMM-Newton and Chandra Observations of neutron stars, pulsars, and supernovae remnants.

NASA/Goddard Space Flight Center, Greenbelt, MD: INTEGRAL-Spectrometer SPI; ACE; STEREO; Swift.

Naval Postgraduate School, Monterey: Modeling of the properties of gallium arsenide material for infrared detectors.

Pacific Northwest National Laboratory (PNNL), Richland: CAST.

Smithsonian Astrophysical Observatory, Cambridge: Chandra-LETGS; X-ray binaries in M31.

Space Telescope Science Institute, Baltimore: Galaxy formation.

University of Arizona, Tucson: cosmic radiation; SOHO/CELIAS; Planet formation; LBT.

University of California, Berkeley: MPG/UCB-Collaboration; Far-infrared detectors; Gallium arsenide centrifuge; Northern lights observations; FAST; INTEGRAL-Spectrometer SPI; CLUSTER/CIS; STEREO.

University of California, San Diego: CLUSTER/EDI; INTEGRAL-Spectrometer SPI; IMPF.

University of Colorado, Boulder: SAMPEX.

University of Iowa, Iowa City: Complex Plasmas; CLUSTER/EDI; IMPF; PKE-Nefedov.

University of Illinois at Urbana-Champaign: FIFLS.

University of Maryland, College Park, MD: SOHO; ACE.

University of New Hampshire, Durham: SEPICA/ACE; CLUSTER; SOHO; FAST; STEREO.

University of Pittsburgh: Galaxy formation.

University of Southern California, Los Angeles: SEM/CELIAS experiment on SOHO.

University of Texas, Austin: Galaxy formation.

University of Toledo: Galaxy formation.

University of Washington, Seattle: CLUSTER/CIS.

University Space Research Association, Moffett Field: SOFIA.

Multinational Collaborations

ASPI, The International Wave Consortium: CNR-IFSI Frascati, Italy; LPCE/CNRS Orleans, France; Dept. of Automatic Control and Systems University of Sheffield, UK.

ASTRO-WISE: LMU München, Universität Bonn, Germany; Sterrewacht Leiden, University of Groningen, The Netherlands; Osservatorio di Capodimonte, Napoli, Italy; Observatoire de Meudon, Paris.

CAST: CERN Geneva Switzerland; TU Darmstadt, MPI für Physik (WHI) München, Germany; Universidad de Zaragoza, Spain; Bogazici University Istanbul, Turkey; Ministry of Science and Technology Zagreb, Croatia; CEA/Saclay DAPNIA-SED, France; Pacific Northwest National Laboratory, Richland, USA.

CDFS, The Chandra Deep Field South: ESO Garching, Astrophysikalisches Institut Potsdam, Germany; IAP Paris, France; Osservatorio Astronomico Trieste; Istituto Nazionale di Fisica Nucleare Trieste, Italy; Associated Universities Washington, Johns Hopkins University Baltimore, Space Telescope Science Institute Baltimore, USA; Center for Astrophysics Hefei, China.

CDS – Coronal Diagnostic Spectrometer for the Solar and Heliospheric Observatory: Rutherford Appleton Laboratory Chilton, Mullard Space Science Laboratory London, University College London, Oxford University, UK; LPSP Verrieres-le-Buisson, Nice Observatory, France; Oslo University, Norway; ETH Zürich, Switzerland; GSFC Greenbelt, NRL Washington, HCO Cambridge, Stanford University, USA; Padova University, Turin University, Italy; MPAe Lindau, Germany.

CELIAS – Experiment for SOHO: MPS Katlenburg-Lindau, TU Braunschweig, Germany; Universität Bern, Switzerland; IKI Moskow, Russia; University of Maryland College Park, University of New Hampshire Durham, University of Southern California Los Angeles, USA.

Chandra: Marshall Space Flight Center Huntsville, Massachusetts Institute of Technology Cambridge, Smithsonian Astrophysical Observatory Cambridge, USA; Space Research Institute Utrecht, The Netherlands; Universität Hamburg, Germany.

CIS-Experiment for CLUSTER: MPS Katlenburg-Lindau Germany; Universität Bern, Switzerland; CESR Toulouse, France; IFSI-CRR Frascati, Italy; Universität Heraklion, Greece; Lockheed Palo Alto Res. Lab., Space Science Lab., Univ. of California Berkeley, Univ. of New Hampshire Durham, Univ. of Washington Seattle, USA.

COSMOS: INAF-Osservatorio Astronomico di Bologna, INAF-Osservatorio Astronomico di Roma, INAF-Osservatorio Astrofisico di Arcetri, INAF/IASF-CNR, Sezione di Milano, IRA-INAF, Bologna, Dipartimento di Astronomia, Università Padova, Dipartimento di Fisica, Università degli Studi Roma Tre, Italy; Harvard-Smithsonian Cen-

tre for Astrophysics, Cambridge, Department of Physics, Carnegie Mellon University, Pittsburg, Institute for Astronomy, University of Hawaii, California Institute of Technology, Pasadena, Department of Astronomy, Yale University, USA; INTEGRAL Science Data Centre, Versoix, Switzerland; Laboratoire d'Astrophysique de Marseille, France.

DOUBLE STAR: MPS Katlenburg-Lindau, Germany; IFSI-CRR Frascati, Italy; CESR Toulouse, France; Space Science Lab., University of California, Berkeley, University of New Hampshire, Durham NH, USA.

EDI-Experiment for CLUSTER: University of New Hampshire Durham, University of California San Diego, USA.

eROSITA: Universität Tübingen,, AIP Potsdam, Universität Hamburg, Remeis-Sternwarte Bamberg, MPA Garching, Germany; IKI Moskau, Russia.

EURO3D Research Training Network for promoting 3D spectroscopy in Europe: Astrophysikalisches Institut Potsdam, ESO Garching, Germany; Institute of Astronomy Cambridge, University of Durham, UK; Sterrewacht Leiden, The Netherlands; CRAL Observatoire de Lyon, Laboratoire d'Astrophysique Marseille, Observatoire de Paris section de Meudon, France; IFCTR-CNR Milano, Italy; IAC La Laguna, Spain.

FAST: SSL-UCB Berkeley, USA; CETP St.Maur, France.

GLAST – Gamma-Ray Burst Monitor: Marshall Space Flight Center Huntsville, University of Huntsville, USA.

GLAST – Gamma-Ray Large Area Space Telescope: Stanford University Palo Alto, Naval Research Laboratory Washington DC, Sonoma State University Rohnert Park, Lockheed Martin Corporation Palo Alto, University of California Santa Cruz, University of Chicago, University of Maryland Greenbelt, NASA Ames Research Center Moffett Field, NASA Goddard Space Flight Center for High Energy Astrophysics Greenbelt, Boston University, University of Utah Salt Lake City, University of Washington Seattle, SLAC Particle Astrophysics Group Palo Alto, USA; ICTP and INFN Trieste, Istituto Nazionale di Fisica Nucleare Trieste, Italy; University of Tokyo, Japan; CEA Saclay, France.

GRAVITY – Instrument for VLT Interferometry: MPIA Heidelberg, German; Observatoire de Paris / LESIA, France; Universität zu Köln, Germany; European Southern Observatory, Garching, Germany.

Herschel – PACS (Photodetector Array Camera and Spectrometer): CSL Liège, Katholieke Universiteit Leuven, Belgium; MPIA Heidelberg, Universität Jena, Germany; OAA/LENS Firenze, IFSI Roma, OAP Padova, Italy; IAC La Laguna, Spain; Universität und TU Wien, Austria; IGRAP Marseilles, CEA Saclay, France.

IMPF – International Microgravity Plasma Facility / IMPACT – International Microgravity Plasma, Aerosol and Cosmic Dust Twin Laboratory: Oxford University, UK; Université d'Orléans CNRS, France; Institute for High Energy Densities Moscow, Russia; University of Iowa, USA.; University of Tromsø, Norway; National Central University Chungli, Taiwan; Eindhoven University of Technology, The Netherlands; University of California, San Diego, USA.; Tohoku University, Kyushu University, Japan; Christian-Albrechts-Universität Kiel, Germany.

INTAS – Cooperation of Western and Eastern European Scientist: France, Germany, Norway, Russia.

ISDC – INTEGRAL Science Data Centre: Observatoire de Geneva Saclay, Switzerland; Service d'Astro-physique Centre d'Etudes de Saclay, France; Rutherford Appleton Laboratory Oxon Dept. of Physics University Southampton, UK; Institut für Astronomie und Astrophysik Tübingen, Germany; Danish Space Research Institute Lyngby, Denmark; University College Dublin, Ireland; Istituto di Fisica Milano, Istituto di Astrofisica Spaziale Frascati, Italy; N. Copernicus Astronomical Center Warsaw, Poland; Space Research Institute of the Russian Academy of Sciences Moscow, Russia; Laboratory for High Energy Astrophysics GSFC Greenbelt, USA.

INTEGRAL-Spectrometer SPI: Centre d'Etude Spatiale des Rayonnements (CESR) Toulouse, CEA Saclay Gif-sur-Yvette, France; Institute de Physique Nucleaire Université de Louvain, Belgium; Istituto di Fisica Cosmica e Tecnologia del CNR Milano, Italy; University de Valencia Burjassot, Spain; University of Birmingham, UK; NASA/GSFC Greenbelt, University of California Berkeley, University of California, San Diego, USA.

ISO-SWS Software and Calibration: SRON Groningen, The Netherlands; KU Leuven, Belgium; ESA Villafranca Spain.

KMOS Study for a VLT multi-IFU near-infrared spectrograph: Universitätssternwarte München, Germany; University of Durham, ATC Edinburgh, University of Oxford, Bristol University, UK.

LBT, Large Binocular Telescope Project: MPIA Heidelberg, MPIfR Bonn, Landessternwarte Heidelberg Königstuhl, Astrophysikalisches Institut Potsdam, Germany; University of Arizona Tucson, USA; Osservatorio Astrofisico di Arcetri Firenze, Italy.

Lockman Hole, optical/NIR identifications: Astrophysikalisches Institut Potsdam, ESO Garching, Germany; Istituto di Radioastronomia del CNR Bologna, Italien; Associated Universities Washington, California Institute of Technology Pasadena, Institute for Astronomy Honolulu, Princeton University Observatory, Pennsylvania State University University Park, USA; Subaru Telescope NAO Hilo, Japan.

OmegaCAM: ESO Garching, LMU München, Universität Bonn, Universitätssternwarte Göttingen, Germany; Ster-

rewacht Leiden, University of Groningen, The Netherlands; Osservatorio di Capodimonte, Napoli, OAP Padua, Italy.

PanSTARRS: MPIA Heidelberg, Germany, University of Hawaii, Harvard University, USA, Johns Hopkins Univ. Baltimore, MD, USA, Universities of Durham, Edinburgh, Belfast, UK.

Plasma-Crystal experiment PKE-Nefedov: IHED Moscow, Russia; University of Iowa, Iowa City, USA; DLR-Köln, Germany; Université d'Orléans CNRS, France.

PK-3 Plus (Plasma-crystal experiment): IHED Moscow, Russia.

PK-4 (Plasma-crystal experiment): IHED Moscow, Russia.

Plasma Physics, Astro-Plasma Physics: International Space Science Institute Bern, Switzerland; Institute Physics of Earth Moscow, Russia; University of Sheffield, UK.

PLASTIC experiment for STEREO: University of New Hampshire, Durham, NASA/GSFC Greenbelt, USA; Universität Bern, Switzerland; Universität Kiel, Germany.

SDSS (Sloan Digital Sky Survey): MPA Garching, MPIA Heidelberg, Germany; Univ. of Washington, Seattle, Fermi National Accelerator Laboratory, Batavia, IL, Univ. of Michigan, Ann Arbor MI, Carnegie Mellon Univ., Pittsburgh, PA, Penn State Univ., University Park PA, Princeton Univ. Observatory, Princeton, NJ, The Institute of Advanced Study Princeton, NJ, Space Telescope Science Institute, Baltimore, MD, Johns Hopkins Univ. Baltimore, MD, USA.

SIMBOL-X: Osservatorio Astronomico di Brera, Italy; CEA Saclay, France.

Swift: NASA/GSFC Greenbelt, Penn State University, USA; University of Leicester, Mullard Space Science Laboratory London, UK; Osservatorio Astronomico Brera, Italy.

XEUS: University of Leicester, UK; SRON Utrecht, The Netherlands; Institut für Astronomie und Astrophysik Tübingen, Germany; CESR Toulouse, France; Institute of Space and Astronautical Science (ISAS), Japan.

XMM-Newton/SSC: Astrophysikalisches Institut Potsdam, Germany; SAP Saclay, CDS Strasbourg, CESR Toulouse, France; University of Leicester, Institute of Astronomy Cambridge, MSSL London, UK.

XMM-Newton/TS: ESTEC Noordwijk, The Netherlands.

XMM-Newton/EPIC: SAP Saclay, IAS Orsay, CESR Toulouse, France; University of Leicester, University Birmingham, UK; CNR Mailand-Palermo-Bologna-Frascati, Osservatorio Astronomico Mailand, Italy; Institut für Astronomie und Astrophysik Tübingen, Germany.

Industrial Collaborations

ADTEC Plasma Technology Co. Ltd., Hiroshima: Development of a low-temperature plasma device for in-vivo sterilisation in medical applications.

Albedo GmbH, Neubiberg; Soft- and hardware developments for PK-3 Plus.

ASTEQ GmbH, Kelkheim: Manufacturing of detector arrays of pressed Ge:Ga, and processing of gallium arsenide probes.

BASF Coatings AG, Münster: Investigations on the scattering properties of micro particles.

Berliner Glas, Berlin: Polishing of the GROND-M3 mirror blank.

Bonerz engineering, Weiler-Simmerberg: Platinum development, electronics development.

Buchberger GmbH, Tuchenbach: Manufacturing of parts for OPTIMA and PANTER manipulators; FIFI-LS; parts for CAST and LUCIFER.

Carl Zeiss, Jena: eROSITA mirror and mandrels.

Cryovac Tieftemperaturtechnik, Troisdorf: Design and construction of the test cryostat for Herschel-PACS.

Drollinger, Birkenfeld: Gilding of detector parts for FIFI-LS.

ECM, Moosinning: Manufacturing of the GROND-M3 mirror blank.

ESS, Landsberg: Servicing of the electrical installation; Manufacturing of electrical devices for the test facilities PANTER, CALIFA and PUMA.

FEE, Idar-Oberstein: Production of VAG-blanks for GROND-Linsen.

Guido Lex Werkzeugbau GmbH, Miesbach: Structural parts for FIFI-LS.

Hans Englett OHG, Berlin: Manufacturing of front covers and measurement devices.

ESL GmbH, Berlin: Manufacturing of circuit boards.

Freyer GmbH, Tübingen: Manufacturing of structural parts for LUCIFER; PANTER.

GEWO, Wörth/Hörlkofen: Structural parts for FIFI-LS.

IMEC, Leuven, Belgium: Manufacturing of cryogenic electronics in new CMOS technology for IR-detectors on Herschel-PACS; FIFI-LS.

Ingenieurbüro Buttler, Essen: Development of front-end electronics for XEUS and eROSITA.

Ingenieurbüro Dohnalek, München: Design FIFI-LS and support on the design of pressed Ge:Ga-arrays.

Ingenieurbüro pfma, Haar-Salmdorf: Design und manufacturing of GROND components.

Ingenieurbüro Steinbach, Jena: Design and manufacturing of the GROND-M3 flip-mirror unit.

Ingenieurbüro Weisz, München: Design and mechanical engineering for LUCIFER; PACS test optics; XEUS mirror technology.

Kayser-Threde GmbH, München: Main contractor for Herschel-PACS; plasma-crystal experiments on the ISS; IMPF/IMPACT; eROSITA.

Korth GmbH, Altenholz: Manufacturing of lenses for GROND.

Kugler GmbH., Salem: Mirrors for OPTIMA, FIFI-LS.

Pantolsky GmbH, Neuried: Supporting the PANTER test facility.

PNSensor, München: Development and Manufacturing of semiconductor detectors.

Pribil D., Unterhaching: Manufacturing of structural parts for LUCIFER.

Sagem, Paris: Manufacturing of filters for OmegaCAM.

SCHOTT GLAS, Mainz: Investigations on the manufacturing of mirrors; XEUS.

Siemens AG, München: Manufacturing of reticles for pn-CCDs.

Siegert Electronics GmbH, Cadolzburg: Read-out electronic boards for FIFI-LS.

Tafelmaier Dünnschichttechnik, Rosenheim: Coating of optical components for GROND.

Technotron, Lindau: Development and manufacturing of electronics boards for eROSITA.

Thomas Markl GmbH, Deisenhofen: Manufacturing of structural parts for PACS and FIFI-LS.

Zeiss, Oberkochen: Polishing of the SPIFFI mirrors.

Activities in Transfer of Know-How

The many cooperations with industry and other research groups leads to a natural transfer of scientific and technical know-how, especially if orders are given to industry. In contrast, we list in the following those cooperations which are financed by industry as well as patents and licenses.

A) Research cooperations financed by industry

Dr. Johannes Heidenhain-Stiftung, Traunreut: Technology development in the field of X-ray optics and spectroscopy; absolute calibration of X-ray CCD systems.

Knoll AG, Ludwigshafen: Analyses of longterm cardiograms.

Linos AG / Rodenstock Präzisionsoptik, München: Identification of malignant melanoma.

MAHLE GmbH, Stuttgart: Image analyses of destruction-free examination of materials.

OHB-System GmbH, Bremen: Pre-investigations for a flexible S/W simulator for small satellites.

PROTEOSYS AG, Mainz: Data analyses in biotechnology.

B 1) Licenses

Ganimed AG, Freiburg: ECG-analyses.

Knoll AG, Ludwigshafen: Pharmacology.

Linos AG / Rodenstock Präzisionsoptik, München: Identification of malignant melanoma.

B 2) Licensing agreements pending

Kayser-Threde GmbH, München: Complex Plasmas.

C) Cooperation with Universities (contracts)

Anaesthesiology:

Klinik für Anästhesiologie, Klinikum Rechts der Isar, TU München.

Scanning Probe Microscopy:

Institut für Kristallographie und Angewandte Mineralogie, Ludwig-Maximilians-Universität, München.

Radio Diagnostics:

Institut für med. Statistik und Epidemiologie, TU München;
Institut für Röntgendiagnostik, TU München.

D) Patents

Verfahren und Einrichtung zur Raumfilterung (D, Eu, USA, J); Pat. 700 544.

Verfahren und Vorrichtung zur Mustererkennung (D, Eu, USA, J); Pat. 825 543.

Teilchenmanipulierung (D, Eu, USA, Japan, Russia); Pat.-Anm. 197 13 637.0.

Melanomerkenung (D); Pat.-Anm. 197 54 909.

Streifendetektor (Eu, USA, Japan); Pat.-Anm. PCT/DE 97/01015.

Verfahren und Vorrichtung zur Segmentierung einer Punkteverteilung (D); Anmeldung: # 199 28 231-5.

Silicon Strip Detector (USA, Pat.No.: VS6,184,562 B1).

Controlled Drift Detector, EP Appl. No. 988 300 89.3.

Leitungsüberführung (D, Eu) PCT/EP 03/03209.

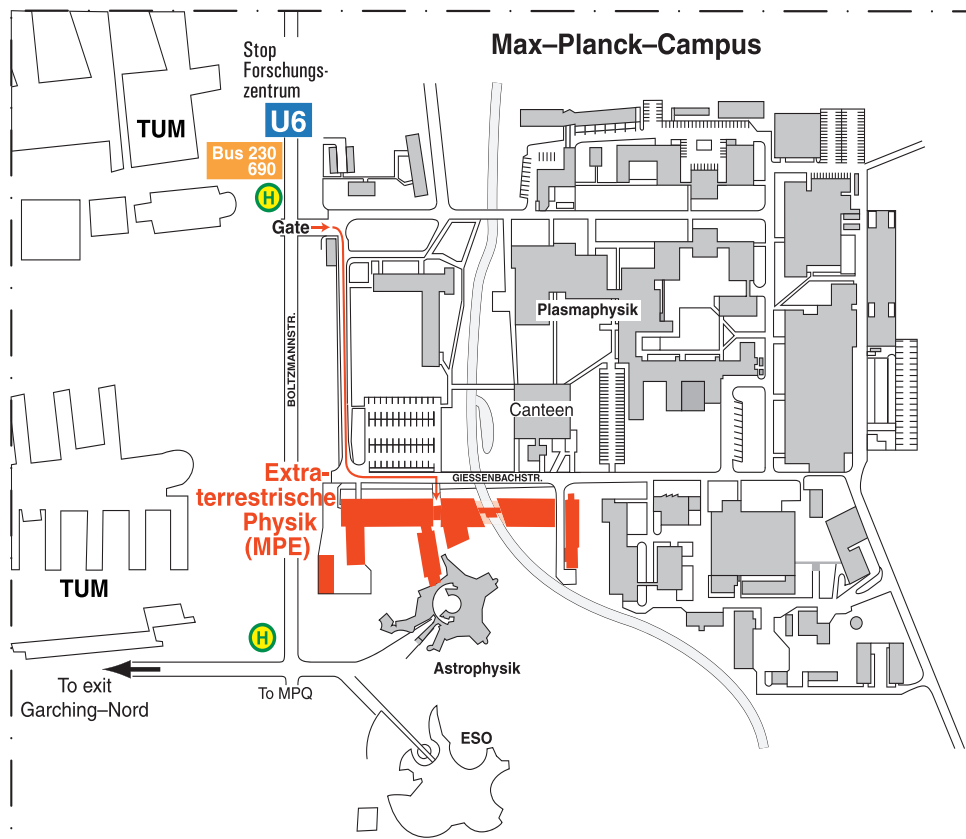
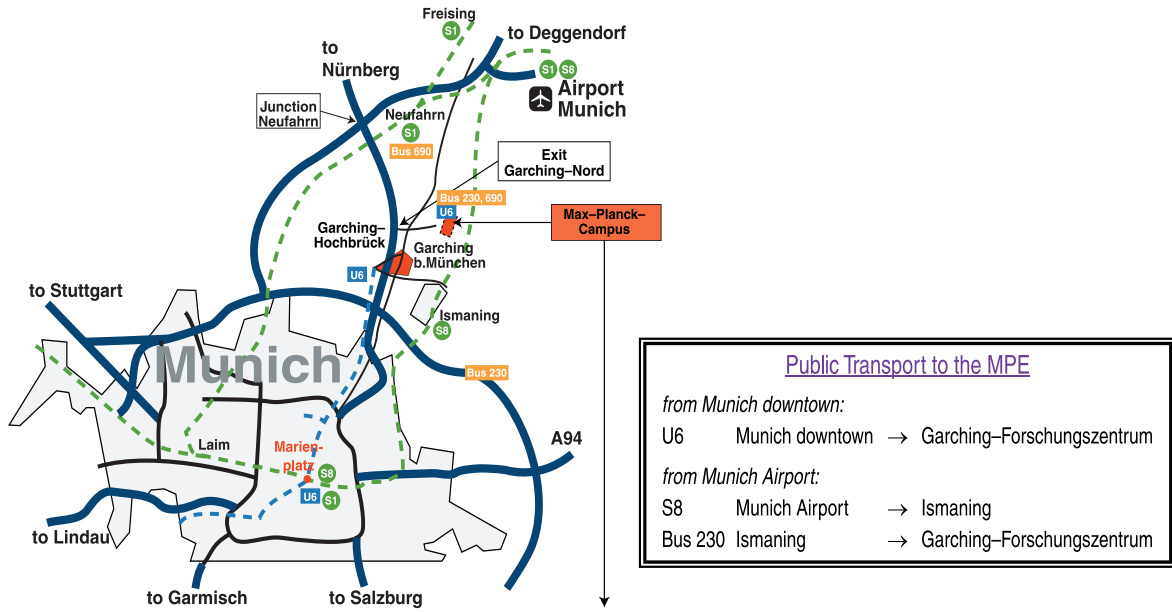
Eintrittsfenster (D) DE 102 60 229.8.

Halbleiterdetektoren: Patenterteilung Deutschland: DE 10 2004 022 948 Patentanmeldung USA: US 11/127,660

Location

Map and Access

Max-Planck-Institut für extraterrestrische Physik (MPE)



Back cover:

The German astronaut Thomas Reiter is experimenting with the MPE plasma crystal experiment PK-3 Plus aboard the International Space Station ISS. PK-3 Plus was lifted from the Russian launch site Baikonur to the ISS by a Progress rocket end of 2005.

